



UNIVERSIDAD DE CHILE
FACULTAD DE CIENCIAS FÍSICAS Y MATEMÁTICAS
DEPARTAMENTO DE GEOLOGÍA

**PROCESOS CONCENTRADORES DE NIOBIO EN DEPÓSITOS ASOCIADOS A
COMPLEJOS CARBONATÍTICOS, PROVINCIA ÍGNEA DEL ALTO PARANAÍBA,
BRASIL**

TESIS PARA OPTAR AL GRADO DE DOCTOR EN CIENCIAS, MENCIÓN GEOLOGÍA

FELIPE VELÁSQUEZ RUIZ

PROFESOR GUÍA:
MARTIN REICH MORALES

MIEMBROS DE LA COMISIÓN:
FERNANDO BARRA PANTOJA
DIEGO MORATA CÉSPEDES
CARLOS SANTIAGO TASSARA

Este trabajo ha sido financiado parcialmente por el Núcleo Milenio Trazadores de Metales en Zonas de Subducción y por la beca doctoral de la Agencia Nacional de Investigación y Desarrollo ANID-21210049.

SANTIAGO DE CHILE
2023

**RESUMEN DE LA TESIS PARA OPTAR AL
GRADO DE: DOCTOR EN CIENCIAS, MENCIÓN
GEOLOGÍA.
POR: FELIPE VELÁSQUEZ RUIZ
FECHA: 2023
PROFESOR GUÍA: MARTIN REICH MORALES**

**PROCESOS CONCENTRADORES DE NIOBIO EN DEPÓSITOS ASOCIADOS A
COMPLEJOS CARBONATÍTICOS, PROVINCIA ÍGNEA DE ALTO PARANAÍBA,
BRASIL**

El niobio (Nb) es un metal de transición litófilo, perteneciente al grupo de los denominados *Elementos de Alta Intensidad de Campo* (HFSE por sus siglas en inglés). Debido a sus múltiples aplicaciones industriales y tecnológicas, el Nb es considerado un elemento crítico o estratégico, considerando además sus fluctuaciones en la demanda global. Esta tesis se centra en el estudio de los procesos mineralizadores que dan origen a los mega-depósitos de Nb asociados a complejos alcalino-carbonatíticos, específicamente en la Provincia Ígnea del Alto Paranaíba (APIP) en Brasil central, los cuales corresponden a la principal fuente de Nb a nivel global. Más del 90% de la producción mundial de Nb está relacionada con la extracción de pirocloro $[(\text{Na},\text{Ca})_2\text{Nb}_2\text{O}_6(\text{OH},\text{F})]$ en los complejos alcalino-carbonatíticos de la APIP, destacándose los mega-depósitos de Nb de Araxá y Catalão II. En la APIP, el pirocloro se encuentra principalmente en rocas ricas en magnetita-apatito-tetraferriflogopita±olivino o foscoritas, que se asocian con carbonatitas, aillikitas y vetas secundarias carbotermales. A pesar de los avances en la comprensión de estos depósitos, existen aspectos fundamentales asociados a la metalogénesis del Nb que permanecen sub-estudiados en la APIP. En particular, el rol del magmatismo alcalino-carbonatítico, la naturaleza del metasomatismo carbotermal asociado (o fenitización) y las características de los procesos mineralizadores que llevan a la formación del pirocloro, la principal fase portadora de Nb en estos depósitos.

La investigación se desarrolla en el depósito de Nb de Boa Vista, localizado en el Complejo Catalão II de la APIP y se estructura de la siguiente forma: el Capítulo 1 corresponde a una introducción general acerca de la metalogénesis del Nb en la APIP y en la cual se presentan los alcances, objetivos y la hipótesis de trabajo. El Capítulo 2 trata sobre la fuente y evolución del magma primario al sistema alcalino-carbonatítico de la APIP, y su vínculo con flujos de lavas ultrapotásicos (kamafugitas). Se propone la existencia de un magma primario sílico-carbonatado ultrapotásico, y posterior a un intenso proceso de fraccionamiento, se generan series de magmas carbonatíticos y alcalinos. En el Capítulo 3 se describe el metasomatismo carbotermal del basamento que aloja la mineralización de Nb en Boa Vista, generado por la liberación de volátiles desde el intrusivo alcalino-carbonatítico. Los resultados indican que dicho proceso, denominado fenitización, se desarrolló de manera sincrónica al emplazamiento intrusivo, proveyendo evidencia de la infiltración de fluidos alrededor de intrusiones carbonatíticas ricas en Nb. El Capítulo 4 reporta el análisis microtextural y de elementos traza *in-situ* en pirocloro, donde se propone que el origen de las foscoritas ricas en Nb estaría relacionado a un proceso de segregación de minerales pesados durante el fraccionamiento de un magma parental carbonatítico. De manera general, la presente tesis doctoral provee nuevos antecedentes acerca de la metalogénesis del Nb asociado a complejos alcalino-carbonatíticos, la principal fuente global de este elemento crítico. Los resultados obtenidos en el Complejo Catalão II pueden extenderse a otros complejos de la APIP, ya que comparten un link genético, incluido el pobemente estudiado Complejo Araxá, que corresponde al mayor depósito de Nb a nivel mundial.

"Si en el oro están comprendidos todos los valores,
en la sencillez están comprendidas todas las virtudes"

Tomás Carrasquilla

A mi madre Martha Lía, Q.E.P.D.

AGRADECIMIENTOS

La presente tesis doctoral, es el resultado de una sinergia entre académicos y laboratorios de diversas universidades chilenas, brasileñas y europeas. En primer lugar, agradezco a mi orientador Dr. Martin Reich por haberme dado la oportunidad de realizar el doctorado en la Universidad de Chile, por guiarme oportunamente en temas geológicos y por su apoyo en la postulación a becas nacionales e internacionales. También agradezco al Dr. Reich por brindarme su apoyo durante el confinamiento global entre los años 2020 y 2021, producto de la pandemia de Covid-19. Agradezco a mi comisión de tesis, formada por los Drs. Fernando Barra y Diego Morata de la Universidad de Chile, y al Dr. Santiago Tassara, de la Universidad de O'Higgins, por la revisión de este documento y el apoyo brindado durante el proceso de graduación.

También, me gustaría agradecer al Dr. Pedro Cordeiro por la obtención de muestras de roca alcalinas y carbonatitas de la APIP, por ayudarme a comprender la geología brasileña y por el puente que hizo con laboratorios brasileños y europeos. Agradezco al Dr. Leonardo Lagoeiro de la *Universidade Federal do Paraná*, por su ayuda con los análisis EBSD. También al *Centro Regional para o Desenvolvimento Tecnológico e Inovação* (CRTI), por su colaboración con los análisis de microsonda electrónica (EMPA). Mil gracias al Dr. Fernando Barra y a Rurik Romero de la Universidad de Chile por su colaboración con los análisis de *laser ablation inductively coupled plasma mass spectrometry* (LA-ICP-MS), y a Christian Nievas por su apoyo en el uso del microscopio electrónico de barrido. Agradezco al Dr. Thomas Angerer de la Universidad de Bonn, por colaborar con los análisis de μ -XRF y un especial agradecimiento al Dr. Sam Broom-Fendley de la Universidad de Exeter por colaborar en varios análisis complementarios de LA-ICP-MS, EMPA y catodoluminiscencia. También, se agradece al Dr. Charles Beard de la Universidad de Cambridge por su apoyo en temas de geoquímica de elementos incompatibles.

Se agradece al proyecto NCN13_065 “Núcleo Milenio Trazadores de Metales en Zonas de Subducción” por apoyar esta investigación a través de la Iniciativa Científica Milenio, a la Agencia Nacional de Investigación y Desarrollo (ANID) por la Beca de Doctorado Nacional No. 21210049 y a la *Society of Economic Geologists* (SEG) por la Beca *Hugh McKinstry Fund*.

Mil gracias a Cristian Pérez Hernández por su valiosa compañía y apoyo, por ofrecerme la oportunidad de entender la cultura chilena y por hacerme más fácil mi estadía en el pre- y pos-confinamiento de Covid-19. De igual modo, agradezco el apoyo incondicional de mis amigas Leidy P. y Alejandra T., por ser una fuente de catarsis y de cercanía con Colombia.

Agradezco a mi familia en Colombia, a mi padre Agustín y a mis hermanas Yaneth, Susana y Renatha por creer en mí siempre, especialmente en mis ocurrencias de ir al exterior a realizar investigación, los quiero mucho y los extrañé todos los días que estuve fuera de Medellín. Finalmente, a mi madre Martha Lía Ruiz, Q.E.P.D., quien es mi ángel, mi motivación y la razón de mi existencia.

TABLA DE CONTENIDO

CAPÍTULO 1: INTRODUCCIÓN	1
1.1. PRESENTACIÓN Y MOTIVACIÓN	1
1.2. CONTEXTO GEOLÓGICO Y EVOLUCIÓN GEODINÁMICA	2
1.3. COMPLEJOS ALCALINO-CARBONATÍTICOS DE LA APIP.....	5
1.4. OBJETIVOS DE LA TESIS	6
1.4.1. ALCANCE Y OBJETIVO GENERAL.....	6
1.4.2. OBJETIVOS ESPECÍFICOS.....	7
1.5. HIPÓTESIS DE TRABAJO	7
1.6. MANUSCRITOS Y PUBLICACIONES	8
CAPÍTULO 2: THE GENETIC LINK BETWEEN KAMAFUGITE MAGMATISM AND ALKALINE-CARBONATITE COMPLEXES IN THE LATE CRETACEOUS ALTO PARANAÍBA IGNEOUS PROVINCE, CENTRAL BRAZIL.....	9
2.1. ABSTRACT	10
2.2. INTRODUCTION	10
2.3. GEOLOGICAL BACKGROUND.....	11
2.3.1. THE ALTO PARANAÍBA IGNEOUS PROVINCE (APIP).....	11
2.3.2. MATA DA CORDA FORMATION KAMAFUGITES.....	12
2.3.3. POTASSIC AND ULTRAPOTASSIC SILICA UNDERSATURATED ROCKS ASSOCIATED WITH THE APIP ALKALINE-CARBONATITE COMPLEXES	13
2.4. METHODS AND SAMPLES	14
2.4.1. GEOPHYSICAL IMAGING.....	14
2.4.2. SAMPLES, WHOLE-ROCK CHEMISTRY, MICRO-XRF AND MINERAL CHEMISTRY.....	15
2.5. RESULTS	16
2.5.1. AEROMAGNETIC MODELLING.....	16
2.5.2. PETROGRAPHY.....	17
2.5.3. MINERAL CHEMISTRY.....	18
2.5.4. WHOLE ROCK CHEMISTRY.....	19
2.6. DISCUSSION.....	20
2.6.1. SPATIAL DISTRIBUTION OF KAMAFUGITE VOLCANISM AND ALKALINE-CARBONATITE COMPLEXES.....	20
2.6.2. POTENTIAL LINKS BETWEEN KAMAFUGITES AND AILLIKITES FROM ALKALINE-CARBONATITE COMPLEXES IN THE APIP	23
2.6.3. MANTLE SOURCE CHARACTERISTICS AND SILICA-UNDERSATURATED MAGMATISM	24
2.6.4. POST-MAGMATIC PROCESSES IN KAMAFUGITE LAVAS.....	26
2.7. CONCLUSIONS	28
2.8. ACKNOWLEDGMENTS	28
2.9. FIGURES.....	29
CAPÍTULO 3: MICROANALYTICAL INVESTIGATION OF K-RICH FENITES FROM THE CATALÃO II ALKALINE-CARBONATITE COMPLEX IN CENTRAL BRAZIL: IMPLICATIONS FOR ORE-FORMING PROCESSES WITHIN THE WORLD'S LARGEST NIOBIUM PROVINCE	40
3.1. ABSTRACT	41
3.2. INTRODUCTION	41
3.3. GEOLOGICAL SETTING	43
3.4. METHODS	44
3.5. RESULTS	45
3.5.1. TEXTURES AND MINERALOGY OF K-RICH FENITES.....	45
3.5.2. CHEMICAL MAPPING OF K-RICH FENITES AND ASSOCIATED CARBONATITES.....	46
3.5.3. MINERAL CHEMISTRY OF K-BEARING SILICATES.....	46
3.5.4. MICROSTRUCTURE OF FENITES	47
3.6. DISCUSSION.....	48
3.6.1. FENITIZATION ASSOCIATED WITH NIOBIUM MINERALIZATION.....	49
3.6.2. TEXTURAL ANALYSIS OF MAGMATIC AND METASOMATIC PHLOGOPITES.....	50

3.6.3.FENITE MICROSTRUCTURE AS A FLUID FLOW INDICATOR IN THE MAGMATIC-HYDROTHERMAL WINDOW	51
3.7. CONCLUSIONS	52
3.8. ACKNOWLEDGMENTS	53
3.9. TABLES	54
3.10. FIGURES.....	55
CAPÍTULO 4: ORIGIN OF CARBONATITE-RELATED NIOBUM DEPOSITS: INSIGHTS FROM PYROCHLORE GEOCHEMISTRY.....	65
4.1. ABSTRACT	66
4.2. INTRODUCTION	67
4.3. GEOLOGICAL SETTING	68
4.3.1.THE CATALÃO II ALKALINE-CARBONATITE COMPLEX AND NOMENCLATURE OF ITS “EXOTIC” ROCKS	68
4.4. SAMPLES AND METHODS.....	70
4.5. RESULTS	71
4.5.1.ROCK TEXTURES AND PARAGENETIC SEQUENCE	71
4.5.2.PYROCHLORE TEXTURES.....	71
4.5.3.PYROCHLORE CHEMICAL COMPOSITION.....	72
4.6. DISCUSSION.....	74
4.6.1.TEXTURAL ANALYSIS OF PYROCHLORE AND ITS RELATIONSHIP WITH MAGMATIC AND CARBOHERMAL PROCESSES	74
4.6.2.INSIGHTS INTO NB ENRICHMENT PROCESSES FROM SOURCE TO ORE.....	76
4.6.3.HEAVY MINERALS TRANSPORT WITHIN A CARBONATITIC SYSTEM.....	77
4.6.4.GENESIS OF PYROCHLORE-RICH PHOSCORITES.....	77
4.7. CONCLUSIONS	78
4.8. ACKNOWLEDGMENTS	79
4.9. DATA AVAILABILITY	79
4.10. TABLES	80
4.11. FIGURES.....	82
CAPÍTULO 5: REVISION OF THE NOMENCLATURE OF APATITE-MAGNETITE-RICH IGNEOUS ROCKS AND ITS INCLUSION WITHIN THE IUGS CLASSIFICATION.....	97
5.1. ABSTRACT	98
5.2. INTRODUCTION	98
5.3. HISTORICAL BACKGROUND ON APATITE-MAGNETITE-RICH IGNEOUS ROCKS	99
5.3.1.NELSONITE.....	99
5.3.2.PHOSCORITE.....	100
5.3.3.BEBEDOURITE	101
5.4. CLASSIFICATION RATIONALE	101
5.5. INTEGRATING APATITE-MAGNETITE-RICH IGNEOUS ROCKS INTO THE IUGS CLASSIFICATION	102
5.6. APPLICATION OF THE REVISION	103
5.6.1.PHOSCORITES AND BEBEDOURITES FROM THE ALTO PARANÁIBA IGNEOUS PROVINCE (APIP).....	103
5.6.2.NELSONITES FROM ANORTHOSITE-LACKING LAYERED MAFIC INTRUSIONS.....	103
5.7. CONCLUDING REMARKS.....	104
5.8. ACKNOWLEDGEMENTS.....	104
5.9. TABLES	105
5.10. FIGURES.....	106
CAPÍTULO 6: CONCLUSIONES	108
BIBLIOGRAPHY	111
ANEXO: MATERIAL SUPLEMENTARIO.....	125

ÍNDICE DE TABLAS

TABLE 1. REPRESENTATIVE ELECTRON MICROPROBE ANALYZER (EMPA) DATA FOR K-RICH MAGMATIC AND HYDROTHERMAL MICAS IN THE BOA VISTA Nb MINE, SOUTHERN PLUG, CATALAO II COMPLEX. ALL ANALYSES ARE INCLUDED IN SD2.....	54
TABLE 2. REPRESENTATIVE EPMA ANALYSES FOR PYROCHLORE IN EACH ROCK TYPE FROM THE BOA VISTA MINE AT CATALÃO II SOUTH.....	80
TABLE 3. SUMMARY OF TRACE ELEMENT CONCENTRATIONS FOR PYROCHLORE IN EACH ROCK TYPE FROM THE BOA VISTA MINE.....	81
TABLE 4. PROPOSED NOMENCLATURE FOR APATITE-MAGNETITE-RICH IGNEOUS ROCKS, COMPRISING FIVE TERMS INCLUDING NELSONITE, PHOSCORITE, BEBEDOURITE, APATITITE, AND MAGNETITITE, AND THEIR RESPECTIVE ROCK-FORMING MINERALS (SOLID CIRCLES). THE CLASSIFICATION WAS MADE BASED ON A RECONCILIATION BETWEEN THE GLOSSARY OF TERMS OF THE IUGS CLASSIFICATION (LE MAITRE, 2002) AND CLASSICAL LITERATURE (WATSON, 1907; WATSON AND TABER, 1913; MOORE, 1940; PHILPOTTS, 1967; YEGOROV, 1993, DARLING AND FLORENCE, 1995; KRASNOVA ET AL., 2004; TEGNER ET AL., 2006; BARBOSA ET AL., 2012). DESPITE THE HIGH VARIETY OF ACCESSORY MINERALS (OPEN CIRCLES), THESE ARE NOT TAKEN INTO ACCOUNT IN THE CLASSIFICATION.....	105

ÍNDICE DE FIGURAS

FIG. 1. (A) MAPA DE AMÉRICA DEL SUR CON LA UBICACIÓN DE LA APIP, EL CRATÓN DE SÃO FRANCISCO Y LA CUENCA DE PARANÁ. (B) MAPA GEOLÓGICO DE LA APIP, CON LA UBICACIÓN DE LOS SEIS COMPLEJOS PRINCIPALES ALCALINO-CARBONATÍTICOS, MODIFICADO A PARTIR DE LAS HOJAS CARTOGRÁFICAS 1:1M BELO HORIZONTE (SE-23) Y GOIÂNIA (SE-22), DEL SERVICIO GEOLÓGICO DE BRASIL	3
FIG. 2. A) MAPA DE UBICACIÓN DE LA PORCIÓN SUR DE AMÉRICA DEL SUR EN GONDWANA OCCIDENTAL. LEYENDA: RPC - CRATÓN RÍO DE LA PLATA, SFC - CRATÓN SÃO FRANCISCO, TC - CRATÓN TANZANIA. B) MAGMATISMO ALCALINO Y TOLEÍTICO DEL MESOZOICO AL PALEÓGENO EN LA PLATAFORMA SUDAMERICANA (TOMADA DE FERREIRA ET AL., 2022).....	4
FIG. 3. GEOMETRÍA COMPARATIVA Y TAMAÑOS DE COMPLEJOS ALCALINO-CARBONATÍTICOS DE LA APIP, INCLUYENDO LOS COMPLEJOS: SERRA NEGRA, SALITRE, ARAXÁ, TAPIRA Y CATALAO I Y II (TOMADO DE NOVAES, 2018).	5
FIG. 4. SIMPLIFIED GEOLOGICAL MAP FOR THE APIP SHOWING THE LOCATION OF THE MATA DA CORDA FORMATION AND THE NEIGHBOURING ALCALINE-CARBONATITE COMPLEXES, MODIFIED FROM THE 1:1M CARTOGRAPHIC SHEETS BELO HORIZONTE (SE-23) AND GOIÂNIA (SE22) OF THE BRAZILIAN GEOLOGICAL SURVEY (CPRM 2020). PREVIOUS OCCURRENCES REPORTED IN THE LITERATURE ARE ALSO SHOWN (E.G., GUARINO ET AL., 2013; MELLUSO ET AL., 2008; GIBSON ET AL., 1994). ABBREVIATIONS: APIP, ALTO PARANAÍBA IGNEOUS PROVINCE; A. 125°, AZIMUTH 125° LINEAMENT; SFC, SÃO FRANCISCO CRATON. THE SAMPLING LOCATIONS COME FROM PATOS DE MINAS AND LAGOA FORMOSA, STATE OF MINAS GERAIS, BRAZIL	29
FIG. 5. (A) OUTCROP OF HIGHLY WEATHERED KAMAFUGITE LAVAS IN MATA DA CORDA CENTRAL. (B) AND (C) CORRESPOND TO DRILL CORES OF A KAMAFUGITE LAVA (SAMPLE FSP13-326) AND A KAMAFUGITE BRECCIA (SAMPLE PH01-139), RESPECTIVELY. (D) AND (E) CORRESPOND TO AN OUTCROP AND A BOREHOLE (SAMPLE RM024-339.5) RESPECTIVELY, OF AN OLIVINE AILLIKITE CUTTING A CALCITE-CARBONATITE DIKE FROM THE CATALÃO II COMPLEX. ABBREVIATIONS: CAL, CALCITE; CPX, CLINOPYROXENE; GO, GORCEIXITE; MAG, MAGNETITE; OL, OLIVINE; PCL, PYROCHLORE.....	30
FIG. 6. (A) ANALYTICAL SIGNAL IMAGES FROM MAGNETIC DATA, SHOWING THE MAGNETIC FABRIC IN THE MATA DA CORDA FORMATION AND THE CONTOURS OF THE SERRA NEGRA, SALITRE, ARAXÁ AND TAPIRA ALCALINE-CARBONATITE COMPLEXES. IN ADDITION, THE TRACE OF THE AZIMUTH 125° LINEAMENT AND ITS THREE COMPONENTS L1, L2 AND L3, ACCORDING TO (ROCHA ET AL. 2014). (B) REDUCTION TO THE POLE IMAGE, WHERE IT IS OBSERVED THAT ALCALINE-CARBONATITE COMPLEXES HAVE A DIPOLE MAGNETIC RESPONSE. IN ADDITION, THREE Dipoles are observed south of MATA DA CORDA, spatially associated with azimuth 125°. ABBREVIATIONS: MCN, MATA DA CORDA NORTH; MCC, MATA DA CORDA CENTRAL; MCS, MATA DA CORDA SOUTH.....	31
FIG. 7. POLARIZED-LIGHT AND SCANNING ELECTRON MICROSCOPE PHOTOMICROGRAPHS OF KAMAFUGITE LAVAS (A-D) AND KAMAFUGITE BRECCIAS (E-F) FROM MATA DA CORDA CENTRAL. G-I ARE OLIVINE AILLIKITE SAMPLES FROM THE CATALÃO II COMPLEX. (A) FINE-GRAINED DIOPSIDE AND APATITE WITH POIKILITIC TEXTURE, WITH PEROVSKITE AND MAGNETITE OIKOCRYSTS. (B) PEROVSKITE AND MAGNETITE MICROCRYSTS SET IN AN ALTERED GROUNDMASS HOSTING VESICLES. (C) ANHEDRAL AGGREGATES OF PHLOGOPITE, CLINOPYROXENE, AND PEROVSKITE. (D) KALSILITE AND CLINOPYROXENE MICROCRYSTS. (E) CHLORITE AND GORCEIXITE VEINLETS IN A KAMAFUGITE BRECCIA. (F) CALCITE VEINLET WITH GLAUCONITE CRYSTALS. (G) OLIVINE AILLIKITE RICH IN OXIDES, IN A CONTACT WITH A CALCITE-CARBONATITE WITH PYROCHLORE. (H) ZONED PHLOGOPITE AND ROUNDED OLIVINE MACROCRYSTS SET IN A MAGNETITE-PHLOGOPITE RICH GROUNDMASS. (I) PARTIALLY ALTERED OLIVINES TO TALC SET IN A MAGNETITE-PHLOGOPITE-RICH GROUNDMASS. ABBREVIATIONS: AP, APATITE; CAL, CALCITE; CHL, CHLORITE; CPX, CLINOPYROXENE (DIOPSIDE); GLT, GLAUCONITE; GO, GORCEIXITE; KLS, KALSILITE; MAG, MAGNETITE; OL, OLIVINE; PCL, PYROCHLORE; PHL, PHLOGOPITE; PRV, PEROVSKITE; TLC, TALC; USP, ULVÖSPINEL	32
FIG. 8. BOXPLOTS SHOWING THE END MEMBER COMPOSITION FOR REPRESENTATIVE SPINEL-GROUP OXIDES IN THE APIP ULTRAPOTASSIC ROCKS (n=210). PLOTS SHOW THE SPINEL GROUP SOLID SOLUTION, INCLUDING MAGNETITE, ULVÖSPINEL, MG-CHROMITE AND MG-FERRITE END MEMBERS, FOR (A) MATA DA CORDA CENTRAL (MCC) KAMAFUGITES, (B) MATA DA CORDA NORTH (MCN) KAMAFUGITES, (C) OLIVINE (OL) AILLIKITES AND (D) DIOPSIDE (DI) AILLIKITES. THE EMPA DATABASE IS PRESENTED IN THE SUPPLEMENTARY MATERIAL 2.....	33

- FIG. 9.** WDS MAPS OF Fe, Ni, Ti, Ca AND Mg SHOWING A POIKILITIC MAGNETITE (MAG) WITH PEROVSKITE (Prv) OIKOCRYSTALS OF A KAMAFUGITE LAVA FROM MATA DA CORDA CENTRAL (SAMPLE PH03-059.5). MAGNETITE SHOWS MARTITIZATION IN THE BROAD DARKER RIM IN THE BSE IMAGE (UPPER LEFT), WHILE PEROVSKITE SHOWS VARIABILITY OF Ca AND Ti BETWEEN THE DIFFERENT INCLUSIONS. THE BAR SCALE IS IN COUNTS.....34
- FIG. 10.** FeO VS CAO DIAGRAM FOR CLINOPYROXENE FROM APIP ULTRAPOTASSIC ROCKS. THE UPPER RIGHT BOX SHOWS THE CLASSIFICATION CORRESPONDING TO A CA-RICH DIOPSIDE.....35
- FIG. 11.** TOTAL ALKALI VS. SILICA DIAGRAM (LE MAITRE 2002) FOR THE MATA DA CORDA KAMAFUGITES. WE ALSO PLOT THE CHEMICAL RESULTS OF OLIVINE AILLIKITES FROM THE CATALÃO II, TAPIRA AND SERRA NEGRA COMPLEXES WITH RED CIRCLES AND DIOPSIDE AILLIKITES OF SALITRE WITH YELLOW CROSSES (SUPPLEMENTARY MATERIAL 1) FOR COMPARISON.....35
- FIG. 12.** VARIATION DIAGRAMS OF SELECTED MAJOR AND OXIDES FOR MATA DA CORDA KAMAFUGITES IN GREEN AND BLUE RECTANGLES. WE ALSO PLOT THE CHEMICAL RESULTS OF OLIVINE AILLIKITES FROM THE CATALÃO II, TAPIRA AND SERRA NEGRA COMPLEXES WITH RED CIRCLES AND DIOPSIDE AILLIKITES OF SALITRE WITH YELLOW CROSSES (SUPPLEMENTARY MATERIAL 1) FOR COMPARISON. BLACK RECTANGLES AND CIRCLES CORRESPOND TO NEAR PRIMARY MELT COMPOSITIONS FOR KAMAFUGITES AND AILLIKITES, RESPECTIVELY. THE FIELDS AND LINES IN (B) CORRESPOND TO SiO₂ VS. CAO CLASSIFICATION FIELDS FOR ULTRAPOTASSIC ROCKS (FOLEY ET AL., 1987).....36
- FIG. 13.** (A), (B) AND (C) CORRESPOND TO REE-NORMALIZED SPIDER DIAGRAMS (NAKAMURA, 1974), COMPARING THE COMPOSITIONS OF MATA DA CORDA KAMAFUGITES, OLIVINE AILLIKITES AND DIOPSIDE AILLIKITES WITH APIP NEAR-PRIMARY MELTS (SUPPLEMENTARY MATERIAL 1). (D) Cr (ppm) VS Zr/Nb DIAGRAM FOR ALL APIP POTASSIC AND ULTRAPOTASSIC ROCKS. (E) Y (ppm) VS SR/Y DIAGRAM, PLOTTED FOR APIP, TORO-ANKOLE AND SAN VENANZO (SV) KAMAFUGITES AND AILLIKITES, SEPARATING TWO FIELDS FOR PRIMARY KAMAFUGITES AND AILLIKITES/(EVOLVED KAMAFUGITES?). (F) Nb (ppm) VS La/Y DIAGRAM FOR APIP ULTRAPOTASSIC ROCKS.....37
- FIG. 14.** INITIAL END VS ⁸⁷Sr/⁸⁶Sr ISOTOPIC DIAGRAM FOR THE APIP LOCALITIES COMPARED TO THE ARCHEAN TO PALEOPROTEROZOIC CRUST OF THE SÃO FRANCISCO CRATON, THE NEOPROTEROZOIC BRASILIA BELT (APIP BASEMENT) AND THE PLIOCENE ILHA DA TRINDADE (TRINDADE ISLAND) IN CENTRAL ATLANTIC. THE COMPILATION OF ISOTOPIC APIP DATA IS SHOWN IN THE SUPPLEMENTARY TABLE 2. ISOTOPIC COMPOSITION OF THE SÃO FRANCISCO CRATON AND THE BRASILIA BELT FROM CARVALHO ET AL. (2019). ISOTOPIC COMPOSITION OF TRINDADE COMPONENTS FROM HALLIDAY ET AL. (1992).....38
- FIG. 15.** EMPLACEMENT MODEL FOR THE MAGMATIC ROCKS OF THE MATA DA CORDA FORMATION (STEPS 1 TO 5) AND FOR A GENERIC APIP ALKALINE-CARBONATITE COMPLEX (STEPS 1 TO 4.2 AND 6 TO 8). RELATIVE DEPTHS OF THE UPPER AND LOWER CRUST AND THE SUBCONTINENTAL LITHOSPHERIC MANTLE CORRESPOND TO THE INITIAL APIP DEPTHS PROPOSED BY GIBSON ET AL. (1995). ABBREVIATIONS: Di, DIOPSIDE; E, APIP EAST; Ol, OLIVINE; SGM, SPINEL GROUP MINERALS; W, APIP WEST.....39
- FIG. 16.** GEOLOGICAL MAP OF THE APIP SHOWING THE LOCATION OF THE SIX MAIN ALKALINE-CARBONATITE COMPLEXES. FIGURE MODIFIED FROM THE 1:1M BELO HORIZONTE (SE-23) AND GOIÂNIA (SE22) CARTOGRAPHIC SHEETS OF THE BRAZILIAN GEOLOGICAL SURVEY (CPRM, 2020). ABBREVIATIONS: APIP, ALTO PARANAÍBA IGNEOUS PROVINCE; SFC, SÃO FRANCISCO CRATON.....55
- FIG. 17.** DETAILED GEOLOGICAL MAP OF THE CATALÃO II COMPLEX, SHOWING THE LOCATION OF THE NORTH AND SOUTH PLUGS, THE NIOBUM AND PHOSPHATE MINES, THE DISTRIBUTION OF MAGMATIC ALKALINE LITHOTYPES, THE SURROUNDING FENITE, AND THE BASEMENT. THE FENITES OF BOA VISTA NB MINE IN THE SOUTH PLUG ARE STUDIED HERE.....56
- FIG. 18.** (A) OUTCROP OF A DISTAL FENITE WITH CALCITE VEINLETS IN THE PIT OF THE BOA VISTA Nb MINE. (B) SWARM DIKE SYSTEM CONTAINING PHOSCORITE AND CALCITE CARBONATITE DIKES, SHOWING A DRAMATIC CHANGE IN THE CARBONATITE DIKE THICKNESS. (C) OUTCROP OF A PERVERSIVE DISTAL FENITIZED BASEMENT ROCK WITH HIGH DENSITY OF CALCITE VEINLETS AND FRACTURES. (D) CORE SAMPLE SHOWING FENITE TEXTURES ASSOCIATED WITH A PYROCHLORE-BEARING (PCL) CALCITE CARBONATITE DIKE (MINERALIZED CC DIKE). THE DIKE SHOWS A PROXIMAL FENITE OF A PHLOGOPITITE AND THE ORIENTED FINE-GRAINED DISTAL FENITE. (E) CORE SAMPLE SCAN SHOWING A BARREN CALCITE CARBONATITE DIKE (BARREN CC DIKE). AS IN (D), PHLOGOPITE METASOMATIC HALOES ARE OBSERVED.....57
- FIG. 19.** PHOTOMICROGRAPHS OF THE CALCITE CARBONATITE DIKES ARE SHOWN IN THE (A), (C) AND (E) IMAGES, WHILE THEIR ASSOCIATED FENITES ARE SHOWN IN THE (B), (D) AND (F) IMAGES. (A) PLANE POLARIZED LIGHT (PPL) IMAGE

SHOWING THE TEXTURE OF A COARSE-GRAINED CALCITE CARBONATITE DIKE. (B) PPL IMAGE SHOWING THE TEXTURE OF AN ORIENTED FINE-GRAINED DISTAL FENITE, MARKED BY PHLOGOPITE. (C) PPL IMAGE CORRESPONDS TO ZONED MAGMATIC CRYSTALS OF PHLOGOPITE CORE AND TETRAFERRIPHLOGOPITE RIM. (D) CROSSED POLARIZED LIGHT (XPL) IMAGE SHOWS IN DETAIL THE FINE-GRAINED ASSOCIATION OF PHLOGOPITE, CALCITE AND ORTHOCLASE (BLACK RECTANGLE IN B). (E) PPL IMAGE CORRESPONDS TO A COARSE-GRAINED ASSOCIATION OF PYROCHLORE, CALCITE AND ZONED PHLOGOPITE-TETRAFERRIPHLOGOPITE CRYSTALS. (F) XPL IMAGE SHOWS THE FINE-GRAINED ORIENTATION OF PHLOGOPITE, ORTHOCLASE AND CALCITE IN THE FENITE. ABBREVIATIONS: AP, APATITE; CAL, CALCITE; CC DIKE, CALCITE CARBONATITE DIKE; MAG, MAGNETITE; OR, ORTHOCLASE; PHL, PHLOGOPITE; PCL, PYROCHLORE; TFPHL, TETRAFERRIPHLOGOPITE58

FIG. 20. CHEMICAL DISTRIBUTION OF K, Mg, P AND Nb IN BARREN (LEFT COLUMN) VS. MINERALIZED (RIGHT COLUMN) CALCITE CARBONATITE DIKES. (A) SCAN OF POLISHED SAMPLE THAT CORRESPONDS TO A BARREN CALCITE CARBONATE DIKE WITH POOR FENITIZATION DEVELOPMENT. (B) SCAN OF POLISHED SAMPLE THAT CORRESPONDS TO A PYROCHLORE-MINERALIZED CALCITE CARBONATITE DIKE WITH INTENSE FENITIZATION. (C), (E) AND (G) SHOW M-EDXRF CHEMICAL MAPS OF K, Mg, AND P-Nb OF THE BARREN CARBONATITE DIKE IN (A), WHILE (D), (F) AND (H) SHOW M-EDXRF MAPS FOR THE SAME ELEMENTS IN THE MINERALIZED CARBONATITE DIKE IN (B). ABBREVIATIONS: AP, APATITE; BA, BARITE; CAL, CALCITE; OR, ORTHOCLASE; PHL, PHLOGOPITE; PCL, PYROCHLORE; TFPHL, TETRAFERRIPHLOGOPITE59

FIG. 21. EMPA DATA FOR PHLOGOPITE, TETRAFERRIPHLOGOPITE AND ANNITE IN THE CALCITE CARBONATITE DIKES, AND IN THE PROXIMAL AND DISTAL FENITES FROM THE BOA VISTA Nb MINE. (A) COMPOSITION OF THE MICAS IN TERMS OF AL, Mg AND TOTAL Fe (A.P.F.U.). THE DASHED LINE SEPARATES THE Mg AND Fe BIOTITE END MEMBERS. (B) AND (C) DIAGRAMS CORRESPOND TO THE VARIATION OF Si vs. Al AND Si vs Fe³⁺ IN A.P.F.U. (D), (E) AND (F) CORRESPOND TO THE DISTRIBUTION OF Mg, Mn, Ti, K AND THE MAGNESIUM-NUMBER (Mg/Mg+Fe²⁺).....60

FIG. 22. FIGURES (A) AND (B) CORRESPOND TO SCANNED DRILL CORES OF BARREN (SAMPLE RM024-253.5) AND MINERALIZED (SAMPLE RM024-329) CALCITE CARBONATITE DIKES, RESPECTIVELY. THE YELLOW RECTANGLES SHOW THE AREAS FOR EBSD ANALYSIS IN C) AND D). FIGURES (C) AND (D) SHOW INVERSE POLE FIGURE MAPS, WHICH DEPICT THE CRYSTALLOGRAPHIC DIRECTIONS FOR ALL MINERAL PHASES USING X (PERPENDICULAR TO DIKE WALL) AND Y (PARALLEL TO DIKE WALL) DIRECTIONS AS A REFERENCE (Z DIRECTION IS PERPENDICULAR TO THE EBSD IMAGES).....61

FIG. 23. INVERSE POLE FIGURE FOR KEY MAGMATIC (A) AND METASOMATIC (B) MINERAL PHASES, ASSOCIATED TO A BARREN CALCITE CARBONATITE DIKE, PREVIOUSLY SHOWN IN FIGURE 7A.....62

FIG. 24. INVERSE POLE FIGURE FOR KEY MAGMATIC (A) AND METASOMATIC (B) MINERAL PHASES, ASSOCIATED TO A MINERALIZED CALCITE CARBONATITE DIKE, PREVIOUSLY SHOWN IN FIGURE 7B.....63

FIG. 25. (A) EBSD MAP OF A MINERALIZED CALCITE CARBONATITE DIKE (Y AXIS AS REFERENCE TO THE WALL DIKE), SHOWING THE DIFFERENT MINERAL PHASES WITH A FALSE COLOR COMPOSITION, HIGHLIGHTING A MAGMATIC PHLOGOPITE (PHL), WITH CRYSTALLIZATION OF CALCITE AND DOLOMITE BETWEEN ITS BASAL CLEAVAGE SPACES IN (001). (B) INVERSE POLE FIGURE MAP OF THE FIGURE IN (A) SHOWING CHANGES OF CRYSTALLOGRAPHIC DIRECTIONS BY FRACTURE ALONG THE CRYSTAL. PHLOGOPITE IS OBSERVED WITH A STRONG AND SPACED BASAL CLEAVAGE PLANE, WHERE CALCITE AND DOLOMITE ARE CRYSTALLIZED IN THE MIDDLE OF THE PHLOGOPITE SHEETS. THE MAGMATIC DIRECTION IS HIGHLIGHTED BY THE RED ARROW IN THE LOWER LEFT CORNER IN (A), WHICH ALMOST COINCIDES WITH THE DIRECTION OF INJECTION OF CARBONATES IN BETWEEN THE PHLOGOPITE SHEETS.64

FIG. 26. (A) SOUTH AMERICA MAP, SHOWING THE LOCATION OF THE APIP, BETWEEN THE SÃO FRANCISCO CRATON AND THE PARANÁ BASIN. (B) GEOLOGICAL MAP OF THE APIP SHOWING THE LOCATION OF THE SIX MAIN ALKALINE-CARBONATITE COMPLEXES, MODIFIED FROM THE 1:1 M BELO HORIZONTE (SE-23) AND GOIÂNIA (SE-22) CARTOGRAPHIC SHEETS OF THE BRAZILIAN GEOLOGICAL SURVEY. SFC, SÃO FRANCISCO CRATON. (C) GEOLOGICAL MAP OF THE CATALÃO II COMPLEX, SHOWING THE LOCATION OF THE NORTH AND SOUTH PLUGS AND THE NIOBIUM AND PHOSPHATE MINES (MODIFIED AFTER PALMIERI ET AL., 2022).82

FIG. 27. (A) BOA VISTA MINE PIT, SHOWING THE SEPARATION OF THE PYROCHLORE-ENRICHED REGOLITH AND THE UPPER HYPOGENE ZONE WHERE DIKE SWARMS OF CARBONATITE, PHOSCORITE, AILLIKITE AND CARBOTHERMAL VEINS ARE BRAIDED. (B) OUTCROP OF A TYPICAL DIKE SWARM OF THE BOA VISTA Nb MINE, LOCATED IN THE RED RECTANGLE OF FIGURE 2A, SHOWING CALCITE CARBONATITE AND TETRAFERRIPHLOGOPITE PHOSCORITE DYKES FENITIZING THE BASEMENT AND BEING INTRUDED BY A PAIR OF OLIVINE AILLIKITES.83

- FIG. 28.** PHOTOS OF REPRESENTATIVE DRILL CORE SAMPLES OF THE DIFFERENT LITHOTYPES FROM THE BOA VISTA MINE. (A) CALCITE CARBONATITE SAMPLE, SHOWING A MIAROLITIC CORE ENVELOPED BY SKELETAL CARBONATES, IN TURN IN CONTACT WITH A MEDIUM TO FINE GRAINED PYROCHLORE-BEARING PHOSCORITE. (B) MEDIUM-GRAINED APATITE-RICH (AP) TETRAFERRIPHLOGOPITE PHOSCORITE WITH MAGNETITE-RICH TRANSITIONS, AND A CARAMEL-COLORED PYROCHLORE CUMULATE. (C) COARSE-GRAINED MAGNETITE-RICH TETRAFERRIPHLOGOPITE PHOSCORITE, WITH LARGE MAGNETITE (MT) AND TETRAFERRIPHLOGOPITE (TFPHL) CRYSTALS, AND COARSE-GRAINED CRYSTALS OF LIGHT BROWN PYROCHLORE (PCL). (D) CARBOHERMAL VEIN WITH CALCITE (CAL), DOLOMITE (DOL), SIDERITE (SID), PYRITE (PY) AND VARIEGATED FINE-GRAINED CARBONATES.....84
- FIG. 29.** BOREHOLE SAMPLES OF THE BOA VISTA Nb MINE. (A) LAYERED CALCITE CARBONATITE WITH CALCITE (CAL), MAGNETITE (MT) AND PYROCHLORE (PCL). (B) CALCITE CARBONATITE WITH DOG TOOTH TEXTURE CARBONATES, INTERCUMULUS APATITE (AP) AND SECONDARY MAGNETITE VEINLETS. (C) MAGNETITE-RICH PHOSCORITE WITH IRREGULAR CALCITE POCKETS. (D) APATITE-RICH PHOSCORITES OF ISOTROPIC TEXTURE WITH A COARSE-GRAINED MAGNETITE-PHLOGOPITE POCKET. (E) SIDERITE-RICH (SID) CARBOHERMAL VEIN WITH VARIEGATED TEXTURE. (F) PHLOGOPITE-RICH (PHL) FENITIZED BASEMENT, BEING DIGESTED BY A CALCITE CARBONATITE.....85
- FIG. 30.** PARAGENETIC SEQUENCE OF MINERAL PHASES IN MAGMATIC AND CARBOHYDROTHERMAL LITHOTYPES, FROM THE BOA VISTA Nb MINE. THE ABUNDANCE OF MINERAL PHASES IS SHOWN ACCORDING TO FOUR ARBITRARY INTERVALS, DIVIDED INTO: (I) TRACE; (II) < 5%, (III) 5 – 20 %, AND (IV) > 20 %.....86
- FIG. 31.** PYROCHLORE (PCL) SPECIMENS IN CALCITE CARBONATITE (CC). (A) BSE IMAGE OF A PYROCHLORE CRYSTAL WITH OSCILLATORY ZONED CORE AND SKELETAL RIM. (B) BSE IMAGE OF DISSOLVED PYROCHLORE WITH IRREGULAR AREAS OF LIGHT AND DARK BSE BRIGHTNESS. (C) PYROCHLORE, APATITE (AP), PHLOGOPITE (PHL), AND CALCITE (CAL) VIEWED UNDER CL, SHOWING A LOW RESPONSE FOR PYROCHLORE UNDER CL.....87
- FIG. 32.** REPRESENTATIVE BSE (A, C-D) AND CL (B) IMAGES OF PYROCHLORE (PCL) IN TETRAFERRIPHLOGOPITE (TFPHL) PHOSCORITE DYKES. (A) PATCHY ZONED PYROCHLORE FROM A MAGNETITE-RICH PHOSCORITE (MP). (B) PYROCHLORE FROM AN APATITE-RICH PHOSCORITE (AP) WITH A MASKED YELLOWISH-BROWN COLOUR CL. GROUNDMASS IS FINE-GRAINED AND ZONED APATITE, WITH A LIGHT BLUE COLOUR ACTIVATED BY Ce³⁺. (C) PATCHY ZONED PYROCHLORE FROM AN APATITE-RICH PHOSCORITE, WITH A ZIRCONOLITE (ZIR) RIM. (D) DISSOLVED PYROCHLORE FROM AN APATITE-RICH PHOSCORITE WITH A SKELETAL RIM.....88
- FIG. 33.** REPRESENTATIVE IMAGES OF PYROCHLORE (PCL) IN A CARBOHERMAL VEIN (CV). (A) AND (B) ARE PPL AND CL IMAGES PYROCHLORE IN A GROUNDMASS OF QAQARSSUKITE-(Ce), SIDERITE AND CALCITE. (C) BSE IMAGE OF EUHEDRAL ZONATION-FREE PYROCHLORE AND BARITE VEINLETS.....89
- FIG. 34.** CLASSIFICATION OF THE PYROCHLORE SUPERGROUP ACCORDING TO ATENCIO ET AL., (2010), INCLUDING SAMPLES FROM THE BOA VISTA AND MORRO DO PADRE MINES OF THE CATALÃO II COMPLEX, AND FROM MINE II/AREA LESTE MINES OF THE CATALÃO I COMPLEX. (A) COMPOSITION AT B-SITE, WHERE MOST SAMPLES PLOT AS PYROCHLORE, WITH TWO BETAFITE OUTSIDERS FROM THE CATALÃO I COMPLEX. (B) COMPOSITION AT A-SITE, WHERE MOST BOA VISTA SAMPLES PLOT AS CALCIOPYROCHLORE, WITH TWO KENOPYROCHLORE OUTLIERS.....90
- FIG. 35.** WDS MAPS SHOWING THE DISTRIBUTION OF Nb, Na AND Ti IN THREE CALCIOPYROCHLORE CRYSTALS WITH OSCILLATORY AND PATCHY ZONATION AND DISSOLVED-SKELETAL TEXTURES. THE BAR SCALE IS IN COUNTS.91
- FIG. 36.** CHONDRITE-NORMALIZED REE DISTRIBUTION OF PYROCHLORE CRYSTALS FROM THE BOA VISTA Nb MINE. THE PYROCHLORE PATTERNS ARE ROUGHLY PARALLEL TO THE RESULTS FOR CARBONATITE AND PHOSCORITE ROCKS FROM THE MORRO DO PADRE Nb MINE (PALMIERI ET AL., 2022), SHOWN IN THE GRAY SHADED FIELD. ..92
- FIG. 37.** COMPOSITION OF B-SITE CATIONS (A) TO (C), AND A-SITE CATIONS (D) TO (E) USING MAJOR, MINOR AND TRACE ELEMENTS IN CALCIOPYROCHLORE CRYSTALS SEPARATED BY ROCK TYPE AND TEXTURE, FOR CALCITE CARBONATITE (CC), CARBOHERMAL VEIN (CV), APATITE-RICH PHOSCORITE (AP), AND MAGNETITE-RICH PHOSCORITE (MP).93
- FIG. 38.** INTENSITY (COUNTS PER SECOND - CPS) VERSUS TIME PLOTS OF LINE SCAN ANALYSES OF A ZONED PYROCHLORE IN CALCITE CARBONATITE. (A) DISTRIBUTION OF SOME RARE EARTH ELEMENTS (REE) WITH INTENSITIES ABOVE 103 CPS, INCLUDING La, Ce, Pr, Nd, Sm, Eu, Gd, Tb, Dy and Ho, WHERE THE REEs FOLLOW THE ZONED PATTERN OF THE MEASURED CRYSTAL, SLIGHTLY ENRICHED TOWARDS THE EDGES. (B) DISTRIBUTION OF SOME HFSE ELEMENTS, INCLUDING V, Hf, Ta, Zr, Th and U, WHERE A DISPERSED BEHAVIOUR IS OBSERVED, WITHOUT FOLLOWING PYROCHLORE ZONING.94

FIG. 39. (A) CL IMAGE OF INTERCUMULUS CALCITE CRYSTAL WITH A Fe^{3+} QUENCHING IN DARK ORANGE CL COLOUR TO THE RIM, AND A YELLOW CL COLOUR ACTIVATED BY Mn^{2+} IN THE CORE. (B) INTERCUMULUS CALCITE CRYSTALS BORDERING MAGNETITE (MT) AND APATITE (AP) GRAINS.....	95
FIG. 40. EMPLACEMENT MODEL FOR CARBONATITE AND PHOSCORITE DYKES AND CARBOTHERMAL VEINS AND ITS PARAGENETIC SEQUENCE IN THE HYPOGENE DIKE SWARM ZONE OF THE BOA VISTA Nb MINE, CATALÃO II SOUTH. PYROCHLORES FROM PANELS (A), (B), (C) AND (D) CORRESPOND TO AN INTERPRETATION FOR BSE AND CL IMAGES FROM FIGURES 6 TO 8.....	96
FIG. 41. MODAL MINERALOGY OF “CLASSIC” NELSONITES AND OF ORE BODIES FROM LAYERED MAFIC INTRUSIONS, PLOTTED IN THE MAGNETITE-ILMENITE-APATITE DIAGRAM (VELÁSQUEZ RUIZ ET AL., 2019; TEGNER ET AL., 2006; DARLING AND FLORENCE, 1995 AND REFERENCES THEREIN).	106
FIG. 42. PHOSCORITE CLASSIFICATION DIAGRAM INITIALLY PROPOSED BY YEGOROV (1993), WHERE THE TERM NELSONITE IS INCLUDED, DESPITE THE FACT THE DIAGRAM DOES NOT CONTAIN AN OXIDE OF Fe-Ti ENDMEMBER. THE VALUES REFER TO RECALCULATED AMOUNTS OF MODAL MINERAL ABUNDANCE.....	107

CAPÍTULO 1: INTRODUCCIÓN

1.1. PRESENTACIÓN Y MOTIVACIÓN

El niobio (Nb) es un metal de transición litófilo con una concentración promedio de 11 ppm (g/t) en la corteza terrestre (Akinfiev et al., 2020). En los últimos años, el Nb ha obtenido una importancia significativa como materia prima crítica debido a su creciente demanda y alto riesgo de suministro (McCaffrey et al., 2023; Williams-Jones and Vasyukova, 2023). La producción mundial de Nb en 2022 se estimó en ~90,000 toneladas métricas (CBMM, 2023), de las cuales alrededor de un 75% se relaciona a la producción de ferroniobio, el cual se utiliza para mejorar las características del acero a partir de metales base como níquel, cobalto o hierro (Williams-Jones y Vasyukova, 2023). Las aleaciones de Nb con dichos metales base pueden mejorar las propiedades del acero tales como resistencia, tenacidad, corrosión o formabilidad. Por otra parte, el 25% restante de la producción de Nb se concentra en aplicaciones especiales, incluido el uso en imanes superconductores, en aleaciones especializadas con titanio (NbTi) o estaño (Nb₃Sn), y en aplicaciones en tecnología de resonancia nuclear magnética y de fusión termonuclear (López y Cramer, 2012; Uglietti et al., 2018; Oliveira et al., 2023).

Debido a su valencia de 5+ y un radio iónico de 0,64 Å en la mayoría de las condiciones redox (Shannon, 1976), el Nb se considera un elemento incompatible en términos de su comportamiento geoquímico, perteneciente al grupo de los denominados elementos de alta intensidad de campo o HFSE (High Field Strength Elements), por sus siglas en inglés. Debido a los bajos coeficientes de partición del Nb en los principales silicatos formadores de roca tales como el olivino, piroxeno, anfíbol o granate, que son del orden de 10⁻¹ a 10⁻⁴ con respecto al fundido silicatado (Green, 1994), el Nb ocurre naturalmente formando óxidos complejos. Por ejemplo, las ocurrencias naturales más importantes de óxido de Nb son: (i) minerales del grupo columbita-tantalita, asociados a pegmatitas graníticas (Tindle and Breaks, 2000; Che et al., 2015; Zhou et al., 2021), y (ii) minerales del grupo del pirocloro, que son comunes en carbonatitas y foscoritas, asociados a complejos alcalino-carbonatíticos (Chakhmouradian y Wall, 2012; Chakhmouradian y Zaitsev, 2012; Broom-Fendley et al., 2021; Beard et al., 2023). Dentro del grupo de minerales de pirocloro, se han identificado siete especies principales según el catión dominante: microlita (Ta⁵⁺), romeíta (Sb⁵⁺), elsmoreita (W⁶⁺), betafita (Ti⁴⁺), ralstonita (Al³⁺), coulselita (Mg²⁺) y pirocloro (Nb⁵⁺) (Atencio et al., 2010, Atencio, 2021).

El pirocloro (Na,Ca)₂Nb₂O₆(OH,F), es la variedad más importante del grupo de minerales de pirocloro y constituye la principal fase mineral portadora del Nb en los complejos alcalino-carbonatíticos de la Provincia Ígnea del Alto Paranaíba (APIP, de sus siglas en inglés), en el centro de Brasil (Cordeiro et al., 2011). En la APIP, el Complejo Araxá (mina CBMM, 26,5 Mt @ 2,5% Nb₂O₅; Cordeiro et al., 2011) y el Complejo Catalão II (mina Boa Vista, 26 Mt @ 0,95% Nb₂O₅) son responsables del ~90% de la producción global de Nb (Palmieri et al., 2022). El pirocloro en la APIP se extrae principalmente del regolito formado por la meteorización de rocas alcalinas y carbonatitas

de dichos complejos (Cordeiro et al., 2011; Mitchel, 2015). Fuera de Brasil, los depósitos más importantes de Nb se encuentran en la mina Niobec en el complejo carbonatítico de Saint Honoré, Canadá (2,6 Mt @0,42 % Nb₂O₅; Vallieres et al., 2013), que aporta aproximadamente el 7 % de la producción mundial de Nb (Vallieres et al., 2013; Williams-Jones and Vasyukova, 2023), mientras que otros depósitos menores como Lovozero, Rusia representan ~1% (Mitchell, 2015; Mitchell et al., 2020).

Estudios a nivel global relacionados con el origen de las mineralizaciones de Nb en distintos ambientes tectónicos, y sus minerales huéspedes (principalmente pirocloro y columbita), han mostrado que los depósitos de Nb se forman usualmente a partir de magmas primarios melilíticos, nefelínicos y alcalinos, configurándose como depósitos diseminados de gran tonelaje y baja ley, típicamente <1% en peso de Nb₂O₅ (Taylor et al., 1967; Wall y Zaitzev, 2004; Mitchell, 2015; Akinfiev et al., 2020). Más allá de los depósitos asociados a intrusivos y pegmatitas alcalinas, el origen de las mineralizaciones de Nb relacionadas a carbonatitas se mantienen escasamente estudiados y poco se conoce acerca de los procesos mineralizadores.

En consecuencia y con el propósito de aportar al conocimiento acerca de la metalogénesis del Nb en complejos carbonatíticos, la presente tesis de doctorado se enfoca en el estudio de los procesos mineralizantes en el depósito de Nb de Boa Vista, en el Complejo Catalão II de la APIP. Asimismo, el proyecto de doctorado aborda la petrogénesis y nomenclatura de las rocas alcalino-carbonatíticas, la caracterización del metasomatismo carbotermal del basamento, y la firma microtextural y geoquímica del pirocloro, la fase principal portadora de Nb.

1.2. CONTEXTO GEOLÓGICO Y EVOLUCIÓN GEODINÁMICA

La Provincia Ígnea de Alto Paranaíba (APIP) del Cretácico Tardío, se encuentra insertada entre los estados de Minas Gerais y Goiás, en Brasil central, abarcando un área total de ~25.000 km² (Gibson et al., 1995). La APIP está compuesta por un grupo de rocas ígneas alcalinas intrusivas y extrusivas potásicas a ultrapotásicas y dicho magmatismo intruye rocas metavolcanosedimentarias en facies anfibolita del Cinturón Neoproterozoico de Brasilia, limitando al sureste por la Cuenca de Paraná y al noroeste por el Cratón São Francisco (Zalan et al., 1990; Barbosa y Sabaté, 2004; Silva et al., 2020; Fig. 1a). La parte oriental del APIP está compuesta por flujos de lavas ultrapotásicas (e.g., lavas de kamafugita), rocas piroclásticas y diatremas de la Formación Mata da Corda (Gibson et al., 1995; Byron, 1999), mientras que la parte occidental consiste en afloramientos de menor escala de diatremas de kamafugita, numerosos cuerpos subvolcánicos de kimberlita (Guarino et al., 2013), y seis complejos alcalino-carbonatíticos, a saber de norte a sur: Catalão II, Catalão I, Serra Negra, Salitre, Araxá y Tapira (Fig. 1b). Las lavas kamafugíticas se originaron entre 90 a 76 Ma, mientras que las kimberlitas se formaron entre 91–80 Ma según edades U-Pb en perovskita (Sgarbi et al., 2004; Guarino et al., 2013; Felgate, 2014). Por otra parte, la formación de los complejos alcalino-carbonatíticos involucró múltiples episodios de magmatismo, datados entre 96 y 78 Ma, con edades ⁴⁰Ar/³⁹Ar en flogopita y U-Pb en perovskita (Guarino et al., 2013; Guarino et al., 2017; Conceição et al., 2020).

El rasgo estructural más importante de la APIP es el lineamiento de Azimut 125°, que corresponde a un conjunto de lineamientos de rumbo NW-SE de ~1,800 km de largo, observados mediante datos aeromagnéticos regionales, pero que también se pueden reconocer como afloramientos de milonitas y diques máficos y ultramáficos (Bardet, 1977; Moraes Rocha et al., 2014). El lineamiento Azimut 125° comprende un complejo sistema de fallas, milonitas y diques con una alta susceptibilidad magnética, que contrasta con el basamento Brasiliano. Estos lineamientos se desarrollaron en tres etapas principales: (i) L1 (950–520 Ma) asociado con el evento Brasiliano, caracterizado por una tectónica compresiva, responsable de formar el Cinturón de Brasilia (Moraes Rocha et al., 2014); (ii) L2 (~180 Ma) correspondiente a un evento extensivo, asociado a la fragmentación de Gondwana; y (iii) L3 (90–80 Ma) asociada al magmatismo alcalino intracontinental (Gibson et al., 1995). Si bien las edades L3 son compatibles con la APIP, su alineamiento discrepa con la tendencia general NNE de la provincia. El emplazamiento del APIP, por lo tanto, probablemente siguió las debilidades regionales NNE en el Cinturón de Brasilia en lugar del lineamiento Azimut 125°.

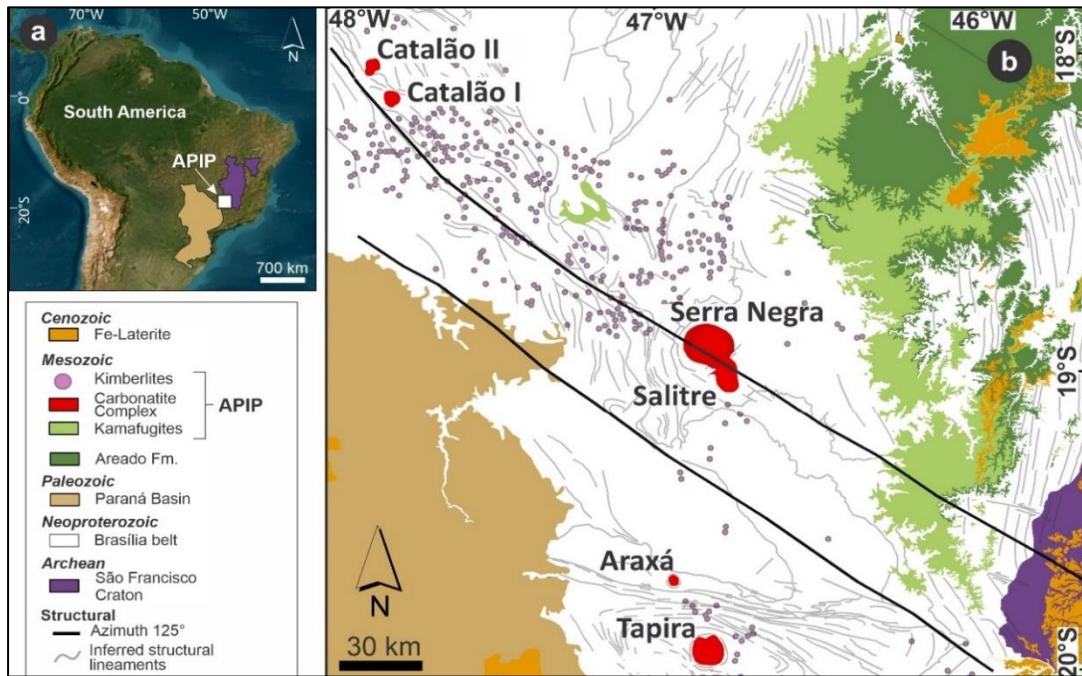


Fig. 1. (a) Mapa de América del Sur con la ubicación de la APIP, el Cratón de São Francisco y la Cuenca de Paraná. (b) Mapa geológico de la APIP, con la ubicación de los seis complejos principales alcalino-carbonatáticos, modificado a partir de las hojas cartográficas 1:1M Belo Horizonte (SE-23) y Goiânia (SE-22), del Servicio Geológico de Brasil.

El inicio del magmatismo en Brasil central en el Cretácico tardío, responsable de generar diversas provincias alcalinas, incluyendo la APIP y la Provincia Alcalina de Goiás, inicialmente se atribuyó al impacto de la pluma mantélica Trindade en la base de la litosfera subcontinental (Gibson et al., 1995; Gibson et al., 1997; Thompson et al., 1998). Los autores citados proponen que la trayectoria de la pluma tuvo una orientación sureste con respecto a la APIP, bordeando el límite

sur del Cratón de São Francisco y el trayecto continuó hacia el este de Brasil, en lo que se conoce como Provincia Alcalina de la Serra do Mar hasta alcanzar su reciente posición debajo de las Islas Trindade-Martin Vaz en el Océano Atlántico medio. Alternativamente, estudios más recientes han abogado por un modelo de rifting relacionado con la apertura del Atlántico sur (Ribeiro et al. 2018). Esta hipótesis se propuso en parte, porque trabajos paleomagnéticos demostraron que la pluma Trindade estaba al menos a 1.000 km fuera de las provincias alcalinas anteriormente mencionadas en el momento de las erupciones (Ernesto et al. 2002; Ribeiro et al. 2018). Una compilación de datos numéricos, geofísicos y geológicos (Fig. 2) apuntan que las tasas de extensión durante la fragmentación de Gondwana occidental, y la presencia de estructuras corticales débiles previas al magmatismo alcalino, contribuyeron a la generación y emplazamiento de múltiples complejos alcalinos en Brasil central y oriental (Ferreira et al., 2022). Dichos autores, apuntan que la composición local del manto, la profundidad y las proporciones de extensión de la corteza controlaron la composición del magma.

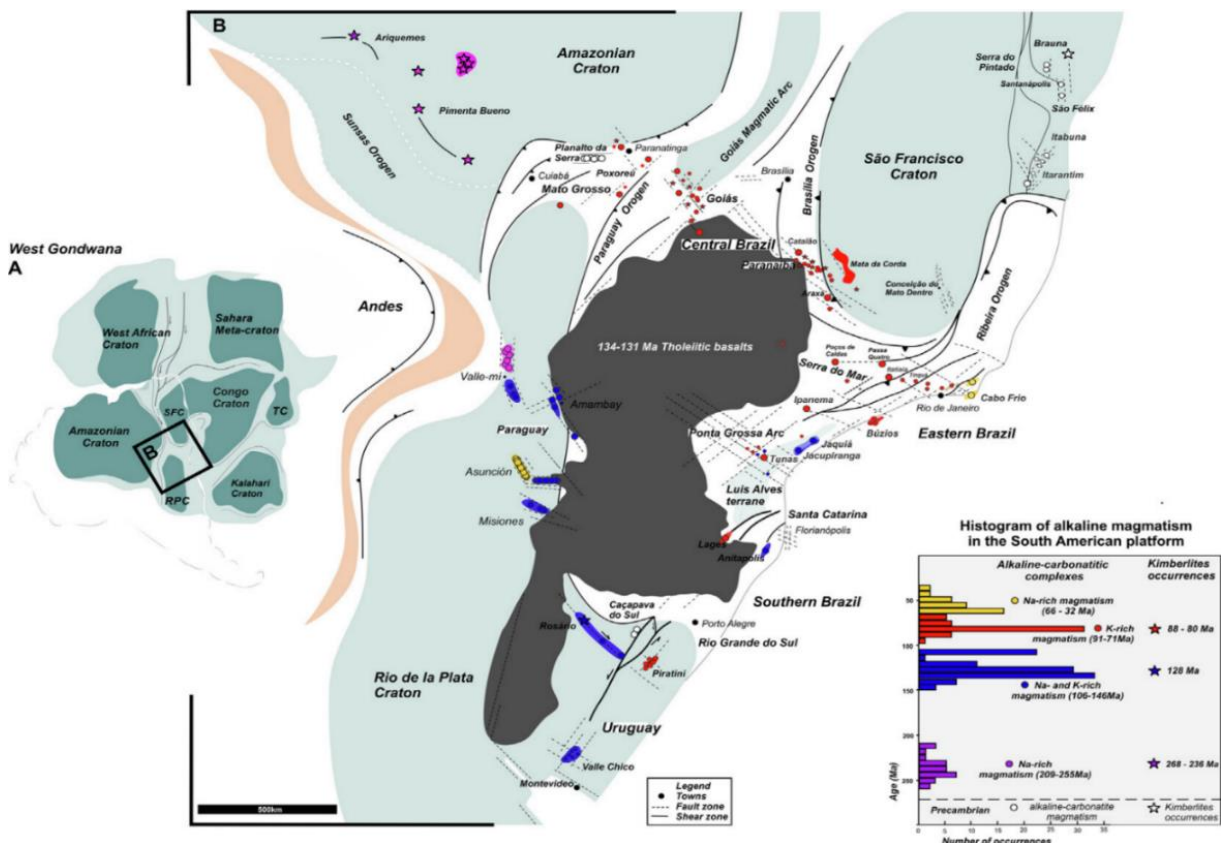


Fig. 2. A) Mapa de ubicación de la porción sur de América del Sur en Gondwana Occidental. Leyenda: RPC - Cratón Río de La Plata, SFC - Cratón São Francisco, TC - Cratón Tanzania. B) Magmatismo alcalino y toleítico del Mesozoico al Paleógeno en la plataforma Sudamericana (tomada de Ferreira et al., 2022).

1.3. COMPLEJOS ALCALINO-CARBONATÍTICOS DE LA APIP

Los complejos alcalino-carbonatíticos de la APIP forman cuerpos intrusivos anulares, ovóides y generalmente cumuláticos (Palmieri et al., 2022; Fig. 3). Dichos complejos se desarrollan en múltiples etapas de fraccionamiento magmático e involucran principalmente cuatro series magmáticas, incluyendo carbonatitas, foscoritas, bebeduritas y rocas alcalinas (Barbosa et al., 2012; Fig. 3). Las capas cumuláticas incluyen rocas de calcita y dolomita (carbonatitas), foscoritas, bebeduritas, lamprófidos ultramáficos (aillikitas) y clinopiroxenitas. En este trabajo, nos referiremos a las foscoritas como rocas ígneas intrusivas ricas en apatito, magnetita y uno de los silicatos, forsterita, diópsido o flogopita. Adicionalmente, definimos a las bebeduritas como rocas ígneas intrusivas, compuestas de cantidades variables, pero aproximadamente similares de olivino, diópsido, apatito, magnetita, flogopita y una fase Ca-Ti, como perovskita, melanita o titanita (Barbosa et al., 2012). La nomenclatura y clasificación de las rocas ígneas ricas en apatito y magnetita serán abordadas en detalle en el Capítulo 5 de la presente tesis.

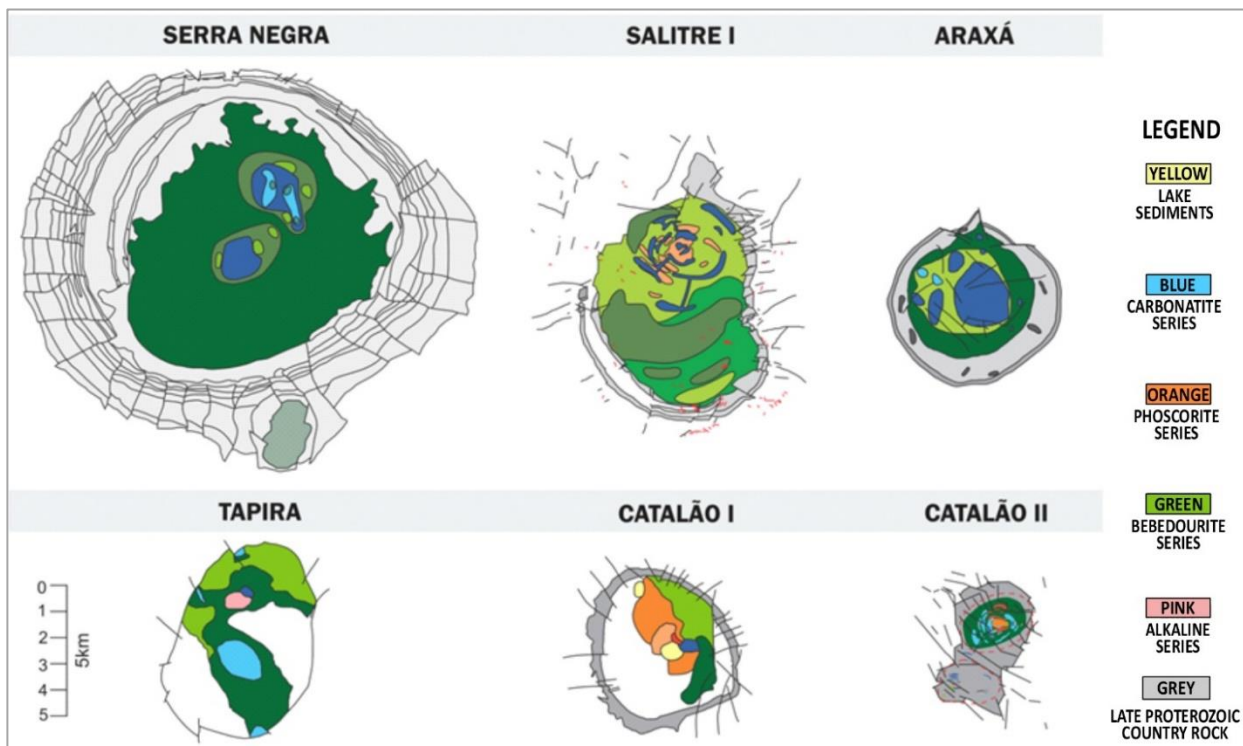


Fig. 3. Geometría comparativa y tamaños de complejos alcalino-carbonatíticos de la APIP, incluyendo los complejos: Serra Negra, Salitre, Araxá, Tapira y Catalao I y II (tomado de Novaes, 2018).

En los complejos alcalino-carbonatíticos de la APIP, las capas cumuláticas alimentan sistemas de enjambres de diques menos profundos, superpuestos a los cumulados intrusivos más profundos (Palmieri et al., 2022). Estos comprenden diques de carbonatita, foscorita, aillikita y vetas carbotermales. Las vetas carbotermales se forman a partir de fluidos ricos en CO₂ de estadios

tardíos y baja temperatura, llamados “fluidos carbotermales” (el equivalente carbonatado al término “hidrotermal”, o rico en agua; Mitchell y Gittins, 2022). Tanto las capas cumuláticas profundas como los enjambres de diques poco profundos son cortados por diques de alkilitas de olivino, asociadas a una fuente más profunda, que se interpretan como el magma parental de los complejos alcalino-carbonatíticos por Brod et al. (2000).

Los diques y cumulados de los complejos alcalino-carbonatíticos de Araxá, Catalão I y II se caracterizan por carbonatitas y foscoritas ricas en pirocloro ($\text{Na, Ca}_2\text{Nb}_2\text{O}_6(\text{OH, F})$). La extracción de los suelos residuales ricos en pirocloro de Araxá, Catalão I y II, resultantes de la intensa meteorización química que han afectado los depósitos primarios, se ha realizado por más de 50 años. Actualmente, la mina CBMM del Complejo Araxá y la mina Boa Vista del Complejo Catalão II, son las dos únicas minas de Nb activas en la APIP y representan alrededor del 80% y 10% de la producción global de Nb, respectivamente, que anualmente varía entre 80,000 a 90,000 toneladas anuales (<https://cbmm.com>).

En particular, el Complejo Catalão II ofrece una oportunidad única para estudiar los procesos carbonatíticos y carbotermales que dieron origen a la mineralización de Nb, debido a que es la única localidad dentro de la APIP donde las operaciones mineras han expuesto parte de la geometría del complejo en profundidad (Palmieri et al., 2022), permitiendo ver relaciones texturales, estructurales y el contacto entre rocas intrusivas y basamento. El complejo Catalão II posee un importante número de labores mineras de extracción Nb, distribuidos en dos *plugs*. El *plug* norte del complejo Catalão II, está compuesto por la mina de Nb Farm y la mina de fósforo Coqueiros, mientras que el *plug* Sur está compuesto por tres minas de Nb, Marcos, Boa Vista y Morro do Padre, siendo Boa Vista la única mina de Nb activa en la actualidad (Palmieri et al., 2022).

1.4. OBJETIVOS DE LA TESIS

1.4.1. Alcance y objetivo general

La presente tesis de doctorado tiene como objetivo amplio proponer un modelo genético que explique la formación de los depósitos de Nb alojados en complejos alcalino-carbonatíticos de la Provincia Ígnea del Alto Paranaíba (APIP), en Brasil central. El estudio propuesto se desarrolla en el Complejo Catalão II sur, parte de la APIP, y específicamente en la mina de Nb de Boa Vista. El enfoque se centra en la petrogénesis de las rocas alcalino-carbonatíticas a escala regional, en la caracterización del metasomatismo carbotermal del basamento o fenitización a escala de depósito, y las características microtexturales y geoquímicas del pirocloro, como fase principal portadora de Nb en el depósito.

1.4.2. Objetivos específicos

1. Examinar el vínculo genético entre el magmatismo de lavas ultrapotásicas (kamafugitas) en la APIP oriental y las aillikitas de los complejos alcalinos-carbonatíticos del APIP occidental, con el propósito de proponer una hipótesis sobre la génesis del magmatismo alcalino desde el manto litosférico subcontinental de la APIP. En esta misma línea, identificar la naturaleza o tipo de magma primario para los complejos alcalino-carbonatíticos, por medio del estudio de la geoquímica de las aillikitas.
2. Identificar la textura, química y microestructura de las fenitas ricas en potasio del basamento metasomatizado, las cuales están en contacto con diques de carbonatitas en la mina Boa Vista, con el propósito de comprender el rol de los fluidos carbotermales en la mineralización de Nb.
3. Realizar una caracterización mineralógica, microtextural y geoquímica detallada del pirocloro de la mina de Nb de Boa Vista del Complejo Catalão II, y proporcionar información sobre el rol de los procesos magmáticos y carbotermales en la mineralización de Nb.
4. Realizar una revisión crítica acerca de la clasificación histórica de las rocas ígneas ricas en apatito-magnetita y su mineralogía, y proponer una clasificación nueva y concisa basada en la mineralogía modal, para unificar la terminología entre el glosario de términos de la IUGS y la literatura clásica, con énfasis en rocas del APIP y otras provincias a nivel mundial.

1.5. HIPÓTESIS DE TRABAJO

A modo general, en esta tesis se testeó la hipótesis que la formación de carbonatitas y rocas asociadas enriquecidas en Nb de la APIP serían el resultado de una cadena de procesos dominanteamente magnáticos, con influencia magnático-carbotermal secundaria.

Se plantea como hipótesis de trabajo, en primer lugar, que la génesis del magma primario responsable del magmatismo alcalino-carbonatítico, estaría relacionada a procesos de fusión parcial del manto litosférico subcontinental en un contexto anorogénico, probablemente con un metasomatismo rico en CO₂. Además, se plantea que el fraccionamiento del magma primario silico-carbonatado generaría un líquido residual alcalino rico en CO₂, formándose reservorios que estarían emplazados en la corteza inferior. Estos magmas pueden experimentar diversas etapas de diferenciación desde la corteza inferior hasta la corteza superior, facilitando el enriquecimiento de los magmas residuales en elementos incompatibles de tipo HFSE, en particular un enriquecimiento sustancial en Nb. El transporte de estos fundidos desde niveles tectono-estratigráficos inferiores, estaría favorecido por un alto contenido de volátiles, en específico, fluidos supercríticos ricos en CO₂ derivados del manto.

Posteriormente al fraccionamiento del magma primario, existiría un proceso de desmezcla o inmiscibilidad, generando dos magmas residuales: (i) un magma parental carbonatítico, enriquecido en CO₂ y elementos incompatibles (entre ellos el Nb), y (ii) un segundo magma parental alcalino, enriquecido en elementos compatibles. El magma parental carbonatítico formaría rocas de las series de carbonatita (e.g., calcita carbonatita y dolomita carbonatita) y simultáneamente existiría formación de fases tales como el pirocloro, magnetita y apatito, que debido a su alto peso específico se

segregarían, formando cúmulos de rocas de foscorita. A su vez, el magma parental alcalino, formaría cúmulos de piroxenitas y bebeduritas, que alimentarían diques de aillikitás. Finalmente, se tiene por objetivo testear que el magma parental carbonatítico exsolvería volátiles al emplazarse en niveles más someros, generando un fluido residual rico en CO₂ que formaría vetas carbotermales así como minerales de alteración metasomática en el basamento.

1.6. MANUSCRITOS Y PUBLICACIONES

Publicaciones y manuscritos resultantes de la tesis doctoral

1. **Velásquez Ruiz, F.**, Cordeiro, P., Reich, M., Motta, J.G., Ribeiro, C., Angerer, T., Bernardes, R. (2022) The genetic link between kamafugite magmatism and alkaline carbonatite complexes in the Late Cretaceous Alto Paranaíba Igneous Province, Central Brazil. *International Geology Review*, v.65, 2148-2170 (CAPÍTULO 2)
2. **Velásquez Ruiz, F.**, Cordeiro, P., Reich, M., Lagoeiro, L., Angerer, T. Microanalytical investigation of K-rich fenites from the Catalão II alkaline-carbonatite complex in Central Brazil: implications for ore-forming processes within the world's largest niobium province. *Journal of Geochemical Exploration* (en revisión) (CAPÍTULO 3).
3. **Velásquez Ruiz, F.**, Reich, M., Broom-Fendley, S., Beard, C.D., Barra, F., Romero, R., Cordeiro, P. (2024) Origin of carbonatite-related niobium deposits: Insights from pyrochlore geochemistry. *Geochimica et Cosmochimica Acta*, v.366, 1-16 (CAPÍTULO 4).
4. **Velásquez Ruiz, F.**, Reich, M., Broom-Fendley, S., Magalhães, N. Revision of the nomenclature of apatite-magnetite-rich igneous rocks and its inclusion within the IUGS classification (a ser sometida) (CAPÍTULO 5).

Resúmenes de congreso y presentaciones en seminarios

1. **Velásquez Ruiz, F.** (2020). Minerales estratégicos: una introducción a la geología de metales raros y tierras raras. VI Seminario de Geología Económica y del Petróleo. Universidad EAFIT, Medellín. (Presentación oral virtual)
2. **Velásquez Ruiz, F.**, Reich, M., Cordeiro, P. (2021). *Magmatic vs hydrothermal processes in the generation of carbonatite-related niobium ores within the Catalão II carbonatite complex, Central Brazil*. PDAC, March, 3-6, Toronto, Canada. (Presentación oral virtual)
3. **Velásquez Ruiz, F.** (2021). *Rochas Kamafugíticas e Alcalinas: Foco na Província Ígnea do Alto Paranaíba*. XV Semana da Geologia UFMG. Belo Horizonte. (Presentación oral virtual)
4. **Velásquez Ruiz, F.**, Reich, M., Broom-Fendley, S., Beard, C.D., Barra, F., Cordeiro, P., Romero, R. (2023). *In-situ trace element and textural analysis of pyrochlore and its use to decipher the origin of carbonatite-hosted niobium deposits*. XVI Congreso Geológico Chileno. Santiago de Chile. (Presentación oral presencial)

**CAPÍTULO 2: THE GENETIC LINK BETWEEN KAMAFUGITE MAGMATISM
AND ALKALINE–CARBONATITE COMPLEXES IN THE LATE CRETACEOUS
ALTO PARANAÍBA IGNEOUS PROVINCE, CENTRAL BRAZIL**

Felipe Velásquez Ruiz^{a,b*}, Pedro Cordeiro^c, Martin Reich^{a,b}, João Gabriel Motta^d, Carlos Cordeiro Ribeiro^e, Thomas Angerer^{f,g}, Renato Borges Bernardes^h

^a*Department of Geology, FCFM, University of Chile, Santiago, Plaza Ercilla 803, Chile*

^b*Millennium Nucleus for Metal Tracing Along Subduction, FCFM, University of Chile, Santiago, Chile*

^c*Mining Engineering Department, Pontifical Catholic University of Chile, Santiago, Chile*

^d*Camborne School of Mines, University of Exeter, Penryn, United Kingdom*

^e*Faculdade de Engenharia, Regional Catalão, Universidade Federal de Goiás, Brazil*

^f*Institute of Mineralogy and Petrography, University of Innsbruck, Austria*

^g*Institute of Earth Sciences, Department of Petrology and Geochemistry, University of Bonn, Germany*

^h*Instituto de Geociências, Universidade de Brasília, Campus Universitário Darcy Ribeiro, Brasília, DF, Brazil*

Published in:

International Geology Review

*Corresponding Author:

E-mail address: fevelasquezru@gmail.com (F.V. Ruiz).

ORCID: 0000-0003-1741-8588

2.1. ABSTRACT

The Late Cretaceous Mata da Corda Formation, located in the eastern part of the Alto Paranaíba Igneous Province (APIP), Central Brazil, is one of the few places on Earth where kamafugite melts reached the surface generating large volumes of lava, pyroclastic rocks and shallow intrusions over an area of 4,500 km². The western part of the APIP, however, is dominated by hundreds of diatreme-like kamafugites and shallow kimberlite intrusions and by the occurrence of multi-stage alkaline-carbonatite complexes. These complexes feature silica-undersaturated K-rich alkaline rocks, such as aillikite, that closely resemble the mineralogy and geochemistry of kamafugite, albeit lacking feldspathoids. The spatial and temporal distribution of kamafugite and aillikite within the APIP suggests a connection between them. In addition, on a regional scale, airborne magnetic data show three highly magnetic dipole-like structures to the south of the Mata da Corda Formation of an undisclosed nature which bear geophysical similar responses to the neighbouring alkaline-carbonatite complexes. Links between kamafugite and aillikite are evaluated by the following chemical and isotopic evidence: (1) kamafugite and aillikite compositions plot in the kamafugite field of Foley's ultrapotassic rock classification; (2) similar CI chondrite-normalized REE distribution, with aillikite enriched up to 2 times in REE compared to kamafugite; (3) both lithologies share almost the same rock-forming minerals; and (4) similar ¹⁴³Nd/¹⁴⁴Nd(i) and ⁸⁷Sr/⁸⁶Sr(i) ratios for all the APIP alkaline-carbonatite rocks, indicating a common source from an enriched lithospheric mantle. Therefore, silica-undersaturated rocks from alkaline-carbonatite complexes display an evolved ultrapotassic affinity indicative of a genetic link.

Keywords: kamafugites; aillikites; alkaline-carbonatite complexes; Mata da Corda Formation; Alto Paranaíba Igneous Province.

2.2. INTRODUCTION

Although extremely rare, ultrapotassic igneous rocks—defined as igneous rocks with K₂O >3 wt.%, MgO >3 wt.% and K₂O/Na₂O >2 (Foley et al. 1987)—are chemically diverse and can be further separated into three distinct end-members: lamproite, kamafugite, and Roman Province-types. Kamafugite has the highest CaO, TiO₂ and K₂O/Al₂O₃ values, and is also silica-undersaturated (Barton 1979; Foley et al. 1987). These features result in a unique mineralogy comprising olivine, diopside, perovskite, certain feldspathoids (kalsilite, melilite and leucite), and accessory minerals such as phlogopite, apatite, among others. Moreover, the presence of kalsilite is an exceptional petrogenetic feature as it occurs (almost) nowhere else, such that kalsilite-bearing rocks include four main rock names in a petrographic classification: kalsilite nephelinite as a special case of nephelinite (*sensu lato*; Oliveira et al. 2022), katungites (melilite dominant), mafurites (kalsilite dominant) and ugandites (leucite dominant; Le Maitre 2002; Tappe et al. 2003; Woolley et al. 1996). The acronym kamafugite is the result of these three rocks (**katungite**, **mafurite** and **ugandite**; Oliveira et al. 2022, and references therein). The archetypal kamafugites occur in the Mid-Miocene to Recent Toro-Ankole province, SW Uganda, in the East African Rift

(Rosenthal et al. 2009; Tappe et al. 2003). Kamafugites also extruded in the Pleistocene San Venanzo and Cupaello localities, Intra-Apennine Province in central Italy (Lustrino et al. 2020). Owing to its ultramafic composition, kamafugite can be used to investigate the composition of the mantle and has been used to clarify the effects of early-stage rifting of the continental crust (Foley et al. 2011), and processes at the supra-subduction mantle wedge (Lustrino et al. 2020). The oldest known kamafugite-carbonatite association is the Mata da Corda Formation in the Alto Paranaíba Igneous Province (APIP), central Brazil, where kamafugites were emplaced around ~90–76 Ma (Brod et al. 2000; Guarino et al. 2013; Melluso et al. 2008; Sgarbi et al. 2004). These rocks represent a unique opportunity to study the generation of ultrapotassic magmas and their potential link to carbonatite magmatism.

The eastern APIP is dominated by the Mata da Corda Formation while the western APIP predominantly consists of carbonatite complexes (Fig. 4). The carbonatite complexes comprise intrusive carbonatite, phoscorite, bebedourite (which is a rock composed of roughly similar amounts of olivine, diopside, apatite, magnetite, phlogopite, and a Ca-Ti phase, such as perovskite, melanite or titanite; Barbosa et al. 2012) and alkaline silicate rocks such as alkaline pyroxenite, and are intruded by several generations of feldspathoid-free olivine aillikite (Gibson et al. 1995; Guarino et al. 2013; Melluso et al. 2008; Thompson et al. 1998). Olivine aillikite is widely distributed throughout the APIP and is both spatially and temporally related to kamafugite (Conceição et al. 2020; Guarino et al. 2013). Olivine aillikite is an ultrabasic rock (<45 wt.% SiO₂), which is frequently ultrapotassic (>3 wt.% K₂O, >3 wt.% MgO and K₂O/Na₂O >2) and has similar mineralogy to the Mata da Corda kamafugite, albeit lacking feldspathoids. Gibson et al. (1995) and Thompson et al. (1998) proposed that the onset of alkaline magmatism in the APIP was a result of the impact of the Trindade mantle plume. However, paleomagnetic studies show that this plume was at least 1,000 km outside of the Paraná province at the time of the eruptions, making this hypothesis improbable (Ernesto et al. 2002; Ribeiro et al. 2018). Moreover, an attempt has been made to connect a common origin for the alkaline-carbonatite complexes and the Mata da Corda kamafugites by means of lithogeochemistry (Brod et al. 2000), again in the above-mentioned mantle plume framework, but showing a chemical connection between the eastern and western ultrapotassic rocks of the APIP.

In this study, we combine geological observations, geophysical imaging, geochemical and mineral chemistry data to unravel the regional setting of kamafugite magmatism in the eastern APIP and evaluate a connection to aillikite in the western APIP alkaline-carbonatite complexes. We report airborne magnetic geophysical data to image regional-scale 2D features of interest, and present a comprehensive set of whole-rock geochemical and isotopic data, and micro-XRF and mineral chemistry data of both the Mata da Corda kamafugite and aillikite from the APIP.

2.3. GEOLOGICAL BACKGROUND

2.3.1. The Alto Paranaíba Igneous Province (APIP)

The potassic to ultrapotassic intrusive and extrusive alkaline igneous rocks of the Alto

Paranaíba Igneous Province encompass a total area of ~25,000 km² (Gibson et al. 1995; Fig. 4). Magmatism took place during the development of the Paraná Basin to the SW (Zalan et al. 1990) but intruded greenschist to amphibolite facies metamorphic rocks of the Neoproterozoic Brasília Belt, at the western border of the São Francisco Craton (Barbosa & Sabaté, 2004; Silva et al. 2020).

An important feature of the APIP area is the Azimuth 125° lineament, which is a group of NW-SE trending, ~1,800 km long lineaments observed in regional aeromagnetic data, but only rarely found as outcrops of mafic and ultramafic rocks (Bardet 1977; Rocha et al. 2014). The Azimuth 125° lineament comprises a complex system of faults, mylonites and dikes with a high magnetic susceptibility that contrasts with the basement. These lineaments developed during three main stages: L1 (950–520 Ma), associated with the Brasiliano event (Rocha et al. 2014), L2 (~180 Ma) during Gondwana fragmentation and L3 (90–80 Ma) which is linked either to the passage of the Trindade mantle plume (Rocha et al. 2014) or to extension following the opening of the South Atlantic (Ferreira et al. 2022). Although L3 ages are compatible with the APIP, their alignment disagrees with the NNE general trend of the province. The emplacement of the APIP, therefore, more likely followed NNE regional weaknesses in the Brasília Belt rather than the Azimuth 125° lineament.

The six main alkaline-carbonatite intrusive complexes of the APIP are Catalão II, Catalão I, Serra Negra, Salitre, Araxá and Tapira, and these encompass the main global resource(s) of niobium and an important source of phosphate (Barbosa et al. 2012; Conceição et al. 2020; Cordeiro et al. 2010, 2011). Moreover, the province hosts numerous kimberlite intrusions (e.g., dikes, plugs, diatremes; Fig. 4; Guarino et al. 2017), some of which are diamond-bearing (Carvalho et al. 2022). The APIP magmatism lasted ~20 Myr, as indicated by U-Pb perovskite dating of ~91–80 Ma for kimberlites, ~90–76 Ma for kamafugites and ~90–78 Ma for olivine aillikites, while carbonatitic rocks show magmatic pulses dated between ~90–70 Ma (Conceição et al. 2020; Felgate, 2014; Guarino et al. 2013; Sgarbi et al. 2004).

2.3.2. Mata da Corda Formation kamafugites

The Mata da Corda Formation crops out in the eastern side of the APIP (Fig. 4) as a ~4,500 km² area of ultramafic, potassic to ultrapotassic lava flows and pyroclastic rocks (Brod et al. 2000). The formation comprises shallow intrusions (Byron, 1999), mainly associated with maar-type volcanic edifices and multiple sequences of extrusive flows and pyroclastics (Carlson et al. 1996) that stand out on higher ground with respect to the surrounding eroded basement rocks. The multiple volcanic centres of Mata da Corda are interpreted as being fed by one or more polyphase intrusive pipes, principally in the localities of Fazenda Grotão, Fazenda Bananal, Água Limpa, Ribeirão da Mata and Serra do Bueno (Byron 1999; Gibson et al. 1994, 1995). Within a typical central part of these volcanic edifices, the rocks of the lower crater facies are dominated by volcanic intrusions and xenolith-rich ultramafic breccia pipes overlain by kamafugite flows and minor lapilli tuffs.

The Mata da Corda extrusive rocks are divided between a basal volcanic unit which encompasses mafurite and ugandite lavas (Sgarbi and Gaspar 2002; Sgarbi et al. 2004), and an upper volcanoclastic unit comprising lapilli, breccia and tuff (Grossi Sad et al. 1971; Melo 2012). U-Pb perovskite ages indicate three main age groups for the lavas: 88–90, 80–81, and 75–76 Ma (Sgarbi et al. 2004). Both the basal volcanic and volcanoclastic units are commonly weathered (Fig. 5a). The Mata da Corda volcanic rocks overlie the Lower Cretaceous Areado Formation, which in turn overlies the Brasília Belt.

2.3.3. Potassic and ultrapotassic silica undersaturated rocks associated with the APIP alkaline-carbonatite complexes

The carbonatites, phoscorites and alkaline silicate rocks of the alkaline-carbonatite complexes make up three magmatic series which form annular intrusive, ovoid-shaped and generally cumulate complexes (Barbosa et al. 2012; Palmieri et al. 2022). Bebedourites are the most representative silica-undersaturated potassic to ultrapotassic intrusive rocks of the APIP alkaline-carbonatitic complexes. The term bebedourite refers to rocks composed of variable but roughly similar amounts of olivine, diopside, apatite, magnetite, phlogopite, and a Ca-Ti phase, such as perovskite, melanite or titanite (Barbosa et al. 2012). Mafic rock-forming minerals such as clinopyroxene and olivine frequently do not exceed 50% of the modal abundances, excluding their classification as pyroxenites or other IUGS ultramafic intrusive rock classification (Le Maitre 2002). Volumetrically, most of the APIP bebedourites are intrusive cumulate rocks which form the outer ring of the complexes. At Salitre (Barbosa et al. 2012) and Tapira (Brod et al. 2013) bebedourite is also associated with diopside aillikite dikes of equivalent mineralogical composition, indicating that bebedourites can also represent melts.

As well as cumulate complexes, shallower dike swarms systems are also present in the APIP, overlying the deeper intrusive cumulates (Palmieri et al. 2022). These comprise carbonatite, phoscorite and diopside aillikite (equivalent to bebedourite). Both the deep cumulates and the shallow dike swarms are cut by a series of olivine aillikites from a deeper source (Brod et al. 2000). Although the olivine aillikites and diopside aillikites formed from different parental magmas, both constitute the silica undersaturated, potassic to ultrapotassic feldspathoid-free volcanic rocks of the APIP alkaline-carbonatite complexes, which we address in this work together with the rocks of the Mata da Corda Formation.

In previous studies, before the publication of the IUGS classification for ultramafic lamprophyres, the mineralogy of the APIP aillikites was challenging to reconcile with established nomenclature, leading to their classification as phlogopite-picrites (Gibson et al. 1995; Brod et al. 2000). Later works by Brod et al. (2000) and Guarino et al. (2013), for example, preserved this established nomenclature despite the silica undersaturation (29.3–36.4 wt.%) and potassium-enrichment (3.1–6.6 wt.%) of the rocks, thus failing to conform with the IUGS picrite nomenclature

(Le Maitre 2002). In this work we refer to these dikes as aillikites, owing to the abundance of carbonate in the matrix and correspondingly high LOI values (6.9–22 wt.%; Brod 2000). The term aillikite is the best fit of the three ultramafic lamprophyre end-members (alnöite, aillikite, damtjernite) of the IUGS classification (Tappe et al. 2005).

The spatial and temporal relationship of the APIP olivine aillikites and alkaline-carbonatite complexes is evident in outcrops at the Catalão II complex, where olivine aillikite is emplaced as late-stage dikes cutting carbonatites (Figs. 5d, e) or as breccia pipes. Similar emplacement styles are also reported in other alkaline carbonatite complexes of the province such as Serra Negra (Grasso 2010), Catalão I (Ribeiro 2008), and Tapira (Brod et al. 2013).

2.4. METHODS AND SAMPLES

2.4.1. Geophysical imaging

Regional aeromagnetic data are used here as a background to interpret the extent and structural context of the APIP rocks on a province scale. In particular, we look for magnetic features and structures that provide insights into the possible connection between the Mata da Corda Formation and unrecognized (concealed) carbonatite complexes. Magnetic geophysical data is useful for interpreting rocks of the APIP in a regional scale (e.g., Cowan et al. 2000; Dentith and Mudge 2014) because of i) the high content of magnetite, perovskite, ulvöspinel or Mg-chromite (Byron 1999; Carlson et al. 1996; Melo 2012); ii) the fact that the emplacement of the APIP represents the latest major geologic magmatic event in the area (Gibson et al. 1995), with minimal post-emplacement structural modification. The airborne magnetic data used here comprises surveys 7, 9 and 10 from the Economic Development Company of Minas Gerais (Codemig) acquired from 2006 to 2008. Data were obtained following flight lines in a N-S direction, with line spacing from 400 to 500 m, and a ground clearance of 100 m. The survey data were interpolated into a regular grid with a side of 125 m with an interpolator that accounts both for across- and in-line data. The magnetic anomaly data for each survey was reduced from the international geomagnetic reference field and reduced from the magnetic pole (RTP; Blakely 1995) for each survey epoch and settings (e.g., inclination and declination) of the magnetic field. The use of the RTP filter in the study area is stable following the moderate magnetic latitude of the study area (<-20 degrees) in the survey epochs (Li 2008). The RTP-reduced magnetic anomaly data from the individual surveys were stitched with a suture region of 128 cells along the region. The RTP-reduced magnetic anomaly maps provide a proxy for the bulk magnetization of the rock bodies in the study area (Pilkington and Tschirhart 2017). The RTP-reduced magnetic anomaly data is further processed with the use of the 3D analytical signal amplitude (ASA) filter (Roest et al. 1992) to enhance the edges of the magnetized bodies (Pilkington and Tschirhart 2017). In the ASA map, the regions of maximum value represent plausible solutions for the edges of the magnetized bodies with a reliable solution in regional survey data regardless of causative body direction (Pilkington and Tschirhart 2017; Roest et al. 1992). The analytical signal amplitude (ASA) and reduction to

the pole images were processed using the Geosoft Oasis Montaj software v. 9.3.

2.4.2. Samples, whole-rock chemistry, micro-XRF and mineral chemistry

We analysed 12 kamafugite lavas of the basal volcanic unit and 8 kamafugite breccias of the upper volcanoclastic unit, which were sampled in the localities of Patos de Minas and Lagoa Formosa, in Mata da Corda Central, retrieved from four boreholes (FSP00, FSP00A, FSP13A and FSP06; Fig. 4). In addition, key samples of olivine aillikites from Catalão II are described in detail and their chemistry is compared with samples from diopside aillikites from Tapira, and kamafugites from the North, Central and South Mata da Corda. In total 20 samples were selected for whole-rock analyses, carried out by ALS Laboratory. Powdered samples were fused with a lithium tetraborate-lithium metaborate flux, and the resulted mold was analyzed by X-ray fluorescence (XRF) spectrometry for SiO_2 , TiO_2 , Al_2O_3 , Fe_2O_3 , MnO , MgO , CaO , Na_2O , K_2O , P_2O_5 . Powders were also dissolved in nitric, hydrochloric and hydrofluoric acid to analyse trace elements by inductively coupled plasma mass spectrometry (ICP-MS), for Rb, Sr, Ba, Cs, Sc, V, Cr, Co, Ga, Ni, Cu, Zn, Y, Zr, Nb, Hf, Ta, La, Ce, Pr, Nd, Sm, Eu, Gd, Tb, Dy, Ho, Er, Tm, Yb, Lu, Pb, Th, U. Whole-rock compositions are reported in the Supplementary Table 1 along with a compilation of published Mata da Corda North and South (in the localities of Presidente Olegario, Malaquías, Santa Rosa, Veridiana, Falcão, Canas and Serra do Bueno), olivine aillikites from Catalão II, diopside aillikites from Tapira and international kamafugite lithogeochemistry data.

Polished thin sections of representative samples were inspected using a polarized microscope and a FEI Quanta 250 scanning electron microscope (SEM) in the Andean Geothermal Center of Excellence (CEGA), Department of Geology, University of Chile in Santiago. Backscattered-electron (BSE) images were obtained using a current of 80 μA , an accelerating voltage of 15 to 20 kV, a beam intensity of $\sim 1 \text{ nA}$, a beam spot size of 5 μm , and a working distance of 10 mm.

Polished thin sections of kamafugites from Mata da Corda central and olivine aillikites of the Catalão II complex were mapped using a Bruker M4 Tornado energy-dispersive micro-X-ray fluorescence (μ -EDXRF) spectrometer at the Institute of Mineralogy and Petrography, University of Innsbruck. The polychromatic beam is focused by a polycapillary lens, resulting in a spot size of 17 μm at 17.48 keV (molybdenum $\text{K}\alpha$). Chemical mapping was performed with a Rh tube and two energy-dispersive Si-drift detectors, at 20 mbar vacuum, 50 kV and 600 nA. The map resolution is $50 \times 50 \mu\text{m}$ and dwell time per pixel was 50 ms. The pixel gray values in a given element map are proportional to the integral of the spectral region around the characteristic X-ray energy of interest (i.e., La or $\text{K}\alpha$ line). Each map is normalized to the minimum and maximum integral intensities. A stochastic fast deconvolution was applied in order to minimize the effect of spectral overlaps in maps (e.g., $\text{Ba-L}\alpha$ on $\text{Ti-K}\alpha$). Composite maps show the intensities of Ca, Ce, Fe, K, Mg, Nb, Nd, Ni, Sm, Ti with different colours.

Electron microprobe analyses (EMPA) were carried out on ten selected kamafugite samples from Mata da Corda Central and three samples of olivine aillikites from the Boa Vista Mine in the Catalão II alkaline-carbonatite complex. The EMPA analyses were performed at the Regional Center for Technological Development and Innovation-CRTI in Goiania, Brazil, using a JEOL JXA 8200 electron microprobe equipped with five wavelength dispersive spectrometers (WDS). The analyses were performed using accelerating voltage of 15 kV and a beam current of 20 nA for oxides and silicates, and 5 nA for carbonates, with a counting time of 20 seconds for all elements. Beam spots sizes of 2 µm, 5 µm and 10 µm were used for oxides, silicates and carbonates, respectively. Synthetic and natural mineral standards of oxides, carbonates, phosphates and silicates were used for calibration. EMPA data were obtained for the primary mineral phases, i.e., perovskite, spinel-group oxides, clinopyroxene, and for secondary mineral phases such as glauconite and apatite (Supplementary Tables 3–7).

2.5. RESULTS

2.5.1. Aeromagnetic modelling

The ASA images from regional airborne magnetic data show a strong magnetic response for the APIP alkaline-carbonatite complexes, lineaments L1, L2 and L3 associated with the 125° azimuth, and the Mata da Corda Formation, in contrast with the poorly magnetic Neoproterozoic basement (Fig. 6a). The strong contrast of the ASA images displays a heterogeneous magnetic response throughout the mapped exposure of the Mata da Corda Formation, with a low magnetic response to the north, a highly magnetic centre, and an intermediate magnetism to the south (Fig. 6a). The low magnetic response for Mata da Corda North is also indicated in the RTP images, where its magnetic response is similar to the basement in those sectors (Fig. 6b).

The alkaline-carbonatite complexes of Serra Negra, Salitre, Araxá and Tapira are highly magnetic (Fig. 6a, b). These complexes display more than one intrusive set and diverse satellite bodies surround the main intrusion (Fig. 9a) with the high signal also retained in the RTP image (Fig. 6b). Other magnetic features include hundreds of small intrusions with strong magnetic highs (Fig. 6a) associated with kimberlite and alkaline plugs that are beyond the scope of this work. In addition, the Salitre, Serra Negra and Mata da Corda cut the 125° azimuth lineament, and there is magnetic discontinuity of the lineament along its L1 and L3 branches (Fig. 6a).

RTP images show that the alkaline-carbonatite complexes of Serra Negra, Salitre, Araxá and Tapira present a dipole-type magnetic response (Fig. 6b). There are also three dipole-type structures very similar to the alkaline-carbonatite complexes south of the Mata da Corda Formation, which are spatially associated with the 125° Azimuth lineament (Fig. 6b). Finally, the ASA and RTP images show that L1, L2 and L3 lineaments are highly magnetic and similar in intensity and morphology, however, the L3 lineament exhibits a reverse polarity in the anomalous magnetic field (Rocha et al. 2014).

2.5.2. Petrography

Kamafugite lavas:

The Mata da Corda basal volcanic unit includes porphyritic and vesicle-rich clinopyroxene-olivine-leucitite-kalsilite lavas (ugandites) and olivine-clinopyroxene-kalsilitite lavas (mafurites), according to the proposed petrographic classification for kalsilite-bearing volcanic rocks by Oliveira et al. (2022). While Mata da Corda North features both ugandite and mafurite lavas, the lava from Mata da Corda Central is predominantly mafurite (Figs. 7a, d). Mafurite lava from Mata da Corda Central consists of clinopyroxene, olivine and phlogopite macrocrysts (Fig. 7c; ~20–30%) (encompassing both xenocrysts and phenocrysts), occurring within a groundmass (~70–80%) of clinopyroxene, magnetite, perovskite, spinel group oxides, kalsilite, phlogopite and glass (Figs. 7a, b, d)), and a variety of accessory minerals such as calcite, chlorite, apatite, gorceixite, zeolites and amygdaloid chalcedony.

Medium- to fine-grained subhedral clinopyroxene (40 µm – 3 mm), is the dominant rock-forming mineral in the lavas from Mata da Corda Central (Figs. 5b and 7a) and accounts for ~50–60% of the macrocrysts, commonly with iso-oriented textures. Isolated grains may contain inclusions (<100 µm) of spinel group minerals (Figs. 7a, c). Olivine is scarce in lavas of Mata da Corda Central, however it is widely reported in Mata da Corda North kamafugites with compositions between Fo₉₀ and Fo₇₃ (Melluso et al. 2008). Spinel group minerals and perovskite microcrysts (Figs. 7a, c) commonly occur as subhedral to anhedral <500 µm grains (Figs. 7a, b). Fine grained kalsilite (<300 µm; Fig. 7d), leucite, phlogopite, and apatite (Fig. 7a) are often altered to clay minerals and gorceixite. Zeolites and chalcedony are restricted to vesicles (Fig. 7b). Ovoid carbonate pockets with sizes between 0.5–3 mm are also common (Fig. 5b).

The spatial distribution of key major elements in rock-forming, accessory and secondary minerals are shown in false colours in Supplementary Figure 1. For Mata da Corda Central kamafugites, perovskite is the most abundant oxide (Supplementary Figure 1 (d,e)). Potassium, reported in red in Supplementary Figure 1(g,h), is mostly retained in the groundmass of both kamafugite lavas and breccias as isolated bright-red grains (Supplementary Figure 1(i)) representing phlogopite and feldspathoid microcrystals.

Kamafugite breccias:

Kamafugite breccia occurs in the upper volcanoclastic unit and consists of hydrothermally-altered reddish green to dark red breccia with veinlets (Figs. 7e, f) with transitional to sharp contacts with kamafugite lavas of the basal volcanic unit. Hydrothermal and veined breccias are so far reported only for Mata da Corda Central. Kamafugite breccias are composed of sub-rounded to sub-angular kamafugitic clasts set within an oxidized matrix predominantly of iron oxides and hydroxides (Fig. 5c) that varies between 10 to 30% of the rock volume. Primary silicate minerals such as clinopyroxene, olivine and phlogopite have been altered mainly to chlorite (Fig. 7e), sericite and clays, while oxide group minerals such as magnetite are altered to hematite or iron hydroxides. The only mineral that is well preserved even with a high degree of alteration is

perovskite. Feldspathoids are commonly altered to sericite and clays.

In addition, white to light ochre, fine-grained calcite veinlets with subordinate apatite and gorceixite (Figs. 7e, f) crosscut the kamafugite breccias (Figs. 5c and 7e, f). These veinlets also occur locally in kamafugite lavas, without an oxidized matrix, with the veinlets containing the same mineralogy but with a higher carbonate content with respect to red kamafugites. Finally, some calcite-rich veins contain well-preserved green glauconite crystals (Fig. 7f), also previously identified in calcite pockets within kamafugite lavas by Byron (1999).

Micro-XRF results show calcite veinlets that are reported in blue in kamafugite breccias (Supplementary Figure 1(g)), and differ from ovoid carbonate pockets of kamafugite lavas as they are not associated with secondary fractures (Supplementary Figure 1(h)). Kamafugite breccias show a clear mobilization of compatible elements such as Ni and Mg, which are hosted within calcite and chlorite veinlets, respectively (Supplementary Figure 1(e,h)). Potassium occurs in high concentrations in secondary K-rich clay minerals and euhedral phlogopite crystals (Supplementary Figure 1(i)) and, in smaller concentrations, in the groundmass.

Olivine aillikites:

These rocks occur as dikes, pipes and small sub-volcanic intrusions crosscutting the APIP alkaline-carbonatite complexes (Fig. 5d, e). The investigated olivine aillikites are clinopyroxene-free dark green porphyritic dikes (Fig. 5d, e) with olivine and phlogopite macrocrysts (20%) set in a groundmass (70%) of glass, perovskite, calcite, spinel group oxides and fine phlogopite laths (Figs. 7g, h). The olivine (~70%) macrocrysts are widely fractured and rounded, with sizes between 500 µm to 2 mm, locally altered to chlorite (Fig. 7i). phlogopite macrocrysts (~30%) are zoned with a dark brown phlogopite core and a yellowish-brown tetraferriphlogopite rim (Fig. 7h). Fine grained spinel group oxides (<100 µm) are common in the groundmass together with perovskite (Fig. 7g). There are also calcite pockets of 1 to 5 mm in diameter (Fig. 5e) randomly distributed in the groundmass.

Micro-XRF results from an olivine aillikite of the Catalão II complex, suggest similar Fe-Ti-Ni oxide composition to those from kamafugite lavas (Supplementary Figure 1(f,i)). In addition, individual calcite pockets lack connections with secondary fractures or vesicles (Supplementary Figure 1(i)).

2.5.3. Mineral Chemistry

Electron probe microanalysis of spinel-group oxides, perovskite and clinopyroxene focused on well-preserved kamafugite lavas, as these are potentially more representative of near-primary compositions than those from kamafugite breccias. The oxide minerals were chosen because they are robust primary magmatic minerals useful for petrogenetic studies and because they have a high magnetic response and therefore complement the interpretation of the geophysical data. The chemistry of clinopyroxene is also examined as it is the most ubiquitous silicate in kamafugite

lavas, compared to other silicates such as olivine, which is scarce in Mata da Corda central. These data are compared with previously published results for oxide phases in Mata da Corda North, olivine aillikites and diopside aillikites (Supplementary Tables 3 and 4), which we will examine in the discussion section.

Spinel-group oxides:

The kamafugite lavas from Mata da Corda Central display a complex solid solution of spinel-group crystals, which are characterized by four end-members including magnetite, ulvöspinel, Mg-chromite and Mg-ferrite (Fig. 8). The most abundant end-member is magnetite ($\bar{x} = 43\%$), followed by ulvöspinel ($\bar{x} = 30\%$) and Mg-ferrite ($\bar{x} = 15\%$) (Fig. 8b). A WDS map for a martitized magnetite microcrystal from Mata da Corda Central lavas shows a titanium and magnesium rich core with slightly higher nickel values at the edges (Fig. 9), associated with secondary oxidation.

Perovskite:

The Ca-Ti-Ce oxide grains correspond to a solid solution between perovskite (CaTiO_3) and loparite $[(\text{Ce,Ca})(\text{Nb,Ti})\text{O}_3]$ end-members (Supplementary Table 4). Perovskites from Mata da Corda Central have low niobium and LREE contents (<1 wt.% Nb_2O_5 , <2 wt.% Ce_2O_3 and <1 wt.% La_2O_3 (Supplementary Figure 2)). Perovskite inclusions within magnetite vary mainly in Ca and Ti (Fig. 9).

Clinopyroxene:

Clinopyroxene is ubiquitous in both Mata da Corda North and Central lavas. The predominant clinopyroxene in Mata da Corda Central is a Ca-rich diopside (Fig. 10). Diopside crystals have high calcium (19.04–26.54 wt.% CaO) and titanium (up to 1.76 wt.% TiO_2) contents. Iron contents are lower (3.03–4.76 wt.% FeO) with than lavas of Mata da Corda North (Melluso et al. 2008) and diopside aillikites from the Salitre carbonatite complex (Barbosa et al. 2012).

2.5.4. Whole rock chemistry

Whole rock chemistry data of the best-preserved kamafugite lavas of the Mata da Corda Central, along with a compilation of published results from Mata da Corda North and South, are reported in the Supplementary Table 1. Owing to the high content of carbonates in secondary veinlets and their associated high LOI values (5.27–15.62%), kamafugite breccias will not be taken into account in these analyses, although the chemistry is also reported in the Supplementary Table 1. We also report chemical data for olivine aillikites from Catalão II, Tapira and Serra Negra and diopside aillikites from Salitre. As expected, kamafugite lavas are characterized by ultramafic SiO_2 -undersaturated compositions (Fig. 11), with SiO_2 between 33.50 wt.% to 40.60 wt.% and MgO varying from 4.5 to 15.5 wt.% MgO . CaO contents are high for kamafugite lavas (4.4 to 14.3

wt.% CaO; Fig. 12b), which is attributed to the calcite pockets in the groundmass. According to the classification of ultrapotassic rocks of Foley et al. (1987), the kamafugite lavas plot in the kamafugite field (Fig. 12b). The degree of data dispersion is high for Fe₂O₃ (13.6–25.3 wt.%), Al₂O₃ (4.3–8.6 wt.%) and TiO₂ (4.7–9.5 wt.%) in kamafugite lavas (Figs. 12c, e). The K₂O content of the lavas from Mata da Corda Central is highly variable, as low as 1.2 wt.% in weathered samples but the most preserved lavas have >3 wt.% K₂O and reaching up to 6.5 wt.% K₂O (Supplementary Table 1), which is attributed to the presence of phlogopite, leucite and kalsilite, but also, as indicated by micro XRF a potassium-rich groundmass (Supplementary Figure 1(g,h)). Furthermore, it is important to note that the K₂O/Na₂O ratio varies from 5.8 to 67.8 (Fig. 12), and together with the high content of MgO (>3 wt.%), these rocks can be classified as ultrapotassic lavas. Although kamafugite lavas show primary carbonate pockets or carbonate globules (ocelli) in the groundmass, which could raise the LOI value, it varies between 6.28 to 9.04% LOI, which is lower than the kamafugite breccias that have values >10% LOI, associated to the high content of secondary carbonate veinlets.

Kamafugite lavas are highly enriched in rare earth elements (REE), with light REE (LREE; Σ La:Eu) ranging from 500 to 2,180 ppm, and heavy REE (HREE; Σ Gd:Lu) varying from 42 to 147 ppm (Supplementary Table 1). Chondrite-normalized REE patterns (Nakamura, 1974), show enrichment in LREE, with respect to HREE (Fig. 13a). Kamafugite lavas have high concentrations of compatible elements such as Ni (182 to 666 ppm) and Cr (160 to 870), attributed to the high concentration of primary magmatic minerals such as clinopyroxene and oxides within the groundmass. In addition to a high content of REE and compatible elements, kamafugites also have elevated values of high field strength elements (HFSE) such as Zr (673 to 837 ppm), Nb (164 to 273 ppm) and Ta (6 to 17 ppm) and the Zr/Nb ratio does not change over an order of magnitude (Fig. 13d). A Nb vs La/Y diagram indicates a positive La/Y trend for kamafugites (Fig. 13f). Finally, the large ion lithophile elements (LILE) display high concentrations, with values up to 4910 Ba, 228 ppm Rb and 1800 ppm Sr.

2.6. DISCUSSION

Spatial relations, geophysical imaging, age determinations and geochemical signatures suggest that the Mata da Corda kamafugites and aillikites (as part of the APIP alkaline-carbonatite complexes) are contemporaneous and were generated in the Late Cretaceous through a common mode of magma production. To unravel the formation of these lithotypes, it is necessary to evaluate the spatial distribution of emplaced magmas, constrain the nature of the magma source and verify whether modification of these magmas suggests consanguinity.

2.6.1. Spatial distribution of kamafugite volcanism and alkaline-carbonatite complexes

The emplacement of the Mata da Corda Formation volcanic rocks —through hundreds of phreatomagmatic eruptive centres (Byron 1999) spread over an area of 4,500 km² (Gibson et al.

1995)—imply rapid magma ascension through a basement undergoing regional extension (Ribeiro et al. 2018), as also happens in neighbouring Late Cretaceous volcanic provinces following the Azimuth 125° lineament, such as the Poxoréu Igneous Province in Mato Grosso State, western Brazil at ~84 Ma (Gibson et al. 1997). The APIP magmatism was initially attributed to the impact of the Trindade mantle plume at the base of the subcontinental lithosphere (Gibson et al. 1995; Gibson et al. 1997; Thompson et al. 1998). These authors propose that the plume-track had a south-east orientation with respect to the APIP, bordering the southern limit of the São Francisco Craton to the Serra do Mar Alkaline Province until reaching its recent position beneath the Trindade-Martin Vaz Islands in the mid-Atlantic Ocean. Alternatively, more recent studies have argued for an incipient rifting model related to far-field stresses during the south Atlantic opening (Ribeiro et al. 2018). This hypothesis was proposed in part because previous works showed by means of paleomagnetic studies that the previous plume was at least 1,000 km outside of the Paraná Province at the time of the eruptions (Ernesto et al. 2002; Ribeiro et al. 2018) and taking into account that the Goiás Alkaline Province ages are almost coeval with respect to the APIP ages (Guarino et al. 2013).

Considering the large volume volcanism over an extended area, a certain degree of variability between different areas of the Mata da Corda would be expected. For example, the magnetic signature of the Mata da Corda Formation shows three magnetically discernible areas (Fig. 6a); low magnetism (Mata da Corda North), high magnetism (Mata da Corda Central) and intermediate magnetism (Mata da Corda South). The ASA further reveals highly magnetic mapped fragments of the Mata da Corda Formation to the northeast of the Serra Negra Complex and the CPRM cartography sheets show Mata da Corda lavas to the northwest of Serra Negra (CPRM 2020), at 900 to 1000 m of elevation, that are disconnected from the main outcrop areas, that occur at ~700 to 800 m of elevation. This disconnection suggests either the emplacement of an originally separate cluster of volcanic centres or that the Mata da Corda Formation was larger than at present and was eroded off in places where current elevation is below 800 m.

Our samples, compared with previously published Mata da Corda kamafugite data, point to lavas with variable chemistry and mineralogy, particularly between the central and north areas (Figs. 8, 10 and 12). Although Mata da Corda North samples have higher SiO₂ (from 33.7 to 42.5 wt.%) and MgO (10.3 to 21.4; Fig. 12a) than those from Mata da Corda Central (Fig. 12a), there is a negative trend from the near-primary kamafugite melts to the Mata da Corda North and Central kamafugites, indicating a continuous fractionation of olivine and clinopyroxene, associated with a crystal settling process. Additionally, the progressive increase of Al₂O₃ and K₂O from near-primary melts to more evolved lavas in Mata da Corda North and Central kamafugites (Figs. 12d, f), indicate restricted or no formation in early stages of minerals with these oxides and perhaps phases such as phlogopite, leucite and kalsilite were formed in late magmatic stages.

The above whole-rock geochemical variations are also observed in EPMA analyses in kamafugites from Mata da Corda North and Central. For example, Ce₂O₃ contents in perovskite reach up to 8 wt.% and ~2 wt.% Nb₂O₅ in Mata da Corda North (Supplementary Fig. 4(a)),

compared to <2 wt.% Ce₂O₃ and <1 wt.% Nb₂O₅ in Mata da Corda Central indicate different generations of extrusive pulses and significant chemical differences between north and central lavas, which in turn can affect the ASA magnetic response. Additionally, Mata da Corda North lavas show higher content of Mg-chromite ($\bar{x} = 33.4\%$) and ulvöspinel ($\bar{x} = 34.8\%$; Fig. 8b), while Mata da Corda Central lavas have a predominance of magnetite ($\bar{x} = 43\%$; Fig. 8a), which is responsible for the high magnetic response (Fig. 6a), compared to Mata da Corda North that has an ulvöspinel predominance. Despite this variable oxide content, REE patterns are similar between kamafugites from the central and northern areas, a feature compatible with the hypothesis of a common mantle source.

Unlike the Mata da Corda Formation, APIP carbonatite complexes are characterized by very large and well-defined dipole anomalies in RTP images and by strong anomalies in ASA images. Several hundred mapped potassic-ultrapotassic intrusions (Fig. 4) show equivalent magnetic signatures in ASA images, albeit much smaller (Fig. 6a). The ASA images show that in addition to a main body, there are also small satellite bodies with a high magnetic intensity, as observed at Araxá, Salitre and Serra Negra (Fig. 6a). This feature is important because it suggests a complex plutonic configuration at depth, with multiple magmatic chambers of different size.

The APIP magnetic data show additional features of unknown origin. A large-scale magnetic anomaly resembling those of the Serra Negra and Salitre complexes is located to the east of the Tapira Complex – the Pratinha anomaly (Louro and Mantovani 2012). This anomaly is interpreted as a deep alkaline-carbonatite complex, with gravimetric data estimating a depth between 400 to 450 m below the surface. Two additional conspicuous dipole-like structures occur in RTP images underneath the Mata da Corda South, but fail to match the general magnetic signature of Mata da Corda volcanics (Fig. 6b). Their full dipole responses are likely to be partially obscured by the intermediate magnetic responses of Mata da Corda South kamafugite cover (ranges from 3,000 to 9,000 nT).

The magnetic data can be thus translated into five main magnetic patterns and their respective geological interpretation: a) Large magnetic anomalies associated with alkaline-carbonatite complexes; b) Equivalent signatures suggesting buried complexes to the south of the Mata da Corda Formation; c) Small magnetic anomalies associated with various kimberlite, kamafugite, and unclassified potassic-ultrapotassic intrusions; d) Large-scale magnetic signatures of variable intensity corresponding to Mata da Corda volcanics, and e) Linear high magnetic signatures of the huge Azimuth 125° lineament (L1, L2 and L3). These diverse geophysical features are compatible with the various emplacement styles observed in the APIP and suggest that the horizontal, largely magnetic, sheets of the Mata da Corda Formation might mask deeper anomalies representing alkaline complexes. Also, the occurrence of disconnected fragments of the Mata da Corda Formation westwards and the various kamafugite plugs spatially close to alkaline-carbonatite complexes (such as Santa Rosa, Canas and Veridiana; Fig. 4), suggests that kamafugite-related volcanism could have extended further west prior to erosion. The spatial relationships between the Mata da Corda kamafugites and alkaline-carbonatite complexes revealed by

geophysics, along with the overlap in the temporal distribution reported in the literature, imply a common mode of parental magma production. Derivation of kamafugites and carbonatites from a common parental magma has been suggested in the APIP (Brod et al. 2000; 2013) and in the Roman Province (Martin et al. 2012). Therefore, assessing whether kamafugites and alkaline-carbonatite complexes can be related to a common magma type depends on assessing their primary magma source.

2.6.2. Potential links between kamafugites and aillikites from alkaline-carbonatite complexes in the APIP

Several published whole-rock analyses of kamafugite from Mata da Corda North show variable Ni (138-890 ppm) and Cr contents (205-1320 ppm; Fig. 14d), olivine with up to Fo₉₀ (Melluso et al. 2008) and whole-rock Mg# up to 60, and many of these kamafugite samples have similar to near-primary mantle-derived melts (Ni >500 ppm, Cr >1000 ppm, Fo₈₆ to Fo₉₁ olivine compositions and Mg# >66; Winter 2001), plotted as black rectangles in Figures 9 and 10. Our kamafugite samples from Mata da Corda Central, on the other hand, show scarce olivine, Ca-richer diopside compositions with respect to diopside crystals from Mata da Corda North (Fig. 12) and much lower Ni (119-666 ppm), Cr (160-870 ppm) and Mg# (<45), indicating variable fractionation of the parental melt. Furthermore, olivine aillikites from Catalão II, Serra Netra and Tapira show variable compositions, e.g., Ni (37-1238 ppm), Cr (68-1450 ppm) and Mg-number (33-58). The most primitive values of those olivine aillikites that are similar to the primary-like kamafugite melts from Mata da Corda North are shown as black circles in Figures 9 and 10. The retention of high Ni contents in primary samples, suggests that there was no early sulphur saturation in the magma (Velásquez Ruiz et al. 2019). Most fractionated samples perhaps correspond to diopside aillikites from Salitre with the most depleted values of Ni (17-654 ppm), Cr (29-782) and Mg# (29-45).

A genetic link between the APIP kamafugites, olivine aillikites and diopside aillikites is supported by several lines of geochemical and mineralogical evidence: (1) the Mata da Corda kamafugites and olivine aillikites have similar rock-forming minerals, (Fig. 8), (with the exception of a lack of feldspathoids for aillikites), and also similar perovskite concentrations, a K-rich groundmass, and primary pockets of carbonates (with no associated secondary fractures), which, despite to the local chemical variability in oxides and silicates (Figs. 8 and 10) demonstrate a common mineralogy and chemistry. (2) Kamafugites and aillikites both plot in the kamafugite field of Foley et al. (1987) (Fig. 12b) and also the Mata da Corda lavas follow the three main chemical criteria to be classified as kamafugites ($MgO > 3\text{wt.\%}$, $K_2O > 3\text{wt.\%}$ and $K_2O/Na_2O > 2$). (3) The REE-normalized patterns for all these ultrapotassic rocks are parallel (Figs. 13a-c), suggesting derivation by fractional crystallization from a single parental magma, and (4) olivine aillikites and diopside aillikites are up to two times richer in REE compared to kamafugites (Figs. 13a-c). Although the Salitre aillikites have a high perovskite concentration (Barbosa et al. 2012), those perovskites show low REE content with respect to the Mata da Corda perovskites by almost an order of magnitude (Supplementary Figure 2(a,b)).

The link between the APIP ultrapotassic rocks is in strong agreement with published Sr and Nd isotope ratios (Fig. 14). Low ϵ_{Nd_i} values (-4.837 to -10.104) and relatively high $^{87}\text{Sr}/^{86}\text{Sr}_i$ values (0.70467 - 0.70623) in Mata da Corda kamafugites (Gibson et al. 1995; Gomes and Comin-Chiaromonti 2005) overlap data from olivine aillikites from Catalao II ($^{87}\text{Sr}/^{86}\text{Sr}_i = 0.70480$ - 0.70551 ; $\epsilon_{\text{Nd}_i} = -7.568$ to -8.602 ; Guarino et al. 2013). In general, the initial $^{143}\text{Nd}/^{144}\text{Nd}$ and $^{87}\text{Sr}/^{86}\text{Sr}$ ratios for all the APIP alkaline carbonatite rocks are similar (Fig. 14), and also indicate a common source from an enriched lithospheric mantle. In addition, the isotopic data of the APIP alkaline-carbonatite rocks are dissimilar from those from Trindade (Fig. 14). In fact, Ferreira et al. (2022) highlights crustal extension, associated with the breakup and dispersal of West Gondwana, as responsible for the generation of alkaline and tholeiitic magmatism between the Mesozoic to Paleogene in the South American platform.

Kimberlite plugs in the APIP, as observed in the ASA image (Fig. 6a) are also spatially associated with kamafugites and have U–Pb perovskite ages between ~ 91 – 80 Ma (Guarino et al., 2013), so they are also temporally related. According to Araujo et al., (2001), kimberlites have a macrocryst assemblage of olivine, set in a groundmass of olivine, ilmenite, phlogopite, spinel, perovskite, carbonate, monticellite, apatite, rare garnet and serpentine. Pyroxene and feldspathoids are absent in the kimberlites, and these do not therefore completely resemble the mineralogy of the Mata da Corda kamafugites. Moreover, the pressure and formation depth of kimberlites must be carefully analysed to consider any link between kamafugites and kimberlites, but this analysis is outside the scope of this work.

2.6.3. Mantle source characteristics and silica-undersaturated magmatism

Generation of strongly silica-undersaturated alkaline magmas can be explained by the presence of enriched components in their mantle source. Foley (1992) proposed that clinopyroxene and mica veining and low-degree wall rock melting (<2%) are responsible for the generation of potassio rich magmas. Mica-amphibole-rutile-ilmenite-diopside (MARID) type veining has been proposed in a deep CO₂-rich mantle source for kamafugites from Toro-Ankole (Rosenthal et al. 2009) and aillikites from Labrador in Canada (a close example of the APIP olivine aillikites; Tappe et al. 2008). Therefore, a metasomatized MARID-like veined mantle is an agent that increases alkaline components in primitive kamafugitic mantle sources (Bizzi et al. 1995; Carlson et al. 1996).

Phlogopite macrocrysts (Fig. 7) and primary carbonate pockets within the Mata da Corda kamafugite lavas (Fig. 5 and Supplementary Figure 1) are key aspects indicating possible metasomatism in the APIP mantle source that, as indicated by $^{143}\text{Nd}/^{144}\text{Nd}_{(i)}$ and $^{87}\text{Sr}/^{86}\text{Sr}_{(i)}$ ratios, comes from an enriched lithospheric mantle (Fig. 14). The availability of deep sources of potassium, CO₂ and H₂O in a pristine magma, implies the presence of a K-bearing mineral phase such as phlogopite or K-richterite (Grégoire et al. 2002, 2003) and a deep CO₂ circulation in the

mantle source. Moderate (<3wt.%) to high K₂O, up to 6 wt.%, Mata da Corda kamafugites and a high K₂O/Na₂O from 5.8 to 67.8 (Fig. 12), point to an extremely K-enriched mantle source associated with metasomatic phlogopite-rich veins, as also proposed by Gibson et al. (1995) and Guarino et al. (2013). These high K₂O/Na₂O ratios coexist with high values of Cr (up to 1,760 ppm) and Ni (up to 2,350 ppm; Supplementary Table 1), which clearly exhibit near-primary enriched, mantle-derived, melt compositions. Furthermore, Na-amphibole is not expected in the APIP source due to the high K₂O/Na₂O ratios, suggesting instead that metasomatic mica, probably phlogopite (Grégoire et al. 2002, 2003), is the principal source of K₂O, and excluding K-richterite for an unlikely low K₂O/Na₂O ratio.

Experimental studies by Martin et al. (2012) point to liquid immiscibility processes between kamafugite and carbonatite melts, with starting materials that are rich in K₂O (2-11wt.%), CO₂ (12-26 wt.%) and extremely poor in SiO₂ (20-32 wt.%). The cited study shows that formation of an initial immiscible carbonatite bubble separating from a kamafugitic liquid is possible at >1200 °C and >1.5 GPa, and given the large number of primary carbonate pockets reported in this work, and carbonates in the groundmass, carbonatite-kamafugite demixing processes are feasible to consider.

In addition, based on major element data (Fig. 12), the trends from near-primary melt composition with their respective less fractionated kamafugite and aillikite samples reveal an intense magmatic fractionation and crystal settle process. The SiO₂ and MgO depletion in both Mata da Corda North and Central lavas, and the slight CaO depletion in Mata da Corda Central indicate early olivine fractionation (\pm clinopyroxene; probably Fe-poor diopside compositions), while a Fe₂O₃, Al₂O₃ and TiO₂ enrichment shows no significant perovskite fractionation nor spinel group minerals in the source. On the contrary, there is depletion in MgO, SiO₂, Fe₂O₃, Al₂O₃, and TiO₂ and CaO enrichment in aillikite samples (Fig. 12), showing early fractionation of olivine and spinel group minerals in the source. Rounded textures in olivines macrocrysts of olivine aillikites (Figs. 7h, i) and their alteration to talc at the edges show disequilibrium and perhaps intense transport from deep sources. This chemical and mineralogical evidence shows that although kamafugites and aillikites have a common enriched lithospheric mantle source, magmatic fractionation processes were different to the east and west of the APIP.

Textural and chemical evidence of primary segregated carbonatite bubbles occur in our kamafugite and aillikite samples (Fig. 5 and Supplementary Figure 1(g,i)), where both specimens have randomly distributed primary calcite bubbles in the matrix (without being associated with secondary fracture zones, as is shown in kamafugite breccias; Supplementary Figure 1(h)). This evidence suggests a possible coalescing of bubbles of carbonatite melt formed from the fractionation of olivine aillikites. In turn, fractionation of HFSE and REE between olivine aillikites and carbonatite dikes in Catalão II, shows preferential partitioning of Ce and Nb into the carbonatite dikes (Supplementary Figure 3), while Ni and Cr remain in olivine aillikites (Supplementary Figure 1(f,i)).

Based on the data presented here, we constructed a conceptual model that links kamafugite

magmatism with the emplacement of alkaline-carbonatite complexes (Fig. 15). In our model, the depths of the upper and lower crust and the subcontinental lithospheric mantle correspond to the initial APIP depths proposed by Gibson et al. (1995). Step 1 comprises low degree melting (<2%) of a CO₂-phlogopite-rich veined peridotite. The phlogopite and carbonate-rich veins were initially proposed by Gibson et al. (2005) and subsequently by Guarino et al., (2013) and explain the enrichment in CaO and volatiles such as CO₂ and H₂O, as well as the low content of Na₂O and the high K₂O/Na₂O ratio, which also denies a Na-rich source (probably poor or lacking in amphibole). Step 2 represents the formation of what could be the first magmatic chamber of an ultrapotassic carbonated-silicate primary magma in the lithospheric mantle in the APIP. Step 3 corresponds to the emplacement of the ultrapotassic carbonated-silicate primary magma at the lithospheric mantle/crust boundary at different points in the APIP, which subsequently generate alkaline-carbonatite complexes to the west side of APIP and kamafugitic magmatism to the east side of APIP. The formation of multiple magma chambers in the APIP crust is mainly explained by the formation of multiple dipoles in the RTP data, as seen in this work (Fig. 6(b)). Step 4 corresponds to fractional crystallization in Mata da Corda kamafugite and aillikite parental magmas. The different mineral phases fractionated early in the Mata da Corda parental magmas (olivine+diopside), with respect to aillikites parental magmas (olivine+spinel group minerals), trigger differences between residual magmas of the east and west sectors in the APIP. The Mata da Corda ultramafic xenoliths described by Byron (1999) as clinopyroxene-rich xenoliths ± olivine, which are moderately to intensely altered in kamafugite lavas, share similar mineralogical characteristics with the APIP bebedourites (Brod 2000), however, bebedourites also appear in the alkaline-carbonatite complexes as a cumulate rock (Barbosa et al. 2012) with variable mineralogy. Step 5 corresponds to the formation of pipes and kamafugite lava flows that generate the Mata da Corda Formation to the east of the APIP. Due to the fissure-type magmatism through the Maar-type volcanoes in the Mata da Corda Formation (Byron 2000), there was an intense degassing process, which would not occur in the alkaline-carbonatite complexes, the latter being intrusive. This could explain why the kamafugite lavas do not have a carbonate-rich groundmass, as is the case for aillikites of the alkaline-carbonatite complexes. To the west side of the APIP on the other hand, carbonatite magma formed in Step 6 either through immiscibility or crystal fractionation from the parental silicate magma, while residual silica undersaturated liquids reach a final fractionation to form a bebedourite cumulate. Step 7 shows a generic APIP alkaline-carbonatite complex. Step 8 represents the intrusion of ultramafic lamprophyres (olivine aillikites) that cut through the APIP complexes and form shallow dike swarm systems.

2.6.4. Post-magmatic processes in kamafugite lavas

It is important to note that physical volcanology has been little addressed since Mata da Corda has been mostly investigated for its geochemical and mineralogical peculiarities in previous literature. As mentioned in chapter 2.2, the Mata da Corda Formation overlies the Areado Formation. The Areado Formation is subdivided between three members, the Quiricó Member that is composed of lacustrine siltstones and argillites, the Tres Barras Member made up of arenites and

the Abaete Member, that is composed of conglomerates from an alluvial fan (Suguió and Barcelos 1983). Although the Areado Formation was deposited in an alluvial-semi desert environment (Suguió and Barcelos 1983), it does not mean that Mata da Corda is characterized by the same paleo-environmental setting. Byron (1999) proposed that Mata da Corda developed via hundreds of phreatomagmatic eruptions and lava flows. One argument supporting this hypothesis is the formation and preservation of green glauconite crystals in red kamafugite lavas, which could indicate that the paleo-environment of Mata da Corda has changed from the Early to Middle-Late Cretaceous. Glauconite is commonly reported in low-latitude, shallow-marine settings at water depths <500 m, temperatures below 15 °C, and under sub-oxic, partially reducing conditions (López-Quirós et al. 2019; Odin 1988; Odin and Matter 1981). Petrographic observations and EPM analyses in this work (Supplementary Table 6) show the presence of glauconite in calcite veinlets in kamafugite breccias from Mata da Corda Central (Fig. 7f). Although these crystals are not abundant, glauconite has high potassium contents (up to 8.38 wt.% K₂O; Supplementary Table 6) and the host rocks have an advanced state of glauconitization, which agrees with phreatomagmatic volcanism. Perhaps, a secondary effect of this phreatomagmatic volcanism is observed in the magnetite crystals with martitization textures (Fig. 9), as evidence of an oxidation processes in Mata da Corda Central lavas.

Lava package thicknesses vary from 2 to 10 m (Fig. 5a) agreeing with low viscosity lavas from diverse Maar-type volcanoes that excavated the Areado Formation and the created the eroded Mata da Corda lava plain (Byron 1999). The multiple Mata da Corda volcanic centres were fed by several polyphase intrusive pipes that comprise breccia pipes and kamafugite intrusions (Gibson et al. 1995), and are overlain by lava flows and pyroclastic rocks of the upper unit of Mata da Corda (Grossi Sad et al. 1971). An estimation of the initial erupted volume developed in Mata da Corda plain was evaluated by Byron (1999). He estimated that the extension of the pre-eroded Mata da Corda spanned 40,000 km² and the lava plain was at least 250 m thick, producing a volume of 10,000 km³ of eruptive ultrapotassic volcanism, akin to a large volume of a fissure-type eruptive style. This is significantly less than the 210,000 km³ estimated for the Columbia River flood basalts (Kasbohm and Schoene 2018), but when compared to other kamafugite provinces, the Mata da Corda lavas represent, together with Toro-Ankole rocks, the largest known eruptive event of kamafugite volcanism in the world.

A hydrothermal event is recorded in kamafugite breccias (Fig. 5c), although it is not possible to discern if it is synchronous to the phreatomagmatic eruptions or if it is post-depositional or late-hydrothermal. It is characterized by the development of hydrothermal breccias with oxidized matrix rich in iron oxides and hydroxides and the generation of secondary calcite-apatite-gorceixite-chlorite veinlets (Fig. 7e and Supplementary Figure 1(h)). Micro-XRF showed remobilization of nickel, magnesium, calcium and iron towards the veinlets (Supplementary Figure 1(e,h)), compared to a kamafugite lava without veinlets (Supplementary Figure 1(d,g)). The presence of fluorapatite, on the other hand (Supplementary Table 7), suggests a progressive increase in the fluorine and phosphorus content within veinlets. The formation of glauconite could be evidence that a phreatomagmatic volcanism acted as a trigger for this hydrothermal event

characterized by addition of Fe-H₂O associated with the red matrix and mobilization of CO₂-P-F present in the veinlets. The high concentrations of P₂O₅ reported here, up to 9 wt.% (Supplementary Table 7), are in agreement with high phosphorus contents previously reported in internal reports from the Morro Azul mining company (up to 27% P₂O₅), and show that the Mata da Corda formation has great potential for phosphorus exploration (Melo 2012).

2.7. CONCLUSIONS

The new regional aeromagnetic data and comprehensive micro-XRF, mineral chemistry, isotopic and whole rock geochemistry of the Mata da Corda lavas and aillikites in the APIP, reveal a genetic link between kamafugite magmatism and alkaline-carbonatite complexes. ASA and RTP images show three dipole structures south of Mata da Corda with magnetic signatures similar to alkaline-carbonatite complexes, which are explained as buried carbonatite complexes underlying Mata da Corda. Kamafugites to the NW of the Serra Negra complex, such as Santa Rosa and Veridiana demonstrate that Mata da Corda extended to the west of the APIP and likely overlaid the alkaline-carbonatite complexes as currently happens at Mata da Corda South, however, most of this evidence disappeared over time due to erosion. The link between kamafugites and aillikites from alkaline-carbonatite complexes is evidenced by: (1) kamafugites and aillikites plotting in the kamafugite field of the ultrapotassic rock classification of Foley (1987); (2) a similar CI chondrite-normalized REE distribution, with aillikites enriched up to 2 times in REE compared to kamafugites; (3) these lithologies share the same rock-forming minerals, except for the lack of feldspathoids in aillikites; and (4) the ¹⁴³Nd/¹⁴⁴Nd_(i) and ⁸⁷Sr/⁸⁶Sr_(i) ratios for all the APIP alkaline-carbonatite rocks are similar, and also indicate a common source from an enriched lithospheric mantle. Our model proposes a multi-stage fractionation process from a primary ultrapotassic carbonated-silicate magma localized in a metasomatized subcontinental lithospheric mantle that ascends and fractionates at different crustal levels, generating numerous alkaline-carbonatite magmatic series (carbonatites, aillikites and bebedourites) to the west of the APIP, and the production of a kamafugitic volcanism of the Mata da Corda Formation to the east of the APIP that probably spread west.

2.8. ACKNOWLEDGMENTS

This work was supported by ANID through Millennium Science Initiative Program (NCN13_065) “Millennium Nucleus for Metal Tracing Along Subduction”, and by ANID-Subdirección de Capital Humano/Doctorado Nacional/2021-21210049. Additional funding for this study was provided by the Hugh McKinstry Fund of the Society of Economic Geologists Foundation Inc. We also thank the Morro Azul Mining Company for providing the samples for this study and the Instituto Federal do Triângulo Mineiro, Campus Patos de Minas, for storing the drill core samples. The contributions of Dr Stephen Foley, an anonymous reviewer and editorial suggestions from Dr Robert J. Stern greatly improved the original manuscript. Authors also thank Dr Sam Broom-Fendley and Dr Ítalo Oliveira for their valuable contributions to the manuscript.

2.9.FIGURES

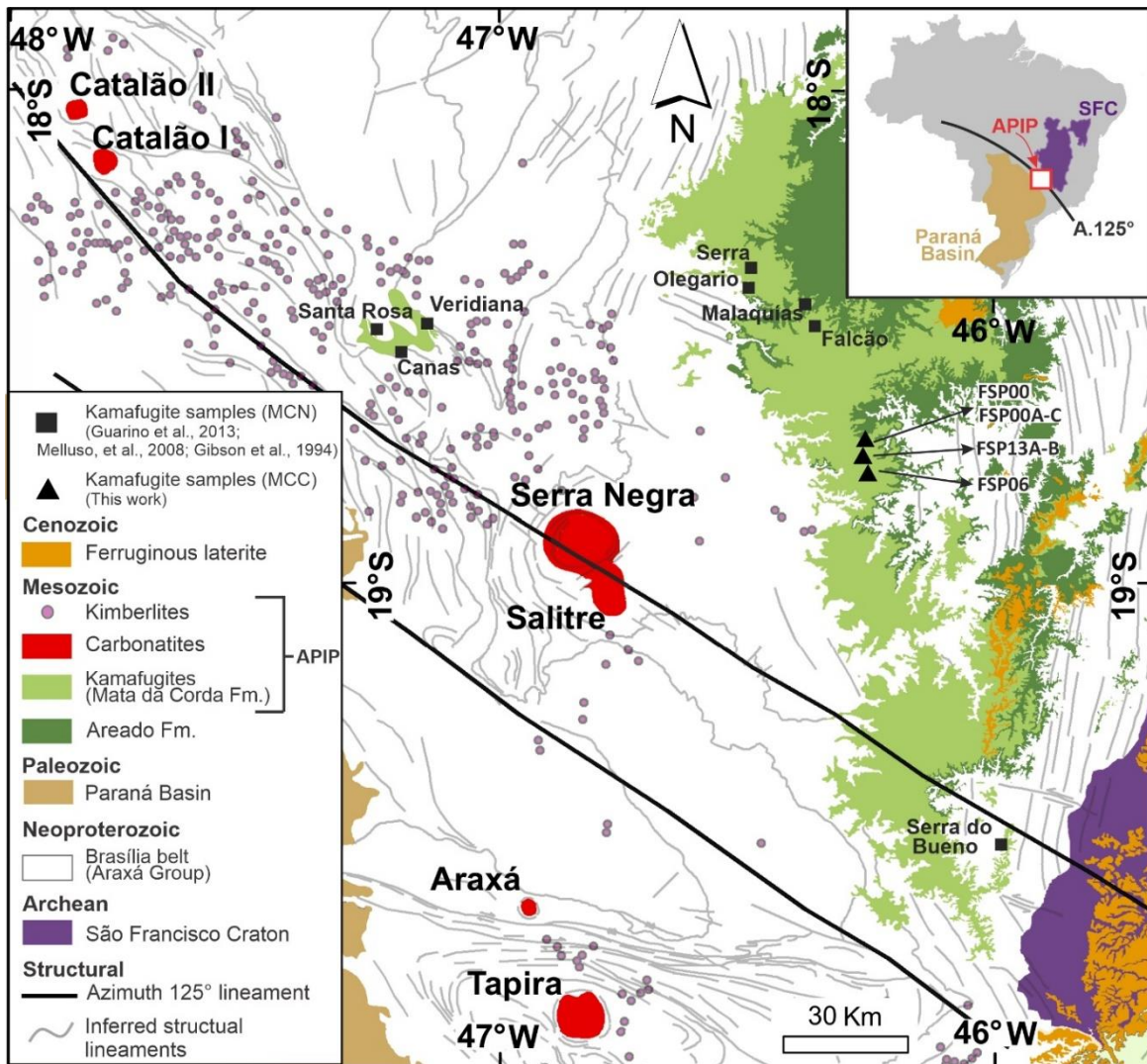


Fig. 4. Simplified geological map for the APIP showing the location of the Mata da Corda Formation and the neighbouring alkaline-carbonatite complexes, modified from the 1:1M cartographic sheets Belo Horizonte (SE-23) and Goiânia (SE22) of the Brazilian Geological Survey (CPRM 2020). Previous occurrences reported in the literature are also shown (e.g., Guarino et al., 2013; Melluso et al., 2008; Gibson et al., 1994). Abbreviations: APIP, Alto Paranaíba Igneous Province; A. 125°, Azimuth 125° lineament; SFC, São Francisco Craton. The sampling locations come from Patos de Minas and Lagoa Formosa, State of Minas Gerais, Brazil.

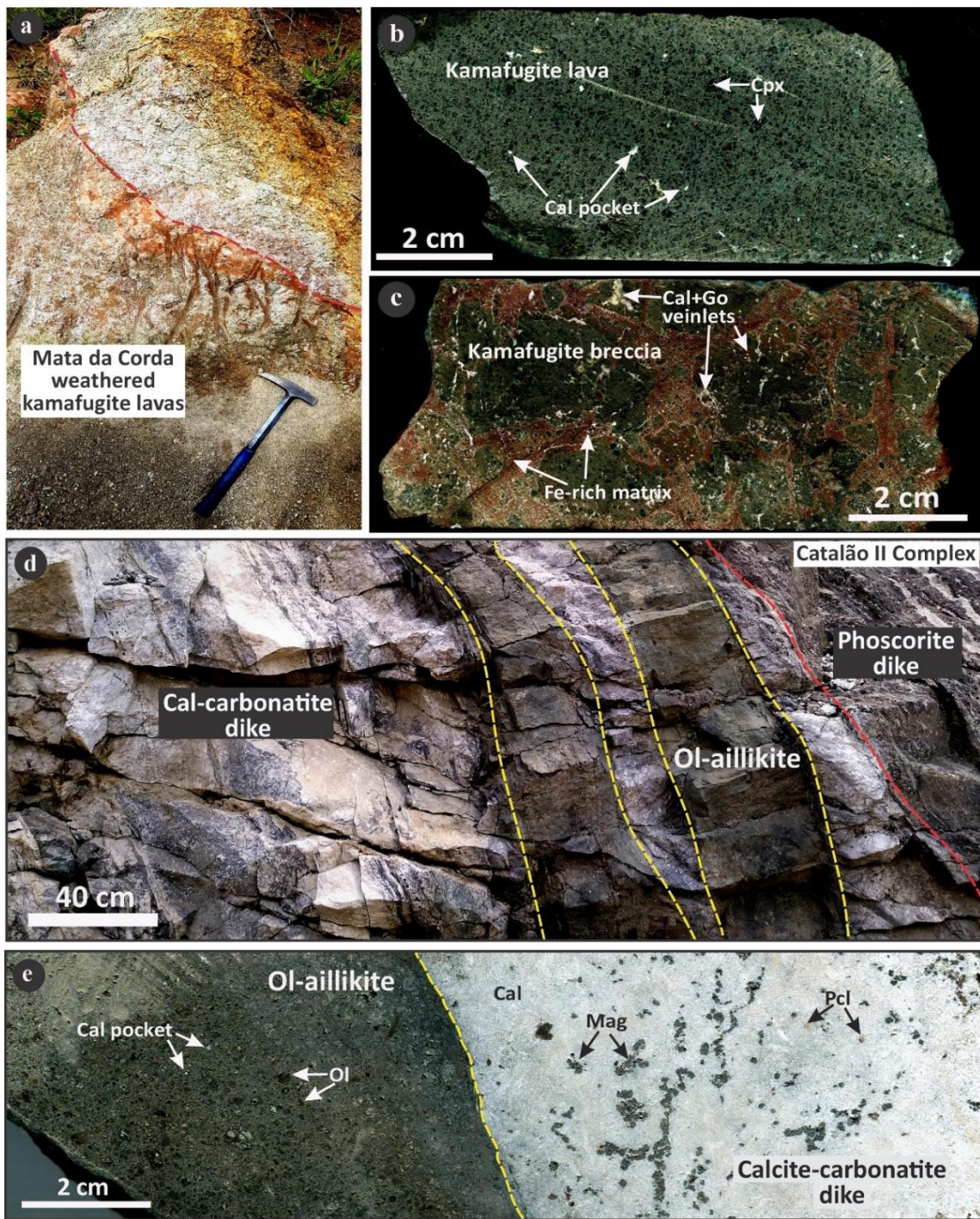


Fig. 5. (a) Outcrop of highly weathered kamafugite lavas in Mata da Corda Central. (b) and (c) correspond to drill cores of a kamafugite lava (sample FSP13-326) and a kamafugite breccia (sample PH01-139), respectively. (d) and (e) correspond to an outcrop and a borehole (sample RM024-339.5) respectively, of an olivine aillikite cutting a calcite-carbonatite dike from the Catalão II complex. Abbreviations: Cal, calcite; CPx, clinopyroxene; Go, gorceixite; Mag, magnetite; Ol, olivine; Pcl, pyrochlore.

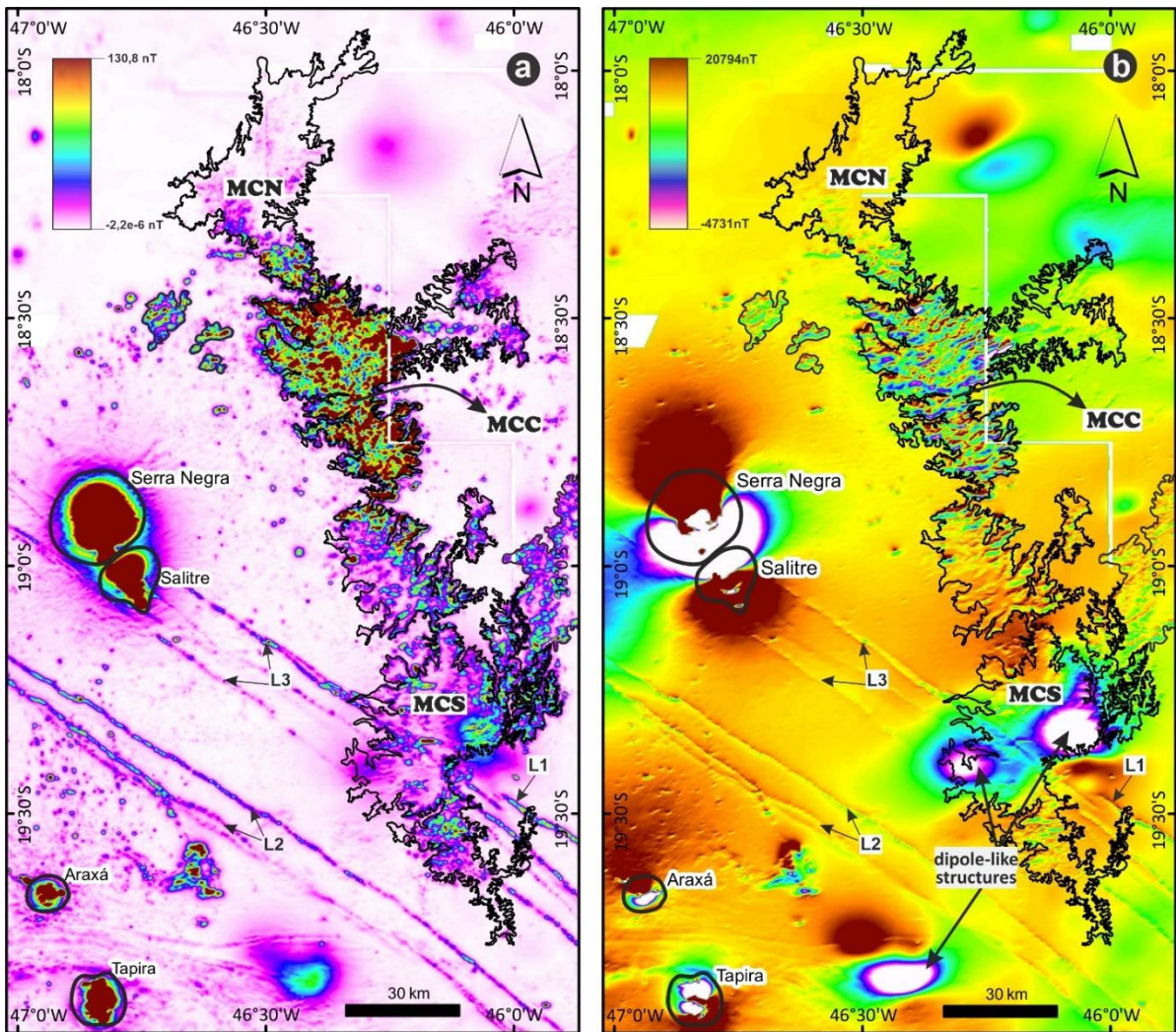


Fig. 6. (a) Analytical signal images from magnetic data, showing the magnetic fabric in the Mata da Corda Formation and the contours of the Serra Negra, Salitre, Araxá and Tapira alkaline-carbonatite complexes. In addition, the trace of the Azimuth 125° lineament and its three components L1, L2 and L3, according to (Rocha et al. 2014). (b) Reduction to the pole image, where it is observed that alkaline-carbonatite complexes have a dipole magnetic response. In addition, three dipoles are observed south of Mata da Corda, spatially associated with Azimuth 125° . Abbreviations: MCN, Mata da Corda North; MCC, Mata da Corda Central; MCS, Mata da Corda South.

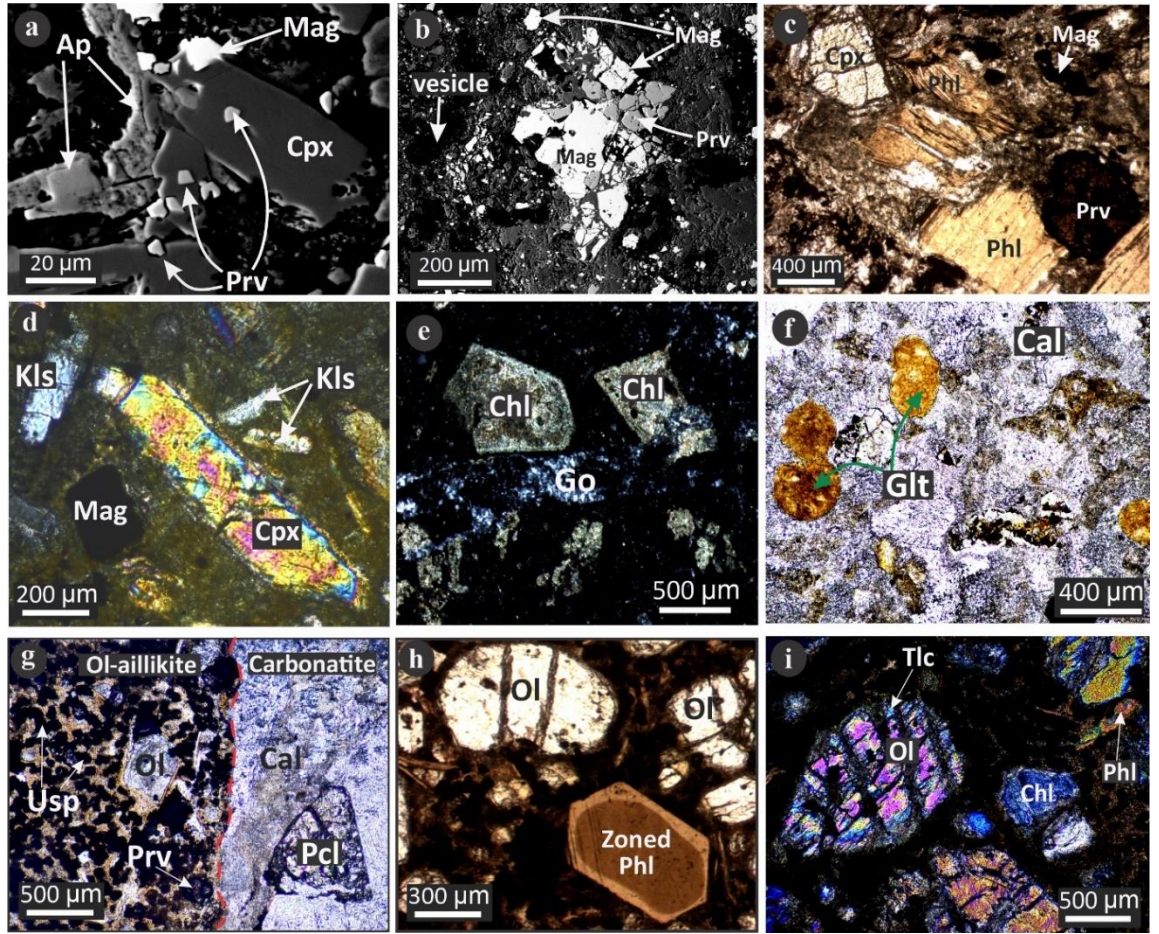
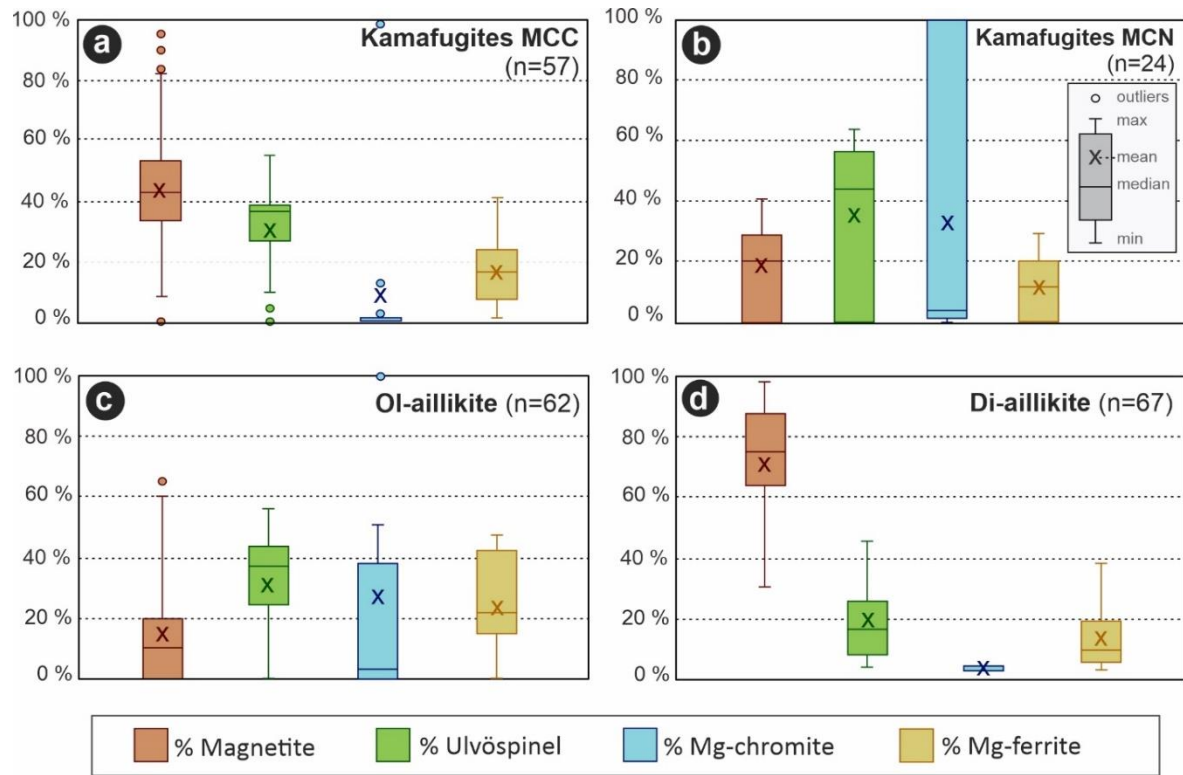


Fig. 7. Polarized-light and scanning electron microscope photomicrographs of kamafugite lavas (a-d) and kamafugite breccias (e-f) from Mata da Corda Central. G-I are olivine aillikite samples from the Catalão II Complex. (a) Fine-grained diopside and apatite with poikilitic texture, with perovskite and magnetite oikocrysts. (b) Perovskite and magnetite microcrysts set in an altered groundmass hosting vesicles. (c) Anhedral aggregates of phlogopite, clinopyroxene, and perovskite. (d) Kalsilite and clinopyroxene microcrysts. (e) Chlorite and gorceixite veinlets in a kamafugite breccia. (f) calcite veinlet with glauconite crystals. (g) Olivine aillikite rich in oxides, in a contact with a calcite-carbonatite with pyrochlore. (h) Zoned phlogopite and rounded olivine macrocrysts set in a magnetite-phlogopite rich groundmass. (i) partially altered olivines to talc set in a magnetite-phlogopite-rich groundmass. Abbreviations: Ap, apatite; Cal, calcite; Chl, chlorite; Cpx, clinopyroxene (diopside); Glt, glauconite; Go, gorceixite; Kls, kalsilite; Mag, Magnetite; Ol, olivine; Pcl, pyrochlore; Phl, phlogopite; Prv, perovskite; Tlc, Talc; Usp, ulvöspinel.



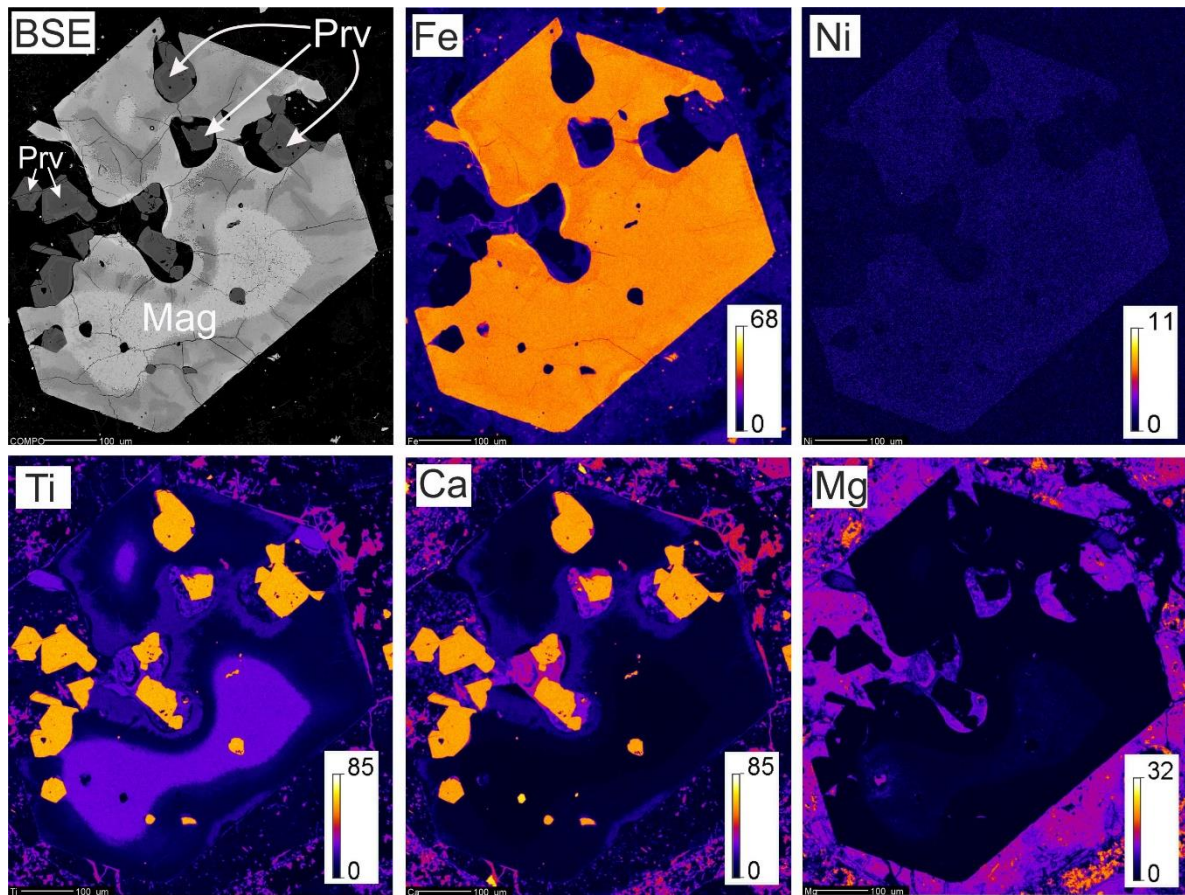


Fig. 9. WDS maps of Fe, Ni, Ti, Ca and Mg showing a poikilitic magnetite (Mag) with perovskite (Prv) oikocrystals of a kamafugite lava from Mata da Corda Central (sample PH03-059.5). Magnetite shows martitization in the broad darker rim in the BSE image (upper left), while perovskite shows variability of Ca and Ti between the different inclusions. The bar scale is in counts.

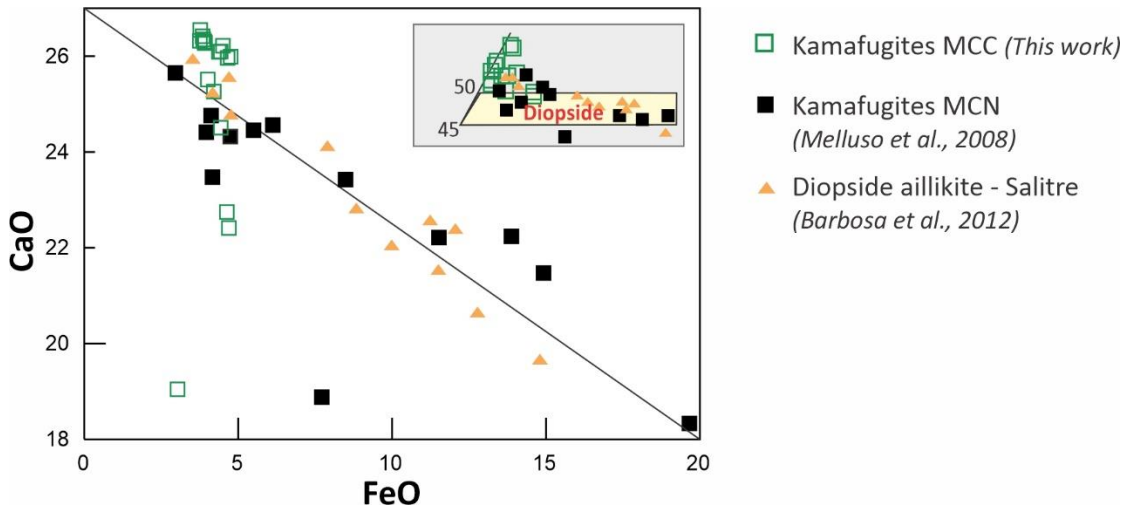


Fig. 10. FeO vs CaO diagram for clinopyroxene from APIP ultrapotassic rocks. The upper right box shows the classification corresponding to a Ca-rich diopside.

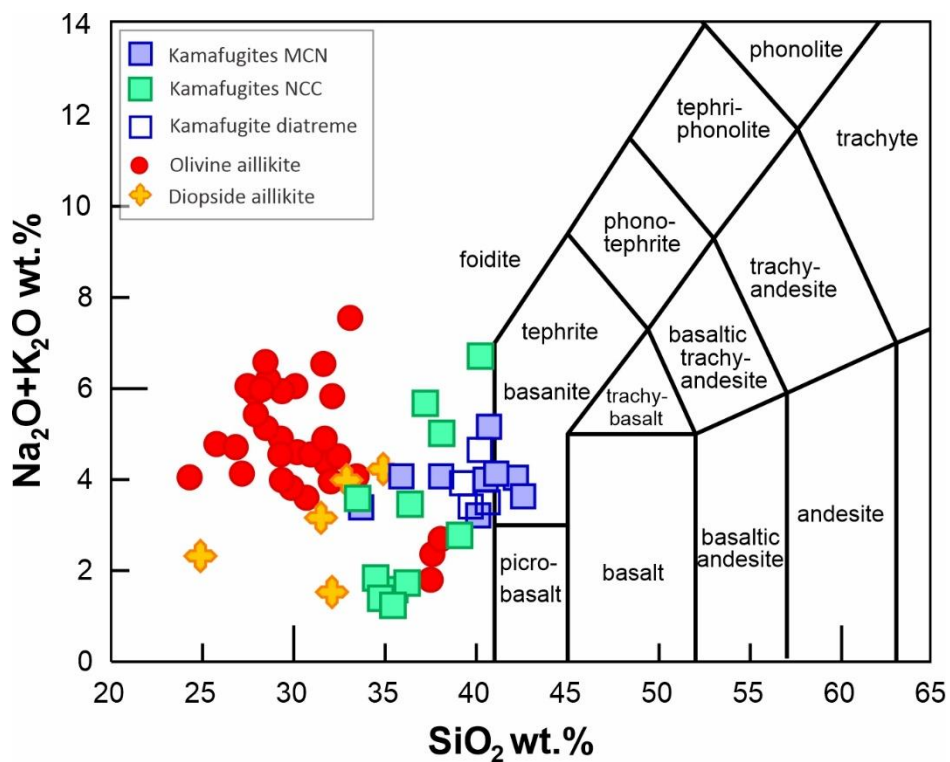


Fig. 11. Total alkali vs. Silica diagram (Le Maitre 2002) for the Mata da Corda kamaufugites. We also plot the chemical results of olivine aillikites from the Catalão II, Tapira and Serra Negra complexes with red circles and diopside aillikites of Salitre with yellow crosses (Supplementary Material 1) for comparison.

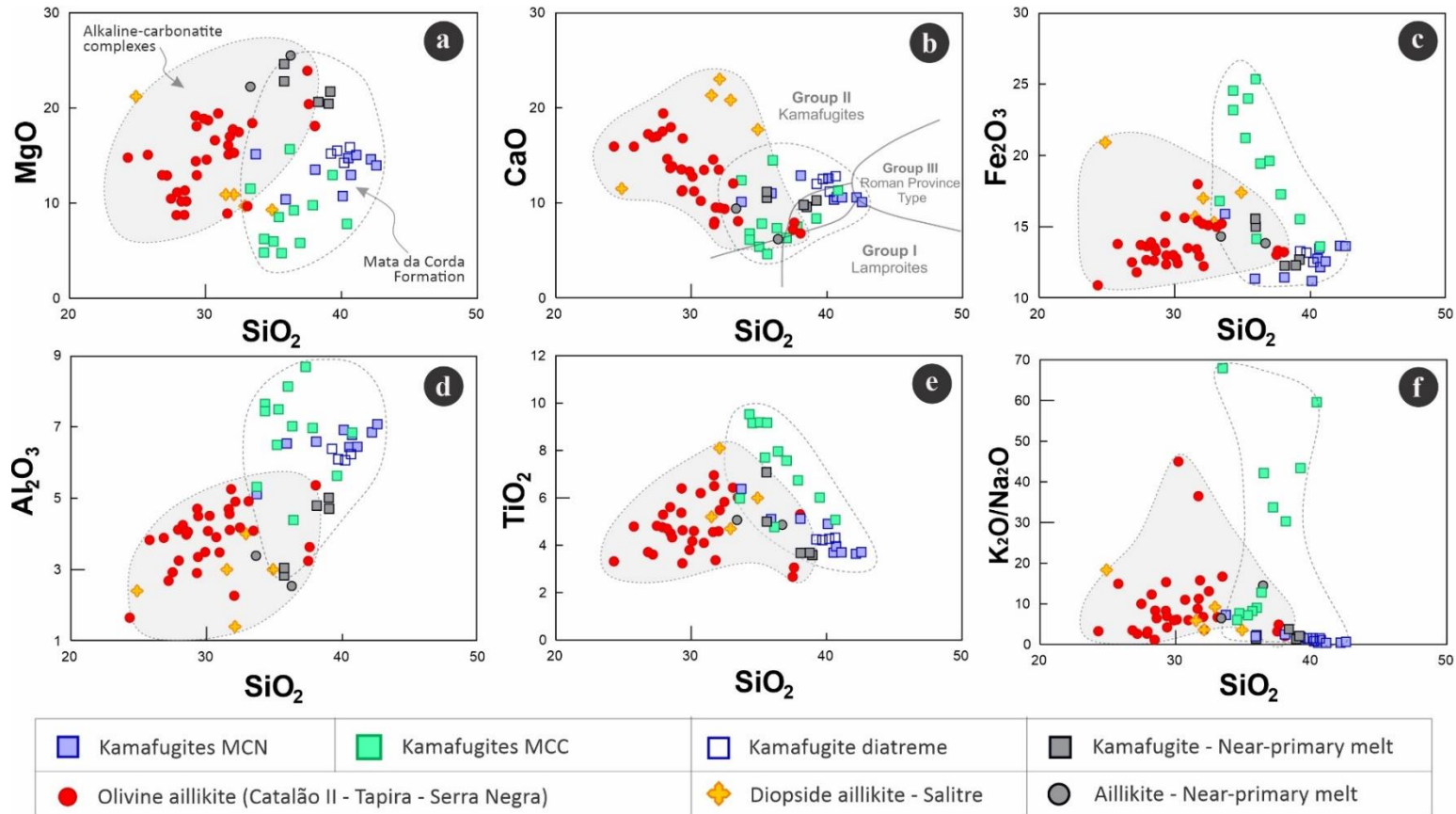


Fig. 12. Variation diagrams of selected major and oxides for Mata da Corda kamafugites in green and blue rectangles. We also plot the chemical results of olivine aillikites from the Catalão II, Tapira and Serra Negra complexes with red circles and diopside aillikites of Salitre with yellow crosses (Supplementary Material 1) for comparison. Black rectangles and circles correspond to near primary melt compositions for kamafugites and aillikites, respectively. The fields and lines in (b) correspond to SiO_2 vs. CaO classification fields for ultrapotassic rocks (Foley et al., 1987).

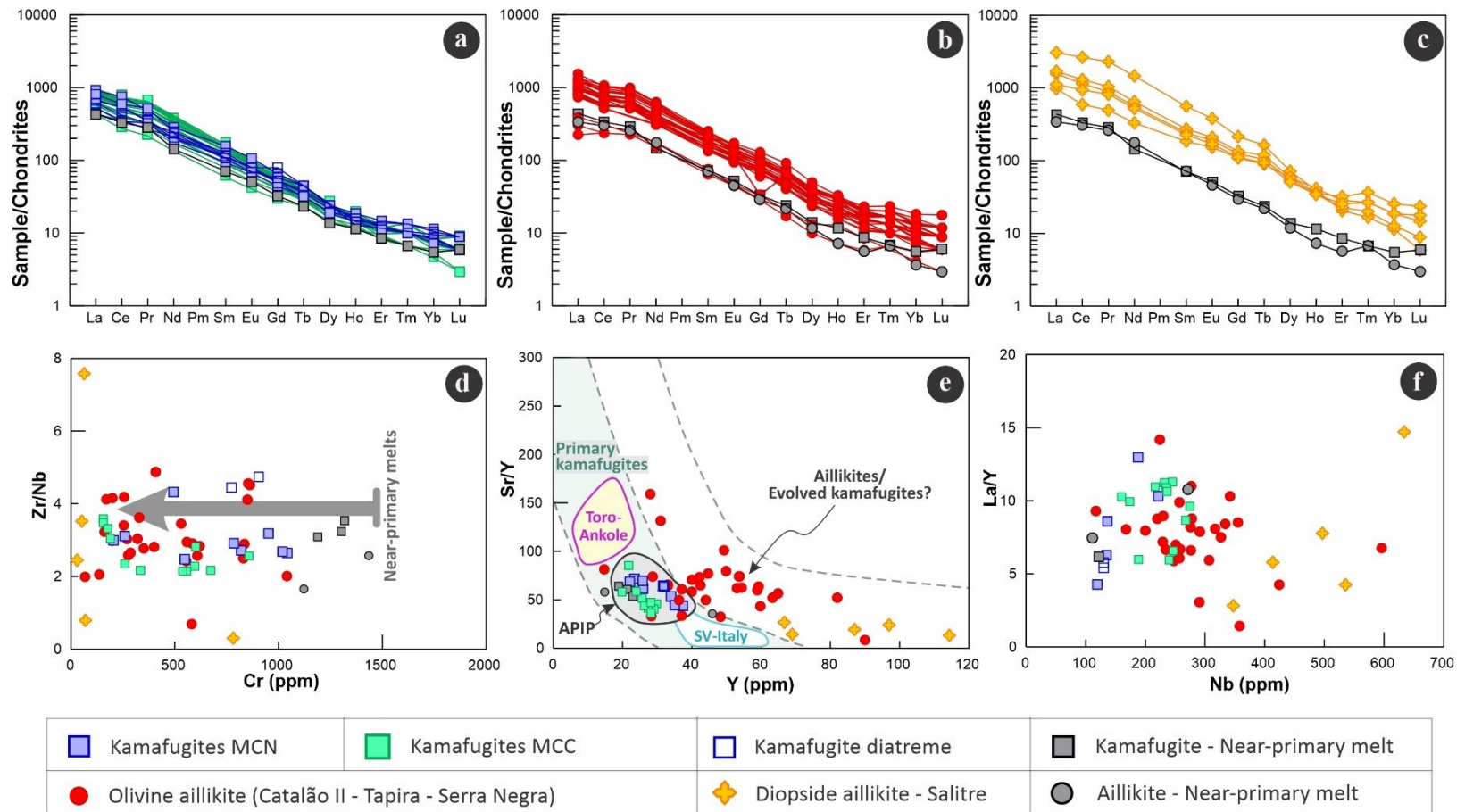


Fig. 13. (a), (b) and (c) correspond to REE-normalized spider diagrams (Nakamura, 1974), comparing the compositions of Mata da Corda kamafugites, olivine aillikites and diopside aillikites with APIP near-primary melts (Supplementary Material 1). (d) Cr (ppm) vs Zr/Nb diagram for all APIP potassic and ultrapotassic rocks. (e) Y (ppm) vs Sr/Y diagram, plotted for APIP, Toro-Ankole and San Venanzo (SV) kamafugites and aillikites, separating two fields for primary kamafugites and aillikites/(evolved kamafugites?). (f) Nb (ppm) vs La/Y diagram for APIP ultrapotassic rocks.

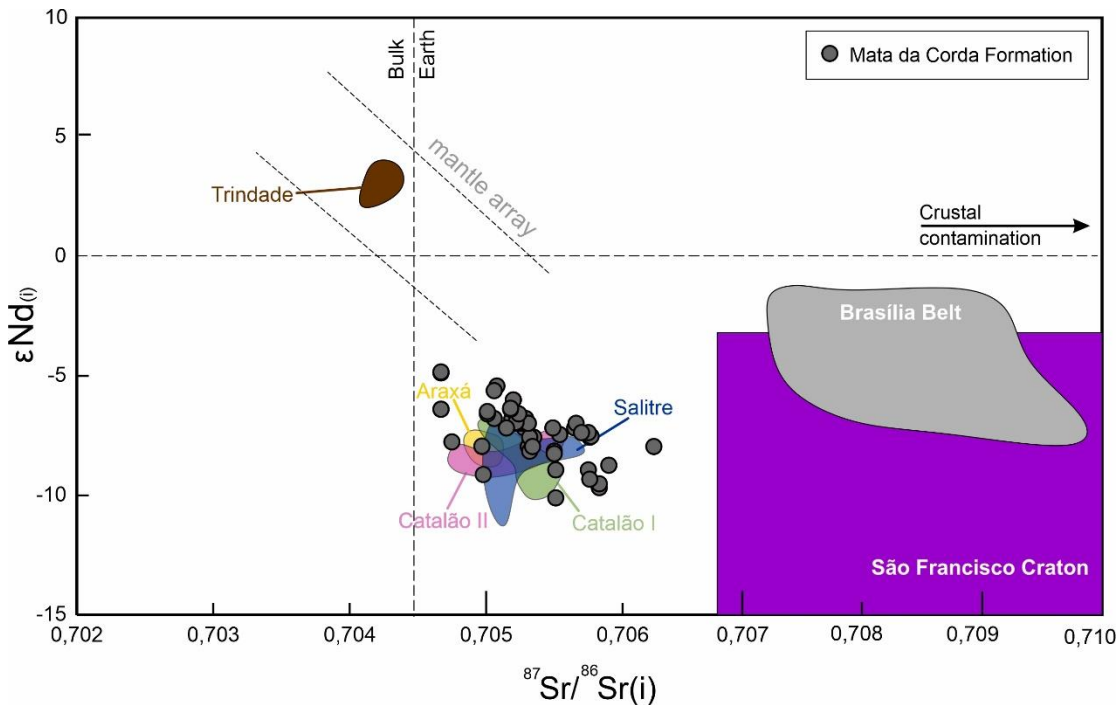


Fig. 14. Initial ϵNd vs $^{87}\text{Sr}/^{86}\text{Sr}$ isotopic diagram for the APIP localities compared to the Archean to Paleoproterozoic crust of the São Francisco Craton, the Neoproterozoic Brasilia Belt (APIP basement) and the Pliocene Ilha da Trindade (Trindade island) in central Atlantic. The compilation of isotopic APIP data is shown in the Supplementary Table 2. Isotopic composition of the São Francisco Craton and the Brasilia Belt from Carvalho et al. (2019). Isotopic composition of Trindade components from Halliday et al. (1992).

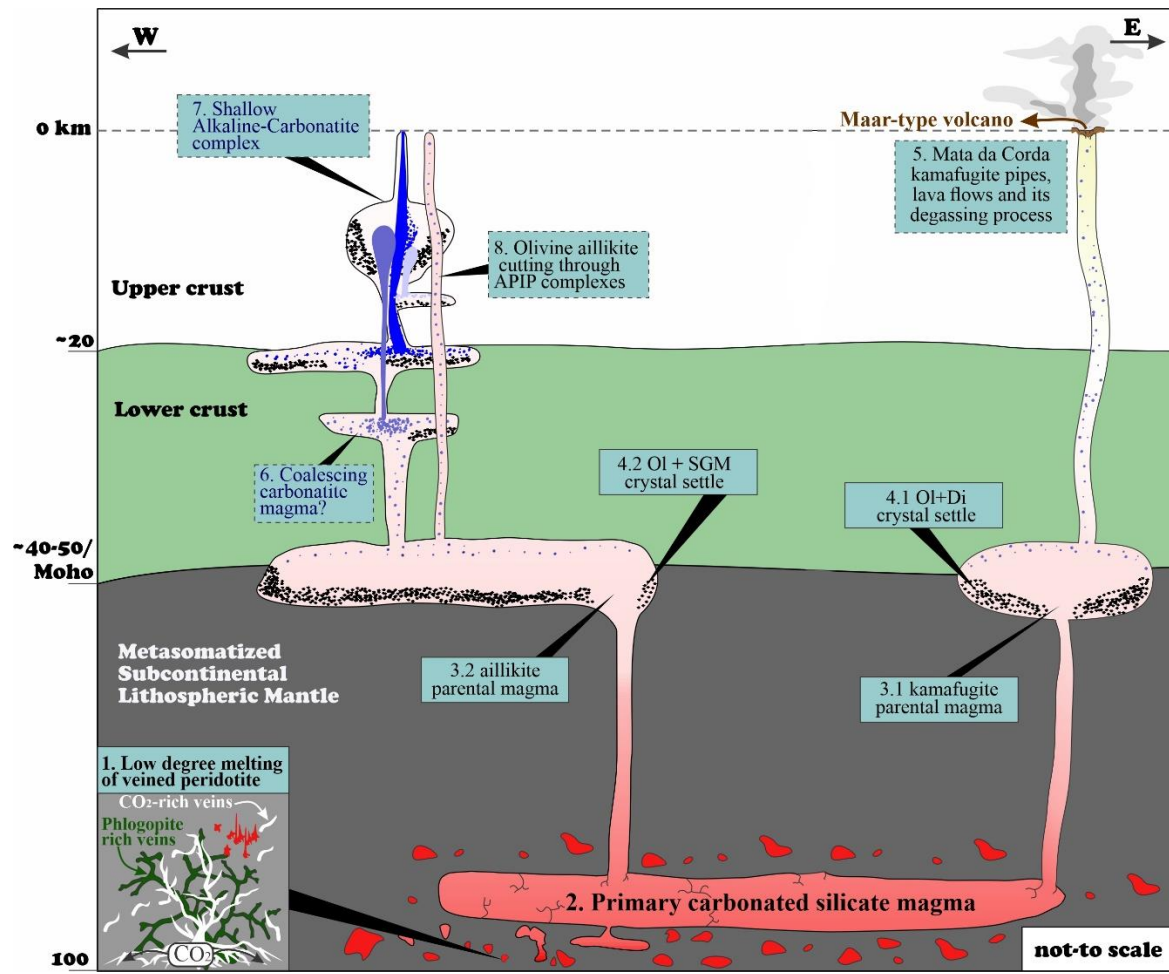


Fig. 15. Emplacement model for the magmatic rocks of the Mata da Corda Formation (steps 1 to 5) and for a generic APIP alkaline-carbonatite complex (steps 1 to 4.2 and 6 to 8). Relative depths of the upper and lower crust and the subcontinental lithospheric mantle correspond to the initial APIP depths proposed by Gibson et al. (1995). Abbreviations: Di, diopside; E, APIP east; Ol, olivine; SGM, spinel group minerals; W, APIP west.

**CAPÍTULO 3: MICROANALYTICAL INVESTIGATION OF K-RICH FENITES
FROM THE CATALÃO II ALKALINE-CARBONATITE COMPLEX IN
CENTRAL BRAZIL: IMPLICATIONS FOR ORE-FORMING PROCESSES
WITHIN THE WORLD'S LARGEST NIOBIUM PROVINCE**

Felipe Velásquez Ruiz*^{a, b}, Pedro Cordeiro^c, Martin Reich^{a, b}, Leonardo Lagoeiro^d,
Thomas Angerer^{e, f}

^aDepartment of Geology, FCFM, University of Chile, Santiago, Plaza Ercilla 803, Chile.

^bMillennium Nucleus for Metal Tracing Along Subduction, FCFM, University of Chile, Santiago, Chile

^cMining Engineering Department, Pontifical Catholic University of Chile, Santiago, Chile

^dDepartment of Geology, Universidade Federal do Paraná, Curitiba, Brazil

^eInstitute of Mineralogy and Petrography, University of Innsbruck, Austria

^fInstitute of Earth Sciences, Department of Petrology and Geochemistry, University of Bonn, Germany

Submitted to:
Journal of Geochemical Exploration

*Corresponding Author:

E-mail address: fevelasquezru@gmail.com (F.V. Ruiz).

3.1. ABSTRACT

Alkaline-carbonatite complexes are the main source of critical raw materials such as niobium (Nb) and rare earth elements (REE), which concentrate through a combination of magmatic and hydrothermal processes. These systems typically occur in close spatial connection with altered country rocks resulting from metasomatic alteration by exsolved K-Na-rich fluids, a process known as fenitization. Thus, the association between Nb-REE-rich carbonatites and fenites provides a unique opportunity for the investigation of hydrothermal alteration processes leading to critical metal enrichment. In this study, we focused on K-rich fenites associated with a shallow dike swarm system in the Boa Vista niobium deposit, the second-largest global producer of Nb, which is hosted within the Catalão II alkaline-carbonatite complex in Central Brazil. We used a combination of micro-analytical techniques including EBSD, EMPA, and μ -EDXRF to unravel the complex micro-textural features of the fenites. Our data suggest that alkaline fluids exsolved vigorously from the carbonatite melts upon dike emplacement and pervasively metasomatized the country rocks, forming a melanocratic proximal fenite (phlogopite), and distal fine-grained orthoclase-phlogopite-calcite fenites. Fluid alteration mobilized soluble cations (K, Fe, Mg, Ba, and Sr) plus S and OH⁻, whereas Nb and REE were retained in the carbonatite dikes. The consistent dike-orthogonal orientation of metasomatic phlogopite and orthoclase grains in the proximal fenite, determined by EBSD, suggests that newly formed metasomatic minerals precipitated from the fenitizing fluids along the flow path. These orientations differ from the isotropic textures defined by primary (magmatic) minerals like pyrochlore, tetraferriphlogopite, dolomite, and calcite. However, and despite the microstructural differences between magmatic and hydrothermal phlogopite, their mineral chemistry is similar, suggesting that fenites are almost synchronous to the emplacement of carbonatites. These data indicate that fenites provide a rich archive of alkali-rich fluid infiltration around Nb-REE-rich carbonatite intrusions.

Keywords: fenite; metasomatism; niobium; carbonatite; phoscorite; Catalão II Complex.

3.2. INTRODUCTION

Fenites are alkali metasomatic rocks composed of highly variable assemblages including K-feldspar, albite, alkali pyroxene, phlogopite, and alkali amphibole. These rocks are formed by alteration—or fenitization—from hydrothermal fluids derived from cooling alkaline magmas or carbonatite intrusions. Fenitizing fluids exsolve from evolved magmas in alkaline-carbonatite complexes can form niobium (Nb)- and rare earth element (REE)-rich micro-mineral assemblages in the country rocks (Elliott et al., 2018). Therefore, metasomatic aureoles are markers of infiltration of alkali-rich fluids around alkaline-carbonatite intrusions and hold potential for the exploration of critical or strategic mineral resources, key for current and emerging technologies (Mudd et al., 2017; Werner et al., 2017).

The term *fenite* was first proposed by Brögger (1921) to describe the metasomatic country rocks of the Fen carbonatite complex, in Norway, but according to the International Union of Geological Sciences (IUGS), it defines as a metasomatic rock associated with both carbonatites and alkaline rocks (Le Maitre, 2002). Therefore, fenitization encompasses all metasomatic processes that involve an alkaline-carbonatite intrusion and its country rock (Morogan, 1994; Le Bas, 2008). A possible classification of fenite uses whole-rock K/Na to distinguish between sodic, intermediate, and potassic endmembers (Verwoerd, 1963). For example, sodic fenites are found in the giant Bayan Obo REE-Nb-Fe deposit in Inner Mongolia, China (Fan et al., 2014; Le Bas, 2008; Liu et al., 2018; Yang and Le Bas, 2004) and also in the Il'mensky-Vishnevogorsky complex in Russia (Nedosekova, 2007), where alkaline amphibole and pyroxene occur within the surrounding metasomatic aureoles (Elliott et al., 2018). Potassic fenites, on the other hand, can contain up to 90% K-feldspar (Elliott et al., 2018); however, an addition of Mg produces phlogopitization of the K-feldspar. Phlogopite-rich fenites can be found at the Cargill complex in Canada, where an intense phlogopitization metasomatized the pyroxenite country rock (Gittins et al., 1975).

Despite the great importance of fenites, few studies are available and hydrothermal processes leading to fenitization are not fully understood. This is relevant not only because fenites are markers of the alkaline alteration that is seldom recorded in the main alkaline-carbonatite intrusions (Elliott et al., 2018), but also because fenites are closely related to economic Nb-REE mineralization and can be used as an exploration attribute to vector towards these key commodities.

The present study focuses on the K-rich fenites from the alkaline-carbonatite Catalão II complex in the Alto Paranaíba Igneous Province, Central Brazil (Fig. 16). This complex is the world's second-largest Nb producer after the Araxá Complex, with reserves above 14.5 Mt @ 1.52% Nb₂O₅ (Cordeiro et al., 2011; Palmieri, 2011). The K-rich fenites occurring in the Catalão II complex have not been studied previously and therefore are key to better understanding the interaction between alkaline-carbonatite magma, exsolved fluids, and its host rocks and ultimately help explain the formation of the world's largest Nb province. This work aims to provide a comprehensive textural, chemical and microstructural characterization of the K-rich fenites in contact with Nb-mineralized and barren dikes in Catalão II using a combination of micro-analytical techniques. The spatial chemical distribution of various elements in these rocks was determined by micro-X-ray fluorescence (μ -EDXRF) imaging and their microstructures were detailed using electron backscatter diffraction (EBSD) techniques. Electron microprobe analysis (EMPA) was used to constrain the major and minor element composition of K-rich mineral phases such as phlogopite, tetraferriphlogopite, and orthoclase, which are ubiquitous minerals with complex textural relationships. Finally, we explain the observed micro-textural and compositional differences and relate the Nb-mineralizing carbonatite event to the formation of proximal and distal fenite haloes.

3.3. GEOLOGICAL SETTING

The Late Cretaceous Alto Paranaíba Igneous Province (APIP) comprises carbonatite, phoscorite, and alkaline magmatic series in a variety of plutonic, sub-volcanic, and volcanic igneous forms (Fig. 16; Gibson et al., 1995). The APIP covers an area of 25,000 km² along the NE margin of the Paraná Basin, where the Neoproterozoic Brasília Belt crops out as metasedimentary and metavolcanosedimentary sequences (Almeida et al., 1981; Silva et al., 2020). This province encompasses kamafugite lavas and breccias of the Mata da Corda Formation (Brod et al., 2000; Velásquez Ruiz et al., 2022) and associated ultrapotassic plugs, in addition to hundreds of kimberlite plugs (Guarino et al., 2013) and six main alkaline-carbonatite complexes, named Catalão I, Catalão II, Serra Negra, Salitre, Araxá and Tapira (Fig. 16). These alkaline-carbonatite complexes were formed as a result of diverse carbonatitic and silica undersaturated magmatic pulses that took place from ~90 to 70 Ma (Conceição et al., 2020; Guarino et al., 2013) and generated important phosphate resources currently under production, with the exception of Serra Negra. Moreover, the Araxá, Catalão I, and Catalão II complexes host the world's largest pyrochlore-related (Na, Ca)₂Nb₂O₆(OH, F) niobium reserves, accounting for more than 80% of the world's current production of the metal. Additionally, these complexes host underexplored resources of rare earth elements, titanium, and vermiculite, rendering the APIP a giant polymetallic province (Cordeiro et al., 2011; Ribeiro et al., 2014).

Among these occurrences, the Catalão II complex (Palmieri, 2022) offers a unique opportunity to study carbonatite-related magmatic and carbohydrothermal processes because it is the only location within the APIP where mining operations are developed at the carbonatite-country rocks contact. The southern plug of the Catalão II complex, named Catalão II South (Fig. 17), is composed of three Nb-rich phoscorite and carbonatite dike swarms—Marcos, Boa Vista and Morro do Padre—hosted within fenitized country rocks. Five main lithotypes configure the magmatic and post-magmatic rocks of Catalão II South, which include: (1) calcite carbonatite dikes, often containing pyrochlore mineralization, (2) ultramafic lamprophyres (aillikites; Velásquez Ruiz et al., 2022), (3) pyrochlore-bearing magnetite-apatite-tetraferriphlogopite phoscorite dikes, (4) late-magmatic REE-rich carbonatite veins (carbothermal veins), with variable amounts of pyrochlore, and (5) fenites associated with all previous lithotypes. Of notice is the absence of olivine in all phoscorites related to the niobium mineralization, as also observed in the Catalão I niobium deposits (Cordeiro et al., 2011)—hence the tetraferriphlogopite phoscorite nomenclature in contrast with the classic olivine phoscorites.

The spatial association of carbonatites and fenites in Catalão II South and the excellent outcrop exposures produced by mining activities makes it an ideal location to investigate late magmatic and metasomatic processes.

3.4. METHODS

Fenite samples were collected from four boreholes (RM024, RM025, RM032 and PCBV), drilled from the pit of the Boa Vista Nb mine in the Catalão II South plug (Fig. 17). Sampling strategy was focused on collecting specimens of both calcite carbonatite dikes—which contain phlogopite and tetraferriphlogopite—and its associated phlogopite-orthoclase fenite. Five representative samples of the calcite carbonatite dikes and the fenitized country rocks were selected. Additionally, samples from other lithologies containing magmatic and late-magmatic phlogopites and tetraferriphlogopites were collected as follows: one aillikite, one apatite-rich phoscorite, one magnetite-rich phoscorite and one carbothermal vein.

The samples show various degrees of fenitization and thus were studied in detail using a combination of polarized light microscopy, scanning electron microscopy (SEM), electron back-scattered diffraction (EBSD), micro-energy dispersive X-ray fluorescence spectrometry (μ -EDXRF), and electron microprobe analysis (EMPA). Microtextural and microstructural observations were carried out using a MIRA 3RM SCAN SEM in the Lactec Institute located at the Federal University of Paraná in Curitiba, Brazil. The SEM is equipped with secondary electron (SE), backscattered electron (BSE), energy dispersive spectrometry (EDS) and electron backscatter diffraction (EBSD) detectors. Analytical conditions for SEM observation were 20 kV of accelerating voltage, beam current of 4 nA, working distance of ~15 mm and a step size of 100 nanometers between the measurements. The EBSD data were acquired using the methodology explained by Taufner et al. (2021). Samples of a barren and mineralized calcite carbonatite dikes in contact with the proximal fenite were cut parallel to the length of the dike to obtain microstructural information of the dike-fenite interface (i.e., X-length, Y-width, Z-depth of dike). EBSD data focused on distinguishing between magmatic vs. metasomatic phlogopite and orthoclase, where the (001), (010) and (100) crystallographic planes were used in the inverse pole figure set, parallel to the above-mentioned SEM X, Y and Z axes. In addition, the crystallographic directions of calcite, dolomite, apatite, magnetite and ilmenite within the barren and mineralized calcite carbonatite dikes were analyzed.

Two representative samples of calcite carbonatite dikes in contact with fenitized country rock from the Boa Vista Nb mine were chemically mapped using a Bruker M4 Tornado energy-dispersive micro-X-ray fluorescence (μ -EDXRF) spectrometer at the Institute of Mineralogy and Petrography, University of Innsbruck. The polychromatic beam was focused by a polycapillary lens, giving a spot size of 17 μm at 17.48 keV (molybdenum K α). The analysis was carried out with a Rh tube and two Si-drift energy dispersion detectors, at 20 mbar vacuum, 50 kV and 600 nA. The resolution of the acquired maps is set to $50 \times 50 \mu\text{m}$, and they were obtained with a dwell time per pixel of 50 ms. The values of the gray pixels in the element maps are comparable to the integral of the spectral region around the X-ray energy of the studied area (of the L α or K α lines). The chemical distribution of K, Mg, Nb and P are shown with different colors. Furthermore, additional maps for the elements Al, Ba, Ce, Fe, S, Si, Ti, Y, and Zr are shown in SD1.

Wavelength-dispersive spectrometry (WDS) analysis was carried out using a JEOL JXA 8200 electron microprobe at the Regional Center for Technological Development and Innovation (CRTI), Universidade Federal de Goiás, Goiania, Brazil. Microprobe analysis was focused on the potassium-rich magmatic and metasomatic minerals, such as phlogopite, tetraferriphlogopite and orthoclase, for the five lithotypes described from the Boa Vista mine (N=145 analyses). The analyses were performed using an accelerating voltage of 15 kV, a beam current of 20 nA, and a beam spot size of 5 μm . A counting time of 20 seconds was used for all elements analyzed. Synthetic and natural mineral standards of silicates were used for calibration. EMPA results and technical specifications of the standards used are provided in SD2.

3.5. RESULTS

3.5.1. Textures and mineralogy of K-rich fenites

In the Boa Vista mine, fenites occur in two main forms, i.e., as pervasive fenite alteration of the basement rocks associated with intense calcite veinlets (Figs. 18a & c), and as fenite haloes closely circumscribed to the mineralized (Figs. 18b & d) and barren (Fig. 18e) calcite carbonatite dike swarms. The fenitized basement rocks comprise silicate-rich lithotypes from the Neoproterozoic Brasilia belt (Silva et al., 2020) and correspond mainly to amphibolites and metarhyolites (Navarro et al., 2013). The basement rock foliation marked by amphiboles (such as hornblende and hastingsite; Navarro et al. 2013) and deflected albite—that locally display NNW orientation—is cut obliquely with respect to the carbonatite intrusion.

The mineralized and barren calcite carbonatite dikes have a highly variable thickness, from metric to decimetric (Fig. 18b), to cm-scale dikes (~1 cm; Fig. 18d). All the calcite carbonatite dikes intruding basement rocks are characterized by the development of fenite haloes, melanocratic with respect to the mesocratic (fenitized) basement rocks due to the higher content of phlogopite (Figs. 18d-e). Since calcite carbonatite dikes lack a clear structural orientation, the occurrence of the fenite haloes is predetermined by the dike structure.

The fenite haloes are texturally divided into two types: (1) a proximal fenite with a phlogopitite halo at the dike-basement rock contact, characterized by fine-grained metasomatic phlogopite (Figs. 18d, e; Fig. 19f), and (2) a distal fenite of variable thickness (Fig. 18d), but generally thicker than the proximal phlogopitite, composed of fine-grained (< 200 μm), phlogopite, orthoclase and calcite (Fig. 19b, d) and subordinate ilmenite and titanite (< 2%). Moreover, the distal fenite has a marked orientation by the fine-grained phlogopite (Fig. 19b, f), and its orientation is almost orthogonal with respect to the dike (Fig. 18d).

In contrast to the oriented fine-grained metasomatic phlogopites in the fenites, the non-oriented magmatic phlogopites (Figs. 19a, c) contained within the calcite carbonatite dikes are coarse-grained (>1 mm) and zoned, with phlogopite cores and a tetraferriphlogopite rims (Fig. 19c, e). Furthermore, magmatic phlogopite and tetraferriphlogopite are associated with coarse-grained

apatite, calcite, dolomite, pyrochlore, magnetite, and ilmenite, as shown in Figures 19a, c and e. Magmatic phlogopite from other Boa Vista lithologies—i.e., phoscorites, aillikites and carbothermal veins—show restricted fenitization and were not included in this study.

3.5.2. Chemical mapping of K-rich fenites and associated carbonatites

Composite chemical maps obtained by μ -EDXRF show the distribution of K, Mg, P and Nb of fenites developed along the barren and mineralized calcite carbonatite dikes, showing the proximal and distal haloes (Fig. 20). Additionally, the distribution of other elements such as Al, Ba, Ce, Fe, S, Si, Ti, Y and Zr is presented in the SD1.

Figure 23a shows a barren calcite carbonatite dike intruding the fenitized basement rock. As seen in Figure 23c, potassium is depleted and unevenly distributed in the fenitized basement, i.e., mostly related to orthoclase. The K content increases progressively from the fenitized basement to the distal and the proximal phlogopite halo; the highest K concentrations are observed within the proximal fenite halo (Fig. 20c). Magnesium, on the other hand, is restricted only to the proximal fenite halo (Fig. 20e), attributed to the formation of fine-grained phlogopite. Despite the absence of pyrochlore within the barren calcite carbonatite dikes, Nb is commonly detected, mainly associated with carbonates (Fig. 20g). Finally, elements such as Al, Fe and Si are mostly associated with amphiboles occurring in the fenitized basement rocks, as shown in SD1. Minor elements such as Ba and S are abundant in the distal fenites, attributed to the formation of barite (SD1).

The mineralized calcite carbonatite dike in Figure 23b is rich in K (Fig. 20d), which is mostly due to the formation of coarse-grained phlogopite and tetraferriphlogopite in comparison to barren one (Fig. 20c). In the mineralized calcite carbonatite dikes, the K content is also higher within the fenitized basement, due to a higher abundance of phlogopite and orthoclase in the distal fenite. Furthermore, mineralized calcite carbonatite dikes contain high P associated with apatite (Fig. 20h), and when compared with the barren calcite carbonatite dikes, Nb is more abundant within the mineralized dikes, mainly associated with coarse-grained pyrochlore (Fig. 19h). Finally, Ti and Zr do not show a clear mineralogical control because both elements are found in the calcite carbonatite dikes and basement rocks (SD1). Cerium and Y are more abundant within the mineralized calcite carbonatite dikes, and are associated with carbonates and pyrochlore (SD1).

3.5.3. Mineral chemistry of K-bearing silicates

Representative electron microprobe analyses of phlogopite from the Boa Vista mine are reported in Table 1. This mica is the focus of analysis because phlogopite is abundant in the distal and proximal fenites, and is also a common magmatic mineral in the calcite carbonatite dikes and other primary lithotypes (e.g., phoscorites, aillikites, carbothermal veins). All EMPA data are presented in SD2.

Phlogopite in the calcite carbonatite dikes:

The analyzed micas in the calcite carbonatite dikes correspond to phlogopite grains with zoned textures defined by phlogopite cores and tetraferriphlogopite rims (Figs. 19c; 21a). The EMPA data show a narrow $\text{Si}_{(\text{iv})}$ compositional range in the phlogopite cores, from 2.73 to 2.96 a.p.f.u., which overlaps the range of the tetraferriglogopite rims (2.74 to 2.89 a.p.f.u.) (Fig. 21a). Moreover, there is a wide range for the compositions of tetrahedral sites such as $\text{Al}_{(\text{iv})}$ and $\text{Fe}^{3+}_{(\text{iv})}$ (Table 1). For instance, phlogopite cores are enriched in $\text{Al}_{(\text{iv})}$ (Fig. 21b), where the composition of Al varies between 1.12 to 12.13 wt.% Al_2O_3 (0.09 to 1.06 a.p.f.u.), whereas tetraferriphlogopite rims are depleted in $\text{Al}_{(\text{iv})}$, with concentrations between 0.03 to 6.83 wt.% Al_2O_3 (0 to 0.57 a.p.f.u.). Conversely, tetraferriphlogopite rims are enriched in $\text{Fe}^{3+}_{(\text{iv})}$, with values varying between 0.53 to 1.24 a.p.f.u., while phlogopite cores are depleted in $\text{Fe}^{3+}_{(\text{iv})}$ (0.04 to 1.17 a.p.f.u.; Fig. 21c).

The EMPA data for Ti, Mn and K for both phlogopite and tetraferriphlogopite show narrow ranges (Figs. 21d to f). Phlogopite cores have TiO_2 contents between 0 to 2.93 wt.% TiO_2 (0 to 0.17 a.p.f.u.), MnO concentrations between 0 to 0.34 wt.% (0 to 0.02 a.p.f.u.), and K_2O contents between 10.5 to 12.3 wt.% (0.98 to 1.23 a.p.f.u.). Tetraferriphlogopite rims, on the other hand, have TiO_2 values between 0 to 0.26 wt.% (0 to 0.01 a.p.f.u.), MnO contents between 0 to 0.15 wt.% (all values around 0 a.p.f.u.), and K_2O concentrations between 11 to 11.8 wt.% (1.00 to 1.07 a.p.f.u.). The Mg-number ($\text{Mg}/(\text{Mg}+\text{Fe}^{2+})$) is higher in the phlogopite rims, with values around 1, when compared to the tetraferriphlogopite cores (0.65 to 1; Fig. 21f).

Phlogopite in the fenites:

Micas from proximal fenites have a phlogopite composition, while the distal micas have an intermediate composition between phlogopite and annite (Fig. 21a). Phlogopites in the proximal fenites have almost the same major element composition than phlogopite cores from calcite carbonatite dikes (Figs. 21b, c, 21d, f). In contrast, significant differences in composition are detected in annites from the distal fenites. For example, the most depleted Si contents are observed in the distal fenites, varying from 2.57 to 2.95 a.p.f.u. In addition, annites from distal fenites have the highest Al values, from 11.1 to 17.4 wt.% Al_2O_3 (1 to 1.43 a.p.f.u.); also, they show depleted values for Fe^{3+} , from 0 to 0.11 a.p.f.u. Annite in the distal fenites are characterized by high Ti, Mn and K concentrations, e.g., for ranging from 0.78 to 3.88 wt.% TiO_2 (0.05 to 0.22 a.p.f.u.), 0.29 to 0.38 wt.% MnO (0.01 to 0.02 a.p.f.u.) and 11 to 11.5 wt.% K_2O (1.07 to 1.14 a.p.f.u.). The Mg-number shows high values, varying between 0.32 to 0.69.

3.5.4. Microstructure of fenites

EBSM analyses were carried out to compare the global crystallographic directions of mineral phases associated with proximal fenites, with respect to primary mineral phases within the barren (Fig. 22a) and mineralized (Fig. 22b) calcite carbonatite dikes. The EBSM maps in Figures

22c and d show the orientations of all the mineral phases present in the barren vs. mineralized samples, at the dike-fenite boundary. Additionally, Figures 23 and 24 show four sets of inverse pole figures for key mineral phases such as phlogopite, calcite, apatite, and orthoclase.

The EBSD map of the barren dike shows that the coarse-grained mineral phases associated with the dike have random orientations (Fig. 22c) and are, thus, isotropic. The individual inverse pole diagrams in Figure 23 confirm crystallographic isotropy for coarse-grained primary calcite and phlogopite within the dike (Fig. 23a), while apatite has a strong alignment of the basal plane (0001) to the Y axis, which corresponds to the plane parallel to the wall dike. The (11̄20) and (12̄10) planes are parallel to the X and Z axes (Fig. 23a), perpendicular to the wall dike, which were not previously seen on the inverse pole figure. In contrast, the proximal fenite EBSD data show an overall orientation pattern that is mainly associated with the basal planes (001) of phlogopite (red) (Fig. 22c). The inverse pole diagrams for fine-grained phlogopite within the proximal fenite (Fig. 23b) shows a strong alignment of the basal plane (001) of phlogopite along the Z axis, which is orthogonal to the dike wall direction; longitudinal crystallographic planes (e.g., 100; 010) are parallel to the X and Y axes (Fig. 23b), corresponding to the length and width of the dike, respectively. Finally, orthoclase shows a preferential orientation of its plane (100) to the Y axis, also orthogonal to the dike wall (Fig. 23b).

The EBSD map of primary mineral phases associated with the mineralized dike (Fig. 22d) show areas of strong apatite concentration with a global predominance of the Z axis direction (associated with the basal plane 0001) also orthogonal to the dike wall. The individual inverse pole diagrams confirm this pattern (Fig. 24a) and show that (11̄20) and (12̄10) planes are parallel to the X axis. In addition, and similarly to what was observed in the barren dike, overall random crystallographic directions are observed for calcite, dolomite, magnetite, ilmenite and monazite-Ce (Fig. 22d, 9a). Unlike the barren dike, there are few orthoclase grains within the proximal fenite, however there is a strong tendency of the basal plane (001) of fine-grained phlogopite to orient along the Y-axis, while the longitudinal planes (e.g., 100, 010) are mostly random in orientation (Fig. 24b).

3.6. DISCUSSION

The microanalytical data of the K-rich fenites associated with mineralized and barren carbonatite dikes at the Boa Vista Nb mine provide new insights on the development of metasomatic textures at the carbonatite-base ment boundary. As described, the Boa Vista mine fenites occur as proximal and distal metasomatic haloes enveloping mineralized and barren calcite carbonatite dikes upon pervasive alteration of amphibolite and metarhyolite basement rocks. In this section, we discuss field observations and micro-analytical data (SEM, EMPA, μ -EDXRF, EBSD), and provide an interpretation for the observed micro-textural and compositional differences, which relate the formation of fenites to the Nb-mineralizing carbonatite event.

3.6.1. Fenitization associated with niobium mineralization

The Araxá Group represents the basement of the Catalão II Complex and includes amphibolites and metarhyolites with Na-K-rich mineral phases such as hornblende, hastingsite and albite (Navarro et al., 2013). However, and despite the presence of these minerals, the basement rocks have a low bulk content of alkalis to be the main source of potassium for fenitization. Previous studies of the Araxá Group indicate that amphibolites have an average of 0.78 wt.% K₂O and 2.08 wt.% Na₂O (Seer et al., 2001), while metarhyolites vary between 2.69 to 4.18 wt.% K₂O and 0.96 to 7.17 wt.% Na₂O (Piauilino, 2018). Therefore, it is likely that the development of phlogopite-bearing pervasive fenitization at Catalão II was highly dependent on the alkali budget from magmatic fluids and the system temperature and pressure (Elliott et al., 2018; Le Bas, 1987; Platt, 1996). The high proportion of phlogopite, orthoclase and calcite in proximal and distal fenites in the Boa vista Nb mine (Fig. 4) indicates that the original mineralogy of the Na-amphibole-rich basement was completely overprinted by the fenitization. Although textural and chemical data indicate that the K source probably comes from carbonatitic liquids, and despite that the basement is low in K₂O, the composition and porosity of the pre-fenitized basement may play an important role in development of metasomatism, where metarhyolites may be more reactive, having at least 2 wt.% of K₂O more than amphibolites.

The μ -EDXRF and EMPA data provides further insights about the K-rich metasomatic event that pervasively affected the basement at the Boa Vista mine (Fig. 20c, d). This event was likely the result of the intrusion of the carbonatite bodies (dikes) into the basement rocks, which formed the proximal and distal phlogopite-orthoclase fenite, plus calcite (Figs. 19b, d). Field observations show that the distal fenites developed over a few meters to up to hundreds of meters surrounding both the north and south plugs of the Catalão II Complex (Fig. 17). In addition to high K contents, large amounts of Mg and water (OH⁻) were necessary to form the widespread hydrothermal phlogopite in the fenites associated with both mineralized and non-mineralized carbonatite dikes (Fig. 20e, f). EMPA results show a higher K content in the proximal and distal fenites, when compared to phlogopites and tetraferriphlogopites from calcite carbonatite dikes (Fig. 21f). The formation of the pervasive proximal fenite, with phlogopites having a K₂O content ranging from 10.99 to 11.54 wt.%, and the formation of a metasomatic fine-grained orthoclase contents of up to Or₉₆ in the distal fenites (SD2), strongly suggest that the excess of K and Mg in the exsolved magmatic fluids were not retained within the calcite carbonatite dikes.

The elemental distribution within the carbonatite dikes suggests that there was a greater input of K along the mineralized structures, supporting a dominantly magmatic source for K and associated elements (Fig. 20d). This is in agreement with μ -EDXRF maps indicating that Nb is dominantly circumscribed to the carbonatite dikes (as well as REE, Ce and Y), i.e., incorporated within pyrochlore in the mineralized and barren calcite carbonatite dikes, respectively (Fig. 20g, h), thus showing that Nb is not mobilized into fenites. Other minor elements in the proximal and

distal fenites show a more mobile behavior, for example Ba occurs as barite within the proximal fenite (SD1). Despite that the budget of immobile elements such as Ti and Nb from the basement was probably low (i.e., 0.51-1.11 wt.% TiO_2 and 22-200 ppm Nb; Piauilino, 2018), the Ti present in the basement rocks likely responded to the fenitization by forming secondary fine-grained phlogopite in the distal fenites, which are characterized by a higher Ti content (up to 0.2 a.p.f.u.), compared to phlogopite from the proximal fenites and from the calcite carbonatite dikes (mainly with Ti contents close to 0 a.p.f.u.; Fig. 21d).

3.6.2. Textural analysis of magmatic and metasomatic phlogopites

The textures and chemistry of magmatic phlogopites within the carbonatite dikes are useful to explore the relative temporality of the magmatic intrusion with respect to the metasomatic stage of fenitization. As described, phlogopite grains within the carbonatite dikes are characterized by a phlogopite core and a tetraferriphlogopite rim (Fig. 19c). Previous studies in the alkaline-carbonatite complexes of Tapira and Catalão I and II have determined that the origin of the tetraferriphlogopite rim in zoned phlogopites may be either magmatic (Brod, 1999) or post-magmatic (Araújo, 1996). Brod et al. (2001), on the other hand, shows by means of EMPA that crystallization of tetraferriphlogopite is likely associated with primary crystallization of carbonatites, possibly during a late magmatic stage.

The EMPA results for the Boa Vista mine show that Fe^{3+} content range of metasomatic phlogopite in the proximal fenites (0 to 1.13 a.p.f.u., fig. 21c) overlap that of magmatic phlogopite cores from calcite carbonatite dikes, and are also similar to aillikites (SD2) considered parental of the alkaline-carbonate system (Brod et al. 2013). In contrast, the composition of tetraferriphlogopite rims presents noticeable differences when compared to both the phlogopite (magmatic) cores and the (metasomatic) proximal fenites (Fig. 21c). It is also observed that as the fenitization recedes, distal fenite micas have a composition closer to the Fe-rich biotite end-member (annite), losing Fe^{3+} and Mg the metasomatic micas and gaining Al and Fe^{2+} (Fig. 21) as they move away from the carbonate intrusion. Therefore, the strikingly similar chemistry observed between the (magmatic) phlogopite cores and the (metasomatic) phlogopite from proximal fenites could be an indicator that the early-stage carbonatite intrusion is almost synchronous with fenitization, or that possibly the carbonatitic intrusive event was so rapid that the chemistry of metasomatic phlogopites did not vary significantly from those of the magmatic phlogopites. The latter is in agreement with a catastrophic pressure release model for a low viscosity carbonatite magma ascent, emplacement and fluid exsolution, i.e., the “pneumatic jackhammer model” (Walter et al., 2021). In the light of this evidence, we distinguish two alternative possibilities to explain the genetic relation between the magmatic phlogopite cores and the metasomatic phlogopites in the proximal fenites: (1) The magmatic phlogopite cores would be xenocrysts representing earlier and, thus, Ti-richer compositions, whereas the tetraferriphlogopite borders represent in-situ crystallization from a more evolved carbonatite magma; (2) Alternatively, the exsolved alkaline fluid came out almost simultaneously with the intrusion of the carbonatite dikes, and promoted a pervasive proximal country-rock alteration that crystallized metasomatic phlogopites similar to magmatic ones. The

tetraferriphlogopite rims within the carbonatite dikes, on the other hand, indicate that the Al budget remained very low even after emplacement in Al-rich country rocks. Therefore, these rims represent a late magmatic event where country-rock assimilation by the residual melts was very, following the line proposed by Brod et al. (2001).

Studies in other alkaline complexes have indicated that the fenitization process is most likely rapid. For example, Skelton et al. (2007) proposed for fenitization of gneissic protolith in the Alnö complex in Sweden that the metasomatic reaction rate was significantly fast, with estimated timescales between 10^2 to 10^4 years. Based on this evidence, and taking into consideration textures and mineral chemistry, we propose that the fenitization process in the Catalão II complex was possibly also fast, and occurred simultaneously with the carbonatite intrusion. It is noted that between the proximal and distal fenite micas there are no visible compositional gaps, indicating that the fenitization was continuous and changes in the composition of the metasomatic micas are a function of the depletion of the element budget regarding the distance. These aspects will need to be evaluated in detail in future studies.

3.6.3. Fenite microstructure as a fluid flow indicator in the magmatic-hydrothermal window

The EBSD analyses provide insights into the use of fenite microstructure as a fluid flow indicator. As described in section 4.4, EBSD maps allow identifying crystallographic orientations of the metasomatic phlogopites in the proximal fenites, in relation to primary (magmatic) mineral orientation within the barren and mineralized calcite carbonatite dikes (Figs. 22-24).

The apatite crystals that are located close to the dike wall (Fig. 22d) mark the original direction of the carbonatitic magma flow (i.e., along the strike of the dikes), which is parallel to its basal axis (0001) (Figs. 23a, 24a). The EBSD results show evidence that the basal apatite axis (0001) is parallel to the dike wall direction for barren calcite carbonatite dikes (Fig. 23a), while the (11 $\bar{2}$ 0) and (12 $\bar{1}$ 0) axes are orthogonal to the dike wall, also showing the direction of the magma flow. These results are consistent with studies documenting magmatic flow directions in dikes using EBSD methods (Chadima et al., 2009; Romeo et al., 2007). Furthermore, inspection of the EMPA composition of phlogopites in the carbonatite dikes point to the Al by Fe³⁺ substitution in tetrahedral sites (Fig. 21b, c), while there are two main exchanges in octahedral sites, Mg by Ti (Fig. 21d), and Mg by Mn (Fig. 21e). These cation exchanges commonly generate micro-cracks, as seen in the middle of the highlighted phlogopite crystal in Figure 25, which produce slight changes in the crystallographic directions in magmatic phlogopites within calcite carbonatite dikes and together with the movement of the crystals within the carbonatite flow, explains its isotropic texture. In addition, we can observe that the spaces generated by the strong basal cleavage plane (001), perpendicular to the phlogopite crystal (Fig. 25), are filled by fine-grained calcite and dolomite.

Finally, EBSD maps provide a detailed view of mineral grain orientation within the fenites (Fig. 22c, d). The EBSD results show that the proximal fenites are characterized by preferential orientations marked by fine-grained metasomatic phlogopite (Fig. 23b). Evidence from the metasomatic phlogopite basal plane (001), which is orthogonal to the dike wall (Fig. 23b), indicate that the metasomatic flux direction into the basement rock. Orientation of the phlogopite grains mark a flux direction that could be used as an alteration vector, where hydrothermal flux direction is orthogonal or near-orthogonal to the magmatic injection direction (i.e., strike of the carbonatite dike) (Fig. 23b), regardless of whether the original country rock had strong foliation. This orientation can be followed into the distal fenite, which shows aligned/foliated textures marked by the fine-grained phlogopites that are orthogonal to the dike wall (Fig. 19b). These features are extensively recognized and mapped at outcrop scale in the Boa Vista mine. Thus, fenite microstructural EBSD mapping at the micro-scale is a powerful tool to unravel fluid flow in carbonatite systems, as it has been recently applied in a variety of other magmatic-hydrothermal settings (e.g., Barbosa and Lagoeiro, 2010; Cook et al., 2017; Malatesta et al., 2021; Yeats et al., 2017).

3.7. CONCLUSIONS

Micro-textural and micro-analytical studies in the Boa Vista Nb mine indicate that the intrusion of the Late Cretaceous Catalão II alkaline-carbonatite complex produced a pervasive potassium-rich fenitization of the Neoproterozoic amphibolite and metarhyolite basement, forming melanocratic proximal fenites of phlogopite and distal phlogopite-orthoclase-calcite fenites. Niobium and REEs were partitioned within the carbonatite dikes forming pyrochlore and REE-rich carbonates; the coarse-grained magmatic phases such as pyrochlore, tetraferriphlogopite, dolomite and calcite in the dikes revealed a dominantly isotropic fabric. The 52rindade52g fluids exsolved from the carbonatite dikes, rich in soluble cations, i.e., K, Mg, Ba and Sr plus S and OH⁻, permeated the basement, without forming significant pyrochlore mineralization. The oriented basal plane of metasomatic phlogopite (001) crystallized orthogonal with respect to the carbonatite dike walls, showing that newly formed metasomatic minerals precipitated from the 52rindade52g fluids along the flow path. The mineral chemistry of metasomatic phlogopites is similar to that of magmatic phlogopite cores, suggesting that the metasomatic event was most likely simultaneous to the carbonatite intrusion, possibly attributed to a catastrophic release of pressure from the low-viscosity carbonatite magma.

This study highlights the importance of fenites as archives of fluid flow, which may provide a broader chemical perspective into the evolution of the alkaline complexes. Further studies are needed, for example, in other APIP complexes such as Araxá, the world's largest Nb producer, as well as other relevant locations around the world. As such, potentially relevant applications of K-rich fenites include their use as markers of metasomatism in alkaline-carbonatite complexes, which may potentially guide mineral exploration.

3.8. ACKNOWLEDGMENTS

This work was supported by ANID through the Millennium Science Initiative grant NCN13_065 “Millennium Nucleus for Metal Tracing Along Subduction”. Felipe Velásquez thanks financial support provided by ANID-Subdirección de Capital Humano/Doctorado Nacional/2021-21210049. This work was also supported by the Hugh McKinstry Fund of the Society of Economic Geologists Foundation Inc. Partial funding for this research was provided by the Brazilian National Council for Scientific and Technological Development (CNPq) under 425412/2018-0 and 305232/2018-5 processes. Finally, this work was supported by “Dirección de Investigación de la Vicerrectoría de Investigación de la Pontificia Universidad Católica de Chile, Concurso Inicio 2020”.

3.9. TABLES

Table 1. Representative electron microprobe analyzer (EMPA) data for K-rich magmatic and hydrothermal micas in the Boa Vista Nb mine, southern plug, Catalao II Complex. All analyses are included in SD2.

Rock Type	K-rich magmatic micas				K-rich hydrothermal micas			
	CC. dike	CC. dike	CC. dike	CC. dike	P. fen	P. fen	D. fen	D. fen
Mineral	Phl	Phl	Tfpchl	Tfpchl	Phl	Phl	Ann	Ann
SiO ₂	39.80	38.99	38.48	39.14	39.92	40.12	36.02	36.13
TiO ₂	1.87	2.33	0.08	0.19	1.94	1.78	3.88	2.41
Al ₂ O ₃	12.08	11.74	0.19	0.03	10.14	10.15	12.98	13.13
FeO	11.10	14.01	20.90	17.57	14.46	14.62	18.96	18.80
MnO	0.18	0.25	0.12	0.09	0.21	0.26	0.36	0.37
MgO	19.89	17.05	21.54	24.20	18.23	18.55	12.53	13.19
CaO	0.00	0.00	0.01	0.00	0.04	0.00	0.00	0.00
Na ₂ O	0.08	0.09	0.13	0.08	0.07	0.06	0.06	0.08
K ₂ O	11.67	11.48	11.02	11.60	11.71	11.83	11.20	11.47
SrO	0.43	0.36	0.32	0.35	0.38	0.40	0.29	0.34
BaO	0.00	0.04	0.00	0.00	0.02	0.01	0.05	0.00
Cl	0.00	0.01	0.05	0.00	0.00	0.00	0.00	0.00
Total	97.1	96.4	92.8	93.3	97.1	97.8	96.3	95.9
Elements, atoms per formula unit (calculated to 11 atoms of oxygen)								
T								
Si	2.890	2.894	2.759	2.752	2.908	2.903	2.750	2.791
Al	1.034	1.027	0.016	0.003	0.871	0.865	1.168	1.195
Fe ³⁺	0.076	0.079	1.225	1.246	0.221	0.232	0.082	0.014
ΣT	4.0	4.0	4.0	4.0	4.0	4.0	4.0	4.0
M								
Ti	0.102	0.130	0.004	0.010	0.106	0.097	0.223	0.140
Mn	0.011	0.016	0.007	0.006	0.013	0.016	0.023	0.024
Mg	2.153	1.887	2.302	2.536	1.980	2.001	1.426	1.519
Fe ²⁺	0.455	0.646	0.000	0.000	0.256	0.229	0.983	1.177
ΣM	2.7	2.7	2.3	2.6	2.4	2.3	2.7	2.9
#Mg	0.83	0.74	1.00	1.00	0.89	0.90	0.59	0.56
I								
Ca	0.000	0.000	0.001	0.000	0.003	0.000	0.000	0.000
Na	0.011	0.013	0.018	0.012	0.010	0.008	0.008	0.012
K	1.081	1.087	1.008	1.041	1.089	1.092	1.091	1.131
ΣI	1.1	1.1	1.0	1.1	1.1	1.1	1.1	1.1
OH								
OH	1.989	1.984	1.992	1.994	1.984	1.984	1.977	1.976
Cl	0.000	0.000	0.001	0.000	0.003	0.000	0.000	0.000
ΣOH	2.0	2.0	2.0	2.0	2.0	2.0	2.0	2.0

¹Abbreviations: CC. dike, calcite carbonatite dike; Ann, annite; D. fen, distal fenite; P. fen, proximal fenite; Phl, phlogopite; Tfpchl, tetraferriphlogopite.

3.10. FIGURES

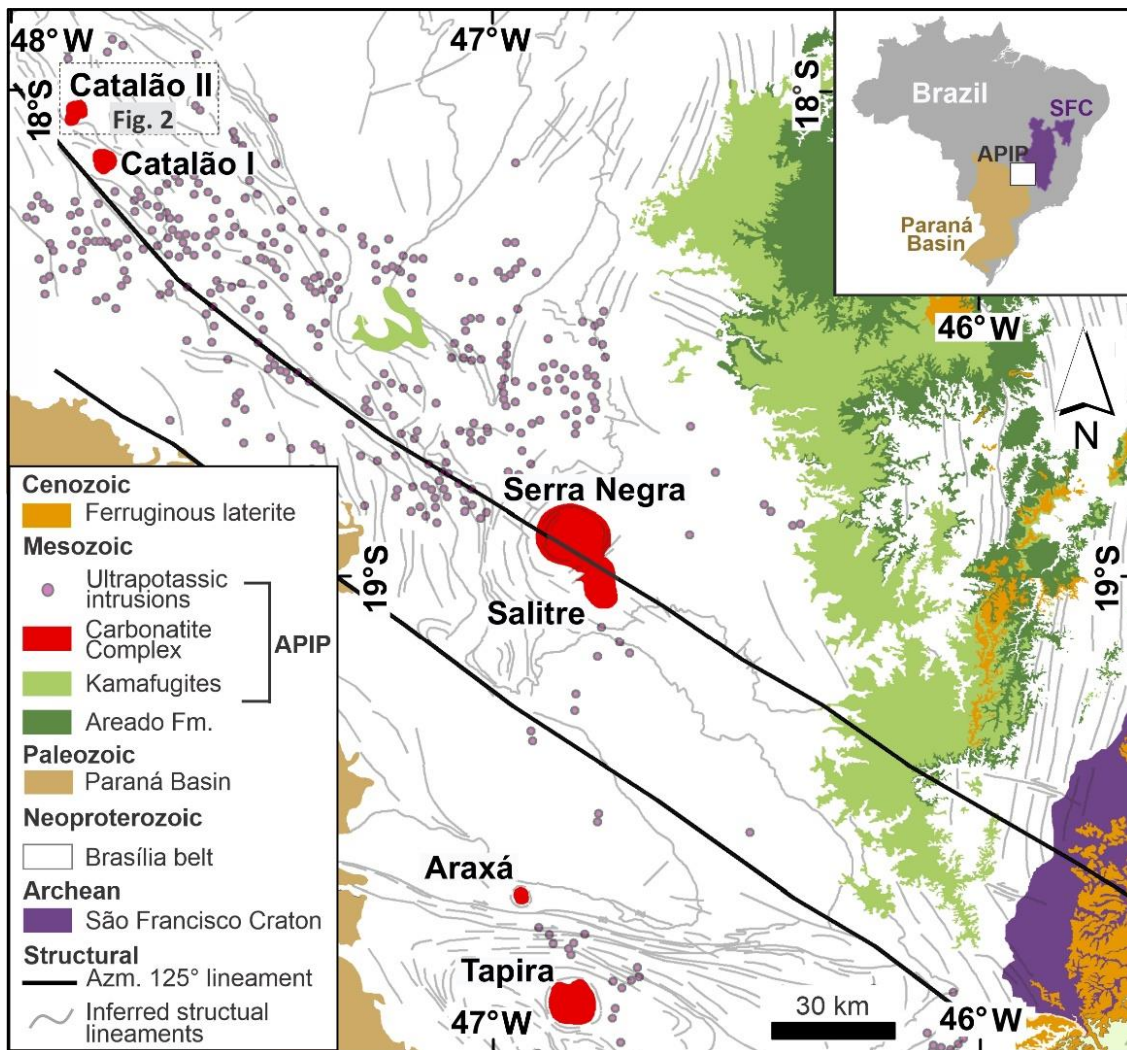


Fig. 16. Geological map of the APIP showing the location of the six main alkaline-carbonatite complexes. Figure modified from the 1:1M Belo Horizonte (SE-23) and Goiânia (SE22) cartographic sheets of the Brazilian Geological Survey (CPRM, 2020). Abbreviations: APIP, Alto Paranaíba Igneous Province; SFC, São Francisco Craton.

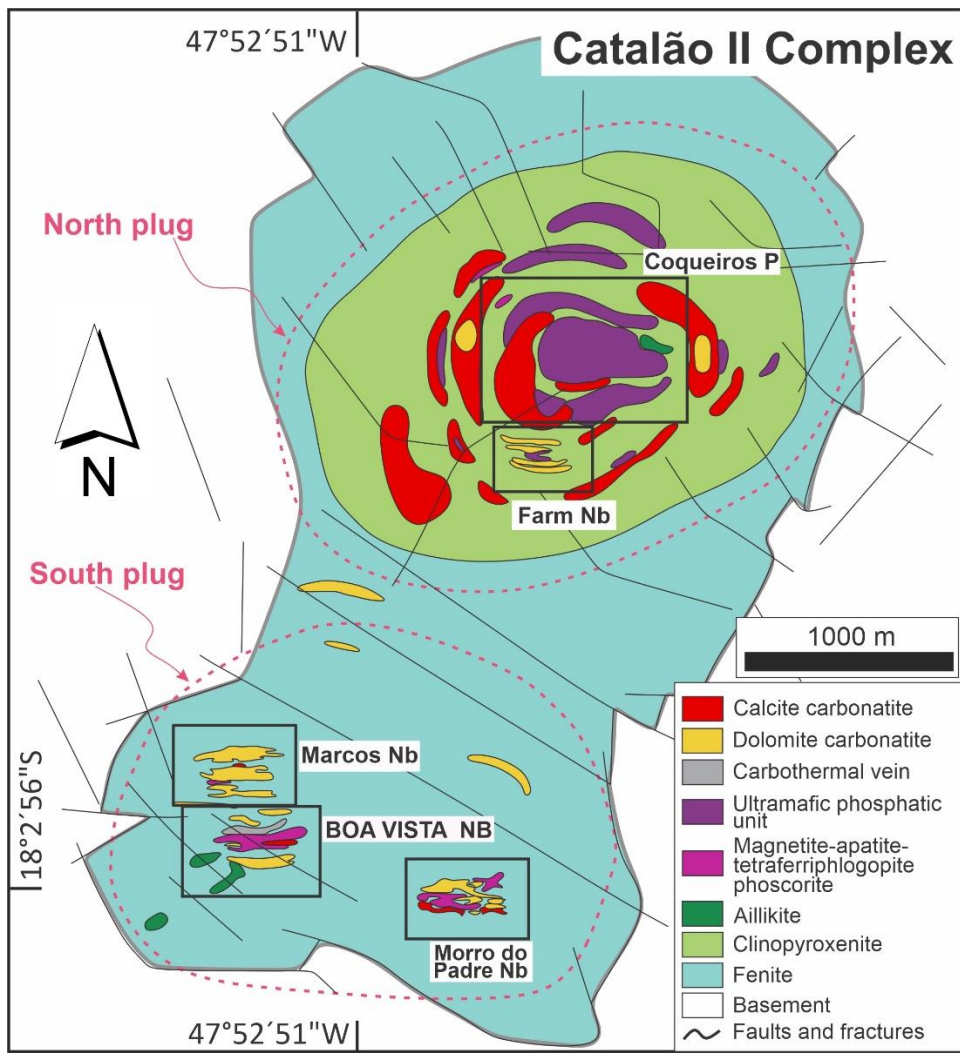


Fig. 17. Detailed geological map of the Catalão II complex, showing the location of the north and south plugs, the niobium and phosphate mines, the distribution of magmatic alkaline lithotypes, the surrounding fenite, and the basement. The fenites of Boa Vista Nb mine in the south plug are studied here.

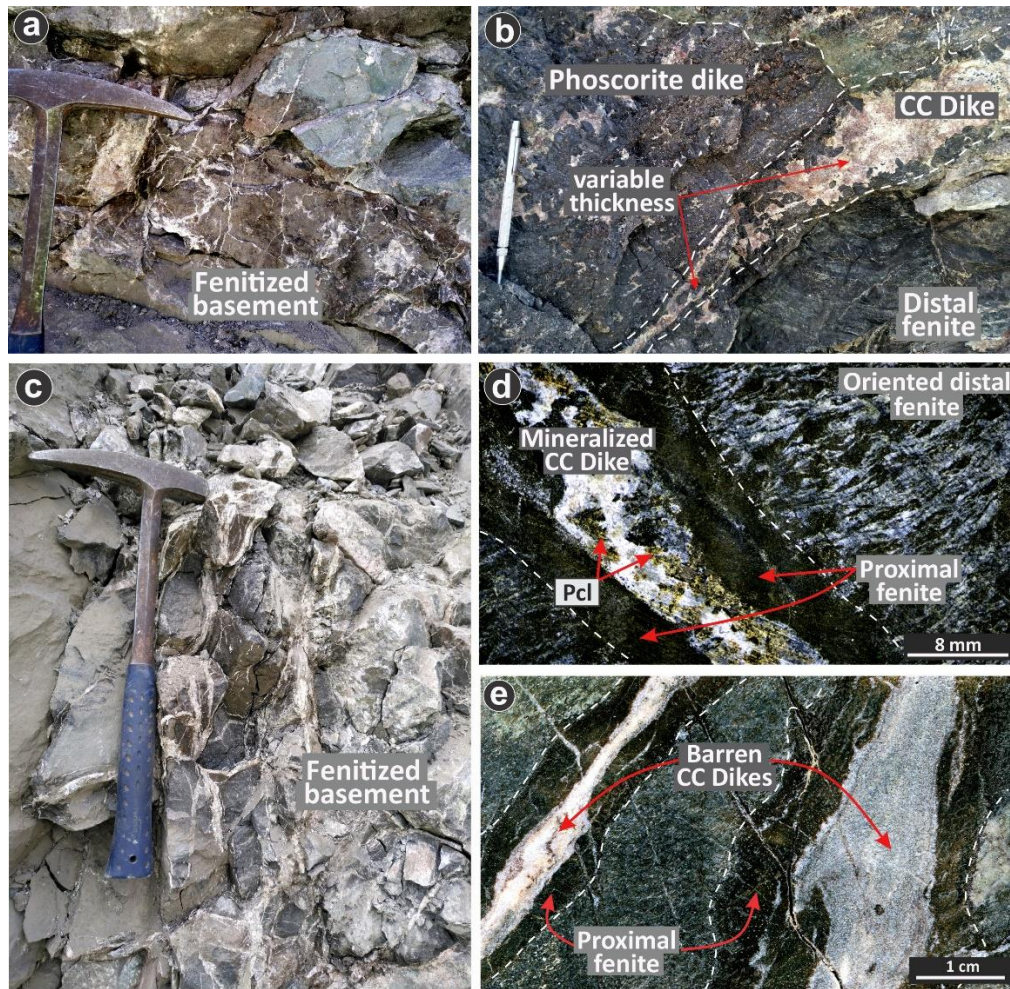


Fig. 18. (a) Outcrop of a distal fenite with calcite veinlets in the pit of the Boa Vista Nb Mine. (b) Swarm dike system containing phoscorite and calcite carbonatite dikes, showing a dramatic change in the carbonatite dike thickness. (c) Outcrop of a pervasive distal fenitized basement rock with high density of calcite veinlets and fractures. (d) Core sample showing fenite textures associated with a pyrochlore-bearing (Pcl) calcite carbonatite dike (Mineralized CC dike). The dike shows a proximal fenite of a phlogopite and the oriented fine-grained distal fenite. (e) Core sample scan showing a barren calcite carbonatite dike (Barren CC dike). As in (d), phlogopite metasomatic haloes are observed.

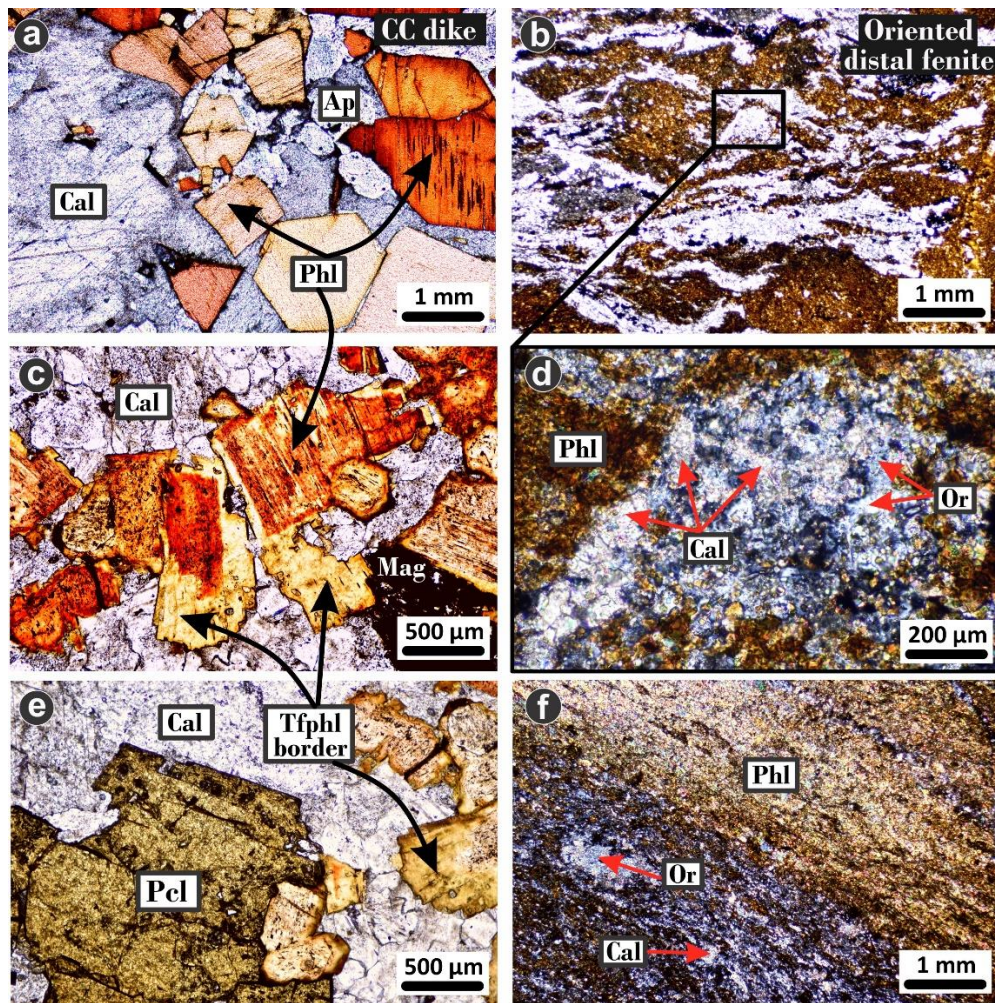


Fig. 19. Photomicrographs of the calcite carbonatite dikes are shown in the (a), (c) and (e) images, while their associated fenites are shown in the (b), (d) and (f) images. (a) Plane polarized light (PPL) image showing the texture of a coarse-grained calcite carbonatite dike. (b) PPL image showing the texture of an oriented fine-grained distal fenite, marked by phlogopite. (c) PPL image corresponds to zoned magmatic crystals of phlogopite core and tetraferriphlogopite rim. (d) Crossed polarized light (XPL) image shows in detail the fine-grained association of phlogopite, calcite and orthoclase (black rectangle in b). (e) PPL image corresponds to a coarse-grained association of pyrochlore, calcite and zoned phlogopite-tetraferriphlogopite crystals. (f) XPL image shows the fine-grained orientation of phlogopite, orthoclase and calcite in the fenite. Abbreviations: Ap, apatite; Cal, calcite; CC dike, calcite carbonatite dike; Mag, magnetite; Or, orthoclase; Phl, Phlogopite; Pcl, pyrochlore; Tfphl, tetraferriphlogopite.

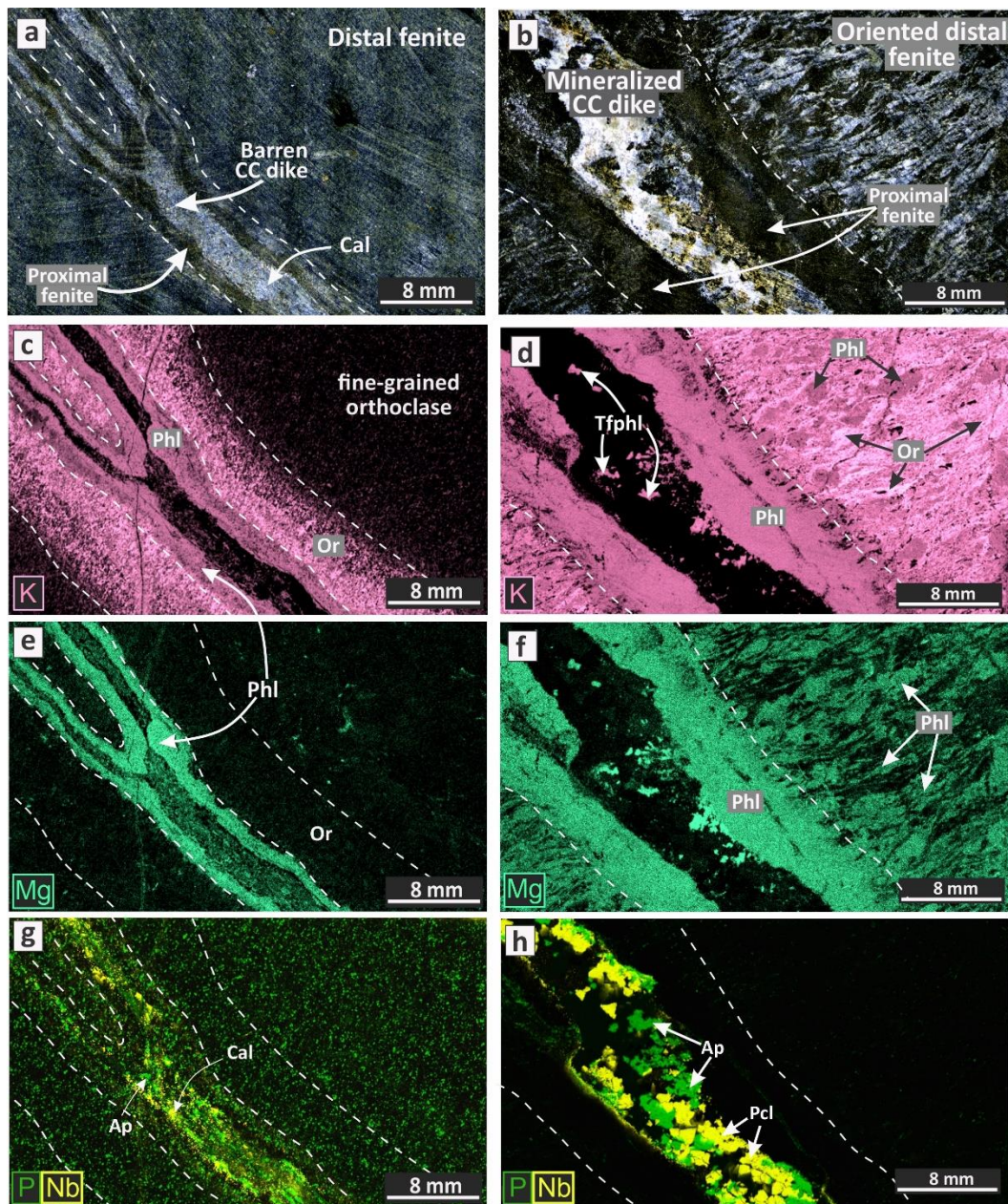


Fig. 20. Chemical distribution of K, Mg, P and Nb in barren (left column) vs. mineralized (right column) calcite carbonatite dikes. (a) Scan of polished sample that corresponds to a barren calcite carbonate dike with poor fenitization development. (b) Scan of polished sample that corresponds to a pyrochlore-mineralized calcite carbonatite dike with intense fenitization. (c), (e) and (g) show μ -EDXRF chemical maps of K, Mg, and P-Nb of the barren carbonatite dike in (a), while (d), (f) and (h) show μ -EDXRF maps for the same elements in the mineralized carbonatite dike in (b). Abbreviations: Ap, apatite; Ba, barite; Cal, calcite; Or, orthoclase; Phl, phlogopite; Pcl, pyrochlore; Tfphl, tetraferriphlogopite.

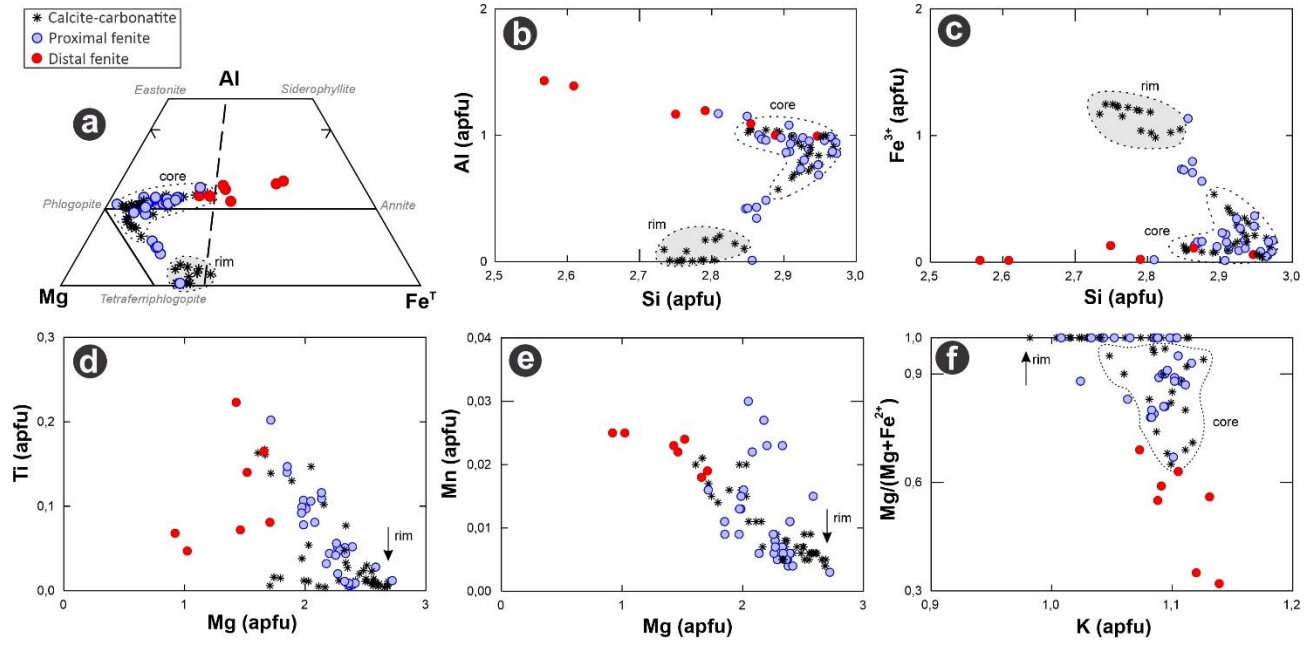


Fig. 21. EMPA data for phlogopite, tetraferriphlogopite and annite in the calcite carbonatite dikes, and in the proximal and distal fenites from the Boa Vista Nb mine. (a) Composition of the micas in terms of Al, Mg and total Fe (a.p.f.u.). The dashed line separates the Mg and Fe biotite end members. (b) and (c) diagrams correspond to the variation of Si vs. Al and Si vs Fe^{3+} in a.p.f.u. (d), (e) and (f) correspond to the distribution of Mg, Mn, Ti, K and the magnesium-number ($\text{Mg}/(\text{Mg}+\text{Fe}^{2+})$).

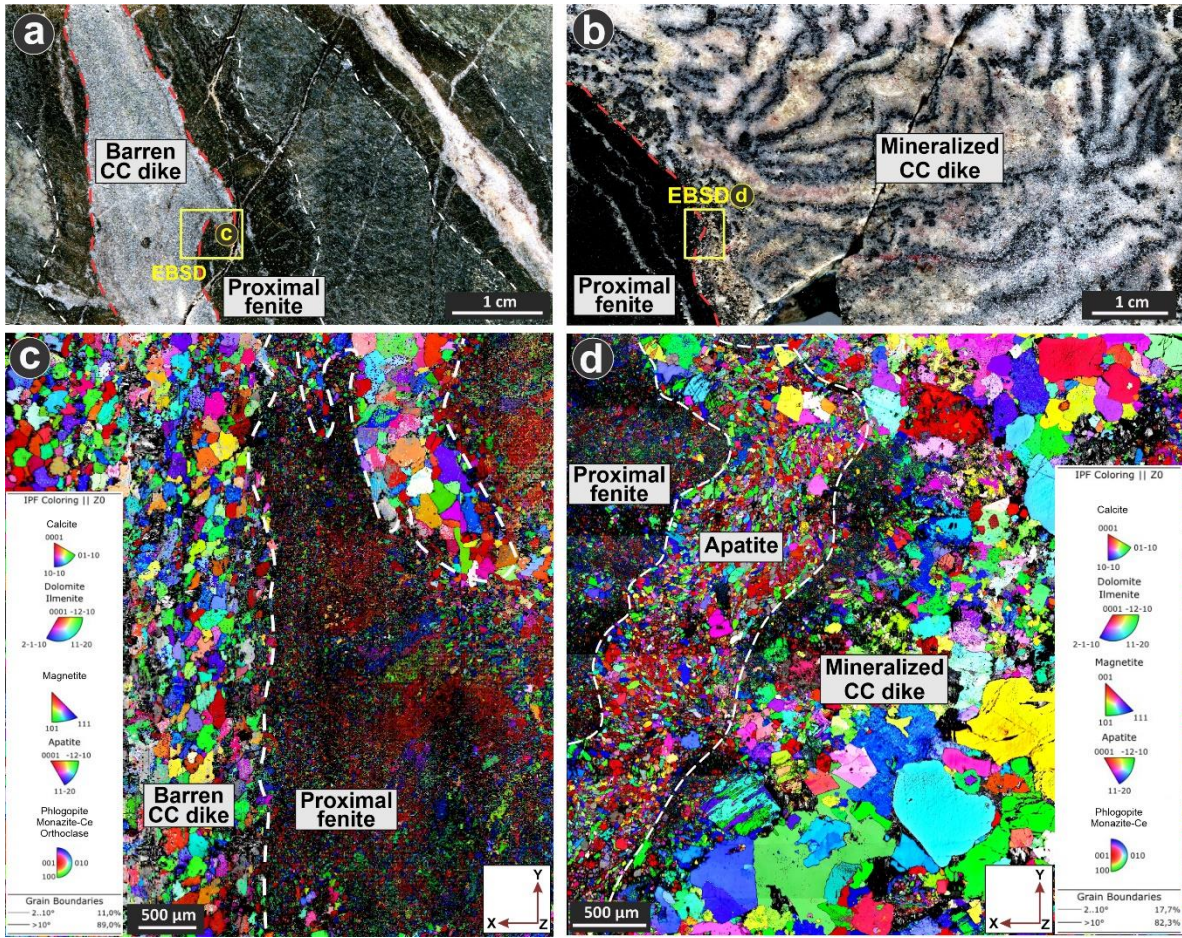


Fig. 22. Figures (a) and (b) correspond to scanned drill cores of barren (sample RM024-253.5) and mineralized (sample RM024-329) calcite carbonatite dikes, respectively. The yellow rectangles show the areas for EBSD analysis in c) and d). Figures (c) and (d) show inverse pole figure maps, which depict the crystallographic directions for all mineral phases using X (perpendicular to dike wall) and Y (parallel to dike wall) directions as a reference (Z direction is perpendicular to the EBSD images).

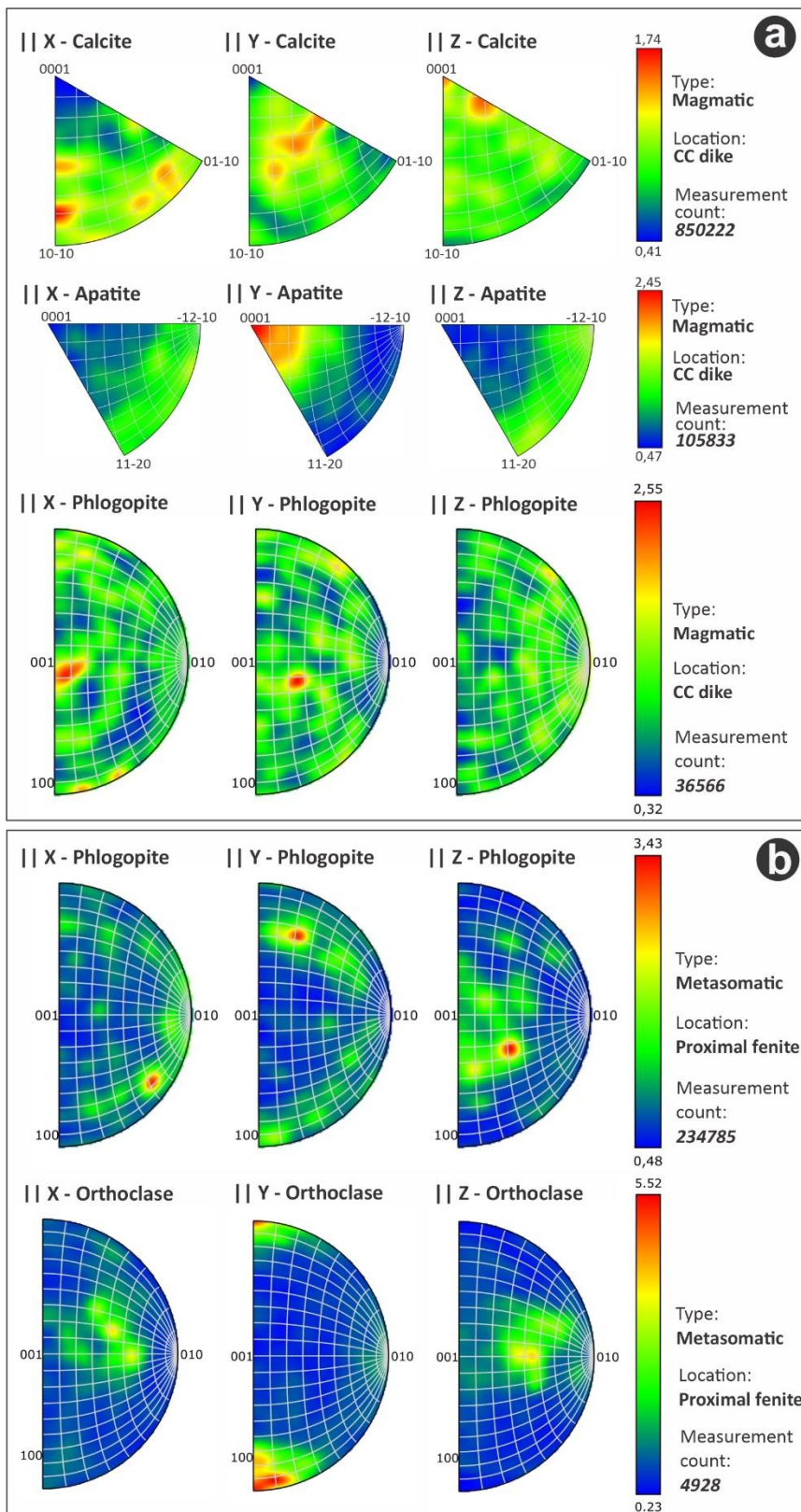


Fig. 23. Inverse pole figure for key magmatic (a) and metasomatic (b) mineral phases, associated to a barren calcite carbonatite dike, previously shown in Figure 7a.

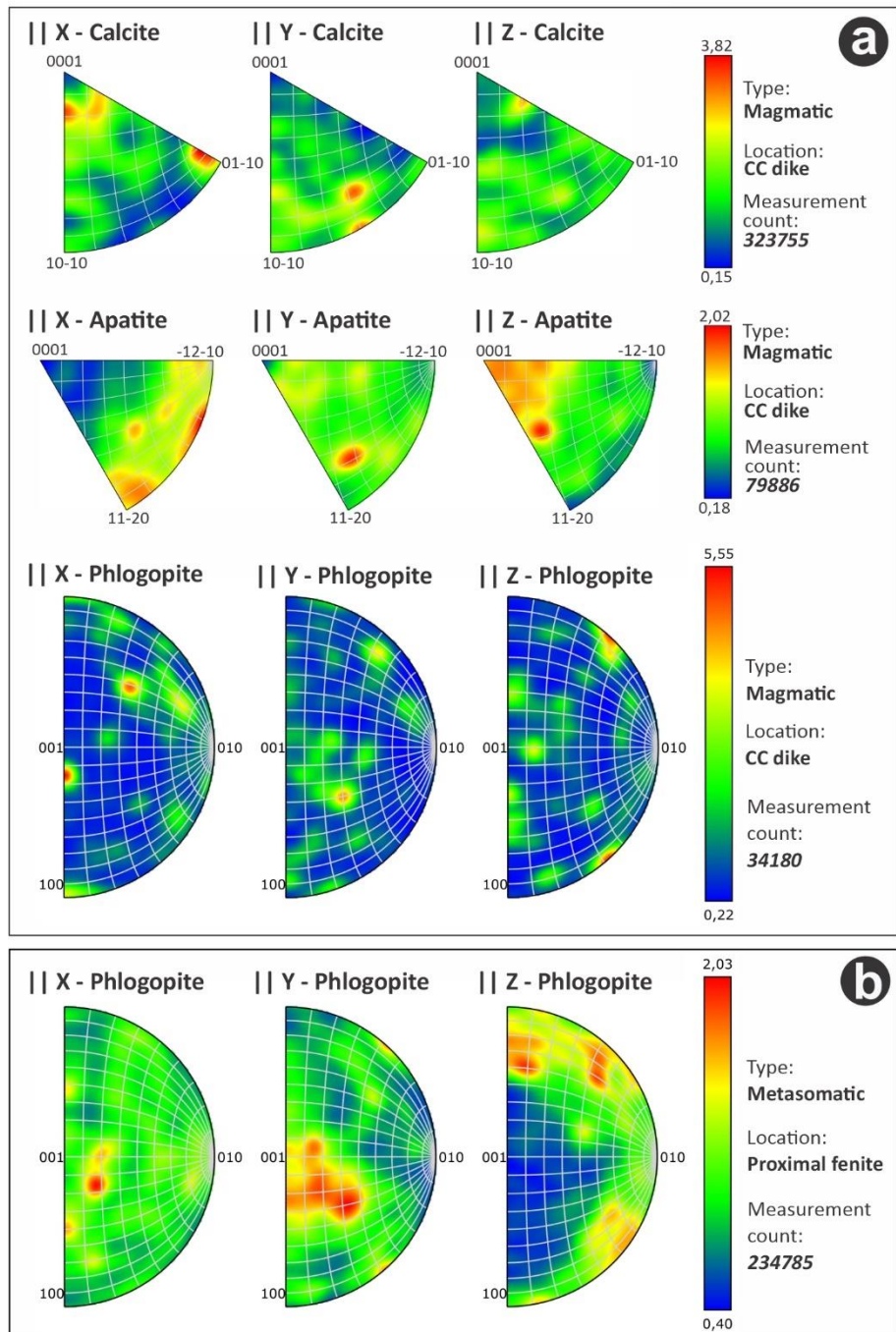


Fig. 24. Inverse pole figure for key magmatic (a) and metasomatic (b) mineral phases, associated to a mineralized calcite carbonatite dike, previously shown in Figure 7b.

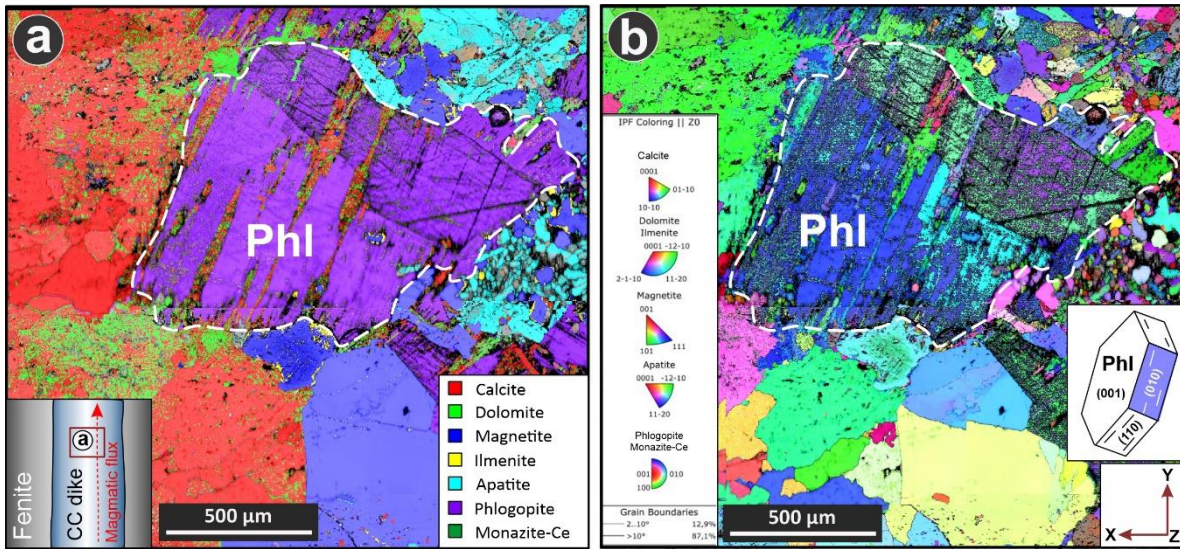


Fig. 25. (a) EBSD map of a mineralized calcite carbonatite dike (Y axis as reference to the wall dike), showing the different mineral phases with a false color composition, highlighting a magmatic phlogopite (Phl), with crystallization of calcite and dolomite between its basal cleavage spaces in (001). (b) Inverse pole figure map of the figure in (a) showing changes of crystallographic directions by fracture along the crystal. Phlogopite is observed with a strong and spaced basal cleavage plane, where calcite and dolomite are crystallized in the middle of the phlogopite sheets. The magmatic direction is highlighted by the red arrow in the lower left corner in (a), which almost coincides with the direction of injection of carbonates in between the phlogopite sheets.

CAPÍTULO 4: ORIGIN OF CARBONATITE-RELATED NIOBIUM DEPOSITS: INSIGHTS FROM PYROCHLORE GEOCHEMISTRY

Felipe Velásquez Ruiz*, a, b, Martin Reich^{a, b}, Sam Broom-Fendley^c, Charles D. Beard^d, Fernando Barra^{a, b}, Rurik Romero^{a, b}, Pedro Cordeiro^e

^aDepartment of Geology, Facultad de Ciencias Físicas y Matemáticas (FCFM), Universidad de Chile, Plaza Ercilla 803, Santiago, Chile.

^bMillennium Nucleus for Metal Tracing Along Subduction, Facultad de Ciencias Físicas y Matemáticas (FCFM), Universidad de Chile, Plaza Ercilla 803, Santiago, Chile.

^cCamborne School of Mines, University of Exeter, Penryn Campus, Cornwall TR10 9FE, UK.

^dDepartment of Earth Sciences, University of Cambridge, Cambridge, UK.

^eDepartment of Mining Engineering, Pontifical Catholic University of Chile, Vicuña Mackenna 4860, Santiago, Chile.

Published in:

Geochimica et Cosmochimica Acta

*Corresponding Author:

E-mail address: fevelasquezru@gmail.com (F.V. Ruiz).

ORCID: 0000-0003-1741-8588

4.1. ABSTRACT

The carbonatite-related Nb deposits of the Alto Paranaíba Igneous Province (APIP) in central Brazil, currently account for ~92% of the global Nb production. In the APIP, pyrochlore is abundant in magnetite–apatite–tetraferriphlogopite±carbonate rocks or phoscorites, occurring as interbedded layers with carbonatites in the lower hypogene zone, feeding dike swarms of phoscorite and calcite carbonatite, and late-stage carbothermal veins in the upper hypogene zone. The origin of the phoscorite–carbonatite association can be explained by three hypotheses: (1) crystal segregation from fractional crystallization, (2) liquid immiscibility, and/or (3) phoscoritic magma formation after basement metasomatism (fenitization). However, it is not well understood whether pyrochlore formation is limited to a carbonatitic event, carbohydrothermal, or both, and this gap of knowledge is addressed in this work. To investigate the petrogenesis of pyrochlore-rich phoscorite, cathodoluminescence (CL) images, chemical maps, and LA-ICP-MS data were acquired of pyrochlore crystals from magmatic and carbothermal rocks from the Boa Vista Nb mine, Catalão II Complex. In the Boa Vista mine, oscillatory and patchy zoning were identified as primary pyrochlore textures commonly recorded at the lower hypogene zone, while secondary dissolution, skeletal and zonation-free textures are registered at shallower depths in the upper hypogene zone. Calciopyrochlore is the dominant Nb phase at the Boa Vista mine, with only two kenopyrochlore outliers. The pyrochlore CI chondrite-normalized REE distribution is consistent with geochemical results of the carbonatite and phoscorite rocks, indicating a magmatic origin for pyrochlore and the presence of pyrochlore antecrysts in carbothermal veins. The Sr/Y vs La and Na vs Ce diagrams in pyrochlore indicate a continuous fractionation pattern, with some mixtures of antecrysts and primary phases. An examination of intercumulus calcite using CL provide evidence of carbonatitic magma residues within tetraferriphlogopite phoscorite dikes and suggests that alkaline–carbonate-rich fluids played a role in transporting heavy minerals (i.e., magnetite, apatite, pyrochlore). Consequently, the textural and chemical evidence in the Boa Vista Nb mine indicates that the origin of pyrochlore-rich phoscorites is the result of physical segregation of heavy minerals from a carbonatite magma by fractional crystallization, leading to the emplacement of pyrochlore-rich carbonatite and phoscorite dikes. The implications at Catalão II may extend to other APIP alkaline–carbonatite complexes, as they share a genetic connection, and should motivate further studies focusing on pyrochlore geochemistry in other carbonatite-related Nb deposits, which will be crucial for advancing our knowledge of global Nb metallogenesis.

Keywords: niobium, phoscorite, carbonatite, carbothermalite, pyrochlore geochemistry.

4.2. INTRODUCTION

Pyrochlore is the most important group of the pyrochlore-supergroup minerals and constitutes the main Nb ore in the carbonatite deposits of the Late Cretaceous Alto Paranaíba Igneous Province (APIP), central Brazil (Cordeiro et al., 2011). The APIP alkaline-carbonatite complexes (Fig. 1b), including the Araxá carbonatite complex (CBMM Nb mine: 896 Mt @ 1.49% Nb₂O₅; Biondi and Braga Junior, 2023) and the Catalão II carbonatite complex (Boa Vista Nb mine: 26 Mt @ 0.95% Nb₂O₅), account for ~92% of the global Nb production over the last 50 years (Palmieri et al., 2022). Pyrochlore is principally extracted from the regolith (Fig. 2a) formed by the weathering of carbonatite and phoscorite rocks (Fig. 2b; Cordeiro et al., 2011; Mitchel, 2015). In addition, the Niobec mine at Saint Honoré, Canada (2.6 Mt @ 0.42% Nb₂O₅; Vallières et al., 2013), contributes approximately 7% of the global Nb production (Vallières et al., 2013), while other minor deposits such as Lovozero, Russia and Pitinga, Brazil represent ~1% (Mitchell, 2015; Mitchell et al., 2020).

Despite the importance of pyrochlore as the main Nb-bearing phase, only a limited number of microanalytical and geochemical studies have been published (Cordeiro et al., 2011; Walter et al., 2018; Klemme et al., 2020; Da Costa et al., 2021; Khan et al., 2021; Zaitsev et al., 2021; Palmieri et al., 2022; Sun et al., 2022; Vasyukova and Williams-Jones, 2023). The common presence of oscillatory zoning in pyrochlore suggests a magmatic origin, but the composition of pyrochlore is highly variable and can be influenced by local processes such as alteration to ferrocolumbite or zirconolite, metamictization, or fenitization. The paucity of comprehensive data raises important questions regarding the formation of pyrochlore in carbonatites either as a result of processes related to carbonatitic magmas or carbothermal fluids (i.e., late stage, low-temperature fluids dominated by CO₂, Mitchell and Gittins, 2022), or a combination of both. Understanding the different origins of pyrochlore in carbonatite systems is crucial for deciphering the implications and geological significance of Nb enrichment processes.

In this study, we provide a comprehensive in-situ geochemical and microtextural characterization of pyrochlore from the Boa Vista Nb mine in Brazil. Here, pyrochlore-bearing phoscorites are intermingled with carbonatites and carbothermal veins, providing a unique opportunity to constrain the geochemical signature of pyrochlore in relation to different rock types and Nb enrichment processes. Our work consists of microtextural observations using scanning electron microscopy (SEM) and optical cathodoluminescence (CL) methods, and in-situ geochemical analysis using a combination of electron microprobe analysis (EPMA) and laser ablation inductively coupled plasma mass spectrometry (LA-ICP-MS) techniques. Our objective is to provide insights on the role of magmatic and secondary carbothermal processes on Nb mineralization within the APIP, explore the potential of pyrochlore as a tracer for Nb enrichment in alkaline-carbonatite complexes, and contribute to the understanding of the origin of pyrochlore mineralization within the world's largest niobium province.

4.3. GEOLOGICAL SETTING

The Late Cretaceous Alto Paranaíba Igneous Province (APIP) in central Brazil (Figs. 1a-b), comprises potassic-to-ultrapotassic intrusive and volcanic alkaline rocks that cover a total area of ~25,000 km² (Gibson et al., 1995). The APIP intrudes greenschist-to-amphibolite facies metamorphic basement rocks of the Neoproterozoic Brasília Belt, located between the NE margin of the Paraná Basin and the SW border of the São Francisco Craton (Barbosa and Sabaté 2004; Silva et al. 2020). The eastern part of the APIP comprises kamafugitic lava flows, pyroclastic rocks and diatremes from the Mata da Corda Formation (Velásquez Ruiz et al., 2023), whereas the western part consists of smaller-scale outcrops of diatreme-like kamafugites, numerous kimberlites (Guarino et al., 2013), and six multi-stage alkaline-carbonatite complexes, namely (from north-to-south): Catalão II, Catalão I, Serra Negra, Salitre, Araxá and Tapira (Fig. 1b). Kimberlites were emplaced between 91–80 Ma and potassic-to-ultrapotassic rocks (kamafugites) from 90 to 76 Ma based on U-Pb perovskite ages (Sgarbi et al. 2004; Guarino et al. 2013; Felgate 2014). The formation of the alkaline-carbonatite complexes involved multiple episodes of carbonatite and silica-undersaturated magmatism with radiometric ages between 96 and 78 Ma (⁴⁰Ar/³⁹Ar phlogopite and U-Pb perovskite ages; Guarino et al. 2013; Guarino et al. 2017; Conceição et al. 2020).

The main structural feature in the APIP is the Azimuth 125° lineament (Fig. 1b), which corresponds to a group of ~1,800 km long NW-SE-trending lineaments identified by regional aeromagnetic data and represented by mylonites and dikes (Moraes Rocha et al. 2014). The development of the Azimuth 125° lineament can be attributed to three distinct tectonic events: (1) the Brasiliano orogeny (950–520 Ma), (2) Gondwana fragmentation (~180 Ma), and (3) an event at ~90–80 Ma, either related to the passage of the Trindade mantle plume (Moraes Rocha et al. 2014; Gibson et al., 1995), or extension following the opening of the South Atlantic (Ferreira et al., 2022).

4.3.1. The Catalão II alkaline-carbonatite complex and nomenclature of its “exotic” rocks

According to the International Union of Geological Sciences (IUGS) Subcommission on the Systematics of Igneous Rocks (Le Maitre, 2002), the “special” or “exotic” igneous rocks comprise pyroclastics, carbonatites, kimberlites, lamproites and lamprophyres. Nonetheless, apatite-magnetite-rich igneous rocks are not included in the IUGS classification, although they are briefly mentioned in its glossary of terms.

The nomenclature for apatite–magnetite-rich rocks in the Catalão II and Catalão I complexes has evolved over time, particularly the change from nelsonites to phoscorites (Cordeiro et al., 2010; Palmieri et al., 2022). According to the IUGS, phoscorite is defined as a rock containing apatite, magnetite and olivine typically associated with carbonatites (Yegorov, 1993; Le Maitre, 2002). However, Krasnova et al. (2004a) expanded this definition as a plutonic ultramafic rock, comprising apatite, magnetite and one of the silicate phases forsterite, diopside or

phlogopite. The predominant silicate mineral in both Morro do Padre and Boa Vista Nb mines is tetraferriphlogopite ($KMg_3Fe^{3+}Si_3O_{10}(OH)_2$) and therefore, plutonic ultramafic rocks with magnetite, apatite, tetraferriphlogopite and pyrochlore as essential minerals are currently referred to as tetraferriphlogopite phoscorites (Palmieri et al., 2022). A similar mineral association is found in the Araxá Complex, where these rocks were named with the predominant mineral ending in "ite" (i.e., magnetite, phlogopite, apatite; Biondi and Braga Junior, 2023), without taking into account the nomenclature of phoscorite rocks.

In contrast, the term bebedourite is derived from the Bebedouro area at Salitre Hill, in the APIP (Barbosa et al., 2012). Initially, Tröger (1928, 1935) defined bebedourite as biotite-perovskite-rich clinopyroxenite with accessory opaque phases, apatite, K-feldspar and olivine. The previous definition was maintained by the IUGS in its glossary of terms. However, this exotic rock type was later redefined by Barbosa et al. (2012) as a cumulate igneous rock, whose rock-forming minerals are diopside, apatite, magnetite, phlogopite, and a Ca–Ti phase (mostly perovskite, more rarely titanite and/or Ti-garnet). However, the nomenclature of this rock type is a current topic of debate.

The last group of exotic rocks that has changed its nomenclature in the APIP alkaline-carbonatite complexes are the ultramafic lamprophyres. These rocks are silica undersaturated (29.3–36.4 wt.%) and potassium-rich (3.1–6.6 wt.%) ultramafic dikes, previously classified as phlogopite-picrites (Gibson et al. 1995; Brod et al. 2000), but later renamed as olivine aillikites (Velasquez et al., 2023) following the classification of ultramafic lamprophyres of Tappe et al., (2005). The APIP olivine aillikites are clinopyroxene-free porphyritic dikes with olivine and phlogopite macrocrysts, set in a groundmass of glass, perovskite, calcite, spinel group oxides and fine phlogopite laths.

The Catalão II alkaline-carbonatite complex is situated in the northern part of the APIP and is located 14 km NW from Catalão I (Figs. 1b-c). The Catalão II complex bifurcates into two small intrusions (North and South) that resulted in the fenitization of the Neoproterozoic metasedimentary basement, leading to the formation of a phlogopite-carbonate-rich (\pm orthoclase) fenite halo that surrounds both the North and South intrusions (Fig. 1c). The age of the Catalão II complex has been determined between ~90 and 82 Ma based on U-Pb age determination of perovskite from aillikite (Guarino et al., 2013). Catalão II North is a stratified intrusion comprising an outer clinopyroxenite cumulate ring and segmented layers of calcite to dolomite carbonatite and an apatite-rich ultramafic unit (mainly phoscorite with variations to bebedourite), which host the Coqueiros phosphate deposit (Fig. 1c). Catalão II South comprises three sets of EW trending dike swarms that occur in the upper hypogene zone, namely Morro do Padre, Marcos and Boa Vista (Fig. 1c). Although geophysical data reveal that these three dike systems are connected by a larger magma chamber below 1,000 m (Palmieri et al., 2022), they present different lithological variations and magnetic anomalies. For example, magnetic anomalies at Catalão II South indicate that Morro do Padre is closer to the source of the magma chamber, while the Boa Vista system is further from the source, modelled as a westward magnetic branch (Palmieri et al., 2022). Lithological

differences between Morro do Padre and Boa Vista have been revealed by drill cores. At Morro do Padre, for example, olivine aillikite and carbothermal veins are rare, while calcite and dolomite carbonatite and tetraferriphlogopite phosphorite dikes are more abundant, compared to Boa Vista, where there is greater exposure of the metavolcanosedimentary basement. There are five main rock types in the Boa Vista dike swarm: (1) Calcite carbonatite dikes with observed variations to dolomite carbonatite and common accessory pyrochlore (Fig. 3a); (2) Tetraferriphlogopite phoscorite, which is host to the pyrochlore ore. It can vary from an apatite-rich (Fig. 3b) to magnetite-rich composition (Fig. 3c); (3) Late-magmatic REE-rich carbothermal veins composed of calcite, dolomite, siderite, strontianite, qaqarssukite-(Ce) and barite with minor pyrite (Fig. 3d). Pyrochlore and apatite are rare in these veins, while magnetite and tetraferriphlogopite are absent; (4) Pyrochlore-lacking K-rich fenites, which is associated with metasomatism of the basement rocks (Figs. 2b). It is composed of fine-grained phlogopite, orthoclase, and calcite; and (5) Pyrochlore-lacking, olivine aillikite crosscutting the alkaline and carbonatite rocks (Fig. 2b). In this study, the focus was on pyrochlore, hence, only the calcite carbonatite dikes, tetraferriphlogopite phoscorite, and carbothermal veins were sampled and investigated.

4.4. SAMPLES AND METHODS

Nine representative pyrochlore-bearing samples were selected from six drill cores (PCBV, RM01, RM016, RM024, RM025 and RM032) from the Boa Vista mine, which is owned by CMOC-Brazil (<https://cmocbrasil.com/en>). The samples consist of four calcite carbonatites, four tetraferriflogopite phoscorites (three apatite-rich and one magnetite-rich), and one carbothermal vein.

Textural characterization of the nine pyrochlore-bearing samples was conducted using polarized light microscopy, back-scattered electron (BSE) petrography using a scanning electron microscope (SEM), and optical cathodoluminescence (CL). The BSE images were acquired using a JEOL JXA 8200 instrument at the Camborne School of Mines, University of Exeter, UK, operating with a 15 kV, 20 nA beam. CL images were also obtained using a CITL Mk5 optical cathodoluminescence microscope at the same institution, operated with a beam current of ~300–500 µA and a corresponding voltage of 8–12 kV.

Electron Probe Micro Analysis (EPMA) of pyrochlore was conducted using JEOL JXA 8200 instruments at the Regional Centre for Technological Development and Innovation (CRTI) in the Universidade Federal de Goiás, Goiania, Brazil, and at the Camborne School of Mines. The analyses were performed with an accelerating voltage of 15 kV, a beam current of 20 nA, and a beam spot size of 5 µm. A counting time of 20 seconds was used to determine the concentrations of Nb₂O₅, Ta₂O₅, SiO₂, TiO₂, ZrO₂, UO₂, ThO₂, La₂O₃, Ce₂O₃, Y₂O₃, FeO, MnO, CaO, BaO, SrO, Na₂O and F. Synthetic and natural mineral standards were used for calibration.

Trace elements concentrations in pyrochlore were determined using laser ablation inductively coupled plasma mass spectrometry (LA-ICP-MS), at the University of Chile and the Camborne School of Mines. At the University of Chile, a Photon Machines Analyte G2 ArF

excimer nanosecond laser (193 nm) was used coupled to a Thermo Fisher Scientific ICAP-Q quadrupole ICP-MS. The laser had a spot size of 30 μm and a repetition rate of 5 Hz, maintaining a fluence of approximately 4 J cm^{-2} . At the Camborne School of Mines, analyses were conducted using a New Wave Research 213 nm Nd-YAG laser coupled to an Agilent 7700 ICP-MS under identical analytical conditions. Trace element analyses were calibrated using the abundance of ^{43}Ca as measured by EPMA. The reference material NIST SRM 612 was used for calibration, and the accuracy was determined through measurement of the secondary standard GSD. Data processing was performed using Iolite software.

4.5. RESULTS

4.5.1. Rock textures and paragenetic sequence

At the Boa Vista and Morro do Padre Nb mines, the deep hypogene zone is characterized by meter size layered calcite carbonatite and tetraferriflogopite phoscorite (Palmieri et al., 2022). In the deeper parts of the complex (>300 m depth), the layered calcite carbonatite is composed of calcite layers (>1 cm) and strings of heavy minerals such as magnetite, apatite and pyrochlore (Fig. 4a). A dog tooth texture with intercumulus apatite, intersected by fine-grained magnetite veinlets is also observed in the calcite carbonatite (Fig. 4b). In the Boa Vista deposit, the upper hypogene zone, which extends from the bottom of the regolith layer (~60 m) to a depth of about 300 m (Fig. 2a), comprises a swarm of calcite carbonatite and tetraferriphlogopite phoscorite dikes, aillikites, and carbothermal veins (Figs. 3-4). At shallow levels (~80 m), the calcite carbonatite dikes display miarolitic cavities filled with fine-grained phoscorite within skeletal coarse carbonate, which in turn is in sharp contact with medium-grained phoscorites (Fig. 3a). The transition from apatite-rich to magnetite-rich zones in tetraferriphlogopite phoscorites is gradual (Fig. 3b). Tetraferriphlogopite phoscorite is the main host of the Nb mineralization, with pyrochlore abundances exceeding 10% in the most enriched zones (Figs. 3b and c). In contrast, pyrochlore is present as an accessory phase in calcite carbonatite (Fig. 4a) and a trace mineral in carbothermal veins. Calcite coarse aggregates are common in apatite- to magnetite-rich tetraferriphlogopite phoscorite (Fig. 4c). Carbothermal veins in the upper section of the hypogene zone display variegated and porous textures (Figs. 3d and 4e). At the contact between the intrusion and basement rocks, pervasive metasomatism resulted in fenitization of the metasedimentary rocks (Fig. 2b). Basement fragments were assimilated by calcite carbonatite, forming a K-rich fenite of phlogopite with orthoclase and carbonates (Fig. 4f). Overall, the magmatic stage includes the formation of carbonatites and apatite- and magnetite-rich phoscorites, whereas the late stage includes carbothermal veins and the fenitized basement rocks (Fig. 5).

4.5.2. Pyrochlore textures

Pyrochlore occurs in calcite carbonatite, tetraferriphlogopite phoscorite, and carbothermal veins. In the calcite carbonatite, the most common primary pyrochlore texture is oscillatory zoning. This zoning is characterized by fine bands of high and low BSE brightness, indicating variations

in the composition of the carbonatitic magma during fractionation (Fig. 6a). Pyrochlore in the tetraferriphlogopite phoscorite exhibits a coarse patchy zonation (Figs. 7a, c). Both zoned textures generally show euhedral to subhedral pseudohexagonal habit despite crystallizing in the isometric system (Fig. 6a and 7a), with few inclusions mainly consisting in tetraferriphlogopite (Fig. 7c) and apatite. These zoned textures are registered at depths varying between 487 to 183 m using exploratory drill cores. Zirconolite rims occur in pyrochlores from apatite-rich phosphorite (not found in other rock type), being the least abundant texture at Boa Vista. Some of these zirconolite-rimmed crystals are broken, indicating that the breakage formed later, but this texture is not common.

Zonation-free dissolution textures occur in pyrochlore in calcite carbonatite and tetraferriphlogopite phoscorite. These textures are characterized by penetrative irregular lobes with contrasting BSE responses (Fig. 6b and 7d). Where dissolution is penetrative, there are no zoned crystals in the same sample. Furthermore, dissolution is non-penetrative at the rims of pyrochlore with oscillatory zonation (Fig. 6a). Dissolved pyrochlore grains typically show subhedral to anhedral habits and contain abundant inclusions, often apatite, in comparison to zoned pyrochlores. A skeletal texture occurs where dissolved pyrochlore shows an increase in apatite inclusions from the rim to the core resulting in crystals with anhedral habit (Fig. 7b). Apatites associated with skeletal pyrochlores present zoned textures under CL, which exhibits a light blue CL colour (Fig. 7b) due to activation by trace quantities of LREE ions mainly Ce³⁺, also seen in apatites from phoscorites of the Catalão I complex (Broom-Fendley et al., 2021). In response to massive apatite inclusions, skeletal pyrochlores present a masked CL response, with a yellowish-brown colour in the rim and dark-brown colour in the core. It is worth noting that this masked CL response appears to be exclusively restricted to samples from the apatite-rich phoscorite, as pyrochlore crystals from the calcite carbonatite (Fig. 6c) or the carbothermal veins (Fig. 8b) do not display a CL response. Zonation-free textures are recorded at depths between 284 to 3 m depth, corresponding to the upper hypogene zone and the regolith.

Zonation-free, non-dissolved pyrochlores are restricted to the carbothermal veins (Figs. 8a, c), registered at shallower depths (<100 m). These pyrochlore grains show euhedral to subhedral habits, typically immersed in a qaqarssukite-(Ce) ($Ba(Ce,REE)(CO_3)2F$) groundmass (Fig. 8b), and also associated with barite veinlets (Fig. 8c). Qaqarssukite-(Ce) has a low response to CL similar to that of pyrochlore (Fig. 8b), attributed to its high LREE content. In contrast, calcite exhibits a high CL response, observed with a yellow CL colour due to activation by Mn²⁺ to dark orange CL colour related to Fe³⁺-quenching.

4.5.3. Pyrochlore chemical composition

The term “pyrochlore” is now used to refer to the pyrochlore-supergroup minerals. The pyrochlore-supergroup follows a general formula of $A_2B_2X_6Y$, where A is a large 8-fold coordinated cation site hosting Na, Ca, Ag, Mn, Sr, Ba, Fe, Pb, Sn, Sb, Bi, Y, REE, Sc, U or Th (Atencio, 2010; 2021). The B site is a 6-fold coordinated cation site that can accommodate Ta, Nb, Ti, Sb, W, V, Sn, Zr, Hf, Fe, Mg, Al, and Si, whereas the X- and Y-sites contain O and an anion,

respectively, but can also host H₂O, F or a vacancy (□). Based on the dominant cation in the B-site, seven main groups have been identified in the pyrochlore-supergroup: microlite (Ta⁵⁺), roméite (Sb⁵⁺), elsmoreite (W⁶⁺), betafite (Ti⁴⁺), ralstonite (Al³⁺), coulsellite (Mg²⁺) and pyrochlore (Nb⁵⁺) (Atencio, 2010, 2021).

Table 1 presents representative EPMA analyses in both zoned and zonation-free pyrochlore crystals from calcite carbonatite, tetraferriphlogopite phoscorite (both apatite-rich and magnetite-rich), and carbothermal veins. The formulae in atoms per formula unit (a.p.f.u.) was calculated on the basis of two B-site cations. Detailed EPMA data ($n = 95$) are available at Mendeley Data (<https://doi.org/10.17632/vs26by5p5b.3>).

According to the pyrochlore-supergroup minerals classification (Atencio et al., 2010), both zoned and zonation-free crystals from Boa Vista fall within the pyrochlore group, as well as samples from Morro do Padre Mine at Catalão II south (Palmieri et al., 2022), and Catalão I complex (Cordeiro et al., 2011), with only two outliers in the betafite group from Catalão I (Fig. 9a). The predominant pyrochlore phase in Boa Vista is calciopyrochlore with only two kenopyrochlore outliers (Fig. 9b). Therefore, calciopyrochlore in Boa Vista has Ca and Na as main cations at A-site, and Nb and Ti at B-site, whereas the concentrations of several elements are below the detection limit of EPMA analysis, corresponding to trace elements that were analyzed by LA-ICP-MS. In contrast, pyrochlore values obtained for Morro do Padre and Mine II/Area Leste deposits show that kenopyrochlore is the second most common pyrochlore phase in Catalão I and II after calciopyrochlore, while natropyrochlore is the least common phase (Fig. 9b). In the St. Honoré deposit, Canada, calciopyrochlore is also an abundant phase (Vasyukova and Williams-Jones, 2023), which in turn has been altered to columbite (Tremblay et al., 2017).

The EPMA data reveal that zoned calciopyrochlore grains display low variability in terms of their Ca content (0.97–1.13 a.p.f.u.), and Nb content (1.50–1.85 a.p.f.u.). However, there is greater variability in Na (0.35–0.80 a.p.f.u.) and Ti (0.15–0.41 a.p.f.u.) contents. At the crystal scale, Nb is homogeneously distributed within zoned crystals (Figs. 10a-b), but there are significant variations in Ti and Na that are supported by WDS maps (Figs. 10a-b), where a Ti-rich core relative to its rim is observed in grains with oscillatory zonation. There is also a non-homogeneous distribution of Na in oscillatory zoned grains.

Zonation-free calciopyrochlores (dissolved/skeletal and without dissolution) display low variability in their Ca (0.91–1.08 a.p.f.u.), Nb (1.72–1.88 a.p.f.u.), Na (0.67–0.79 a.p.f.u.) and Ti (0.12–0.25 a.p.f.u.) contents, with respect to zoned crystals. At crystal scale, dissolved-skeletal calciopyrochlore shows a heterogeneous Ti distribution with contrasting high/low Ti peaks distributed throughout the grain, where the primary zoned texture is completely obliterated. An inverse relationship between Na and Ti contents is evident in both zoned and dissolved-skeletal textures (Fig. 10c).

Table 2 provides a summary of the concentrations of minor and trace elements found in pyrochlore samples from calcite carbonatite, tetraferriphlogopite phoscorite (apatite- and

magnetite-rich), and carbothermal veins from the Boa Vista mine. These concentrations are reported in Mendeley Data (<https://doi.org/10.17632/vs26by5p5b.3>).

The pyrochlore data display a CI chondrite-normalized REE distribution characterized by an enrichment of LREEs and a depletion of HREEs (Fig. 11). Additionally, a positive Ce anomaly and a slight negative Eu anomaly is observed in the REE pattern (Fig. 11), which is consistent with geochemical data from carbonatite and phoscorite rocks in the Morro do Padre mine (Palmieri et al., 2022). The consistent REE-normalized pyrochlore patterns for carbonatite, phoscorites and carbothermal veins suggest the presence of antecrysts in carbothermal veins.

The variation diagrams of Figure 12 provide insights into the major, minor and trace element contents of pyrochlore, revealing key trends for immobile HFSE, REE elements, as well as Na and Sr. Firstly, both Nb vs Ti and Nb vs Zr exhibit a negative relationship for the majority of pyrochlore samples with zoned and zonation-free textures. Moderate scattering of data points indicates mixtures of antecrysts and primary pyrochlore phases. Pyrochlores from apatite-rich phoscorites with patchy zoned textures show a positive relationship that is associated with the formation of zirconolite at grain rims (Figs. 12a-b). On the other hand, the Zr vs Hf patterns show a consistent positive relationship (Fig. 12c), where primary pyrochlore textures are enriched in Zr and Hf compared to secondary textures, which are relatively depleted in those elements. For A-site cations, an inverse correlation can be observed between Na–Ce and Sr/Y–La. Here, primary pyrochlore textures are more enriched in La, Ce and Y, while secondary textures are more depleted in these elements (Figs. 12d-e).

Line scan analysis of a zoned pyrochlore using LA-ICP-MS shows some insights into the behaviour of REE and HFSE elements (Figs. 13a-b). The LREEs including La, Ce, Pr and Nd that count above 10^5 counts per second (cps) follow the oscillatory zoned pattern, with the rims slightly more enriched in LREE with respect to the core (Fig. 13a). The zoning pattern is a little more scattered for REEs that are counted below 10^5 cps (e.g., Sm, Eu, Gd, Tb, Dy and Ho). In contrast, there is no correlation between the zoned pyrochlore texture and the behaviour of HFSE elements, as was seen for the REE (Fig. 13b). The Ta and U have a very dispersed core-to-rim pattern with large variations, with CPS varying up to two orders of magnitude in a single zoned pyrochlore grain (Fig. 13b).

4.6. DISCUSSION

4.6.1. Textural analysis of pyrochlore and its relationship with magmatic and carbothermal processes

The various pyrochlore textures in samples from the Boa Vista deposit depict a complex multi-stage evolution. This evolution encompasses the transition from primary zoned pyrochlores to zonation-free pyrochlores (dissolved/skeletal and without dissolution). In alkaline–carbonatite systems, zoned pyrochlores with magmatic origin have been identified in the Loe-Shilman

Carbonatite Complex (Khan et al., 2021), the Kerimasi volcano in Tanzania (Zaitsev et al., 2021), and the Kaiserstuhl volcanic complex, in SW Germany (Walter et al., 2018). Analogous to the previous examples, in the Morro do Padre deposit, a magmatic origin is attributed to the phosphorites and carbonatites with pyrochlore mineralization—many of them with zoned textures—supported by country-rock xenoliths within dikes, and by the occurrence of a 140 m thick layered sill with a phoscorite-to-carbonatite layering that represent ponding (Palmieri et al., 2022).

Similarly to Morro do Padre, the pyrochlore-bearing phoscorite and carbonatite rocks in the lower hypogene zone of the Boa Vista deposit display layering (Fig. 4a), attributed to a magmatic origin. Exploratory drill cores show that zoned pyrochlore textures in carbonatite and phosphorite rocks are common at depths between 487 to 183 m, corresponding to the lower hypogene zone, while zonation-free textures are shallower, commonly recorded in the upper hypogene zone and the regolith (284 to 3 m depth). The above suggests that the zoned textures were formed in an earlier primary magmatic stage, since they are more abundant at depth, while the zonation-free textures were formed (or perhaps reworked) in a later secondary magmatic stage during the emplacement of dike swarms. Following the formation of zoned pyrochlore cores at depth (Figs. 6a and 7a), these grains were subject to further crystallization (overgrowths) during the emplacement of the carbonatite-phoscorite dike swarm (Fig. 7c), resulting in zoned rims due to compositional change of the carbonatite magma during fractionation. These overgrowth zones subsequently experience resorption at shallower depths, as evidenced by dissolution/skeletal textures with abundant apatite inclusions (Figs. 6b, 7b and 7d). Because some oscillatory zoned pyrochlores have dissolution textures at their rims, perhaps dissolution is not always penetrative as observed in calcite carbonatite grains.

In contrast, pyrochlores from carbothermal veins record a distinct origin. One hypothesis could support the notion that these zonation-free, non-dissolved pyrochlores (Fig. 8c) are generated from carbothermal fluids (late-stage, low-temperature, CO₂-rich fluids; Mitchell and Gittins, 2022). However, the chondrite-normalized REE distribution for all pyrochlore crystals from Boa Vista are parallel to the geochemical results of carbonatite and phoscorite rocks from the Morro do Padre mine (Fig. 11). Thus, pyrochlores from carbothermal veins probably crystallized from a carbonatite magma, corresponding to antecrysts that are not in chemical equilibrium with the surrounding carbothermal liquid. Regarding the previous evidence, the use of LA-ICP-MS data in pyrochlore could be a tool for future studies in other carbonatite-related Nb deposits to corroborate whether the origin of pyrochlore is magmatic or carbohydrothermal. For example, Biondi and Braga Junior (2023) propose the presence of hydrothermal pyrochlore in the Araxá Complex, based on the presence of phlogopite and apatite inclusions, which according to the authors was not observed in any other rocks based on their textural analyses, without taking into account the chemistry of major or trace elements of pyrochlore.

4.6.2. Insights into Nb enrichment processes from source to ore

The Nb enrichment processes in Boa Vista, as part of the Catalão II South intrusion, includes the production, fractionation and emplacement of alkaline and carbonatite magmas, with massive formation of pyrochlore, accumulated in economically exploitable quantities in tetraferriphlogopite phoscorites. The most recent model in the generation of alkaline-carbonatite magmatism in the APIP, has shown through regional aeromagnetic data and comprehensive lithogeochemical and isotopic data, a multi-stage fractionation process from a primary ultrapotassic carbonated-silicate magma (i.e., Ni >500 ppm, Cr >1000 ppm, up to Fo₉₀ olivine compositions, K₂O >3 wt.%, MgO >3 wt.%, and K₂O/Na₂O >2), localized in a metasomatized subcontinental lithospheric mantle that ascends and fractionates at different crustal levels (Velásquez et al., 2023), generating numerous alkaline-carbonatite complexes to the west of the APIP, and the production of a kamafugitic volcanism of the Mata da Corda Formation to the east of the APIP.

The geochemical signatures of aillikites at both Catalão II North and South is similar to the composition of the previously described primary magma that, together with the presence of carbonatite pockets, is attributed as a parental magma to the carbonatites (Brod et al., 2000; Velásquez Ruiz et al., 2023). Aillikite dikes from Morro do Padre show concentrations from 200 to 400 ppm Nb and a Nb/Ta ratio ranging between 17.4 and 29.2, while carbonatite dikes reach up to ~2000 ppm Nb and a Nb/Ta ratio ranging 54.1 to 10,395 (Palmieri, 2011). The progressive increase in Nb concentration and the Nb/Ta ratio provides evidence of an advanced degree of fractionation, leading to Nb enrichment in the carbonatite magma compared to its parental aillikite.

In contrast, pyrochlore geochemistry reveals some details about its crystallization from a carbonatite magma. As seen in Chapter 5.1, zoned pyrochlores are recorded in cumulate carbonatite and phoscorite rocks in the lower hypogene zone, while zonation-free textures are recorded in dike swarms in the upper hypogene zone and the regolith. The EPMA and *in-situ* LA-ICP-MS data on a zoned pyrochlore of a calcite carbonatite gives an idea of the behaviour of HFSE and REE elements. For example, the WDS maps show that the Nb content in zoned textures (even in zonation-free textures) does not vary for a single crystal (Fig. 10), as is expected since Nb is the main cation in the B site for calciopyrochlore. In addition, WDS maps show that Ti follows the zoned pattern of the texture (Fig. 10). However, the line scan analysis shows that there is an erratic incorporation of Ta and U in the pyrochlore structure that varies the CPS by two orders of magnitude (Fig. 13b), which does not follow the zoned pattern of the crystal. Therefore, the Ta and U concentrations from *in-situ* pyrochlore analysis should be taken carefully. The line scan analysis also reveals that the REEs follow the zoned pattern of pyrochlore (Fig. 13a), being slightly more enriched towards the edges. The above, together with the formation of qaqarssukite-(Ce) in carbothermalites, could indicate that the REEs are preferentially concentrating in late-stage CO₂-rich carbothermal fluids. The dispersed behaviour in Nb vs Ti, Nb vs Zr, and Na vs Ce (Fig. 12a-d) can be attributed to the mixing of antecrysts with primary phases. However, the Sr/Y vs La diagram (Fig. 12e) marks a defined negative pattern without decoupling, suggesting a process of magmatic fractionation without unmixing.

4.6.3. Heavy minerals transport within a carbonatitic system

Rock-forming minerals in phoscorites are apatite and magnetite, plus one of the silicate phases forsterite, diopside or phlogopite. Outside of the alkaline-carbonatite complexes, this mineralogy resembles those found in other geodynamic settings, such as Iron Oxide Apatite (IOA) or Kiruna-type deposits (Knipping et al., 2015a; Ovalle et al., 2018; Rojas et al., 2018; Reich et al., 2022), which form massive apatite-magnetite-rich rocks. One of the theories to explain the formation of these rocks is the magnetite transport model where magnetite is the first liquidus phase to form in hydrothermal fluids and is transported via a buoyancy mechanism. In this model, H₂O bubbles nucleate on magnetite crystal surfaces, and then the bubble-magnetite pairs rise when the buoyancy force $F^{\text{buoyancy}} > 0$, according to the equation $F^{\text{buoyancy}} = (V_{\text{bubble}} \cdot \Delta\rho_{\text{bubble}} - V_{\text{mgt}} \cdot \Delta\rho_{\text{mgt}}) \cdot g$ (Knipping et al., 2015b), where V_{bubble} and V_{mgt} are the volumes of bubble and magnetite, respectively, g is gravitational force, and $\Delta\rho$ is the density difference between melt and bubble ($\Delta\rho_{\text{bubble}}$) or between magnetite and melt ($\Delta\rho_{\text{mgt}}$). In Boa Vista, important evidence regarding the transport mechanism can be found in intercumulus calcite within tetraferriphlogopite phoscorites. A closer examination of intercumulus calcite using CL surrounding magnetite and apatite crystals (Figs. 14a-b), provides evidence of carbonatitic liquid residues within tetraferriphlogopite phoscorite dikes which suggests that alkaline–carbonate-rich fluids played a role in transporting heavy minerals, perhaps through the buoyancy mechanism previously described. The SEM and CL images in pyrochlore and apatite (Figs. 6 to 8), along with CL images in intercumulus carbonates (Fig. 14), could indicate that the formation of tetraferriphlogopite phoscorite dikes involves a mixture of crystal transport and in situ crystallization from a carbonatite magma.

4.6.4. Genesis of pyrochlore-rich phoscorites

Three hypotheses have been proposed regarding the formation of phoscorites associated with carbonatites: (i) crystal segregation due to fractional crystallization (Cordeiro et al., 2010, Palmieri et al., 2022), (ii) liquid immiscibility between carbonatite and phoscorite melts as proposed at Palabora, South Africa (Giebel et al., 2019) and Kovdor, Russia (Krasnova et al., 2004b) and, (iii) formation of a phoscoritic residual magma during fenitization from a parental carbonatitic magma as suggested for St. Honoré, Canada (Williams-Jones and Vasyukova, 2023).

Textural evidence from drill core observations suggests that there are cumulate carbonatite-phoscorite layers in the lower hypogene zone, at depths greater than 300 m in the Boa Vista deposit. Being cumulates, these rocks do not represent liquid bulk compositions. Furthermore, the pyrochlore compositions show no evidence of decoupling as a possible indicator of unmixing, beyond the mixing of primary pyrochlore phases with antecrysts. As mentioned above, there is no evidence of a phoscoritic magma at the Catalão II Complex, either derived from fenitization or as a byproduct of immiscibility. Similar evidence is revealed for the Morro do Padre deposit, where those cumulate carbonatite-phoscorite pairs suggest crystal settling from a parental magma and interstitial carbonate extraction through filter pressing (Palmieri et al., 2022).

In the St. Honoré Complex, Nb mineralization is interpreted as the result of the basement fenitization forming a phoscoritic magma, where pyrochlore is associated with the fenite halos (Williams-Jones and Vasyukova, 2023). This differs from the Catalão II (Palmieri et al., 2022) and Catalão I complexes (Cordeiro et al., 2010), where there is development of a pyrochlore-absent K-rich fenite, whereas the Nb mineralization is primary circumscribed to tetraferriphlogopite phoscorite from the layers and dikes (Palmieri et al., 2022). Therefore, our observations do not support the formation of a phoscoritic magma due to carbohydrothermal activity or the immiscibility of a carbonatitic/phoscoritic pair.

Based on textural and chemical evidence observed in primary zoned and secondary zonation-free pyrochlore, a conceptual model is proposed (Fig. 15). In this model, the primary magma of the Catalão II Complex is a kamafugite-like ultrapotassic magma that generated aillikites containing abundant lobular carbonate pockets, which coalesced to form a parental carbonatite magma (Velásquez Ruiz et al., 2023). Subsequent fractionation of the parental carbonatite magma involved physical segregation of heavy minerals, including magnetite, apatite, phlogopite, pyrochlore (Fig. 15a), resulting in the formation of cumulates consisting of metric layers of phoscorites and carbonatites. Following this initial stage, a two-step exsolution phase driven by alkaline–carbonate-rich fluids helped mobilize some heavy minerals such as magnetite towards the upper hypogene zone, while other minerals such as pyrochlore and apatite were reworked/dissolved and in situ crystallized forming: (i) pyrochlore-rich tetraferriphlogopite phoscorites dikes, and (ii) carbonatite dikes containing traces of pyrochlore, which later dehydrated to form REE-rich carbothermal veins (Fig. 15b-d). A fraction of the alkaline–carbonate-rich fluids were separated from the intrusion and escaped into the surrounding basement rocks forming phlogopite-rich fenites (Fig. 15b).

4.7. CONCLUSIONS

The Boa Vista mine, located south of the alkaline-carbonatite Catalão II Complex, is the second largest Nb resource in the world after Araxá, with both occurring in the Alto Paranaíba Igneous Province, Central Brazil. Exploratory drill cores and petrographic analysis reveal that niobium mineralization is controlled by the presence of pyrochlore in tetraferriphlogopite phosphorites, which occur as cumulate layers in the lower hypogene zone, and as dike swarms in the upper hypogene zone, both cases associated with carbonatite rocks. Detailed observations using SEM and CL reveal two groups of textures in pyrochlore grains, a first group of zoned pyrochlores from the lower hypogene zone, where zonation forms in response to magmatic fractionation, and a second group of zonation-free pyrochlores located in the upper hypogene zone, formed by secondary processes including transport and reworking, as evidenced by the presence of dissolved and skeletal secondary grains. Furthermore, in-situ pyrochlore LA-ICP-MS data show additional evidence of magmatic fractionation, where Sr/Y vs La and Na vs Ce plots do not show decoupling as evidence of immiscibility. The REE-normalized pyrochlore patterns are consistent with the geochemical data from carbonatite and phoscorite rocks and suggest a magmatic origin for the Boa Vista pyrochlores. Because pyrochlores from carbothermal veins follow a similar pattern to

magmatic grains, these pyrochlores correspond to antecrysts that are not in chemical equilibrium with the surrounding carbothermal fluid. Therefore, there is no evidence of pyrochlore formation from carbohydrothermal fluids in Boa Vista. Intercumulus calcite within tetraferriphlogopite phoscorite dikes is interpreted as remnants of carbonatitic magma, supporting the hypothesis that alkaline–carbonate-rich fluids play a crucial role in the transport of heavy minerals, such as magnetite, apatite and pyrochlore. Based on textural and chemical evidence, we propose that tetraferriphlogopite phoscorites were formed by the segregation of heavy minerals from a carbonatite magma, forming cumulates in the lower hypogene zone, and later transported (with *in situ* crystallization) in dike swarms in the upper hypogene zone. Results from this study should motivate further studies focusing on pyrochlore geochemistry in carbonatite-related Nb deposits that will be crucial for advancing our knowledge of global Nb metallogenesis, which is key since Nb has been classified as critical due to exposure to supply restrictions related to increased global demand.

4.8. ACKNOWLEDGMENTS

This work was supported by ANID through the Millennium Science Initiative grant NCN13_065 “Millennium Nucleus for Metal Tracing Along Subduction”. Felipe Velásquez thanks financial support provided by ANID-Subdirección de Capital Humano/Doctorado Nacional/2021-21210049. Additional funding was provided by the Hugh McKinstry Fund of the Society of Economic Geologists Foundation Inc. Sam Broom-Fendley acknowledges NERC grants NE/X015114/1, NE/V008935/1 and NE/R013403/1. The authors also thank the company CMOC Brazil for enabling analysis inside the Boa Vista Pit, and the contributions from three anonymous reviewers and editorial suggestions from Dr. Gleb Pokrovski, which greatly improved the original manuscript.

4.9. DATA AVAILABILITY

Data are available through EPMA and LA-ICP-MS Pyrochlore data at <https://doi.org/10.17632/vs26by5p5b.3>.

4.10. TABLES

Table 2. Representative EPMA analyses for pyrochlore in each rock type from the Boa Vista mine at Catalão II South.

Rock type	Calcite carbonatite			Apatite-rich phoscorite			Magnetite-rich phoscorite			Carbothermal vein		
	Oscillatory	Dissolved	Skeletal	Patchy	Patchy	Skeletal	Patchy	Patchy	Patchy	Unzoned	Unzoned	Unzoned
Texture												
Nb₂O₅	60.32	67.58	52.22	67.59	55.69	64.08	59.41	62.10	59.31	63.16	66.07	67.06
Ta₂O₅	bdl	0.09	0.08	0.11	bdl	bdl	bdl	bdl	bdl	bdl	0.11	bdl
SiO₂	0.84	0.03	2.97	0.01	0.03	bdl	bdl	bdl	0.18	0.43	0.23	0.01
TiO₂	6.10	3.00	4.88	3.43	7.58	4.42	5.91	5.32	6.28	4.92	4.13	3.75
ZrO₂	0.18	bdl	0.10	bdl	1.19	bdl	0.75	0.11	0.73	0.19	0.12	bdl
UO₂	0.82	0.44	0.33	0.64	0.42	0.38	0.35	0.40	0.54	0.81	0.69	0.45
ThO₂	1.70	0.51	1.31	0.02	4.09	1.90	2.54	2.00	2.21	0.30	0.21	0.22
La₂O₃	0.84	0.27	0.39	0.68	0.59	0.80	0.75	0.59	0.89	0.57	0.39	0.35
Ce₂O₃	1.97	0.85	7.38	1.21	3.49	1.94	3.05	2.59	2.21	1.28	1.00	0.88
Y₂O₃	1.04	1.27	0.80	1.17	0.92	1.28	0.08	0.78	0.34	1.22	1.10	1.11
FeO	0.45	0.07	2.33	0.07	0.20	0.14	0.34	0.10	0.26	0.11	bdl	0.03
CaO	15.34	15.63	3.07	15.68	15.90	15.11	16.06	15.00	16.41	16.15	16.02	16.08
BaO	bdl	bdl	15.56	bdl	bdl	bdl	bdl	bdl	bdl	bdl	bdl	bdl
SrO	1.50	1.39	1.56	1.10	0.63	1.84	1.14	1.29	1.05	1.66	1.66	1.59
Na₂O	6.04	6.41	0.05	6.04	4.67	6.28	5.08	5.78	4.66	5.66	5.95	6.26
F	bdl	0.05	bdl	0.04	0.02	bdl	0.01	bdl	0.02	bdl	0.02	bdl
Total	97.1	97.6	93.0	97.8	95.4	98.2	95.5	96.1	95.1	96.5	97.7	97.8
<i>a.p.f.u. on the basis of two B-site cations</i>												
Nb	1.663	1.860	1.557	1.842	1.599	1.794	1.696	1.748	1.672	1.742	1.794	1.830
Ta	bdl	0.001	0.001	0.002	bdl	bdl	bdl	bdl	bdl	bdl	0.002	bdl
Si	0.051	0.002	0.196	0.001	0.002	bdl	bdl	bdl	0.011	0.026	0.014	bdl
Ti	0.280	0.137	0.242	0.155	0.362	0.206	0.281	0.249	0.294	0.226	0.186	0.170
Zr	0.005	bdl	0.003	bdl	0.037	bdl	0.023	0.003	0.022	0.006	0.003	bdl
ΣB-site	2.0	2.0	2.0	2.0	2.0	2.0	2.0	2.0	2.0	2.0	2.0	2.0
U	0.011	0.006	0.005	0.009	0.006	0.005	0.005	0.006	0.007	0.011	0.009	0.006
Th	0.024	0.007	0.020	bdl	0.059	0.027	0.037	0.028	0.031	0.004	0.003	0.003
La	0.019	0.006	0.009	0.015	0.014	0.018	0.017	0.014	0.020	0.013	0.009	0.008
Ce	0.044	0.019	0.178	0.027	0.081	0.044	0.071	0.059	0.050	0.029	0.022	0.019
Y	0.034	0.041	0.028	0.037	0.031	0.042	0.003	0.026	0.011	0.040	0.035	0.036
Fe₂	0.023	0.003	0.129	0.004	0.011	0.007	0.018	0.005	0.014	0.006	bdl	0.001
Ca	1.003	1.019	0.217	1.013	1.082	1.003	1.087	1.001	1.096	1.056	1.031	1.040
Ba	bdl	bdl	0.402	bdl	bdl	bdl	bdl	bdl	bdl	bdl	bdl	bdl
Sr	0.053	0.049	0.060	0.038	0.023	0.066	0.042	0.047	0.038	0.059	0.058	0.056
Na	0.714	0.757	0.006	0.706	0.575	0.754	0.622	0.698	0.563	0.669	0.693	0.733
A□-site	0.076	0.092	0.946	0.149	0.118	0.034	0.100	0.118	0.168	0.114	0.140	0.098
ΣA-site	2.0	2.0	2.0	2.0	2.0	2.0	2.0	2.0	2.0	2.0	2.0	2.0
F	bdl	0.011	bdl	0.009	0.004	bdl	0.003	bdl	0.004	bdl	0.003	bdl
(OH,O,O₂,H₂O)²	1.0	0.989	1.0	0.991	0.996	1.0	0.997	1.0	0.996	1.0	0.997	1.0
ΣY-site	1.0	1.0	1.0	1.0	1.0	1.0	1.0	1.0	1.0	1.0	1.0	1.0

Abbreviations: Av., average; max., maximum; min, minimum; bdl, below detection limit.

Table 3. Summary of trace element concentrations for pyrochlore in each rock type from the Boa Vista mine.

Element ($\mu\text{g/g}$)	Calcite (n=11)			carbonatite			Apatite-rich phoscorite (n=23)			Magnetite-rich phoscorite (n=8)			Carbothermal (n=10)			vein
	Max.	Min.	Av.	Max.	Min.	Av.	Max.	Min.	Av.	Max.	Min.	Av.	Max.	Min.	Av.	
Mg	4310	bdl	254	580	bdl	67	93	25	64	990	bdl	151				
Al	22.7	bdl	3.6	45	bdl	2.4	3.2	bdl	0.9	900	bdl	98.5				
Si	90000	bdl	10919	5900	bdl	bdl	1770	151	1058	2410	bdl	5420				
K	1873	bdl	bdl	888	223	623	1370	922	1265	721	341	507				
V	16	2.3	9.8	22.1	1.5	6.1	15	3.3	11.5	13.3	5.5	9.7				
Mn	180	30	88	1300	10	143	130	43	102	232	15	47				
Sr	14600	7130	11904	24700	5340	13861	13100	9000	9895	16000	11300	14070				
Y	155	20	77	502	13	91	76	34	58	49	28	31				
Zr	4910	154	2416	13800	170	2927	6770	705	4642	2310	980	1675				
Ba	5100	113	945	98000	107	4830	870	175	294	4160	486	1510				
La	9140	1620	5709	8150	2000	3753	7600	3520	4249	4820	2900	4112				
Ce	31800	4130	17978	51100	6320	14703	18900	11510	12800	14000	7180	10995				
Pr	2530	354	1580	3290	516	1086	1750	1027	1166	835	506	744				
Nd	7020	966	4339	11300	1290	3365	5480	3180	3590	2550	1560	2212				
Sm	687	75	335	1900	90	437	510	278	356	270	160	225				
Eu	190	16	87	359	21	76	98	56	75	35	22	31				
Gd	1190	bdl	89	1090	43	217	183	100	132	134	83	118				
Tb	27.6	3.7	12.8	84.4	2.7	15.3	13.8	7.1	11	6.9	4.3	6				
Dy	77	9.7	41.8	328	6.2	53.2	44.2	20.2	34.8	17.1	11.4	14.9				
Ho	8.3	0.9	4.7	32.1	0.6	5.4	4.4	1.8	3.5	1.8	1.2	1.5				
Er	22.2	1.6	11.5	65	1	9.8	6.9	3	5.5	4.6	1.8	3.1				
Tm	1.9	0.1	0.8	5.5	bdl	0.8	0.6	0.2	0.4	0.5	0	0.2				
Yb	8.7	0.2	4.1	17.9	bdl	3.3	2.4	0.8	1.7	2.1	0.2	0.9				
Lu	0.6	0	0.3	1.2	bdl	0.2	0.2	0.1	0.1	0.2	0	0.1				
Hf	480	14	195	657	16	155	298	54	207	116	56	89				
Ta	4390	1	1117	231	23	75	1330	36	425	73	3	16				
W	59.9	6.8	18.7	64.2	2.3	23.7	12.8	2.8	4.5	28.3	8.4	15.3				
Pb	233	71	128	711	50	153	189	139	171	277	43	86				
Th	25500	437	12028	77600	2240	13383	18500	11400	15956	2790	1340	2261				
U	81000	1	19132	3260	34	606	1345	1	461	1090	60	267				

Abbreviations: min, minimum; max., maximum; Av., average; bdl, below detection limit.

4.11. FIGURES

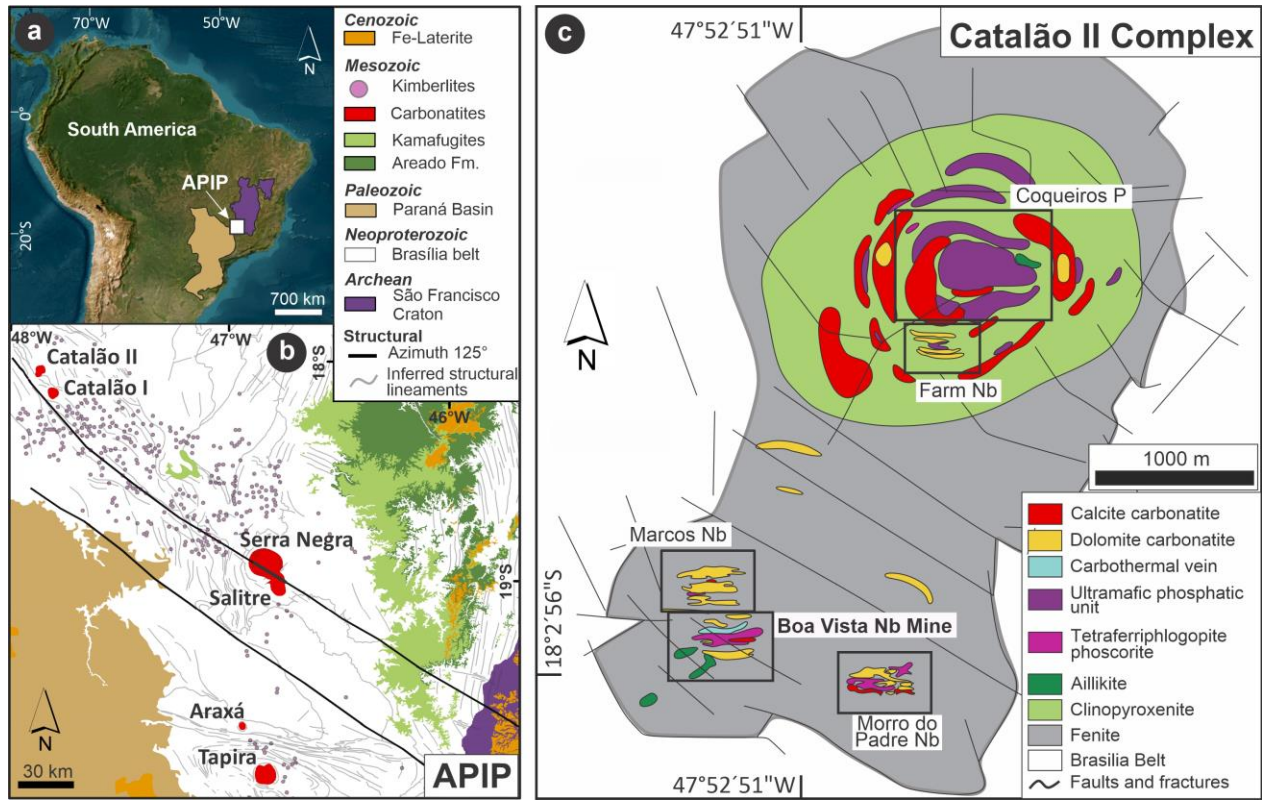


Fig. 26. (a) South America map, showing the location of the APIP, between the São Francisco craton and the Paraná Basin. (b) Geological map of the APIP showing the location of the six main alkaline-carbonatite complexes, modified from the 1:1 M Belo Horizonte (SE-23) and Goiânia (SE-22) cartographic sheets of the Brazilian Geological Survey. SFC, São Francisco Craton. (c) Geological map of the Catalão II complex, showing the location of the north and south plugs and the niobium and phosphate mines (modified after Palmieri et al., 2022).

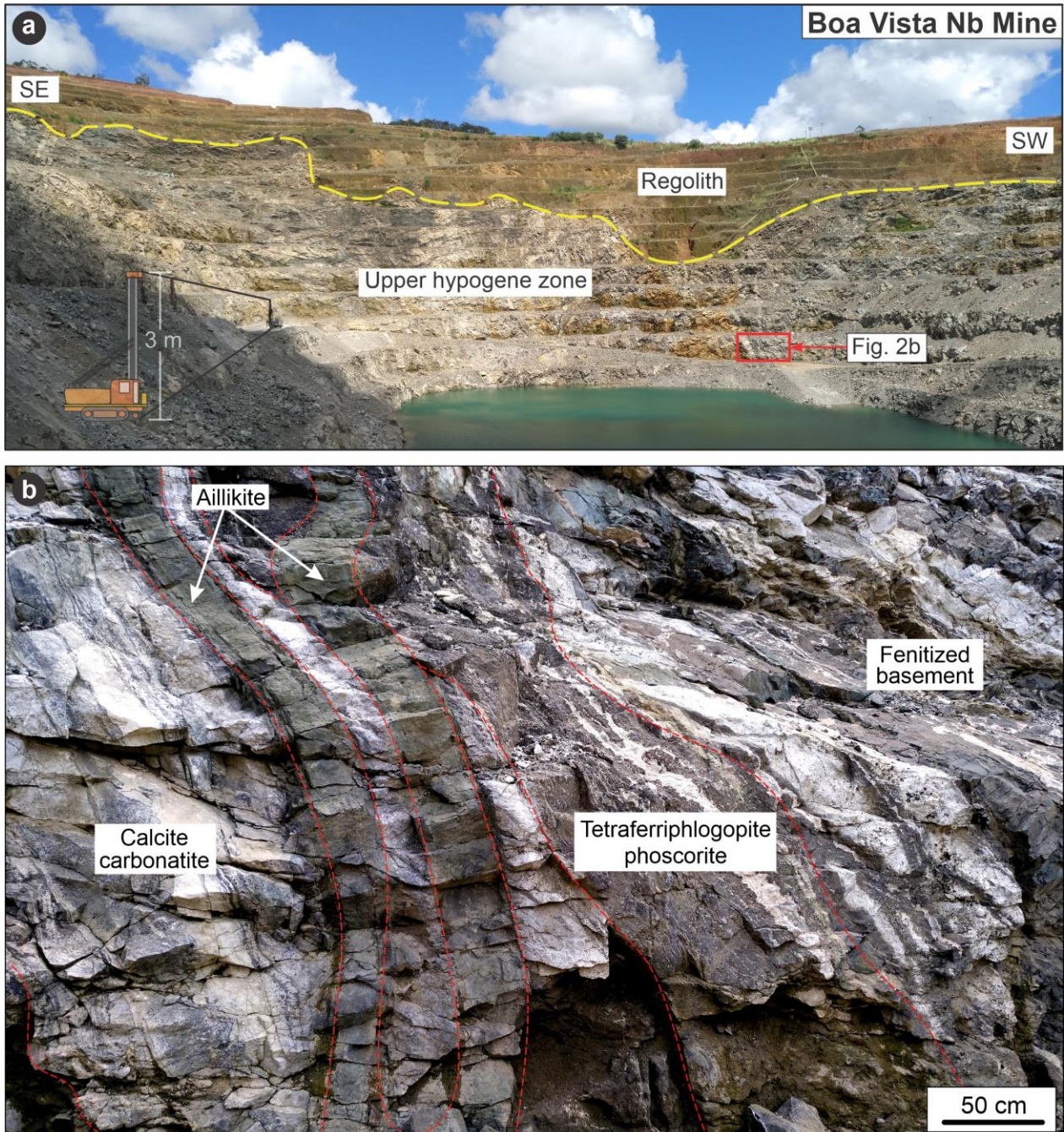


Fig. 27. (a) Boa Vista mine pit, showing the separation of the pyrochlore-enriched regolith and the upper hypogene zone where dike swarms of carbonatite, phoscorite, aillikite and carbothermal veins are braided. (b) Outcrop of a typical dike swarm of the Boa Vista Nb mine, located in the red rectangle of Figure 2a, showing calcite carbonatite and tetraferriphlogopite phoscorite dykes fenitizing the basement and being intruded by a pair of olivine aillikites.

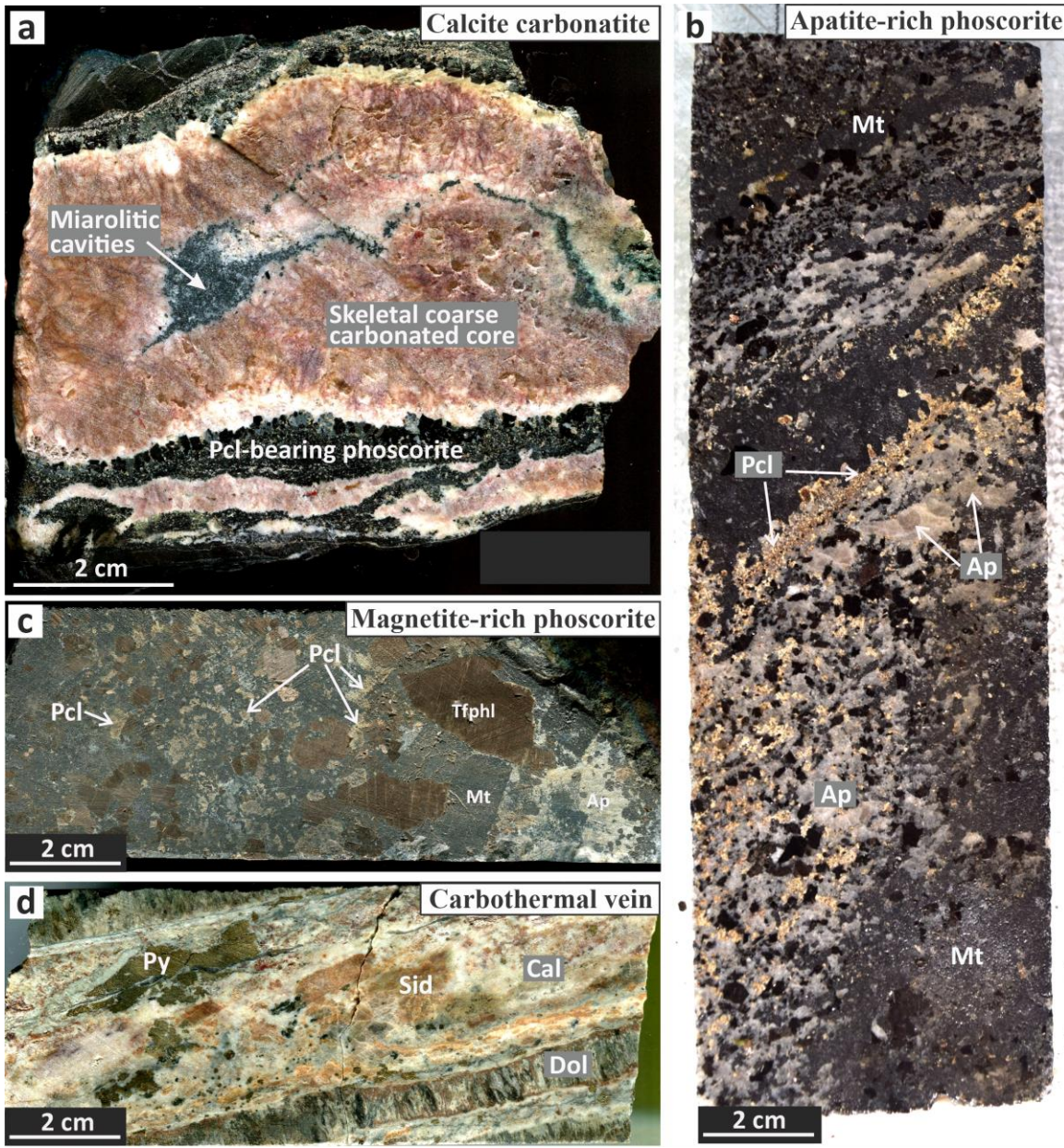


Fig. 28. Photos of representative drill core samples of the different lithotypes from the Boa Vista mine. (a) calcite carbonatite sample, showing a miarolitic core enveloped by skeletal carbonates, in turn in contact with a medium to fine grained pyrochlore-bearing phoscorite. (b) Medium-grained apatite-rich (Ap) tetraferriphlogopite phoscorite with magnetite-rich transitions, and a caramel-colored pyrochlore cumulate. (c) Coarse-grained magnetite-rich tetraferriphlogopite phoscorite, with large magnetite (Mt) and tetraferriphlogopite (Tfphl) crystals, and coarse-grained crystals of light brown pyrochlore (Pcl). (d) Carbothermal vein with calcite (Cal), dolomite (Dol), siderite (Sid), pyrite (Py) and variegated fine-grained carbonates.

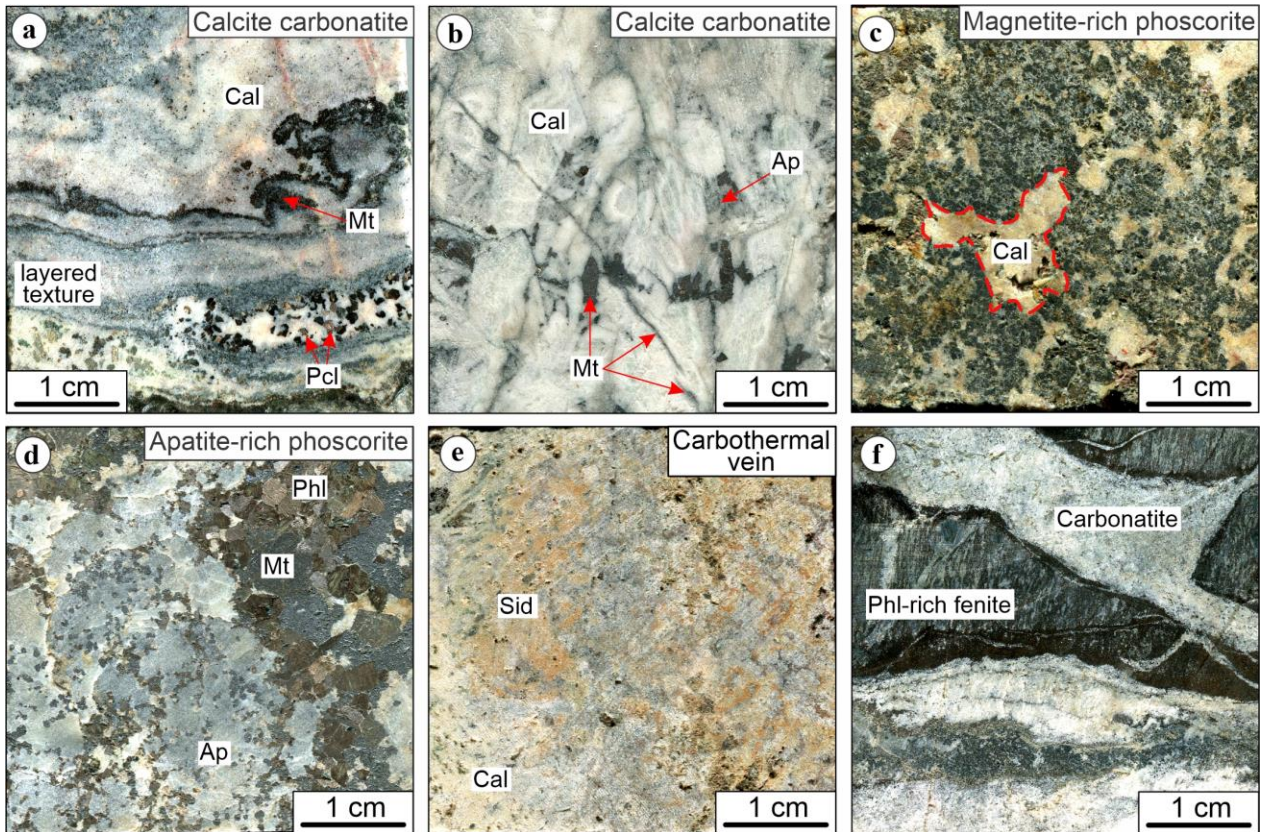


Fig. 29. Borehole samples of the Boa Vista Nb mine. (a) Layered calcite carbonatite with calcite (Cal), magnetite (Mt) and pyrochlore (Pcl). (b) Calcite carbonatite with dog tooth texture carbonates, intercumulus apatite (Ap) and secondary magnetite veinlets. (c) Magnetite-rich phoscorite with irregular calcite pockets. (d) Apatite-rich phoscorites of isotropic texture with a coarse-grained magnetite-phlogopite pocket. (e) Siderite-rich (Sid) carbothermal vein with variegated texture. (f) Phlogopite-rich (Phl) fenitized basement, being digested by a calcite carbonatite.

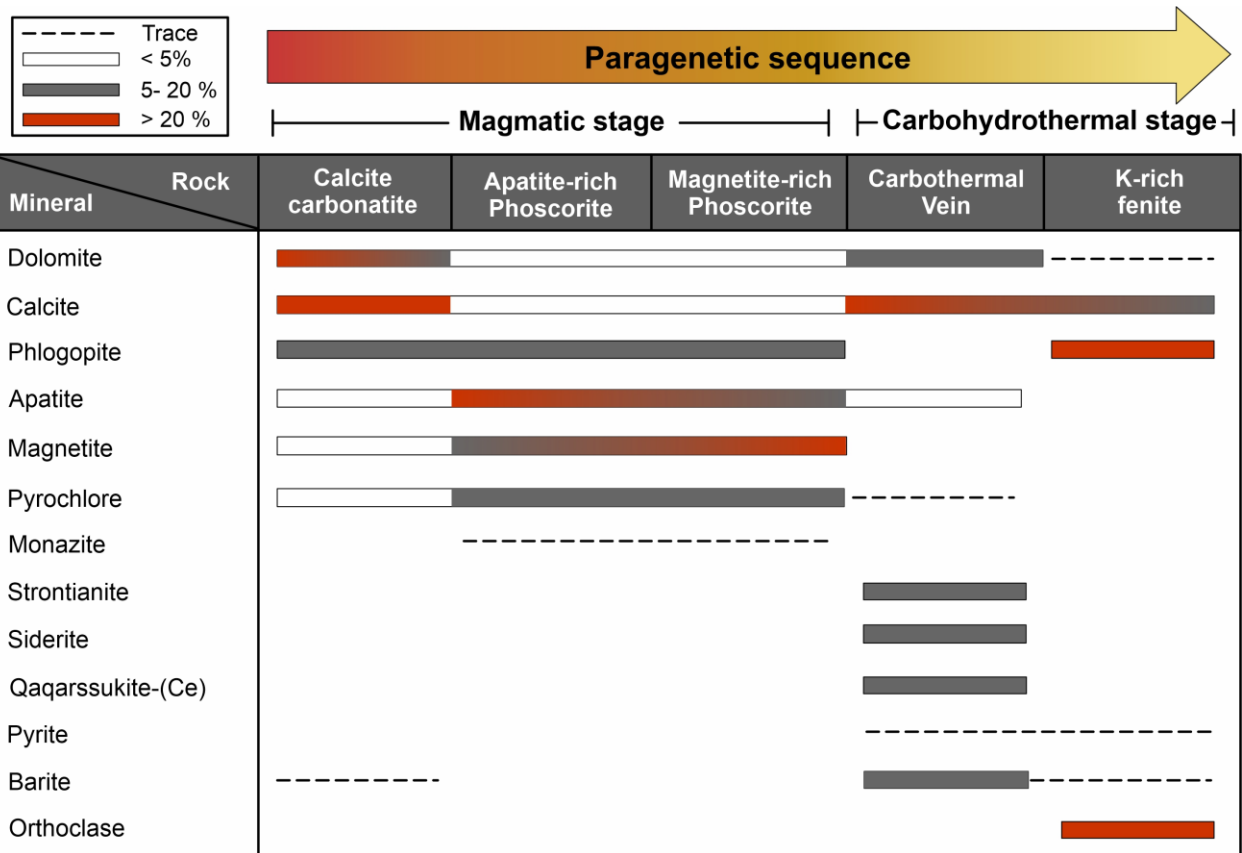


Fig. 30. Paragenetic sequence of mineral phases in magmatic and carbohydrothermal lithotypes, from the Boa Vista Nb mine. The abundance of mineral phases is shown according to four arbitrary intervals, divided into: (i) Trace; (ii) < 5%, (iii) 5 – 20 %, and (iv) > 20 %.

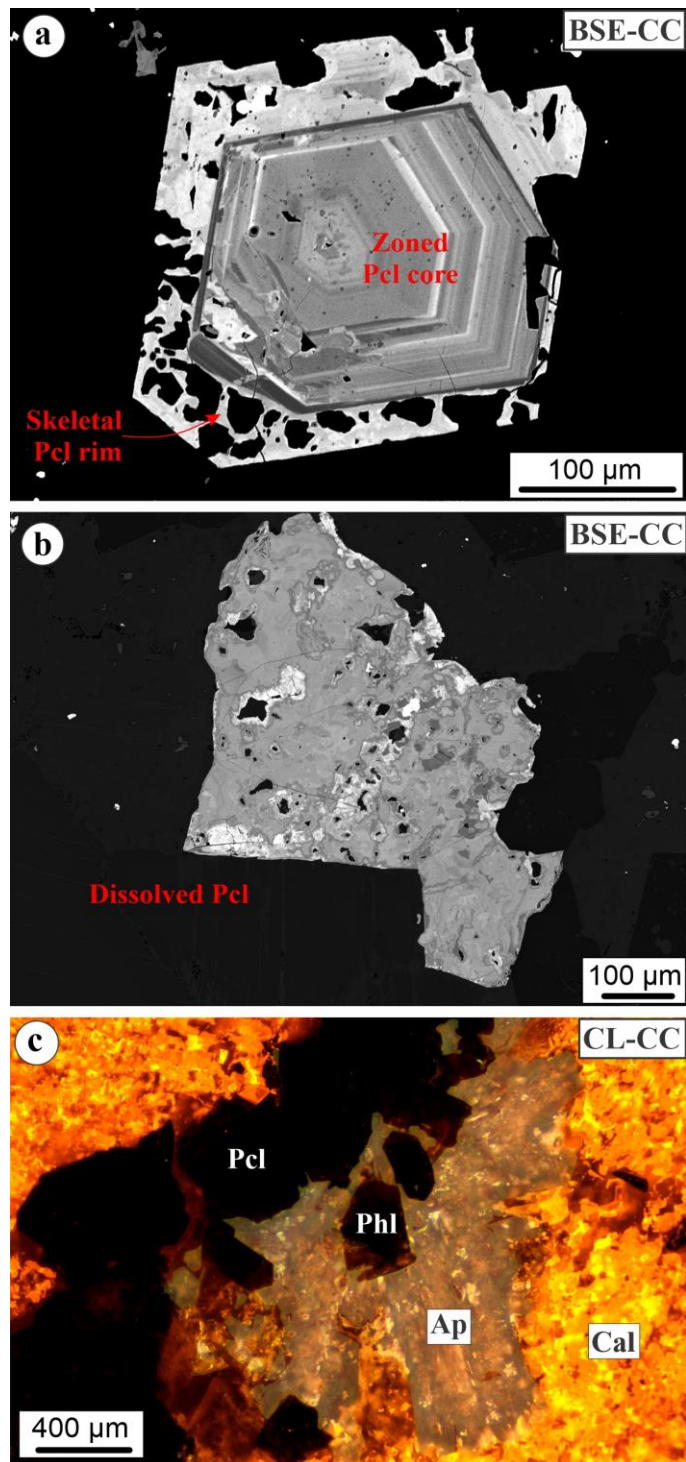


Fig. 31. Pyrochlore (Pcl) specimens in calcite carbonatite (CC). (a) BSE image of a pyrochlore crystal with oscillatory zoned core and skeletal rim. (b) BSE image of dissolved pyrochlore with irregular areas of light and dark BSE brightness. (c) Pyrochlore, apatite (Ap), phlogopite (phl), and calcite (Cal) viewed under CL, showing a low response for pyrochlore under CL.

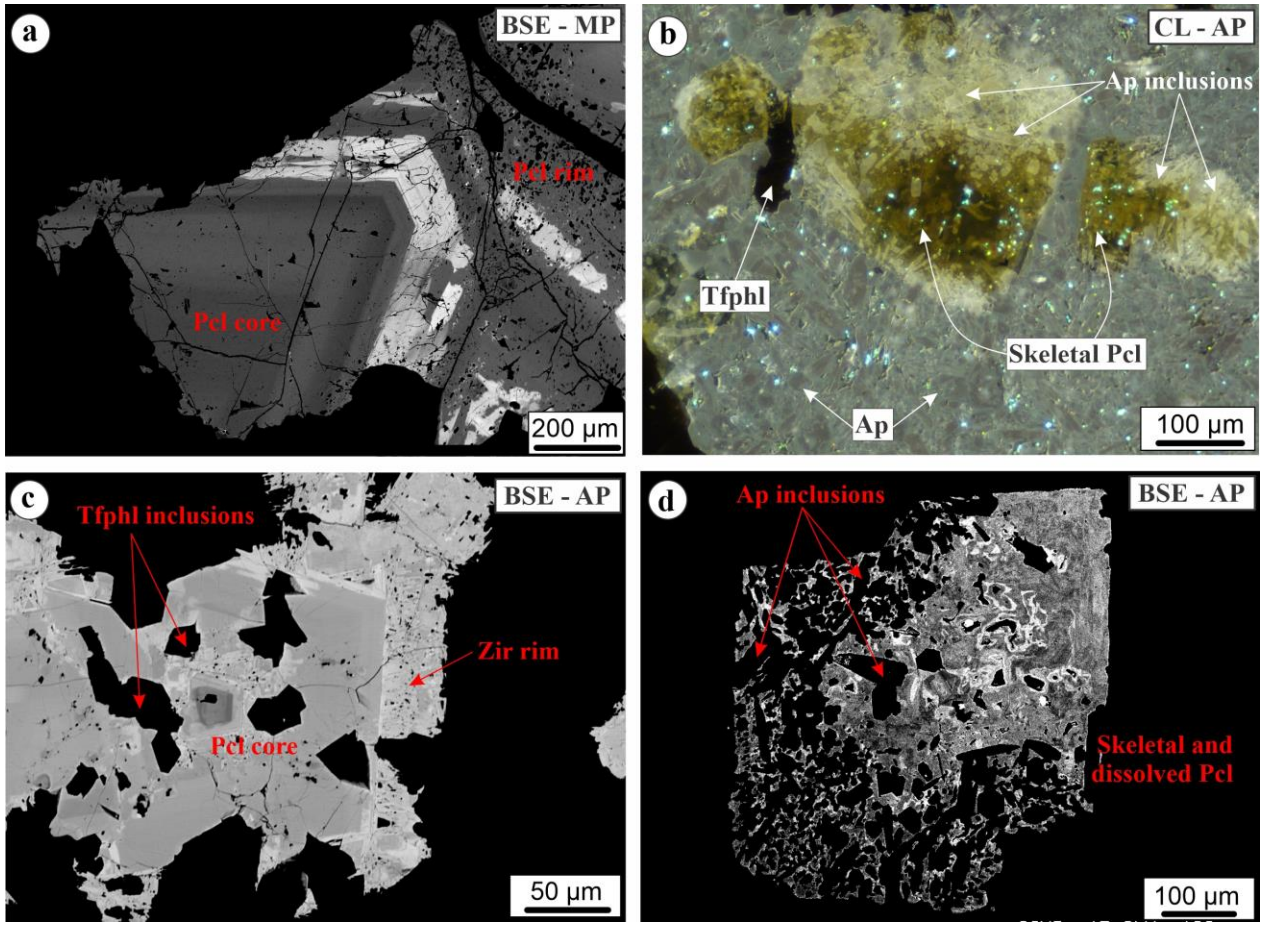


Fig. 32. Representative BSE (a, c-d) and CL (b) images of pyrochlore (Pcl) in tetraferriphlogopite (Tfphl) phoscorite dykes. (a) Patchy zoned pyrochlore from a magnetite-rich phoscorite (MP). (b) Pyrochlore from an apatite-rich phoscorite (AP) with a masked yellowish-brown colour CL. Groundmass is fine-grained and zoned apatite, with a light blue colour activated by Ce³⁺. (c) Patchy zoned pyrochlore from an apatite-rich phoscorite, with a zirconolite (Zir) rim. (d) Dissolved pyrochlore from an apatite-rich phoscorite with a skeletal rim.

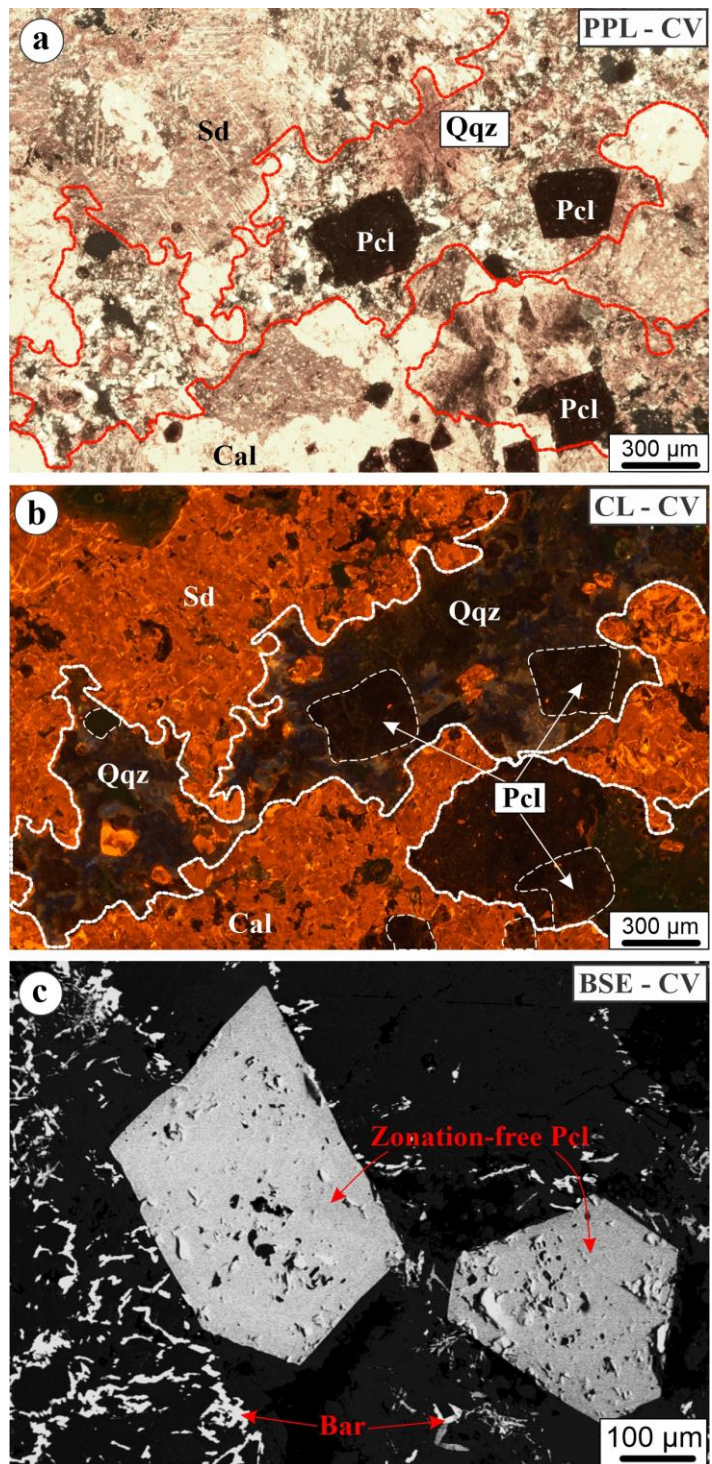


Fig. 33. Representative images of pyrochlore (Pcl) in a carbothermal vein (CV). (a) and (b) are PPL and CL images pyrochlore in a groundmass of qaqarssukite-(Ce), siderite and calcite. (c) BSE image of euhedral zonation-free pyrochlore and barite veinlets.

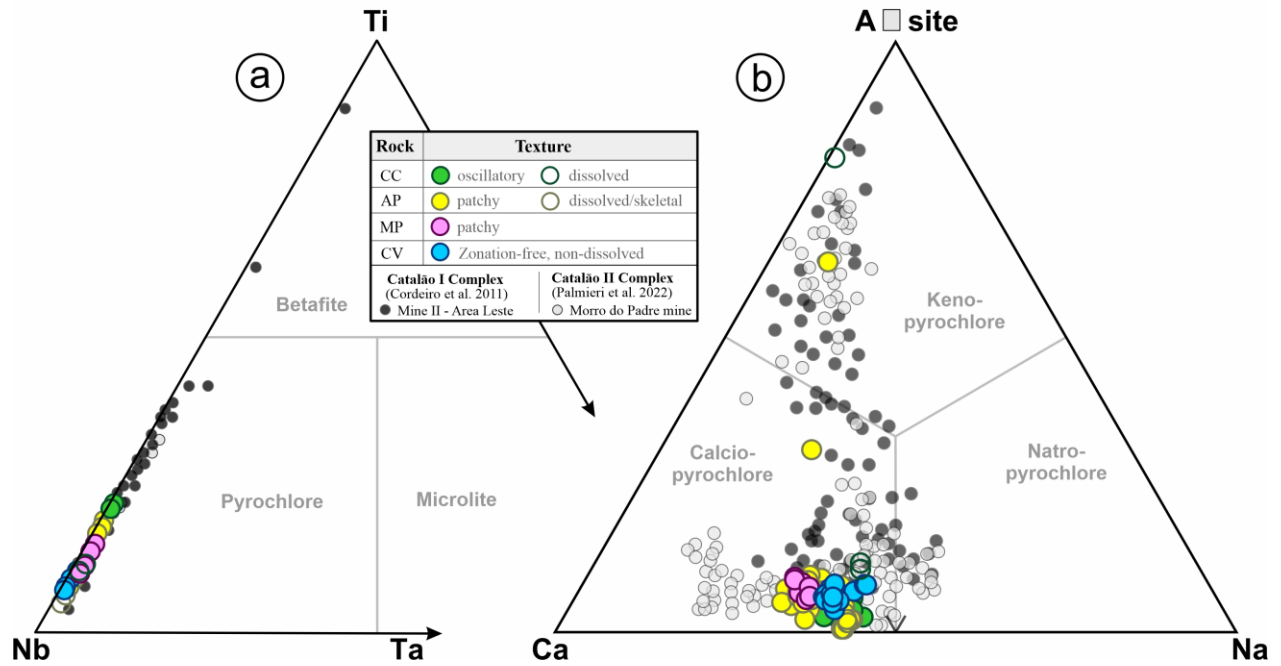


Fig. 34. Classification of the pyrochlore supergroup according to Atencio et al., (2010), including samples from the Boa Vista and Morro do Padre mines of the Catalão II Complex, and from Mine II/Area Leste mines of the Catalão I complex. (a) Composition at B-site, where most samples plot as pyrochlore, with two betafite outsiders from the Catalão I complex. (b) Composition at A-site, where most Boa Vista samples plot as calciopyrochlore, with two kenopyrochlore outliers.

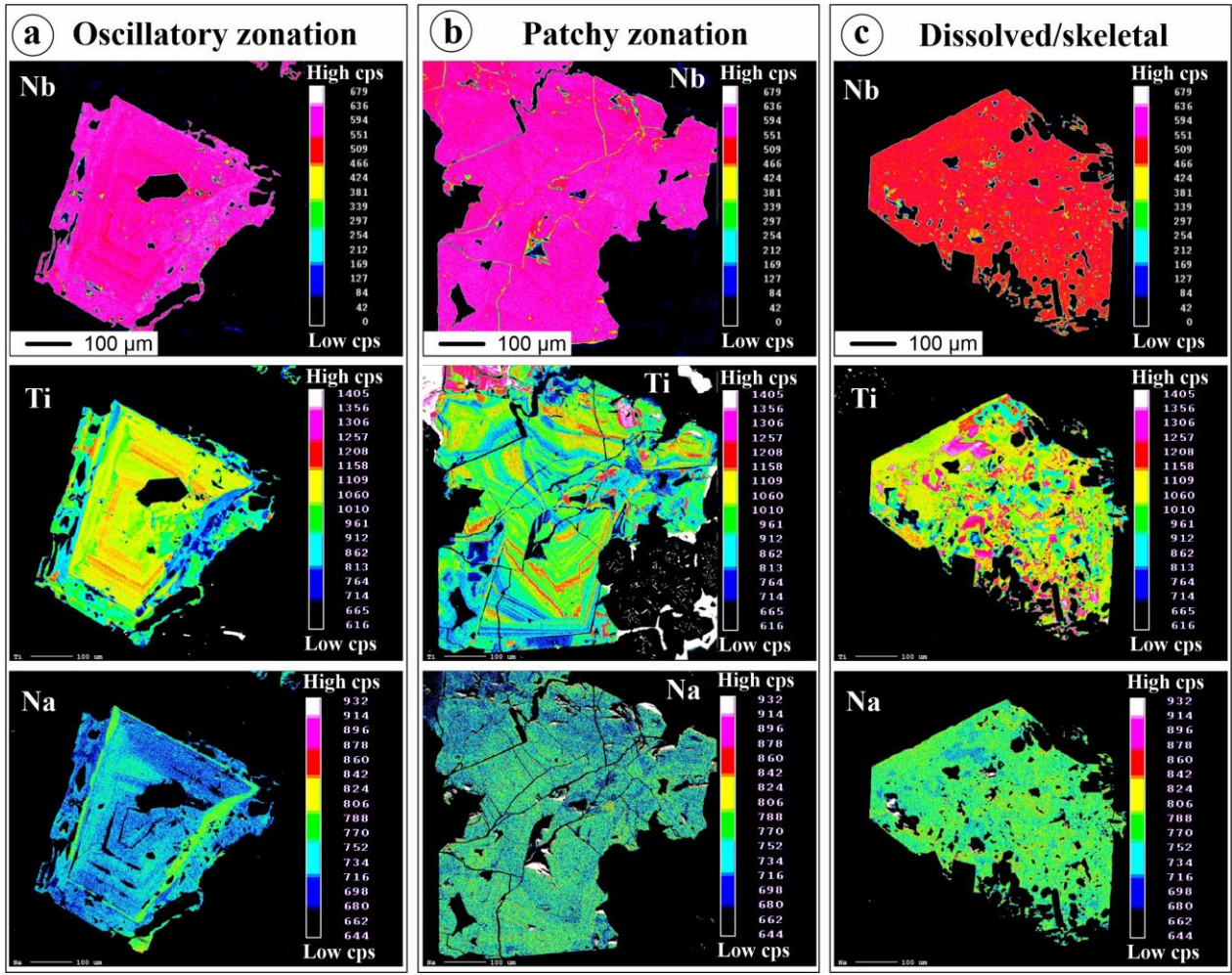


Fig. 35. WDS maps showing the distribution of Nb, Na and Ti in three calciopyrochlore crystals with oscillatory and patchy zonation and dissolved-skeletal textures. The bar scale is in counts.

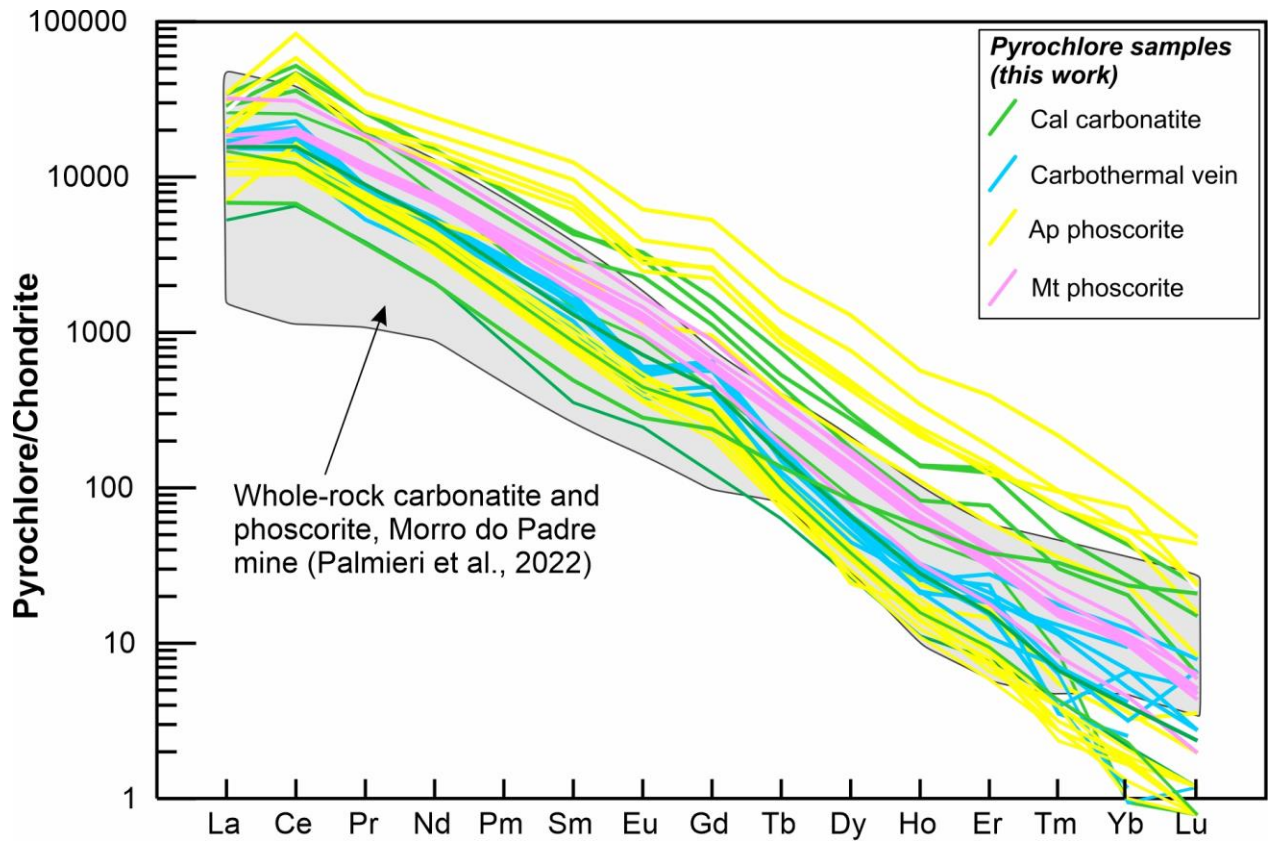


Fig. 36. Chondrite-normalized REE distribution of pyrochlore crystals from the Boa Vista Nb Mine. The pyrochlore patterns are roughly parallel to the results for carbonatite and phoscorite rocks from the Morro do Padre Nb Mine (Palmieri et al., 2022), shown in the gray shaded field.

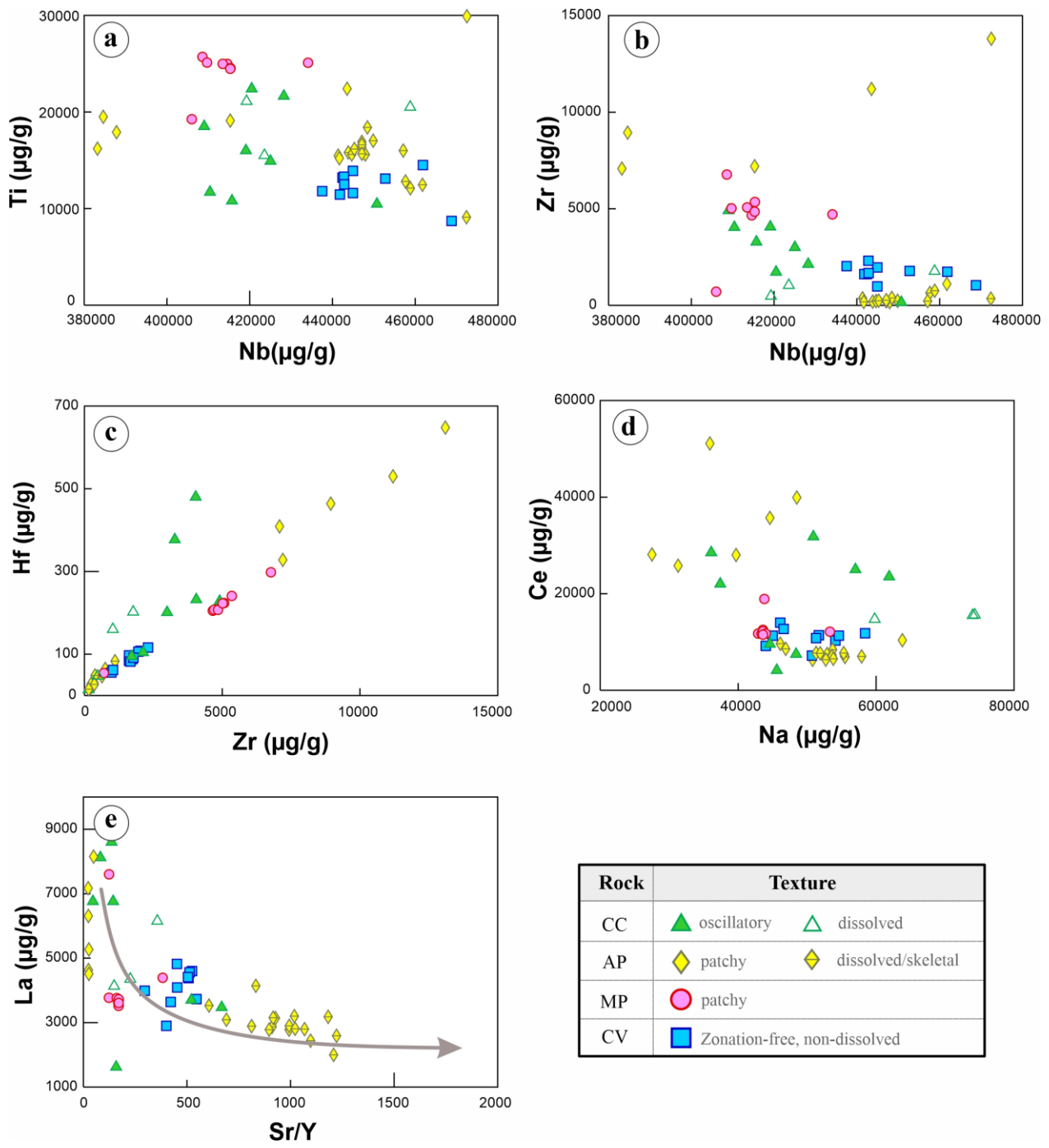


Fig. 37. Composition of B-site cations (a) to (c), and A-site cations (d) to (e) using major, minor and trace elements in calciopyrochlore crystals separated by rock type and texture, for calcite carbonatite (CC), carbothermal vein (CV), apatite-rich phoscorite (AP), and magnetite-rich phoscorite (MP).

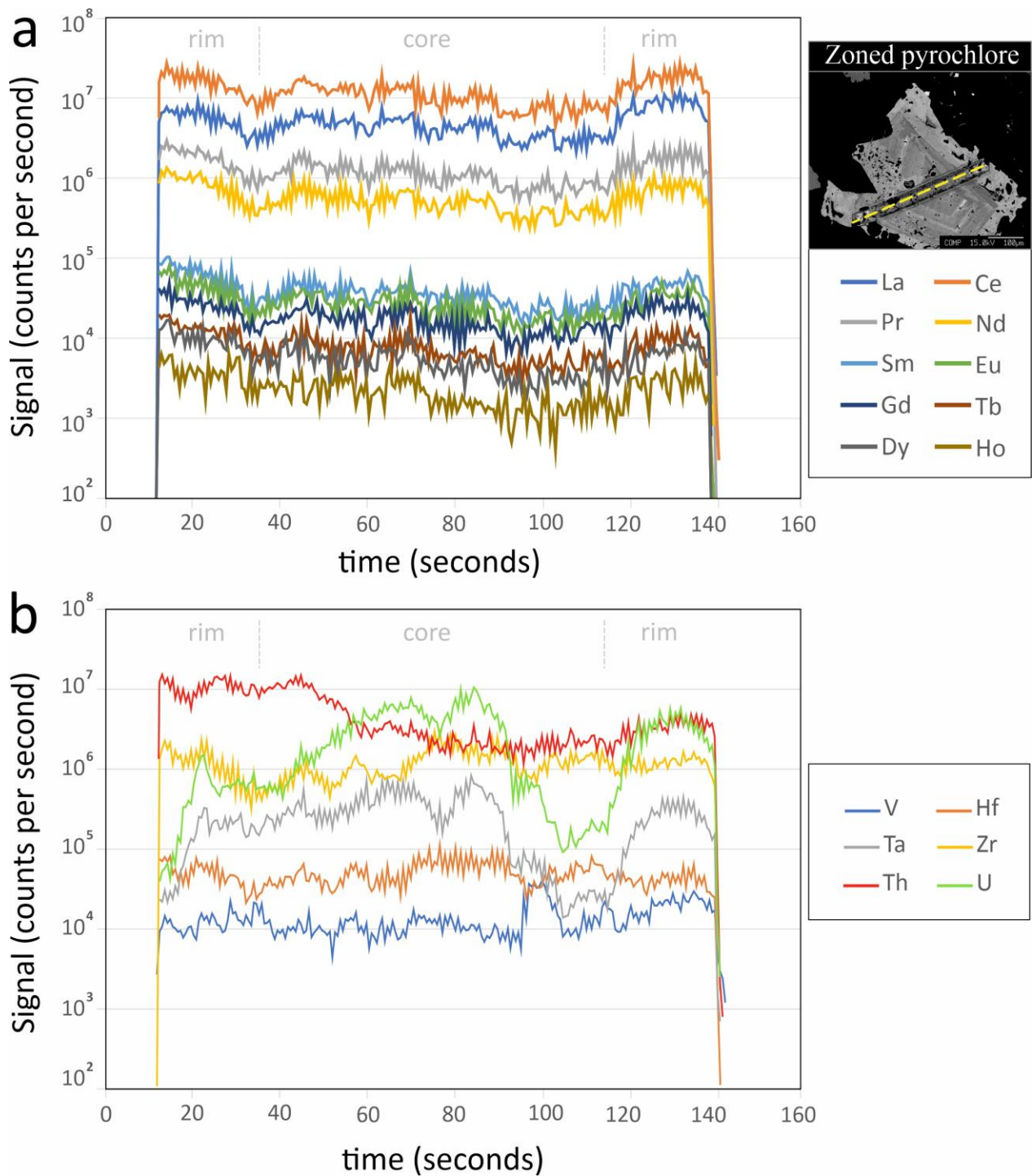


Fig. 38. Intensity (counts per second - cps) versus time plots of line scan analyses of a zoned pyrochlore in calcite carbonatite. (a) Distribution of some rare earth elements (REE) with intensities above 10³ cps, including La, Ce, Pr, Nd, Sm, Eu, Gd, Tb, Dy and Ho, where the REEs follow the zoned pattern of the measured crystal, slightly enriched towards the edges. (b) Distribution of some HFSE elements, including V, Hf, Ta, Zr, Th and U, where a dispersed behaviour is observed, without following pyrochlore zoning.

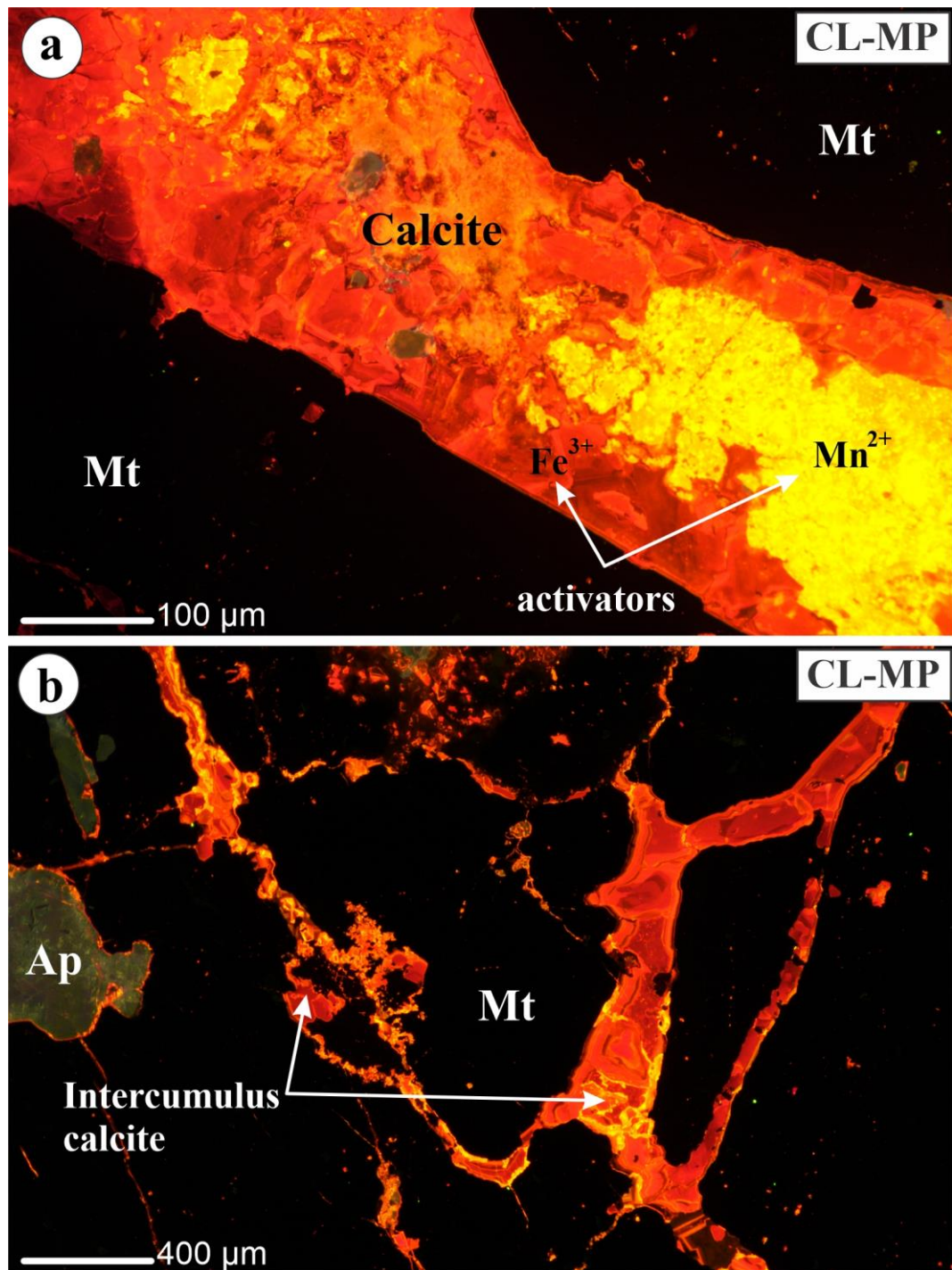


Fig. 39. (a) CL image of intercumulus calcite crystal with a Fe^{3+} quenching in dark orange CL colour to the rim, and a yellow CL colour activated by Mn^{2+} in the core. (b) Intercumulus calcite crystals bordering magnetite (Mt) and apatite (Ap) grains.

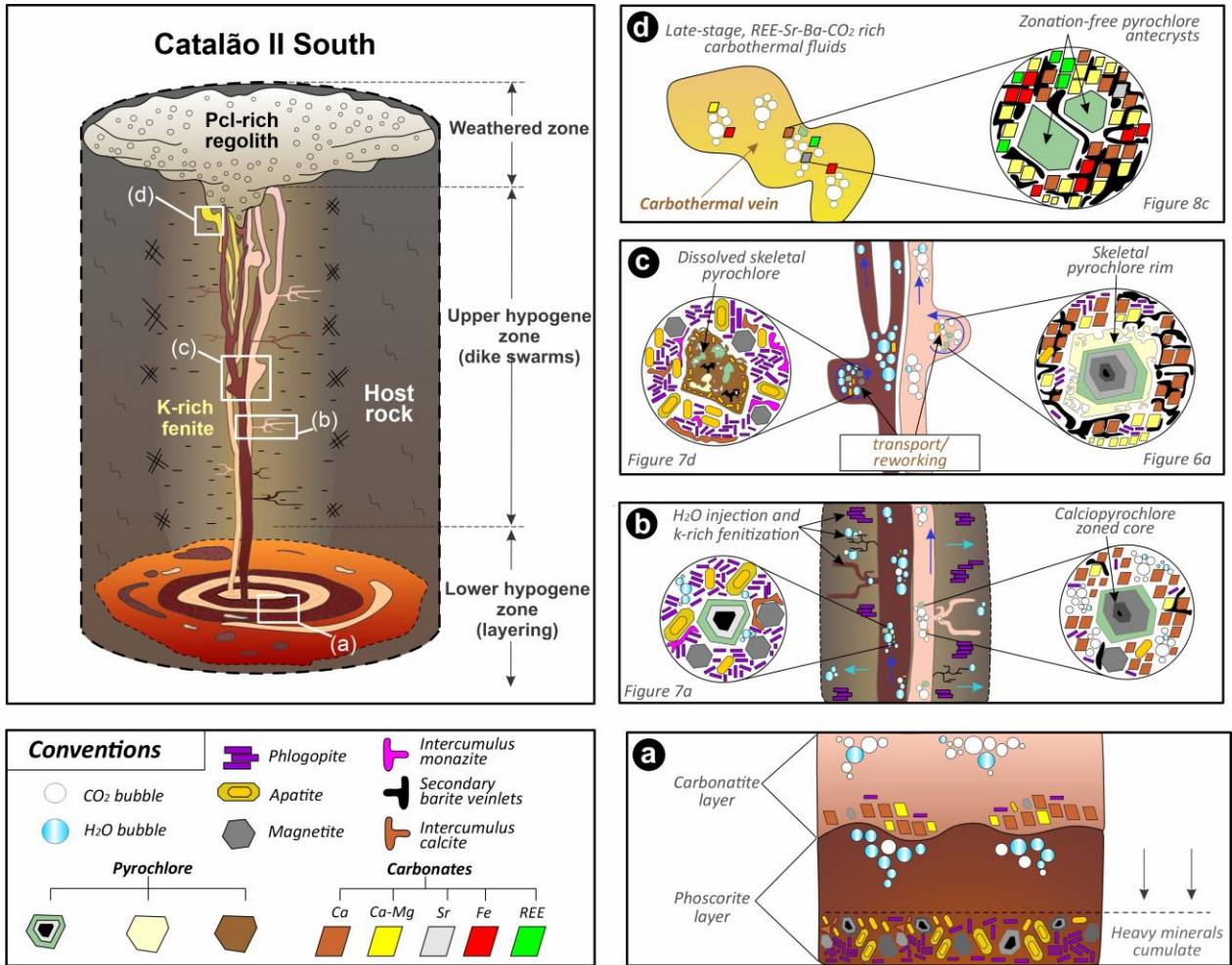


Fig. 40. Emplacement model for carbonatite and phoscorite dykes and carbothermal veins and its paragenetic sequence in the hypogene dike swarm zone of the Boa Vista Nb mine, Catalão II South. Pyrochlores from panels (a), (b), (c) and (d) correspond to an interpretation for BSE and CL images from Figures 6 to 8.

CAPÍTULO 5: REVISION OF THE NOMENCLATURE OF APATITE-MAGNETITE-RICH IGNEOUS ROCKS AND ITS INCLUSION WITHIN THE IUGS CLASSIFICATION

Felipe Velásquez Ruiz^{* a, b}, Martin Reich^{a, b}, Sam Broom-Fendley^c, Nivea Magalhães^c

^aDepartment of Geology, FCFM, University of Chile, Santiago, Plaza Ercilla 803, Chile.

^bMillennium Nucleus for Metal Tracing Along Subduction, FCFM, University of Chile, Santiago, Plaza Ercilla 803, Chile.

^cCamborne School of Mines, University of Exeter, Penryn Campus, Cornwall TR10 9FE, United Kingdom.

*Corresponding Author:

E-mail address: fevelasquezru@gmail.com (F.V. Ruiz).

ORCID: 0000-0003-1741-8588

5.1. ABSTRACT

Although rare, igneous rocks with greater than 50% modal apatite and magnetite can originate from both alkaline and subalkaline rock series. However, the absence of a classification for apatite-magnetite-rich igneous rocks in the International Union of Geological Sciences (IUGS) hinders their correct classification. Of particular concern is a deficiency in differentiating phoscorites, nelsonites, and bebedourites which occur in alkaline–carbonatitic complexes. Since P_2O_5 -F-Cl-OH-rich magmas generally lose their volatiles and alkalis to the basement during emplacement, a chemistry-based nomenclature for these rocks is challenging and tends to be unrepresentative. Here we propose a classification based on modal mineralogy reconciliating IUGS terms and the classical literature. Following the IUGS scheme, only five names are required for the petrographic classification of apatite-magnetite-rich igneous rocks: (1) *nelsonite*, a rock composed of apatite and the Fe-Ti oxides ilmenite, Ti-rich magnetite, or rutile; (2) *phoscorite*, composed of apatite, magnetite and one of the silicates forsterite, diopside or phlogopite (silicates <50% modal); (3) *bebedourite*, composed of apatite, magnetite, a Ca–Ti phase (perovskite or garnet), and one of the silicates forsterite, diopside or phlogopite (silicates <50% modal); (4) *apatitite*, for rocks with more than 90% modal of apatite; and (5) *magnetitite*, for rocks with more than 90% modal of magnetite. The terms of the previous classification only refer to the rock-forming minerals, despite the high variability of accessory minerals that may be present in the abovementioned rocks. Finally, for apatite-magnetite-rich rocks in iron oxide-apatite (IOA) and iron oxide copper-gold (IOCG) deposits, often formed or modified by post-magmatic hydrothermal processes, it is recommended to name the modal mineral composition (e.g., magnetite-apatite or apatite-magnetite), followed by the type of host structure, such as massive tabular bodies, breccias, veins, or stockworks.

Keywords: bebedourite; IOA deposit; IOCG deposit; nelsonite; phoscorite.

5.2. INTRODUCTION

The International Union of Geological Sciences (IUGS) Subcommission on the Systematics of Igneous Rocks has made a great effort towards the classification and nomenclature of most igneous rocks (Streckeisen, 1978; Le Maitre, 1989, 2002), and acts as a referee to ensure terminological agreement between researchers. As part of the IUGS classification, “special” or “exotic” rocks—comprising pyroclastics, carbonatites, kimberlites, lamproites and lamprophyres—need to be addressed first, and anything not considered a “special/exotic” rock type is then classified into either the plutonic or volcanic classifications, which represent the majority of igneous rocks (Le Maitre, 2002). However, several information gaps remain regarding the classification and nomenclature of these rocks. Some issues have been addressed, for example: (1) the nomenclature of ultramafic lamprophyres (Tappe et al., 2005); (2) the classification of kalsilite-bearing volcanic rocks and kimberlites (Scott-Smith et al., 2013; Oliveira et al., 2022); and (3) the classification of carbonatites (Mitchell, 2005; Mitchell and Gittins, 2022). Nonetheless, the rare group of igneous rocks composed of (mainly) apatite and magnetite are not included in the IUGS classification, although they are briefly mentioned in its glossary of terms.

Some of the terms relating to apatite-magnetite igneous rocks include nelsonites, phoscorites and bebedourites (Le Maitre, 2002); however, the classification of these rocks remains unclear to date. This ambiguity gives rise to unknowns for researchers who cannot find a reliable nomenclature system. On one hand, Darling and Florence (1995) state that nelsonite rocks occur in association with anorthosite suite rocks, whereas Philpotts (1967) discusses the magnetite-apatite ore bodies of the Kiruna iron deposit in Sweden, as also nelsonites. The phoscorite classification from Yegorov (1993), on the other hand, includes the name nelsonite as a subdivision of phoscorite, while Krasnova et al. (2004) point out that phoscorites almost always occur in association with carbonatites, stating that "... *there is no accepted nomenclature for the subdivision of phoscorites varieties*". This ambiguity of terms has been reflected, for example, in the Alto Paranaíba Igneous Province (APIP) in Brazil, where some of the apatite-magnetite-rich rocks in the alkaline-carbonatite complexes have been assigned as nelsonites (Cordeiro et al., 2011; Palmieri, 2011) and phoscorites (Palmieri et al., 2022), demonstrating the need for a clearer nomenclature. Finally, the term bebedourite is outdated in the IUGS glossary of terms, and differs from the most-recent definition proposed by Barbosa et al. (2012).

In this paper, we review the historical classification of apatite-magnetite-rich igneous rocks and their mineralogy, and propose a new and concise classification based on modal mineralogy, to unify the terminology between the IUGS glossary of terms and the classical literature. We also give some recommendations for naming the post-magmatic/hydrothermal apatite-magnetite-rich rocks which form high-grade iron ore bodies in iron oxide-apatite (IOA) or "Kiruna-type" deposits, and in iron oxide copper-gold (IOCG) deposits.

5.3. HISTORICAL BACKGROUND ON APATITE-MAGNETITE-RICH IGNEOUS ROCKS

5.3.1. Nelsonite

Nelsonite was named after the Amherst-Nelson counties area, Virginia, USA (Watson, 1907). Watson and Taber (1913) originally defined nelsonite as "*dikelike bodies of an even-granular, ultrabasic igneous rock composed essentially of the ore minerals ilmenite and apatite with sometimes rutile as the dominant mineral*". Later works refer to nelsonite as a rare igneous rock largely composed of apatite and Fe-Ti oxides (magnetite, ilmenite or rutile) and also mention that most nelsonites occur in association with rocks in anorthosite suites (Moore, 1940; Philpotts, 1967; Darling and Florence, 1995; Tegner et al., 2006). This last definition has been widely used, making reference to the classical nelsonites from Roseland Piney in Virginia, USA, Cheney Pond and Port Leyden in New York, USA, Hesnes in Norway, and St. Charles in Quebec, Canada (Fig. 41), but also for the apatite-magnetite-ilmenite-rich orebodies from layered mafic intrusions such as the Bushveld Complex, South Africa (Tegner et al., 2006) or the Grader layered intrusion in Quebec, Canada (Charlier et al., 2008). Thus, the term nelsonite has been frequently used in a broad sense to refer to deposits that consist of Ti-rich magnetite, which is commonly found in association with anorthositic complexes and layered mafic intrusions (Zhou et al., 2005; Tegner et al., 2006,

Charlier et al., 2008; Velásquez Ruiz et al., 2019; Reich et al., 2022). The latter has led to some authors to loosely apply the term nelsonite to the massive magnetite-apatite ore bodies that constitute IOA or “Kiruna-type” deposits (e.g., Philpotts, 1967). However, the particular use of this term within the IOA context is incorrect, considering that these rocks are magmatic-hydrothermal in origin and, strictly, are not genetically associated with anorthosites or layered mafic intrusions (Reich et al., 2022, and references therein). Finally, it is relevant to note that the IUGS define nelsonite as a rock where the mineral constituents are apatite and ilmenite, with or without rutile, quoting the work of Watson (1907). Contrary to previous classical literature, magnetite is not included in this definition, and no reference is made to the close association of nelsonites with anorthosites.

5.3.2. Phoscorite

Phoscorites are plutonic ultramafic rocks and the name is a mnemonic term originating from the company "*Phosphate Development Corporation*", referring to the magnetite, olivine and apatite rocks that ringed the Loolekop carbonatite intrusion of the Palabora Complex in South Africa (Russell et al., 1954; Le Maitre, 2002; Krasnova et al., 2004). Currently, there are known to be 21 localities around the world with phoscorite rocks (Gittins, 1966; Johnson, 1966; Philpotts, 1967; Davies, 1974; Glagolev, 1974; Basu and Mayila, 1986; Verwoerd, 1986; Egorov, 1991; Yegorov, 1993; Kogarko, 1997). The majority of phoscorites are associated with carbonatites (Krasnova et al., 2004), with only one exception located in the Barchinskiy complex in Kazakhstan (Borodin et al., 1973). Since there are more than 500 known carbonatite localities around the globe (Woolley and Kjarsgaard, 2008), the small number of phoscorites evidences the scarcity of these rocks.

The rock-forming minerals comprising phoscorites include apatite, magnetite, and olivine (Le Maitre, 2002). Other rock-forming minerals include calcite, dolomite, phlogopite, tetraferriphlogopite, diopside, richterite, schorlomite, and ilmenite. Although to-date there is no accepted nomenclature for phoscorite subdivisions, phoscorite varieties can be mono-, bi- and poly-mineralic, as depicted in the phoscorite classification diagram initially proposed by Yegorov (1993; Fig. 42). In the aforementioned diagram, Yegorov (1993) includes a field for nelsonite where the Fe-Ti oxide is not considered. This is problematic since it mixes two definitions of apatite-magnetite-rich rocks.

Phoscorites include a wide variety of accessory minerals such as pyrochlore, baddeleyite, zirconolite, spinel, perovskite, pyrrhotite, among others (Krasnova et al., 2004). The abundance of economically mineable accessory minerals such as pyrochlore, increases the importance of studying phoscorites. For example, large pyrochlore endowments occur in phoscorites from the alkaline-carbonatitic complexes of the APIP in Brazil (e.g., Araxá and Catalão I and II), which represent more than 90% of the World’s Nb production (Cordeiro et al., 2010; Palmieri et al., 2022). Apatite has also been extracted to obtain phosphorus mainly for fertilizers, in the Kola Alkaline Province, in the Palabora Carbonatite Complex, as well as the Coqueiros Mine in Catalão II, among others (Giebel et al., 2008; Broom-Fendley et al., 2021).

Due to the highly variable mineral assemblages, Krasnova et al. (2004) proposed to define phoscorites as “*plutonic ultramafic rocks, comprising magnetite, apatite, and one of the silicates, forsterite, diopside or phlogopite*”. This definition helps to: (1) expand the nomenclature initially proposed by Le Maitre (2002), and (2) includes olivine-lacking phoscorites from other alkaline-carbonatite complexes beyond the classical carbonatitic complexes, to avoid overlap or confusion with nelsonites and their monomineralic and polymineralic derivatives.

5.3.3. Bebedourite

The term bebedourite is derived from the Bebedouro area at Salitre Hill, Minas Gerais State, Brazil (Barbosa et al., 2012). Initially, Tröger (1928, 1935) defined bebedourite as biotite-perovskite-rich clinopyroxenite with accessory opaque phases, apatite, K-feldspar and olivine. Subsequently, new exploration programs at the Salitre and Tapira complexes revealed varieties of clinopyroxenites with less than 50% modal silicate contents, combined with a large amount of opaque minerals (Brod et al., 2004). Because the clinopyroxene content in this new group of rocks does not fit the IUGS definition to be named as “*clinopyroxenite*”, due to the significantly high opaque content, the definition of bebedourite had to be changed. Thus, Barbosa et al. (2012) renamed the term bebedourite as a cumulate igneous rock, whose rock-forming minerals are diopside, apatite, magnetite, phlogopite, and a Ca–Ti phase (mostly perovskite, more rarely titanite and/or Ti-garnet), with modal silicate mineral contents less than 50%. Similar to phoscorites and nelsonites, bebedourites have modal compositional variations, and subdivisions may be common such as monomineralic varieties (such as perovskitite), and bi- or poly-mineralic variations (Barbosa et al., 2020). The latest version of Le Maitre (2002) has the same definition of Tröger (1928, 1935), so it is important to update the nomenclature with the new petrological works in the area.

5.4. CLASSIFICATION RATIONALE

Currently, there is no classification for apatite-magnetite-rich igneous rocks within the IUGS, and the terms for nelsonite, phoscorite and bebedourite (Le Maitre, 2002), are out of date. The most recent revisions and classifications of the “special/exotic” rocks have shown that these revisions must be based on modal mineralogy (Mitchell, 2005; Tappe et al., 2005; Oliveira et al., 2022). A classification based on bulk rock composition commonly does not reflect the modal mineralogy and may also not represent the melt composition (Mitchel and Gittins, 2022). This is most pertinent for phoscorites owing to their association with alkaline-carbonatite complexes. These complexes develop pervasive fenitization/hydrothermalism (Elliott et al., 2018) representing the loss of volatiles and alkalis to the basement during emplacement, thus a chemistry-based classification becomes unrepresentative. Nelsonites, phoscorites and bebedourites with cumulate textures form as a result of mineral segregation after fractionation/immiscibility (Velásquez Ruiz et al., 2019), and a bulk rock composition also does not represent the composition of the parental melt. For these reasons, we argue that a classification based on modal mineralogy is the most appropriate approach, and also is an opportunity to establish limits between the rock-forming minerals, which often overlap as is the current case between phoscorites and nelsonites. In addition,

the need to eliminate the term nelsonite as a subtype of phoscorite in the Yegorov (1993) classification is vital to differentiate between these two rock types. This is mostly due to the fact that, genetically, nelsonites are mostly associated with anorthosites and layered mafic intrusions, whereas phoscorites are more often associated with alkaline-carbonatite complexes.

As an example, Mitchel and Gittins (2022) suggest revising the classification of carbonatites and carbothermalites by using the modally-dominant carbonate to define the root name (i.e., carbonatites with dominant calcite are calcite carbonatites). For cases where significant amounts of non-carbonates occur, adding a prefix to the root name acknowledges this (e.g., phlogopite calcite carbonatite). For kalsilite-bearing volcanic rocks, Oliveira et al. (2022) consider the coexistence between kalsilite and nepheline for potassic and ultrapotassic volcanic rocks, such as ugandites, mafurites, katungites and kalsilite nephelinites, using a classification based on the coexistence of six rock-forming minerals (clinopyroxene, olivine, nepheline, leucite, melilite and kalsilite).

5.5. INTEGRATING APATITE-MAGNETITE-RICH IGNEOUS ROCKS INTO THE IUGS CLASSIFICATION

The summary of the proposed classification is found in Table 4, requiring only five names as follows: *nelsonite*, a rock composed of apatite and the Fe-Ti oxides (ilmenite, magnetite, or rutile); *phoscorite*, a rock composed of apatite, magnetite and one of the silicates forsterite, diopside or phlogopite (silicates <50% modal); *bebedourite*, a rock composed of apatite, magnetite, a Ca–Ti phase (perovskite or garnet), and one of the silicates forsterite, diopside or phlogopite (silicates <50% modal); *apatitite*, a rock with more than 90% modal of apatite; *magnetitite*, rocks with more than 90% modal of magnetite. Apatitite and magnetitite are considered monomineralic variations of nelsonite, phoscorite and bebedourite and there is also the possibility of other monomineralic varieties, where, according to the IUGS, it is recommended to use the name of the most abundant mineral ending in "ite", for example: perovskitite or ilmenitite. For all those polymimetic varieties that do not have all the essential minerals, it is recommended to use the root name, and specify the missing mineral in the descriptions (e.g., perovskite-lacking bebedourite). Despite the high variability of accessory minerals, the terms in the above classification and their mono- and poly-mineral derivatives only refer to rock-forming minerals. However, we also highlight common accessory minerals according to the literature (Table 4), and these are not taken into account in the classification.

Importantly, the recommendation above is specifically designed for igneous rocks and does not include hydrothermal ore deposits. It is well documented that apatite-magnetite-rich rocks in IOA and IOCG deposits predominantly form by a combination of magmatic and hydrothermal processes operating in upper crustal silicate magma reservoirs (Williams et al., 2005; Groves et al., 2010; Barton, 2014; Reich et al., 2022; Skirrow, 2022). In these cases, it is recommended to name the modal mineral composition in descending order, followed by the type of host structure, such as

massive tabular bodies, breccias, veins, veinlets and, stockworks (e.g., magnetite-apatite vein). The term nelsonite should be avoided.

5.6. APPLICATION OF THE REVISION

5.6.1. Phoscorites and bebedourites from the Alto Paranaíba Igneous Province (APIP)

The alkaline-carbonatite rocks of the APIP have a highly variable mineralogy, which has led to different terms being assigned over time. At the Catalão I complex, Cordeiro et al. (2010) documented the presence of phoscorites *sensu stricto*, and some olivine-lacking end members, which are classified as nelsonites, using the classification diagram of Yegorov (1993; Figure 42). In this case, two different rock types overlap (i.e., phoscorites and nelsonites), which in terms of classification may be problematic. However, our new classification scheme (Table 4) allows these olivine-lacking end members to be directly classified within the phoscorite series, instead of nelsonites. Furthermore, in the Catalão II complex, tetraferriphlogopite often occurs in phoscorites as the indicative silicate instead of olivine; in this case, the term phoscorite could be used despite the fact that the rock does not have olivine, as proposed in Palmieri et al. (2022). This rock type is named tetraferriphlogopite phoscorite. Finally, in most alkaline-carbonatite complexes in the APIP, perovskite-apatite-magnetite-phlogopite-rich cumulate rocks occur, including monomineralic or polymimetic varieties. According to our classification scheme (Table 4), these olivine-lacking and phlogopite-bearing rocks can be called bebedourites, as previously proposed by Barbosa et al. (2012; 2020).

5.6.2. Nelsonites from anorthosite-lacking layered mafic intrusions

Layered mafic intrusions are of great economic importance due to their high content of platinum group elements (PGE) (Charlier, et al. 2015, Cawthorn and Walraven, 1998, Pang et al., 2008; Zhou et al., 2005), which are concentrated in ore-rich layers during the segregation of heavy minerals (e.g., base metal sulfides, chromite, ilmenite and magnetite). Some layered mafic intrusions have anorthosite and magnetite-ilmenite-apatite-rich layers, the latter called nelsonites, such as the Bushveld Complex in South Africa (Tegner et al., 2006). However, some other layered mafic intrusions lack anorthosites, as is the case of the Emeishan Large Igneous Province, SW China (Liu et al., 2015; Pang et al., 2008) and the São Tomé intrusion, NE Brazil (Velásquez Ruiz et al., 2019). In these cases, authors have refrained from assigning the term nelsonite to their magnetite-ilmenite-apatite-rich layers, despite being magma-derived, mostly because they are not associated with anorthosites. With this new proposal of classification, the magma-derived magnetite-ilmenite-apatite-rich layers from anorthosite-lacking layered mafic intrusions could be named as nelsonites, since they match the classification criteria in Table 4.

5.7. CONCLUDING REMARKS

Here we present an improved and more precise classification for apatite-magnetite-rich igneous rocks, focusing on the modal mineralogy. The terms proposed include nelsonite, phoscorite, bebedourite, apatitite and magnetitite. We stress that the suggested naming of the apatite-magnetite-rich rocks cannot be varied beyond the presence of the rock-forming minerals, regardless of the nature or amount of accessory minerals present. Moreover, we note that this classification must be used strictly for igneous rocks, and therefore should not be applied to post-magmatic or magmatic-hydrothermal rocks, for example magnetite-apatite ore bodies in IOA or Kiruna-type deposit, and IOCG systems. Although it is common but not restrictive, phoscorites and bebedourites are more associated with alkaline-carbonatite complexes, whereas nelsonites are more associated with anorthosite rock suites and layered mafic intrusions. Finally, we encourage researchers to use the currently proposed classification and to persist in investigating these often called “exotic” rock types. Despite their rarity, apatite-magnetite-rich igneous rocks hold significant economic importance as they serve as a source of phosphorus (P), iron (Fe), titanium (Ti), vanadium (V), as well as critical elements including niobium (Nb), platinum group elements (PGE), and rare earth elements (REE).

5.8. ACKNOWLEDGEMENTS

The authors thank Dr. Pedro Cordeiro and Bruno Abilio for their contributions in understanding the alkaline-carbonatite rocks of the APIP.

5.9.TABLES

Table 4. Proposed nomenclature for apatite-magnetite-rich igneous rocks, comprising five terms including nelsonite, phoscorite, bebedourite, apatitite, and magnetitite, and their respective rock-forming minerals (solid circles). The classification was made based on a reconciliation between the glossary of terms of the IUGS classification (Le Maitre, 2002) and classical literature (Watson, 1907; Watson and Taber, 1913; Moore, 1940; Philpotts, 1967; Yegorov, 1993, Darling and Florence, 1995; Krasnova et al., 2004; Tegner et al., 2006; Barbosa et al., 2012). Despite the high variety of accessory minerals (open circles), these are not taken into account in the classification.

Rock type	Mineral assembly					Other common accessory minerals
	Apatite	Magnetite	Silicate*	Fe-Ti oxide**	Ca-Ti phase***	
Nelsonite	●	●	○	●	○	Chromite, tellurides, platinum-group elements (PGE), base metal sulphides, arsenides.
Phoscorite	●	●	●	○	○	Calcite, dolomite, amphibole, baddeleyite, zirconolite, pyrochlore, spinel.
Bebedourite	●	●	●	○	●	Calcite, dolomite, amphibole, baddeleyite, zirconolite, pyrochlore, spinel.
Apatitite	●	○	○	○	○	Calcite, dolomite, baddeleyite, pyrochlore, PGE.
Magnetitite	○	●	○	○	○	Calcite, dolomite, baddeleyite, pyrochlore, PGE.

*Forsterite, diopside, or phlogopite (<50% modal); **Ilmenite, or rutile; ***Perovskite, or Ti-garnet.

5.10. FIGURES

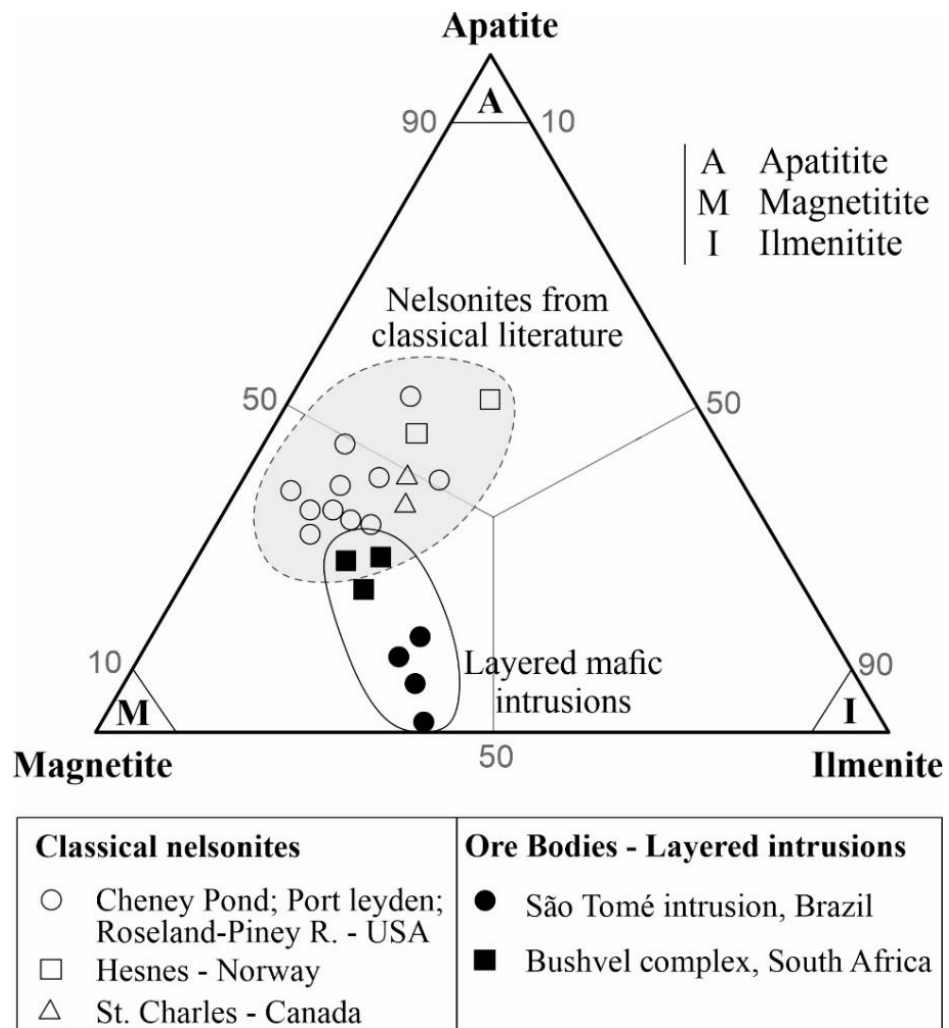


Fig. 41. Modal mineralogy of “classic” nelsonites and of ore bodies from layered mafic intrusions, plotted in the magnetite-ilmenite-apatite diagram (Velásquez Ruiz et al., 2019; Tegner et al., 2006; Darling and Florence, 1995 and references therein).

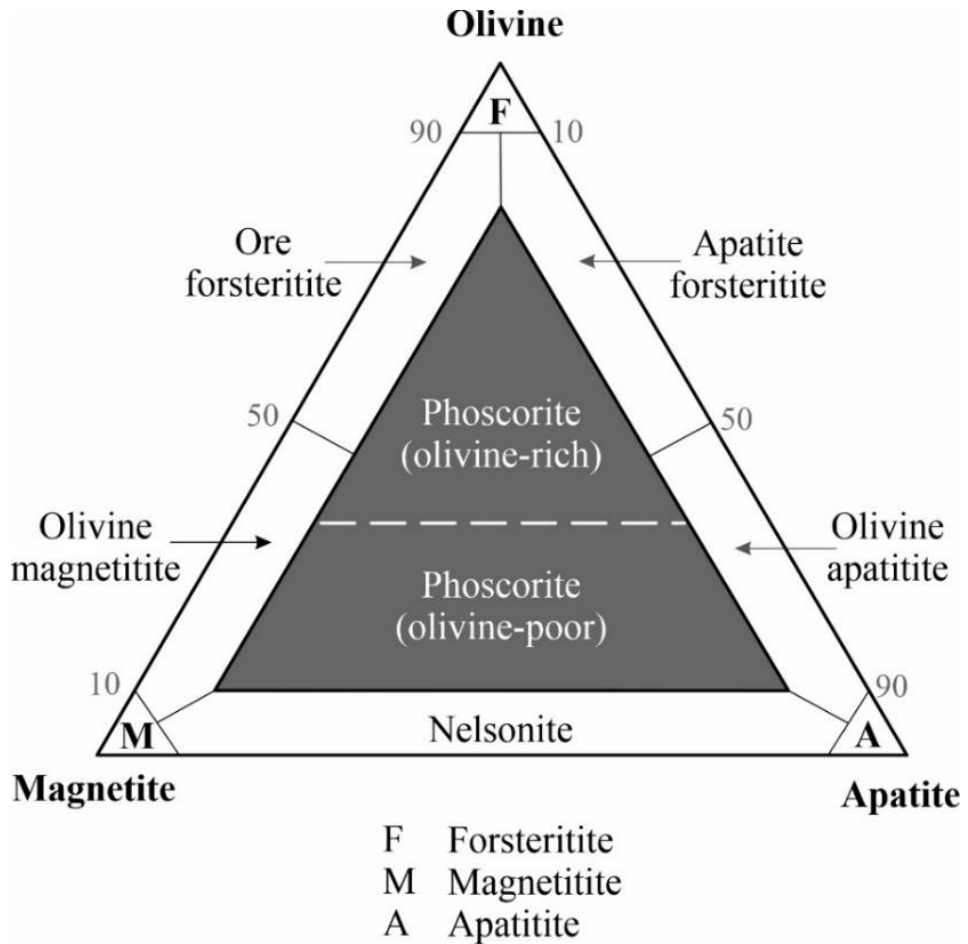


Fig. 42. Phoscorite classification diagram initially proposed by Yegorov (1993), where the term nelsonite is included, despite the fact the diagram does not contain an oxide of Fe-Ti endmember. The values refer to recalculated amounts of modal mineral abundance.

CAPÍTULO 6: CONCLUSIONES

La presente tesis de doctorado aborda de una manera integral los procesos mineralizantes en la mina de Nb Boa Vista del Complejo Catalão II, localizada al extremo noroeste de la Provincia Ígnea del Alto Paranaíba (APIP), en Brasil central, y su impacto en el entendimiento de los complejos alcalino-carbonatíticos. Dentro de los temas estudiados, se abordó la petrogénesis y nomenclatura de las rocas alcalino-carbonatíticas de la APIP, la caracterización del metasomatismo carbotermal del basamento y la caracterización geoquímica del mineral pirocloro, el cual constituye la mena principal de Nb en este tipo de depósitos.

En el Capítulo 2 se reportan datos geológicos y geoquímicos que apuntan a un vínculo genético entre lavas ultrapotásicas de la Formación Mata da Corda y aillikitas de complejos alcalino-carbonatíticos de la APIP. Por medio de datos aeromagnéticos regionales, las imágenes ASA y RTP mostraron tres estructuras dipolares al sur de Mata da Corda con firmas magnéticas similares a los complejos alcalino-carbonatíticos, que se explican como complejos carbonatíticos enterrados debajo de Mata da Corda. Evidencias adicionales muestran el vínculo entre kamafugitas y aillikitas, por ejemplo: (1) datos geoquímicos de ambas litologías plotean en el campo de kamafugita en la clasificación de rocas ultrapotásicas de Foley, (1987); (2) la distribución de REEs normalizados por condritos, es similar; (3) ambas litologías comparten minerales formadores de roca similares, excepto por la falta de feldespatoides en aillikitas; y (4) las razones $^{143}\text{Nd}/^{144}\text{Nd}_{(i)}$ y $^{87}\text{Sr}/^{86}\text{Sr}_{(i)}$ para todas las rocas alcalinas y carbonatitas de la APIP son similares, indicando una fuente común asociada a un manto litosférico enriquecido. El modelo propuesto involucra procesos de fraccionamiento en múltiples etapas a partir de un magma primario silico-carbonatado ultrapotásico, localizado en el manto litosférico subcontinental probablemente metasomatizado, que asciende y se fracciona en diferentes niveles de la corteza terrestre, generando series magmáticas carbonatíticas y alcalinas (aillikitas) hacia el oeste del APIP, y la producción del volcanismo kamafugítico de la Formación Mata da Corda al este del APIP.

En el Capítulo 3, por medio de datos microtexturales (usando EBSD) y datos geoquímicos (usando EMPA y μ -XRF) en la Mina Boa Vista, se observó que la intrusión del Complejo Catalão II produjo una fenitización o metasomatismo pervasivo rico en potasio en el basamento metavolcanosedimentario del Grupo Brasília. Dicho metasomatismo se caracteriza por un primer grupo de fenitas proximales melanocráticas de flogopitita, y un segundo grupo de fenitas distales de flogopita-ortoclasa-calcita; ambas fenitas, o halos feníticos, están orientados ortogonalmente a las paredes de diques carbonatíticos. Se propone que los fluidos derivados del magma, ricos en cationes solubles de K, Mg, Ba y Sr, más S y OH⁻, permearon el basamento sin formar una mineralización significativa de pirocloro. Datos EBSD mostraron que el plano basal de la flogopita secundaria (001) cristalizó ortogonalmente con respecto a las paredes del dique de carbonatita, lo que muestra que la flogopita cristalizó a lo largo de la trayectoria del flujo. La química mineral de las flogopitas metasomáticas es similar a la de los núcleos de flogopita magmática, lo que sugiere que el evento metasomático probablemente fue simultáneo a la intrusión de carbonatita.

En el Capítulo 4 se estudiaron la microtextura y geoquímica de pirocloros de rocas magmáticas y vetas carbotermales de la mina Boa Vista, por medio de SEM, catodoluminiscencia, EMPA y LA-ICP-MS. Se observaron texturas zonadas oscilatorias y parcheadas de origen magmático en granos de pirocloro de carbonatitas y foscoritas. Además, se observaron pirocloros secundarios con texturas de disolución y esqueletales en carbonatitas y foscoritas y cristales no zonados en vetas carbotermales. La formación de pirocloros con texturas de disolución, esqueletales y no zonados se atribuye a procesos secundarios de transporte y retrabajo de cristales, durante el emplazamiento de la intrusión carbonatítica. El análisis geoquímico del pirocloro en Boa Vista mostró un predominio de calcio-pirocloro, la variedad de pirocloro rico en Ca y Nb. Las tendencias de elementos traza en pirocloro, usando los diagramas tipo Harker Sr/Y vs La, Na vs Ce y Zr vs Hf, son consistentes para un proceso de fraccionamiento continuo y no indican ningún desacoplamiento que sea evidencia de inmiscibilidad líquida. Además, los patrones normalizados de REEs en pirocloro son homogéneos y consistentes con datos geoquímicos de roca total de carbonatitas y foscoritas de la mina vecina Morro do Padre, incluyendo pirocloros de vetas carbotermales; toda esta evidencia sugiere un origen magmático para el pirocloro en Catalão II. Esto último implica que pirocloros de vetas carbotermales corresponden a xenocristales primarios transportados y retrabajados. Con base en datos texturales y geoquímicos en pirocloros de la Mina Boa Vista, se propone que las rocas ricas en pirocloro-apatito-magnetita (foscoritas) se formaron mediante la segregación de minerales pesados durante el fraccionamiento de un magma parental carbonatítico. Estos minerales formaron cumulados en la zona hipogénica inferior y luego se emplazaron como diques en la zona hipogénica superior, transportados por el magma carbonatítico parental.

En el Capítulo 5 se realizó una revisión de la nomenclatura de rocas de magnetita y apatito, con énfasis en las rocas asociadas a la mineralización de Nb en el APIP. Se propuso además una clasificación para las rocas ígneas ricas en apatito-magnetita, basada en su mineralogía modal, unificando la terminología entre el glosario de términos de la IUGS y la literatura clásica. La clasificación incluyó los siguientes términos: (1) *nelsonita*, roca compuesta de apatito y los óxidos de Fe-Ti ilmenita, magnetita rica en Ti o rutilo; (2) *foscorita*, roca compuesta de apatito, magnetita y uno de los silicatos forsterita, diópsido o flogopita (silicatos <50% modal); (3) *bebedurita*, roca compuesta de apatito, magnetita, una fase de Ca-Ti (perovskita o granate) y uno de los silicatos forsterita, diópsido o flogopita (silicatos <50% modal); (4) *apatitita*, roca con más del 90% modal de apatito; y (5) *magnetitita*, roca con más del 90% modal de magnetita. Finalmente, para rocas ricas en apatito-magnetita en el contexto de depósitos de tipo óxido de hierro-apatito (IOA) o “tipo Kiruna”, y depósitos de óxido de hierro-cobre-oro (IOCG), se recomienda nombrar el tipo de estructura huésped, como cuerpos tabulares masivos, brechas, vetas o *stockworks*, seguido de la composición mineral modal (e.g., magnetita-apatito o apatito-magnetita).

De manera general, la presente tesis doctoral permitió abordar aspectos clave sobre los procesos concentradores de Nb en mega-depósitos de pirocloro asociados a complejos alcalino-carbonatíticos de la APIP, en Brasil central. Los factores clave para la fuente, génesis y emplazamiento de complejos alcalino-carbonatíticos ricos en pirocloro, incluye un manto

litosférico subcontinental metasomatizado y enriquecido en CO₂ en un ambiente de extensión intracontinental, como responsable del origen de un magma primario silico-carbonatado ultrapotásico, que asciende, se fracciona y desmezcla en diferentes niveles de la corteza terrestre. Empleando datos geoquímicos y texturales en cristales de pirocloro de la Mina Boa Vista del Complejo Catalão II sur, se propuso que las foscoritas ricas en pirocloro, asociadas a carbonatitas, resultan de la segregación de minerales pesados durante el fraccionamiento de un magma parental carbonatítico. Los resultados obtenidos en el Complejo Catalão II pueden extenderse a otros complejos de la APIP, ya que comparten un link genético, incluido el pobemente estudiado Complejo Araxá, que corresponde al mayor depósito de Nb a nivel mundial. Finalmente, el modelo metalogenético para el Nb propuesto en esta tesis doctoral, podría tener aplicaciones clave en exploración mineral, específicamente para los tres posibles complejos alcalino-carbonatíticos no exhumados, que fueron encontrados al sur de la Formación Mata da Corda, en el extremo sureste de la APIP (Capítulo 2), toda vez que podría ser de interés económico para la exploración de Nb, fósforo (P) y minerales ricos en tierras raras (REE).

BIBLIOGRAPHY

- Akinfiev, N.N., Korzhinskaya, V.S., Kotova, N.P., Redkin, A.F., Zotov, A.V., 2020. Niobium and Tantalum in Hydrothermal Fluids: Thermodynamic description of Hydroxide and Hydroxofluoride Complexes. *Geochim. Cosmochim. Acta.*, 280, 102-115.
- Almeida, F.F.M., Hasui, Y., Brito Neves, B.B., Fuck, R.A., 1981. Brazilian structural provinces: An introduction. *Earth-Sci. Rev.*, 17(1–2), 1–29.
- Araújo, D.P., 1996. Metassomatismo no complexo carbonatítico Catalão-I: implicações para a composição do magma carbonatítico e para o metassomatismo carbonatítico no manto superior. Unpublished MSc Thesis, University of Brasilia, Brasilia.
- Araujo, A.L.N., Carlson, R.W., Gaspar, J.C., Buzzi, L.A., 2001. Petrology of kamafugites and kimberlites from the Alto Paranaíba Alkaline Province, Minas Gerais, Brazil. *Contrib. Mineral. Petrol.*, 142, 163-177.
- Atencio, D., 2021. Pyrochlore Supergroup Minerals Nomenclature: An Update. *Front. Chem.*, 9, 713368.
- Atencio, D., Andrade, M., Christy, A., Gieré, R., Kartashov, P., 2010. The pyrochlore supergroup of minerals: nomenclature. *Can. Mineral.* 48, 569-594.
- Barbosa, E.S.R., Brod, J.A., Junqueira-Brod, T.C., Dantas, E.L., Cordeiro, P.F.O., Gomide, C.S., 2012. Bebedourite from its type area (Salitre I complex): A key petrogenetic series in the Late-Cretaceous Alto Paranaíba kamafugite-carbonatite-phoscorite association, Central Brazil. *Lithos*, 144–145, 56–72.
- Barbosa, P.F., Lagoeiro, L., 2010. Crystallographic texture of the magnetite-hematite transformation: Evidence for topotactic relationships in natural samples from Quadrilátero Ferrífero, Brazil. *American Mineralogist*, 95(1), 118–125.
- Barbosa, J.S.F., Sabaté, P., 2004. Archean and Paleoproterozoic crust of the São Francisco Craton, Bahia, Brazil: Geodynamic features. *Precambrian Res.*, 133, 1–27.
- Bardet, M.G., 1977. Géologie du diamante. Troisième partie : Gisements de diamants d'Asie, d'Amérique, d'Europe et d'Australasie : In Mémoires du Bur. Res. Geol. Min., 83 (p. 169).
- Barton, M., 1979. A comparative study of some minerals occurring in the potassium-rich alkaline rocks of the Leucite Hills, Wyoming, the Vico volcano, western Italy, and the Toro Ankole region, Uganda. *Neues Jahrb. Mineral.*, 137, 113–134.
- Barton, M.D., 2014. in *Treatise of Geochemistry*, Vol. 13 (eds. Holland, H. & Turekian, K.), 515–536 (Univ. Arizona).
- Basu, N.K., Mayila, A., 1986. Petrographic and chemical characteristics of the Panda Hill carbonatite complex, Tanzania. *J. Afr. Earth Sci.*, 5, 589-598.

- Beard, C.D., Goodenough, K.M., Borst, A.M., Wall, F., Siegfried, P.R., Deady, E.A., Pohl, C., Hutchison, W., Finch, A.A., Walter, B.F., Elliott, H.A.L., Brauch, K., 2023. Alkaline-Silicate REE-HFSE Systems. *Econ. Geol.*, 118 (1), 117–208.
- Biondi, J. C., Braga Junior, J. M., 2023. Geology and mineralization of Nb, P, Fe and light rare earth elements of the Araxá alkaline-carbonatite complex, Minas Gerais state, Brazil. *J. South Am. Earth Sci.* 131, 104623.
- Bizzi, L.A., DeWit, M.J., Smith, C.B., McDonald, I., Armstrong, R.A., 1995. Heterogeneous enriched mantle materials and Dupal-type magmatism along the SW margin of the São Francisco Craton, Brazil. *Journal of Geodynamics*, 20(4), 469–491.
- Blakely, R.J., 1995. Potential theory in gravity and magnetic applications (Cambridge). <https://doi.org/10.1017/CBO9780511549816>
- Borodin, L.S., Lapin, A.V., Kharchenkov, A.G., 1973. Rare Metal Camaforites. Nauka, Moscow, 176 pp. (in Russian).
- Brod, J.A., 1999. Petrology and geochemistry of the Tapira alkaline complex, Minas Gerais State, Brazil. Unpublished PhD thesis, University of Durham, UK.
- Brod, J.A., Gaspar, J.C., de Araújo, D.P., Gibson, S.A., Thompson, R.N., Junqueira-Brod, T.C., 2001. Phlogopite and tetra-ferriphlogopite from Brazilian carbonatite complexes: petrogenetic constraints and implications for mineral-chemistry systematics. *Journal of Asian Earth Sciences*, 19(2001), 265–296.
- Brod, J.A., Gibson, S.A., Thompson, R.N., Junqueira-Brod, T.C., Seer, H.J., Moraes, L.C., Boaventura, G.R., 2000. The Kamafugite-Carbonatite Association in the Alto Paranaíba Igneous Province (Apip) Southeastern Brazil. *Braz. J. Geol.*, 30 (3), 408–412.
- Brod, J.A., Junqueira-Brod, T.C., Gaspar, J.C., Petrinovic, I.A., Valente, S.C., Corval, A., 2013. Decoupling of paired elements, crossover REE patterns, and mirrored spider diagrams: Fingerprinting liquid immiscibility in the Tapira alkalinecarbonatite complex, SE Brazil. *J. South Am. Earth Sci.*, 41, 41–56.
- Brögger, W.G., 1921. Die eruptivegestein des kristianiagebietes, IV. Das fengebiet in telemark. Norvegen. *Naturv.*, 9:150–167.
- Broom-Fendley, S., Siegfried, P. R., Wall, F., O'Neill, M., Brooker, R.A., Fallon, E.K., Pickles, J.R., Banks, D.A., 2021. The origin and composition of carbonatite-derived carbonate-bearing fluorapatite deposits. *Miner. Depos.*, 56, 863–884.
- Byron, M., 1999. Physical volcanology and lithogeochemistry of the Mata da Corda Formation, Minas Gerais, Brazil: PhD thesis, Carleton University.
- Carlson, R.W., Esperança, S., Svissero, D.P., 1996. Chemical and Os isotopic study of Cretaceous potassic rocks from Southern Brazil. *Contrib. Miner. Petrol.*, 125, 393–405.

- Carvalho, M.O., Valeriano, C.M., Neto, C.C.A., Oliveira, G.D., Heilbron, M., 2019. The Vazante and Canastra groups revisited: Sm-Nd and Sr isotopes — evidence for contribution from Tonian intraplate magmatism during passive margin development along the SW São Francisco margin, Brazil. *Braz. J. Geol.*, 49(1):e20180081.
- Carvalho, L.D.V., Jalowitzki, T., Scholz, R., Gonçalves, G.O., Rocha, M.P., Pereira, R.S., Lana, C., de Castro, M.P., Queiroga, G., and Fuck, R.A., 2022. An exotic Cretaceous kimberlite linked to metasomatized lithospheric mantle beneath the southwestern margin of the São Francisco Craton, Brazil. *Geoscience Frontiers*, 13(1), 101281.
- CBMM, 2023. Niobium production of Companhia Brasileira de Metalurgia e Mineração (CBMM) in 2021, by product. <https://cbmm.com/en/> (accessed 31 July 2023).
- Chadima, M., Cajz, V., Týcová, P., 2009. On the interpretation of normal and inverse magnetic fabric in dikes: examples from the Eger Graben, NW Bohemian Massif. *Tectonophysics*, 466(1-2), 47-63.
- Chakhmouradian, A.R., Wall, F., 2012. Rare earth elements: Minerals, mines, magnets (and more). *Elements*, 8, 333–340.
- Chakhmouradian, A.R., Zaitsev, A.N., 2012. Rare earth mineralization in igneous rocks: Sources and processes. *Elements*, 8, 347–353.
- Charlier, B., Sakoma, E., Sauvé, M., Stanaway, K., Auwera, J.V., Duchesne, J.C., 2008. The Grader layered intrusion (Havre-Saint-Pierre Anorthosite, Quebec) and genesis of nelsonite and other Fe–Ti–P ores. *Lithos*, 101 (3–4), 359–378.
- Che, X.D., Wu, F.Y., Wang, R.C., Gerdes, A., Ji, W.Q., Zhao, Z.H., Yang, J.H., Zhu, Z.Y., 2015. In situ U–Pb isotopic dating of columbite–tantalite by LA–ICP–MS. *Ore Geol. Rev.*, 65(4), 979–989.
- Conceição, F.T., Vasconcelos, P.M., Godoy, L.H., Navarro, G.R.B., 2020. $^{40}\text{Ar}/^{39}\text{Ar}$ geochronological evidence for multiple magmatic events during the emplacement of Tapira alkaline-carbonatite complex, Minas Gerais, Brazil. *J. South Am. Earth Sci.*, 97(November 2019).
- Cook, N.J., Ciobanu, C.L., Ehrig, K., Slattery, A., Verdugo-Ihl, M.R., Courtney-Davies, L., Gao, W., 2017. Advances and Opportunities in Ore Mineralogy. *Minerals*, 7(12), 233.
- Cordeiro, P.F.O., Brod, J.A., Palmieri, M., de Oliveira, C.G., Barbosa, E.S.R., Santos, R.V., Gaspar, J. C., Assis, L.C., 2011. The Catalão I niobium deposit, central Brazil: Resources, geology and pyrochlore chemistry. *Ore Geol. Rev.*, 41(1), 112–121.
- Cordeiro, P.F.O., Brod, J.A., Dantas, E.L., Barbosa, E.S.R., 2010. Mineral chemistry, isotope geochemistry and petrogenesis of niobium-rich rocks from the Catalão I carbonatite-phoscorite complex, Central Brazil. *Lithos*, 118 (3–4), 223–237.

- Cowan, D.R., Tompkins, L.A., Cowan, S., 2000. Screening kimberlite magnetic anomalies in magnetically active areas. *Exploration Geophysics*, 31(2), 66–72.
- CPRM., 2020. Folha cartográfica Belo_Horizonte_SE-23: Serviço Geológico do Brasil – CPRM. <http://geosgb.cprm.gov.br/geosgb/downloads.html>
- Da Costa, R., Roseiro, J., Figueiras, J., Rodrigues, P. C. R., Mateus, A., 2021. Pyrochlore from the Bailundo Carbonatite Complex (Angola): Compositional variation and implications to mineral exploration. *J. Afr. Earth Sci.* 177, 104154.
- Darling, R.S., Florence, F.P., 1995. Apatite light rare earth element chemistry of the port leyden nelsonite, Adirondack Highlands, New York: implications for the origin of nelsonite in anorthosite suite rocks. *Econ. Geol.*, 90, 964-968.
- Davies, K.A., 1947. The phosphate deposits of the Eastern province, Uganda. *Econ. Geol.*, 42, 137-146.
- Dentith, M.C., Mudge, S.T., 2014. Geophysics for the Mineral Exploration Geoscientist (Cambridge). <https://doi.org/https://doi.org/10.1017/CBO9781139024358>
- Egorov, L.S., 1991. Ijolite-Carbonatite Plutonism. Nedra, Leningrad, 260 pp. (in Russian).
- Elliott, H.A.L., Wall, F., Chakhmouradian, A.R., Siegfried, P.R., Dahlgren, S., Weatherley, S., Finch, A.A., Marks, M.A.W., Dowman, E., Deady, E., 2018. Fenites associated with carbonatite complexes: A review. *Ore Geol. Rev.*, 93(2017), 38–59.
- Ernesto, M., Marques, L.S., Piccirillo, E.M., Molina, E.C., Ussami, N., Comin-Chiaromonti, P., Bellieni, G., 2002. Paraná Magmatic Province-Tristan da Cunha plume system: Fixed versus mobile plume, petrogenetic considerations and alternative heat sources. *Journal of Volcanology and Geothermal Research*, 118(1–2), 15–36.
- Fan, H.R., Hu, F.F., Yang, K.F., Pirajno, F., Liu, X., Wang, K.Y., 2014. Integrated U-Pb and Sm-Nd geochronology for a REE-rich carbonatite dyke at the giant Bayan Obo REE deposit, Northern China. *Ore Geol. Rev.*, 63, 510–519.
- Felgate, M.R., 2014, The petrogenesis of Brazilian kimberlites and kamafugites intruded along the 125° lineament: improved geochemical and geochronological constraints on magmatism in Rondonia and the Alto Paranaiba Igneous Province [The University of Melbourne].
- Ferreira, A., Conceição R.V., Mizusaki A.M.P., 2022. Mesozoic to Cenozoic alkaline and tholeiitic magmatism related to West Gondwana break-up and dispersal. *Gondwana Res.*, 106 (2022) 15–33.
- Foley, S., 1992. Vein-plus-wall-rock melting mechanisms in the lithosphere and the origin of potassic alkaline magmas. *Lithos*, 28, 435–453.
- Foley, S.F., Venturelli, G., Green, D.H., Toscani, L., 1987. The ultrapotassic rocks: Characteristics, classification, and constraints for petrogenetic models. *Earth-Sci. Rev.*, 24(2), 81–134.

- Foley, S.F., Jacob, D.E., O'Neill, H.S.C., 2011. Trace element variations in olivine phenocrysts from Ugandan potassic rocks as clues to the chemical characteristics of parental magmas: *Contrib. Miner. Petrol.*, 162(1), 1–20.
- Gibson, S.A., Thompson, R.N., Leonardos, O.H., Dickin, A.P., Mitchell, J.G., 1995. The late cretaceous impact of the trindade mantle plume: Evidence from large-volume, mafic, potassic magmatism in SE Brazil. *J. Petrol.*, 36, 189–229.
- Gibson, S.A., Thompson, R.N., Weska, R.K., Dickin, A.P. and Leonardos, O.H., 1997. Late Cretaceous rift-related upwelling and melting of the Trindade starting mantle plume head beneath western Brazil. *Contrib. to Mineral. Petrol.*, 126, 303–314.
- Giebel, R. J., Marks, M. A. W., Gauert, C. D. K., Markl, G., 2019. A model for the formation of carbonatite-phoscorite assemblages based on the compositional variations of mica and apatite from the Palabora Carbonatite Complex, South Africa. *Lithos* 324–325, 89–104.
- Gittins, J., 1966. Summaries and bibliographies of carbonatite complexes. Pp. 417–570 in: *Carbonatites* (O.F. Tuttle and J. Gittins, editors). Wiley, New York.
- Gittins, J., Allen, C.R., Cooper, A.F., 1975. Phlogopitization of pyroxenite; its bearing on the composition of carbonatite magmas. *Geological Magazine*, 112(5), 503–507.
- Glagolev, A.A., Korchagin, A.M., Kharchenkov, A.G., 1974. Arbarastakh and Inagli Alkaline-Ultrabasic Massifs. Nauka, Moscow, 175 pp. (in Russian).
- Grasso, C.B., 2010. Petrologia do complexo alcalino-carbonatítico de Serra Negra, MG: Universidade de Brasília, Brazil, (p. 164).
- Green, T.H., 1994. Experimental studies of trace-element partitioning applicable to igneous petrogenesis – Sedona 16 years later. *Chem. Geol.*, 117, 1–36.
- Grégoire, M., Bell, D., and Le Roex, A., 2002. Trace element geochemistry of phlogopite-rich mafic mantle xenoliths: Their classification and their relationship to phlogopite-bearing peridotites and kimberlites revisited. *Contrib. Miner. Petrol.*, 142(5), 603–625.
- Grégoire, M., Bell, D.R., Le Roex, A.P., 2003. Garnet lherzolites from the Kaapvaal Craton (South Africa): Trace element evidence for a metasomatic history. *J. Petrol.*, 44(4), 629–657.
- Grossi Sad, J.H., Cardoso, R.N., Da Costa, M.T., 1971. Formações cretácicas em Minas Gerais: uma revisão. *Braz. J. Geol.*, 1, 2–13.
- Groves, D.I., Bierlein, F.P., Meinert, L. D., Hitzman, M.W., 2010. Iron oxide copper-gold (IOCG) deposits through Earth history: implications for origin, lithospheric setting, and distinction from other epigenetic iron oxide deposits. *Econ. Geol.* 105, 641–654.
- Guarino, V., Wu, F.Y., Lustrino, M., Melluso, L., Brotzu, P., Gomes, C. de B., Ruberti, E., Tassinari, C. C.G., Svisero, D.P., 2013. U-Pb ages, Sr-Nd- isotope geochemistry, and petrogenesis of kimberlites, kamafugites and phlogopite-picrites of the Alto Paranaíba

Igneous Province, Brazil. *Chem. Geol.*, 353, 65–82.

- Guarino, V., Wu, F.Y., Melluso, L., de Barros Gomes, C., Tassinari, C.C.G., Ruberti, E., Brilli, M., 2017. U–Pb ages, geochemistry, C–O–Nd–Sr–Hf isotopes and petrogenesis of the Catalão II carbonatitic complex (Alto Paranaíba Igneous Province, Brazil): implications for regional-scale heterogeneities in the Brazilian carbonatite associations. *International Journal of Earth Sciences*, 106(6), 1963–1989.
- Halliday, A., Davies, G., Lee, D., Tommasini, S., Paslick, C., Fitton, J., James, D., 1992. Lead isotope evidence for young trace element enrichment in the oceanic upper mantle. *Nature*, 359(1992), 623–627.
- Johnson, R.L., 1966. The Shawa and Dorowa carbonatite complexes, Rhodesia. Pp. 205–224 in: Carbonatites (O.F. Tuttle and J. Gittins, editors). Wiley, New York.
- Kasbohm, J., Schoene, B., 2018. Rapid eruption of the Columbia River flood basalt and correlation with the mid-Miocene climate optimum. *Science Advances*, 4(9), 1–9.
- Khan, A., Faisal, S., Ullah, Z., Ali, L., Ghaffari, A., Nawab, J., Rashid, M., 2021. Pyrochlore-group minerals from the Loe-Shilman Carbonatite Complex, NW Pakistan: implications for evolution of carbonatite system. *Period. di Mineral.* 90, 277–287.
- Klemme, S., Berndt, J., 2020. Trace element partitioning between pyrochlore, microlite, fersmite and silicate melts. *Geochem. Trans.* 21, 9.
- Knipping, J. L., Bilenker, L. D., Simon, A. C., Reich, M., Barra, F., Deditius, A. P., Wölle, M., Heinrich, C. A., Holtz, F., Munizaga, R., 2015a. Trace elements in magnetite from massive iron oxide-apatite deposits indicate a combined formation by igneous and magmatic-hydrothermal processes. *Geochim. Cosmochim. Acta* 171, 15–38.
- Knipping, J. L., Bilenker, L. D., Simon, A. C., Reich, M., Barra, F., Deditius, A. P., Lundstrom, C., Bindeman, I., Munizaga, R., 2015b. Giant Kiruna-type deposits form by efficient flotation of magmatic magnetite suspensions. *Geology* 43 (7), 591–594.
- Kogarko, L.N., Suddaby, P., Watkins, P., 1997. Geochemical evolution of carbonatite melts in Polar Siberia. *Geochemistry International*, 35, 113–118.
- Krasnova, N. I., Petrov, T. G., Balaganskaya, E. G., Garcia, D., Moutte, J., Zaitsev, A. N., Wall, F., 2004a. Introduction to phoscorites: occurrence, composition, nomenclature and petrogenesis, in: Wall, F., Zaitsev, A.N. (eds.), Phoscorites and Carbonatites from Mantle to Mine: the key example of the Kola Alkaline Province. The Mineralogical Society Series. Mineralogical Society of Great Britain and Ireland, London, pp. 45–74.
- Krasnova, N. I., Balaganskaya, E. G., Garcia, D., 2004b. Kovdor – classic phoscorites and carbonatites, in: Wall, F., Zaitsev, A.N. (eds.), Phoscorites and Carbonatites from Mantle to Mine: the key example of the Kola Alkaline Province. The Mineralogical Society Series. Mineralogical Society of Great Britain and Ireland, London, pp. 99–132.

- Le Bas, M., 2008. Fenites associated with carbonatites. *Can. Mineral.*, 46, 1033–1050.
- Le Bas, M.J., 1987. Nephelinites and carbonatites. In *Alkaline Igneous Rocks*. Geological, pp 53–83.
- Le Maitre, R.W., 2002. *Igneous Rocks: A Classification and Glossary Terms*, Second ed. Univ. (Cambridge).
- Li, X., 2008, Magnetic reduction-to-the-pole at low latitudes: Observations and considerations. *Leading Edge* (Tulsa, OK), 27(8), 990–1002. <https://doi.org/10.1190/1.2967550>
- Liu, S., Fan, H-R., Yang, K-F., Hu, F-F., Rusk, B., Liu, X., Li, X-C., Yang, Z-F., Wang, Q-W., Wang, K-Y., 2018. Fenitization in the giant Bayan Obo REE-Nb-Fe deposit: implication for REE mineralization. *Ore Geol. Rev.*, 94, 290–309.
- López, J., Cramer, T., 2014. Ambiente geológico del complejo Mitú y perspectivas de ocurrencias minerales de niobio y tantalio en el territorio colombiano. *Geo. Colombiana*, 37, 75–95.
- López-Quirós, A., Escutia, C., Sánchez-Navas, A., Nieto, F., García-Casco, A., Martín-Algarra, A., Evangelinos, D., Salabarnada, A., 2019. Glaucony authigenesis, maturity and alteration in the Weddell Sea: An indicator of paleoenvironmental conditions before the onset of Antarctic glaciation. *Sci. Rep.*, 9(1), 1–12.
- Louro, V.H.A., Mantovani, M.S.M., 2012. 3D inversion and modeling of magnetic and gravimetric data characterizing the geophysical anomaly source in Pratinha I in the southeast of Brazil. *Journal of Applied Geophysics*, 80, 110–120.
- Lustrino, M., Ronca, S., Caracausi, A., Ventura Bordenca, C., Agostini, S., Faraone, D. B., 2020. Strongly SiO₂-undersaturated, CaO-rich kamafugitic Pleistocene magmatism in Central Italy (San Venanzo volcanic complex) and the role of shallow depth limestone assimilation. *Earth-Sci. Rev.* 208(February), 103256.
- Malatesta, C., Crispini, L., Ildefonse, B., Federico, L., Lisker, F., Läufer, A., 2021. Microstructures of epidote-prehnite bearing damaged granitoids (northern Victoria Land, Antarctica): clues for the interaction between faulting and hydrothermal fluids. *Journal of Structural Geology*, 147(2021), 104350.
- Martin, L.H.J., Schmidt, M.W., Mattsson, H.B., Ulmer, P., Hametner, K., Günther, D., 2012. Element partitioning between immiscible carbonatite-kamafugite melts with application to the Italian ultrapotassic suite. *Chem. Geol.*, 320–321, 96–112.
- McCaffrey, D.M., Nassar, N.T., Jowitt, S.M., Padilla, A.J., Bird, L.R., 2023. Embedded critical material flow: The case of niobium, the United States, and China. *Resour. Conserv. Recycl.* 188, 106698.
- Melluso, L., Lustrino, M., Ruberti, E., Brotzu, P., de Barros Gomes, C., Morbidelli, L., Morra, V., Svisero, D.P., D'Amelio, F., 2008. Major- and trace-element composition of olivine,

perovskite, clinopyroxene, Cr-Fe-Ti oxides, phlogopite and host kamafugites and kimberlites, Alto Paranaíba, Brazil. *Can. Mineral.*, 46(1), 19–40.

Melo, M.G., 2012. A origem do fosfato nas rochas vulcânicas e vulcanoclásticas do Grupo Mata da Corda nas regiões de Patos de Minas e Presidente Olegário, MG, Master's Thesis, [Universidade Federal de Ouro Preto].

Mitchell, R.H., 2005. Carbonatites and carbonatites and carbonatites. *Can. Mineral.*, 43, 2049–2068.

Mitchell, R.H., 2015. Primary and secondary niobium mineral deposits associated with carbonatites. *Ore Geol. Rev.* 65, 626-641.

Mitchell, R.H., Gittins, J., 2022. Carbonatites and carbothermalites: A revised classification. *Lithos*, 430–431, 106861.

Mitchell, R.H., Wahl, R., Cohen, A., 2020. Mineralogy and genesis of pyrochlore apatitite from The Good Hope Carbonatite, Ontario: A potential niobium deposit. *Mineral. Mag.*, 1–11.

Moore, C.H., 1940. Origin of the nelsonite dikes of Amherst County, Virginia. *Econ. Geol.*, 35, 629-645.

Moraes Rocha, L.G. Pires, A.C.B., Carmelo, A.C., Araújo Filho, J.O., 2014. Geophysical characterization of the Azimuth 125° lineament with aeromagnetic data: Contributions to the geology of central Brazil. *Precambrian Res.* 249, 273–287.

Morogan, V., 1994. Ijolite versus carbonatite as sources of fenitization. *Terra Nova*, 6(2), 166–176.

Mudd, G.M., Jowitt, S.M., Werner, T.T., 2017. The world's by-product and critical metal resources part I: uncertainties, current reporting practices, implications and grounds for optimism. *Ore Geol. Rev.*, 86, 924-938.

Nakamura, N., 1974. Determination of REE, Ba, Fe, Mg, Na and K in carbonaceous and ordinary chondrites. *Geochim. Cosmochim. Acta*, 38(5), 757–775.

Navarro, G.R.B., Zanardo, A., Conceição, F.T., 2013. O Grupo Araxá na região sul-sudoeste do Estado de Goiás. *Geologia USP. Série Científica*, 13(2), 5–28.

Nedosekova, I.L., 2007. New data on carbonatites of the Il'mensky-Vishnevogorsky alkaline complex, the southern Urals, Russia. *Geology of Ore Deposits*, 49(2), 129–146.

Novaes, L.C., 2018, Processos metalogenéticos associados a complexos alcalino-carbonatíticos da Província Ígnea Alto Paranaíba, Sudeste Brasileiro. BsC Thesis, Universidade Federal do Paraná.

Odin, G.S., 1988. Green Marine Clays. Elsevier Science 1988 (ed.); Develop Se.

Odin, Gilles S., Matter, A., 1981. De glauconiarum origine: *Sedimentology*, 28(5), 611–641.

- Oliveira, L., Pereira, M., Pacheli Heitman, A., Filho, J., Oliveira, C., Ziolek, M., 2023, Niobium: The Focus on Catalytic Application in the Conversion of Biomass and Biomass Derivatives. *Molecules* 28, 1527.
- Oliveira, I. Brod, J.A., Junqueira-Brod, T.C., Reimold, W.U. Fuck, R.A., 2022. The IUGS Nomenclature on Kalsilite-Bearing Volcanic Rocks: A Critical Appraisal and Recommendations. *J. Petrol.* 2022, 63, 1–14.
- Ovalle, J. T., La Cruz, N. L., Reich, M., Barra, F., Simon, A. C., Konecke, B. A., Morata, D., 2018. Formation of massive iron deposits linked to explosive volcanic eruptions. *Sci. Rep.* 8, 14855.
- Palmieri, M., 2011, The carbonatite-related Morro do Padre niobium deposit, Catalão II Complex, central Brazil, Master's Thesis [Universidade de Brasília].
- Palmieri, M., Brod, J.Á., Cordeiro P., Gaspar, J.C., Ribeiro, P.A., de Asis, L.C., Junqueira-Brod, T.C., Milanezi, B.P., Machado, A.S., Jácomo, M.H., 2022. The carbonatite-related Morro do Padre niobium deposit, Catalão II Complex, central Brazil. *Econ. Geol.*, 117 (7), 1497–1520.
- Philpotts, A.R., 1967. Origin of certain iron-titanium oxide and apatite rocks. *Econ. Geol.*, 62, 303–315.
- Piauilino, P.F., 2018. Estudo geoquímico e isotópico de anfibolitos e rochas metassedimentares da Sequência Metavulcanossedimentar Veríssimo e Grupo Araxá, Pires do Rio – GO. Master Thesis, University of Brasília, Brasil.
- Pilkington, M., Tschirhart, V., 2017. Practical considerations in the use of edge detectors for geologic mapping using magnetic data: *Geophysics*, 82(3), J1–J8.
- Platt, R.G., 1996. The ijolite-series rocks. In R. H. Mitchell (Ed.), Undersaturated alkaline rocks: mineralogy, petrogenesis, and economic potential. No. 24 in Mineralogical Association of Canada Short Course Series (Mineralogi, pp. 101–122).
- Reich, M., Simon, A. C., Barra, F., Palma, G., Hou, T., Bilenker, L., 2022. Formation of iron oxide-apatite deposits. *Nat. Rev. Earth Environ.* 3, 758–775.
- Ribeiro, A.C., 2008, Geologia, geometalurgia, controles e gênese dos depósitos de fósforo, terras raras e titânio do complexo carbonatítico Catalão I, GO: Universidade de Brasília, Brazil (p. 508).
- Ribeiro, C.C., Brod, J.A., Junqueira-Brod, T.C., Gaspar, J.C., Palmieri, M., Cordeiro, P.F.O., Torres, M.G., Grasso, C.B., Barbosa, E.S.R., Barbosa, P.A., Ferrari, A.J., 2014. Potencial e controles metalogenéticos de ETR, Ti e Nb em províncias alcalino-carbonatáticas 912 brasileiras. In CPRM (Ed.). Metalogenia das Províncias Tectônicas do Brasil (pp. 559–589).
- Ribeiro, A.C., Riccomini, C., Leite, J.A.D., 2018. Origin of the largest South American transcontinental water divide. *Sci. Rep.* 8(1), 1–8.
- Roest, W.R., Verhoef, J., Pilkington, M., 1992. Magnetic interpretation using the 3-D analytic

- signal. *Geophysics*, 57(1), 116–125.
- Rojas, P. A., Barra, F., Deditius, A., Reich, M., Simon, A.C., Roberts, M., Rojo, M., 2018. New contributions to the understanding of Kiruna-type iron oxide-apatite deposits revealed by magnetite ore and gangue mineral geochemistry at the El Romeral deposit, Chile. *Ore Geol. Rev.* 93, 413-435.
- Romeo, I., Capote, R., Lunar, R., Cayzer, N., 2007. Polymineralic orientation analysis of magmatic rocks using electron back-scatter diffraction: implications for igneous fabric origin and evolution. *Tectonophysics*, 444 (1-4), 45-62.
- Rosenthal, A., Foley, S.F., Pearson, D.G., Nowell, G.M., Tappe, S., 2009. Petrogenesis of strongly alkaline primitive volcanic rocks at the propagating tip of the western branch of the East African Rift. *Earth and Planetary Science Letters*, 284(1–2), 236–248.
- Russell, H.D., Hiemstra, S.A., Groeneveld, D., 1954. The mineralogy and petrology of the carbonatite at Loolekop, Eastern Transvaal. *Transactions of the Geological Society of South Africa*, 57, 197-208.
- Scott-Smith, B.H., Nowicki, T.E., Russell, J.K., Webb, K.J., Mitchell, R.H., Hetman, C.M., Harder, M., Skinner, E.M.W., Robey, J.A., 2013. Kimberlite terminology and classification. D. G. Pearson et al. (eds.), *Proceedings of 10th International Kimberlite Conference*. Doi:10.1007/978-81-322-1173-0.
- Seer, H.J., Brod, J.A., Reinhardt, F., Pimentel, M., Boaventura, R., Dardenne, M.A., 2001. Grupo Araxá em sua área tipo: Um fragmento de crosta oceânica neoproterozóica na Faixa de Dobramentos Brasília. *Revista Brasileira de Geociências*, 31(3), 385–396.
- Sgarbi, P.B.A., Gaspar, J.C., 2002. Geochemistry of the Santo Antônio da Barra Kamafugites. *Journal of South American Earth Sciences*, 14, 889–901.
- Sgarbi, P.B.A., Heaman, L.M., Gaspar, J.C., 2004. U-Pb perovskite ages for brazilian kamafugitic rocks: Further support for a temporal link to a mantle plume hotspot track: *J. South Am. Earth Sci.*, 16(8), 715–724.
- Shannon, R.D., 1976. Revised effective ionic radii and systematic studies of interatomic distances in halides and chalcogenides. *Acta Crystallogr. Sect. A* 32, 751–767.
- Silva, A.J.C.A., Simões, L.S.A., DuFrane, S.A., Sá Alkmin, L.A., Cerri, R.I., 2020. U–Pb ages of detrital zircon grains for the Canastra Group and Passos Nappe units and U–Pb and Lu–Hf isotope analyses from orthogneisses: Provenance and tectonic implications, southern Brasília Belt, Brazil. *Precambrian Res.*, 346, 105771.
- Skelton, A., Hode Vuorinen, J., Arghe, F., Fallick, A., 2007. Fluid-rock interaction at a carbonatite-gneiss contact, Alnö, Sweden. *Contrib. Miner. Petrol.*, 154(1), 75–90.

- Skirrow, R.G., 2022. Iron oxide copper-gold (IOCG) deposits—a review (part 1): settings, mineralogy, ore geochemistry and classification. *Ore Geol. Rev.*, 140, 104569.
- Streckeisen, A., 1978. Classification and nomenclature of volcanic rocks, lamprophyres, carbonatites and melilitic rocks: recommendations and suggestions, IUGS Subcommission on the Systematics of Igneous Rocks. *Neues Jahrbuch für Mineralogie, Abhandlungen*, 134, 1–14.
- Suguió, K., Barcelos, J.H., 1983. Paleoclimatic evidence from the Areado Formation, Cretaceous of the São Francisco Basin, State of Minas Gerais, Brazil. *Braz. J. Geol.*, 13(4), 229–231.
- Sun, Z., Qin, K., Mao, Y., Tang, D., Wang, F., Evans, N.J., Zhou, Q., 2022. Mineral Chemistry of Pyrochlore Supergroup Minerals from the Boziguuer Nb-Ta-Zr-Rb-REE Deposit, NW China: Implications for Nb Enrichment by Alkaline Magma Differentiation. *Minerals* 12, 785.
- Tappe, S., Foley, S.F., Jenner, G.A., Heaman, L.M., Kjarsgaard, B.A., Romer, R.L., Stracke, A., Joyce, N., Hoefs, J., 2006. Genesis of ultramafic lamprophyres and carbonatites at Aillik Bay, Labrador: A consequence of incipient lithospheric thinning beneath the North Atlantic Craton. *J. Petrol.*, 47(7), 1261–1315.
- Tappe, S., Foley, S.F., Jenner, G.A., Kjarsgaard, B.A., 2005. Integrating ultramafic lamprophyres into the IUGS classification of igneous rocks: Rationale and implications: *J. Petrol.*, 46(9), 1893–1900.
- Tappe, S., Foley, S.F., Kjarsgaard, B.A., Romer, R.L., Heaman, L.M., Stracke, A., Jenner, G.A., 2008. Between carbonatite and lamproite-Diamondiferous Torngat ultramafic lamprophyres formed by carbonate-fluxed melting of cratonic MARID-type metasomes: *Geochim. Cosmochim. Acta*, 72(13), 3258–3286.
- Tappe, S., Foley, S.F., Pearson, D.G., 2003. The Kamafugites of Uganda: a mineralogical and geochemical comparison with their Italian and Brazilian analogues. *Periodico Di Mineralogia*, 72, 51–77.
- Taufner, R., Lagoeiro, L., Cavalcante, C., Barbosa, P., Silveira, C.S., 2021. Deformation mechanisms accommodating progressive simple shear thrusting of quartzite and metacarbonate in the southwestern Espinhaço Range, Brazil. *J. South Am. Earth Sci.*, 107, 102944.
- Taylor Jr, H.P., Frechen, J., Degens, E.T., 1967. Oxygen and carbon isotope studies of carbonatites from the Laacher See District, West Germany and the Alnö District, Sweden. *Geochim. Cosmochim. Acta*, 31, 407–430.
- Tegner, C., Cawthorn, R.G., Kruger, F.J., 2006. Cyclicity in the Main and Upper Zones of the Bushveld Complex, South Africa: Crystallization from a Zoned Magma Sheet. *J. Petrol.*, 47 (11), 2257–2279.
- Thompson, R.N., Gibson, S.A., Mitghell, J.G., Dickin, A.P., Leonardos, O.H., Brod, J.A.,

- Greenwood, J.G., 1998. Migrating Cretaceous-Eocene magmatism in the Serra do Mar Alkaline Province, SE Brazil: melts from the deflected Trindade mantle plume? *J. Petrol.*, 39(8), 1493–1526.
- Thompson, R.N., Leonardos, O.H., Turner, S.E., Mitghell, J.G., Dickin, A.P., 1994. The Serra do Bueno potassic diatreme: a possible hypabyssal equivalent of the ultramafic alkaline volcanics in the Late Cretaceous Alto Paranaiba Igneous Province, SE Brazil. *Mineralogical Magazine*, 58, 357–373.
- Tindle, A., Breaks, F., 2000. Columbite-tantalite mineral chemistry from rare-element granitic pegmatites: Separation Lakeh area, N.W. Ontario, Canada. *Mineral. Petrol.*, 70, 165–198.
- Tremblay, J., Bédard, L. P., Matton, G., 2017. Columbitization of fluorcalciopyrochlore by hydrothermalism at the Saint-Honoré alkaline complex, Québec (Canada): New insights on halite in carbonatites. *Ore Geol. Rev.* 91, 695–707.
- Tröger, W.E., 1928. Alkaligesteine aus der Serra do Salitre im westlichen Minas Geraes, Brasilien. *Centralblatt für Mineralogie, Geologie und Paläontologie*, Abteilung A, 202–204.
- Tröger, W.E., 1935. Speziell Petrographie der Eruptivegesteine – Ein nomenklatur Kompendium. Verlag der Deutschen Mineralogischen Gesellschaft, Berlin.
- Uglietti, D.; Sedlak, K.; Wesche, R.; Bruzzone, P.; Muzzi, L.; della Corte, A. Progressing in cable-in-conduit for fusion magnets: From ITER to low cost, high performance DEMO. *Supercond. Sci. Technol.* 2018, 31, 055004.
- Vallierès, D., Pelletier, P., Gaultier, P., Ferlatte, G., Tremblay, J. -F., Sirois, R., 2013. Update on Niobec expansion: NI 43-101. https://www.miningdataonline.com/reports/Niobec_12102013_TR.pdf (accessed 31 July 2023).
- Vasyukova, O. V., Williams-Jones, A.E., 2023. A new model for the origin of pyrochlore: Evidence from the St Honoré Carbonatite, Canada. *Chem. Geol.* 632, 121549.
- Velásquez Ruiz, F., Cordeiro, P., Reich, M., Motta, J.G., Ribeiro, C., Angerer, T., Bernardes, R. (2022) The genetic link between kamafugite magmatism and alkaline carbonatite complexes in the Late Cretaceous Alto Paranaíba Igneous Province, Central Brazil. *International Geology Review*, v.65, 2148-2170 (CAPÍTULO 2)
- Velásquez Ruiz, F., Giustina M.E.S.D., Oliveira C.G., Dantas E.L., Hollanda M.H.B., 2019. The 3.5 Ga São Tomé layered mafic-ultramafic intrusion, NE Brazil: insights into a Paleoarchean Fe-Ti-V oxide mineralization and its reworking during West Gondwana assembly. *Precambrian Res.*, 326, 462-478.
- Verwoerd, W.J., 1963. South African carbonatites and their probable mode of origin. *Ann. Univ. Stellenbosch*, 41:121–233.

- Wall, F., Zaitsev, A.N., 2004. Phoscorites and Carbonatites from mantle to mine: the key example of the Kola Alkaline Province. The Mineralogical Society of Great Britain & Irland, Series 10, London.
- Walter, B.F., Giebel, R.J., Steele-MacInnis, M., Marks, M.A.W., Kolb, J., Mark, G., 2021. Fluids associated with carbonatitic magmatism: A critical review and implications for carbonatite magma ascent. *Earth-Sci. Rev.*, 215, 103509.
- Walter, B. F., Parsapoor, A., Braunger, S., Marks, M. A. W., Wenzel, T., Martin, M., Markl, G., 2018. Pyrochlore as a monitor for magmatic and hydrothermal processes in carbonatites from the Kaiserstuhl volcanic complex (SW Germany). *Chem. Geol.* 498, 1-16.
- Watson, T.L., 1907. Occurrence of Rutile in Virginia, *Econ. Geol.*, 2, 493-504.
- Watson, T.L., Taber, S., 1913. Geology of the Titanium and Apatite Deposits of Virginia. University of Virginia, Charlottesville. Bulletin No. III-A.
- Werner, T.T., Mudd, G.M., Jowitt, S.M., 2017. The world's by-product and critical metal resources part II: A method for quantifying the resources of rarely reported metals. *Ore Geol. Rev.*, 80, 658-675.
- Williams, P.J., Barton, M.D., Johnson, D.A., Fontboté, L., de Haller, A., Mark, G., Oliver, N.H.S., Marschik, R., 2005. Iron oxide copper-gold deposits: geology, space-time distribution, and possible modes of origin. *Econ. Geol.*, 100th Anniv. Vol., 371–405.
- Williams-Jones, A.E., Vasyukova, O.V., 2023. Niobium, Critical Metal, and Progeny of the Mantle. *Econ. Geol.* 118 (4), 837–855.
- Winter, J.D., 2001. An Introduction to Igneous and Metamorphic Petrology: PrenticeHall (p. 697).
- Woolley, A.R., Bergman, S.C., Edgar, A.D., Le Bas, M.J., Mitchell, R.H., Rock, N.M.S., Scott Smith, B.H., 1996. Classification of Lamprophyres, Lamproites, Kimberlites, and the Kalsilic, Melilitic and Leucitic rocks. *Canadian Mineralogist*, 34, 175–186.
- Woolley, A., Kjarsgaard, K., 2008. Carbonatite occurrences of the world: map and database. Geological Survey of Canada. 5796, p. 28.
- Yang, X.M., Le Bas, M.J., 2004. Chemical compositions of carbonate minerals from Bayan Obo, Inner Mongolia, China: Implications for petrogenesis. *Lithos*, 72(1–2), 97–116.
- Yeats, C.J., Hollis, S.P., Halfpenny, A., Corona, J.C., LaFlamme, C., Southam, G., Fiorentini, M., Herrington, R.J., Spratt, J., 2017. Actively forming Kuroko-type volcanic-hosted massive sulfide (VHMS) mineralization at Iheya North, Okinawa Trough, Japan. *Ore Geol. Rev.*, 84(2017), 20-41.
- Yegorov, L. S., 1993. Phoscorites of the Maymecha–Kotuy ijolite–carbonatite association. *Int. Geol. Rev.* 35, 346–358.

- Zalan, P.V., Wolff, S., Astolfi, M.A.M., Vieira, I.S., Concelcao, J.C.J., Appi, V.T., Neto, E.V.S., Cerqueira, J.R., Marques, A., 1990. The Parana Basin, Brazil: Chapter 33: Part II. Selected Analog Interior Cratonic Basins: Analog Basins. In *Interior Cratonic Basins* (p. 708).
- Zaitsev, A. N., Spratt, J., Shtukenberg, A. G., Zolotarev, A. A., Britvin, S. N., Petrov, S. V., Kuptsova, A. V., Antonov, A. V., 2021. Oscillatory- and sector-zoned pyrochlore from carbonatites of the Kerimasi volcano, Gregory rift, Tanzania. *Mineral. Mag.* 85, 532–553.
- Zhou, M.F., Robinson, P.T., Lesher, C.M., Keays, R.R., Zhang, C.J., Malpas, J., 2005. Geochemistry, petrogenesis and metallogenesis of the Panzhihua gabbroic layered intrusion and associated Fe–Ti–V oxide deposits, Sichuan Province, SW China. *J. Petrol.*, 46 (11), 2253–2280.
- Zhou, Q., Qin, K., Tang, D., 2021. Mineralogy of columbite-group minerals from the rare-element pegmatite dykes in the East-Qinling orogen, central China: Implications for formation times and ore genesis. *J. Asian Earth Sci.*, 218, 104879.

ANEXO: MATERIAL SUPLEMENTARIO

Material supplementario del Capítulo 2

Los datos de química de roca total en muestras de kamafugia y olivino aillikita, junto con los datos de microsonda electrónica para óxidos del grupo de la espinela, perovskita, clinopiroxeno y glauconita, están disponibles a través del enlace: <https://doi.org/10.1080/00206814.2022.2127127>

Material supplementario del Capítulo 3

Los datos de micro fluorescencia de rayos X para muestras de carbonatita y fenita, junto con datos de microsonda electrónica para flogopita y ortoclas, están disponibles a través del enlace: <https://doi.org/10.17632/mygc3pt7rg.1>

Material supplementario del Capítulo 4

Los datos de elementos mayores en microsonda electrónica y elementos menores y traza en LA-ICP-MS en pirocloro están disponibles a través del enlace: <https://doi.org/10.17632/vs26by5p5b.3>